Systems Biology Analyses of Hematopoietic Cells

Milewicz, Hanna

Awarding institution:
King's College London

Systems Biology Analyses of Hematopoietic Cells

Hanna Jadwiga Milewicz

A THESIS PRESENTED FOR THE DEGREE OF DOCTOR OF PHILOSOPHY

KING'S COLLEGE LONDON

2012

Declaration

I hereby declare that I alone composed this thesis and that the work is my own, except where stated otherwise.

Hanna Milewicz
September 2012

Acknowledgements

Thank you to my primary supervisor Dr. Shaun Thomas for giving me the opportunity to work in your laboratory and for guiding me so well throughout this time. I am extremely grateful and indebted for the expertise, inspiration and for introducing me to the philosophy of 'Systems Biology'. I also would like to thank Prof. Farzin Farzaneh for his ideas and guidance of my work and Prof. GJ Mufti for giving me the opportunity to work in the Department of Haematological Medicine.

I would like to acknowledge our collaborators without whom this work would not be possible to complete. I would never have learnt so much without the opportunity to work within other laboratories: Prof. Tony N, Dr. Leo Carlin and all lab members for giving me the opportunity to learn advanced imaging techniques. Prof. Marcotte, Dr. Daniel Boutz and lab members for the training in proteomics and mass spectrometry. Dr.Dariusz Ladon for the help in cytogenetics. Dr. Paul Lavender and Dr. Audrey Kelly for the help in isolating chromatin.

To Dr. Steve Orr, thanks for his advice and especially for the help in analysing proteomics data. To all my fellow colleagues in the Department of Haematological Medicine, thanks for being so supportive during my stay at the Institute. I would like to thank Leukaemia Lymphoma Research for funding my PhD studies.

To my family, thank you for all the support and encouragement.

A mosaic consists of thousands of little stones. Some are blue, some are green, some are yellow, some are gold. When we bring our faces close to the mosaic, we can admire the beauty of each stone. But as we step back from it, we can see that all these little stones reveal to us a beautiful picture, telling a story none of these stones can tell by itself."

-- Henri Nouwen

List of abbreviations

ACN	Acetonitrile
APC	antigen presenting cells
APEX	absolute protein expression
BCR	B cell receptor
BSA	bovine serum albumin
C/NM	chromatin & nuclear matrix
CBP	Calmodulin binding peptide
Cdc42	cell division cycle 42
CFP	cyan fluorescent protein
ChIP	chromatin immunoprecipitation
CLL	chronic lymphocytic leukaemia
CMTMR	5-(and-6)-(((4-chloromethyl)benzoyl)amino)-tetramethylrhodamine
Col	Colcemid
CRIB	Cdc42/Rac-interactive binding
CTL	Cytotoxic T lymphocytes
Cycs	cytochrome C
DetOut	DetergentOut removal kit
DH	DBl homology
DHR2	Dock-homology region-2
DSB	double strand breaks
DTT	Dithiothreitol
ESI	electrospray ionisation
F	free
F-actin	filamentous actin
FASP	Filter-Aided Sample Preparation
FC- combined	Fold change combined
FITC	Fluorescein isothiocyanate
FLIM	Fluorescence Lifetime Imaging Microscopy
FRET	Förster Resonance Energy Transfer
FSC	forward scatter

GAP	GTPase-activating protein
GDI	guanine nucleotide dissociation inhibitor
GDP	guanosine diphosphate GEF guanine exchange factor
GEF	guanine nucleotide exchange factor
GFP	green fluorescent protein
GrB	Granzyme B
hnRNP	heterogeneous nuclear ribonucleoprotein
HPRD	human protein reference database
Hsp	heat-shock protein
HTS	high-throughput-screening
I-FISH	Interphase FISH
IAA	Iodoacetamide
IFN	interferon
IS	immunological synapse
iTRAQ	isobaric Tags for Relative and Absolute Quantification
LB	Luria-Bertoni
LC	liquid chromatography
LCMS/MS	liquid chromatography tandem mass spectrometry
LTQ	LTQ-Orbitrap mass spectrometer
LUMIER	luminescence-based mammalian interactome mapping
m/z	mass to charge ratio
mAb	monoclonal antibody
MALDI	matrix assisted laser desorption ionisation
Mat2A	Methionine adenosyltransferase 2 A
MHC	major histocompatibility complex
M.nase	micrococcal nuclease
MPM	Multiphoton microscopy
MS	mass spectrometry
MTOC	microtubule organizing center
Nap1L	nucleosome assembly protein 1-like
NChIP	native chromatin immunoprecipitation
NFκB	nuclear factor kappa B
NK cell	natural killer cell

NKIS	activating NK cell immunological synapse
OMIM	McKusick's Online Mendelian Inheritance in Man
P	pellet
p-γH2AX	phospho-γH2AX
PAK1	p21-activayted kinase 1
PBMC	Peripheral blood mononuclear cells
PBS	Phosphate buffered saline
PH	pleckstrin-homology
PI	Propodium Iodide
PI3K1	p85α subunit of phosphatidylinositol 3-kinase
PMA	Phorbol 12-myristate 13-acetate
PMSF	Phenylmethanesulfonylfluoride
PP6	protein phosphatase 6
PRC	pre-replication complex
r	distance between two fluorophores
R_0	Förster distance
RFP	red fluorescent protein
Rpa3	replication protein 3
RPMI	Rosswell Park Memorial Institute medium
RT	Reverse Transcriptase
SD	Standard deviation
SILAC	Stable Isotope Labeling with Amino acids in cell Culture
SMAC	supramolecular activation cluster
SSC	side scatter
τ	fluorescence lifetime
TAP	tandem affinity purification
TCR	T cell receptor
TCSPC	time-correlated single photon counting
TFE	Trifluorethanol
Velos	Velos-Orbitrap mass spectrometer
w XL	with formaldehyde crosslinking
w/o XL	without formaldehyde crosslinking
Y2H	yeast-two-hybrid

Abstract

The focus of my thesis is to apply systems biology approaches to obtain a better understanding of complex cellular systems. In particular, my work concentrates on the function of haematological cells.

The first part of the thesis applies a novel, predictive strategy to identify new regulators of a signalling pathway in human immune cells. Cdc42 is a membrane associated GTPase that is an important regulator of cytoskeleton rearrangements and is required for natural killer (NK) cell activation. Previous work had shown that Cdc42 activity oscillates during NK immune surveillance after an initial increase, suggesting that Cdc42 activity is regulated in NK cells by a number of signalling molecules. The aim of the project is to predict proteins required for Cdc42 activity in NK cells and test the predictions. Using a bioinformatics methodology, 13 different proteins were predicted to interact with Cdc42 and form feedback loops. To determine whether any of the predicted proteins were required for Cdc42 activity, NK cells were transfected with a Cdc42 biosensor, each of the predicted targets was downregulated with siRNA and Cdc42 activity was quantified by FRET/FLIM microscopy in the presence of target cells. The screen identified AKT1 and the p85α subunit of PI3K as novel regulators of Cdc42 activity. Depletion of each of these targets also results in an impaired cellular cytotoxic response. This proof of principle study demonstrates the power of a predictive approach in the NK immune surveillance context to identify novel regulators of Cdc42.

The second part of my thesis is based on using a predictive methodology, called the ‘Phenolog approach’ to predict novel proteins involved in cancer. To determine whether the predicated proteins are required to maintain genome stability, two of the predicted targets were tested using a human primary T cell system, in which cellular mechanisms are normal. Quiescent T cells were transfected with siRNA, the cells were stimulated to enter the cell cycle and chromosome integrity was analysed by interphase FISH. The two predicted targets tested were AND1, a DNA replication protein, and SEC13, a component of the nuclear pore complex. Depletion of each of the targets led to a number of chromosomal abnormalities,

indicating that their normal expression during the $G_0 \rightarrow G_1$ transition is required to maintain genome stability.

The third part of my thesis focuses on the systematic analyses of the chromatin proteome of T cells during cell cycle progression and identifying changes in the proteome caused by depleting the DNA replication protein Mcm7. Reducing the induction of Mcm7 causes DNA damage, premature chromatid separation and genome instability (291). Initially, the chromatin proteome obtained by a native, non-crosslinked chromatin extraction method was compared with that obtained after formaldehyde crosslinking. In addition, the methodology was compared with the proteome obtained previously using the CSK extraction method (290). To analyse the effects of depleting Mcm7, quiescent primary T cells were transfected with Mcm7 siRNA and the cells were stimulated to enter the cell cycle. The proteins were crosslinked with formaldehyde, chromatin was isolated and the chromatin-bound proteome in Mcm7-depleted and control cells were analysed by LC-MS/MS. Changes in the nuclear proteome caused by depleting Mcm7 were quantified by a label-free spectral counting method. Network analyses (HumanNet) were used to identify protein interaction sub-networks. The analyses identified that downregulation of Mcm7 affects a number of processes, including DNA replication, DNA damage, transcription and ribosome biogenesis.

Supplementary Data

In the appendix of this thesis, the complete mass spectrometry data of all proteins identified in Chapter 5 and Chapter 6 are provided, as well as spread sheets of the analyses and high-resolution images of the protein interaction networks.

The CD provided with this thesis contains the following supplementary information:

Folder Chapter 5:

S 5.2.2.Detergent removal summary
S 5.2.3 Cellular location summary
S 5.2.5 Network S2 Native Seedset
S 5.2.5 Network S2 XL Seedset
S 5.2.5_S2 Native sub-network 1
S 5.2.5_S2 Native sub-network 2
S 5.2.5_S2 Native sub-network 3
S 5.2.5_S2 XL sub-network 1
S 5.2.5_S2 XL sub-network 2
S 5.2.5_S2 XL sub-network 3

Folder Chapter 6:

S 6.2.4 Mcm7 knockdown S1 LTQ Analysis
S 6.2.4 Mcm7 knockdown S1 Velos Analysis
S 6.2.4 Mcm7 knockdown S2 LTQ Analysis
S 6.2.5 Network combined_high resolution
S 6.2.5 Network S1 Velos_high resolution
S 6.2.5 Network S1 LTQ_high resolution
S 6.2.5 Network S2 LTQ_high resolution

TABLE OF CONTENTS

Chapter 1

1. Introduction

1.1 Systems biology

The focus of my thesis is to apply systems biology approaches to obtain a better understanding of complex biological systems, with the aim of answering biological questions about hematopoietic cells. Systems Biology is defined as a “ground-breaking scientific approach that seeks to understand how all the individual components of a biological system interact in time and space to determine the functioning of the system” (1). The concept of Systems Biology is to integrate large amounts of data from different sources in order to understand the physiology and to model the complexity of cell function, which leads potentially to improvement in our knowledge of health and disease (1). Even the simplest living cell is an incredibly complex molecular machine, which we only understand in part. Information contained in the DNA and mRNA encodes tens of thousands of proteins that differ in their function, localisation and dynamics. Each protein interacts with other proteins and various small molecules and their activity is highly dependent on the cellular environment. “Viewed as a whole, a cell is like an immense city with people and objects and buzzing with activity” (https://www.systemsbiology.org/research). Until recently biologists tried to understand organisms and biological systems by examining individual components isolated from a large network, such as individual genes or proteins, to understand their biological functions. Over the past few years, Systems Biology approaches have gained more and more importance as ways of trying to understand complex biological systems. Systems Biology uses novel combinatorial, multi-disciplinary approaches to model global networks of proteins in a cell, for example in response to a specific stimulus, rather than only analysing individual, isolated constituents of the network. Such analyses may incorporate high throughput data sets or high content wet-lab experiments, combined with computational approaches to enable us to model and predict cellular functions. This is possible due to the progress made in the last few years in molecular biology, computer science and measurement technologies. Thus, Systems Biology uses a holistic rather than a reductionist approach to understand biological complexity, using a range of cross disciplinary expertise (278).

Predictive biology is an important component of Systems Biology. For example, it is possible to predict new genes that are important in human diseases based on data on different organisms. The “Phenolog” approach uses information about the functions of orthologous genes in different species, that has been accumulated in publically-available databases, to predict novel, functionally important genes in humans (248). I used Phenolog predictions in Chapter 4 and this approach is described in more detail in the Introduction to that Chapter. To integrate all of the accumulated data, Systems Biology enables researchers to merge complexity though the use of network based approaches (29, 55). Building molecular networks will help to link molecular states to physiological states and diseases (322, 330). Moreover, System Biology approaches are one of the first steps toward developing personal medicine (55). The strategy is to take available information and build networks out of individual components, analogous to a wiring diagram. Perturbing one or more components of a cellular network allows us to understand the role of a gene (and the protein it encodes) in a specific biological system (192). Important tools to populate a regulatory network and observing changes in its dynamic behaviour include bioinformatics, proteomics using high-content mass spectrometry, microarrays to monitor the expression levels of mRNA transcripts or RNA deep sequencing to analyse transcriptomes. Mass spectrometry has applications in several areas, including proteomics, metabolomics or interactome mapping. Applying these techniques results in a greatly increased volume of complex, interconnected data (112). Visualisation of large datasets is key in helping to understand biological systems, such as signalling, regulation of gene expression or metabolism and protein:protein interactions (140). There are also many visualisation tools to support the analysis of protein networks. One of these is Cytoscape software (338), which has become one of the most popular tools for visualising protein:protein interactions and analysing biological networks. Measuring and validating protein:protein interactions is important and a gold standard for measuring protein:protein interactions *in vivo* is to employ Förster Resonance Energy Transfer (FRET) with multiphoton Fluorescence Lifetime Imaging Microscopy (FLIM) (228). This method is described in 1.2 below and is used in Chapter 3 to identify regulators of Cdc42 in NK cells. In Chapter 5 I

identified protein interaction networks bound to the chromatin of T cells and analysed changes in Chapter 6 which occur when one of the components of the system, Mcm7, is down regulated. This employed high-content mass spectrometry, described in 1.1.1 below.

1.1.1. Mass spectrometry

Mass spectrometry (MS) is a powerful tool, which can be used to analyse cellular proteomes. Two basic methodologies are employed. In the first, individual proteins in cell lysates are separated before MS analysis and this can be achieved by a number of different biochemical fractionation methods. In the traditional method, protein mixtures of a cell lysate are separated by gel electrophoresis, such as SDS-PAGE or 2-D gels separating on size (SDS-PAGE) and pI (isoelectric focussing, IEF). Bands of a particular molecular weight are cut out form the gel and the protein(s) contained in the gel slice are then digested by a proteolytic enzyme such as Trypsin. Trypsin cleaves proteins at specific amino acids, namely at the carboxyl side of lysine or arginine, except when followed by proline. The mass and charge (m/z) of all peptides can be predicted based on the sequences of protein-encoding genes in the organism under study. The Tryptic peptides are then separated by liquid chromatography (LC) and analysed by MS. An alternative and commonly applied method is to digest all proteins in a cell lysate with Trypsin, releasing thousands of peptides. The peptides are then separated by one-dimensional LC, such as a C18 reverse phase column, or by two-dimensional LC, for instance employing a cation exchange column followed by a C18 column. In the next step, the separated peptide mixtures are analysed using MS. The peptides are ionised using electrospray ionisation (ESI) or matrix assisted laser desorption ionisation (MALDI) that causes ionisation of the peptides. These ions are then introduced into an electric field, which sorts them according to their mass to charge ratio (m/z). For the LTQ quadrupole linear ion trap instrument (Thermo Finnegan) used in part of my study, described in Chapter 5 and 6, ions are collected and trapped in a plane between electrodes. When a specified number of ions have been collected (or after a specific time) the ions are ejected from the trap. In the LTQ instrument, the rate of increase in the ejection voltage allows different m/z ions to be ejected at different

times and analysed, which creates an MS spectrum. However, in my study I used an LTQ-Orbitrap machine. The ions ejected from the LTQ are directed into the Orbitrap, which increases the accuracy of the m/z measurements, as described below. Identification of the m/z for a given ion can be used to identify some peptides. However, a more accurate amino acid composition is required for many, which can be achieved by selecting peptides individually in the ion trap and fragmenting each one by collision-induced dissociation (CID). In CID, the molecular ions are accelerated by an electrical potential and allowed to collide with molecules of either helium, nitrogen or argon. The collision results in bond breakage and the fragment ions can then be analysed to give an accurate amino acid composition.

I used two Orbitap-based mass spectrometers (168, 235) in my studies. The first, an LTQ-Orbitrap, described above, and the second, a Velos-Orbitrap machine. The first uses the LTQ as the front-end ion trap and the second an improved Velos ion trap front end. Ions trapped by the LTQ or Velos are then injected orthogonally into the Orbitrap, which uses an oscillating electrostatic field between two non-linear electrodes. Ions oscillate around the central electrode and the frequency of oscillation is inversely proportional to the square root of the m/z. The Orbitrap has improved mass accuracy (1 ppm for the Velos-Orbitrap), resolution and dynamic range over previous ion trap technologies and is easy to use for routine analyses. Another advantage is that certain ions that circulate in the Orbitrap can be selected for a longer period prior to fragmentation by CID. In all cases, the m/z and amino acid composition of the peptides are then used to identify the protein, using human reference databases containing the sequences of proteins predicted to be encoded by all protein encoding genes (*e.g.* using MASCOT or SEQUEST).

1.1.2. Quantification of protein expression by mass spectrometry

In comparison with other classical methods in protein biochemistry, such as ELISA or western blots, the quantification of differences in protein abundance by mass spectrometry is technically challenging. Of the many thousands of proteomics studies published to date, until recently only a fraction provided a comprehensive quantification by MS and reports quantifying proteins in mixtures reliably are very

limited (27, 28). This is due to the fact that the MS signal intensity or peak height of a peptide does not correlate directly with the abundance of the protein. Different peptides have a different tendency to ionise and some ionise more easily than others due to their different chemical structures and properties. The ionisation and peak height also strongly depend on the buffers used to dissolve the peptides, which may hinder or promote ionisation of specific peptides. Therefore, spectra obtained from MS analyses have to be interpreted carefully and other means have been developed to enable more reliable peptide quantification.

Several techniques have been developed for relative and absolute quantification. One common method for relative quantification is *in vivo* stable isotope labelling prior to MS analysis. Metabolic labelling of proteins can be accomplished by the addition of isotopically labelled amino acids to cell culture (referred to as “Stable Isotope Labeling with Amino acids in cell Culture” (SILAC)) (284). In this approach, two different cell cultures, such as control and cells treated *e.g.* with a drug or cytokine, are cultured in media containing amino acids labelled with a stable heavy isotope, such as ^{13}C-arginine, or light isotope (^{12}C-arginine) respectively. During cell growth in culture, the cells incorporate the ^{13}C- or ^{12}C-arginine respectively into all newly-synthesised proteins. Proteins isolated from the two different cell cultures are later combined and analysed together by MS. However, the MS analysis can distinguish the same peptides from the two different cell cultures, because they will have different m/z values. This is due to the fact that the heavy isotope labelled cells have a higher m/z and the different characteristic MS spectra can be used for relative quantification (18).

A more recent *in vitro* labelling technique has been developed for quantification, called iTRAQ (isobaric Tags for Relative and Absolute Quantification) (123). Similar to SILAC, this approach employs isotope-coded covalent tags and allows the quantification of proteins derived from different experimental sources, which can be pooled and analysed at the same time. The peptides derived from each sample are labelled with specific mass tags and, due to the specific construction of the tag, each tag will fragment with a different MS/MS pattern and will produce different fragmentation m/z. The ratio of different peak intensities for a protein is then used

for relative quantification. The labelling allows either a 4-plex or 8-plex format, which enables four or eight experimental samples to be quantified in the same MS/MS analysis.

Advances in label-free quantification approaches have also been developed, based on advanced statistical methods. Absolute protein expression (APEX) was developed by our collaborator, Prof. Marcotte at the University of Texas at Austin (394). Earlier attempts failed to develop absolute quantification methods by only taking the peak height of peptides into account and by disregarding the information about peptide counts. Due to the fact that the peptide count is strongly dependent on the physicochemical properties of the peptide, the MS detection is heavily dependent on the size of the protein. A large protein will result in the identification of a larger number of peptides, as compared with a small protein and thus each peptide will have a different probability of detection by MS (233). The APEX method improves the basic spectral counting methods by including a correction factor for each protein that accounts for variable peptide detection by MS techniques. This APEX tool can be used for standard, label-free tandem MS experiments and the method provides a Z–score for the identification of statistically significant differences in protein abundances between samples. This method was successfully applied in our recent study, which quantifies changes in chromatin and nuclear matrix-bound proteins in human T cells during entry into the first cell cycle from quiescence (290).

1.1.3. Protein:protein interaction networks

Identifying protein:protein interactions is important for understanding processes occurring in the cell (136, 142, 207, 225) and the underlying basis for the work in Chapter 3 and 6 of my thesis is the identification of protein networks. There are many techniques for identifying protein:protein interactions (345), however the dataset of protein:protein interactions for human cells is incomplete and although the interactions are based on experimental evidence, each has a different probability of being correct. Computational methods are being applied to these datasets to increase the probability of predicting protein:protein interactions (345).

Protein interactions can be classified into different types, depending on their strength of binding, their specificity, localisation of the binding partner and the existence of complementary protein binding domains in each of the interacting subunits (344). The specificity of interactions is characterized by the structural and physicochemical properties of the two interacting proteins. Therefore, there are conservation of interaction domains in similar proteins. This is important for understanding the effects of mutations in cancers. A recent study showed that reconstruction of protein networks based on interaction domains can provide important insights into the molecular mechanisms which occur in human genetic diseases. They built a network of 4,222 protein:protein interactions and mapped the positional relationships of changes in amino acid sequences caused by gene mutations. Their findings suggest that in-frame mutations alter specific protein:protein interaction surfaces and those mutations play an important role in the pathogenesis of many diseases. They also showed that the location of the mutations at interaction surfaces is crucial in understanding the genotype-phenotype relationships. Based on this, they also predicted new disease-causing genes based on identifying the proteins which interact with known disease mutations (protein:protein interaction through the *same* interaction surface in which the mutation(s) occur) (407).

The most common experimental approaches used to provide experimental evidence for protein:protein and domain:domain interactions are yeast-two-hybrid methods (Y2H) (126, 322) and affinity purification, or pull-down approaches (313). The yeast two-hybrid method is based on the fact that a functional transcription factor can be generated by binding separate activation and DNA binding domains together *via* protein:protein interaction. A downstream reporter is then activated when a binary interaction occurs. However, Y2H also detects non-specific interactions (102). This technique is limited by itself and generates many false positives and misses protein interactions detected by other methods, such as tandem affinity purification (TAP). In the TAP method, fusion proteins are generated with a TAP tag, comprised of (N- to C-terminal) Protein A-TEV protease site-Calmodulin binding peptide (CBP). The TAP tag allows binding of the bait protein

(with associated proteins) to IgG-coated beads and this can then be cleaved enzymatically (300). After a second round of affinity purification on Calmodulin, the proteins are eluted with EGTA, Trypsinised and binding proteins can be identified by MS (6). For instance, mapping protein interactions of Nanog, a transcription factor involved in stem cell self-renewal, in ES cells identified associated proteins (such as Oct4) using FLAG and streptavidin tandem affinity purification followed by MS (403). Another research group developed LUMIER (luminescence-based mammalian interactome mapping) (35), a high-throughput technology to map protein:protein interactions systematically in mammalian cells and they applied to it the TGFβ- pathway. This approach uses the *Renilla* luciferease enzyme fused to the bait protein, which is then expressed with the prey FLAG tag protein. The prey protein is then immunoprecipitated using anti-FLAG agarose beads and the interaction between the prey and bait is determined using a luciferase assay (35). However, affinity-purification methodologies work best for tightly bound protein:protein complexes. A common disadvantage of these methods is the poor overlap between screens run by different groups analysing samples from the same organisms. However, data from different techniques can be combined to provide greater certainty of the observed protein:protein interactions.

Numerous large scale projects have been carried out focusing on mapping protein:protein interactions partners using model organisms such as *S.cerevisae* and *E.coli* (351). Mapping such data to the human orthologues of such proteins further improves the likelihood of protein:protein interaction data being correct. This was formalised as the Phenolog approach (248), described above and in the introduction to Chapter 4 (248). These methods have been complemented by a large-scale analysis of soluble protein complexes in two human cell lines, which was reported very recently (156). However, these data have yet to be incorporated into analyses of combined datasets. Despite the progress in identifying protein interactions, the mapping is not complete and, as stated above, the data on individual interactions can differ depending on the technique used.

A recent and more straightforward strategy to study the protein interactome is based on computational methods for predicting protein interaction. Computational

methods allow the construction of systematic protein networks (59, 142) and generate protein interaction maps for a cell or organelle. The interaction map analyses are based on the fact that many interactions are conserved between species (‘interlogs”) (399). Generation of protein networks is strongly based on existing databases *e.g.* HPRD, MIPS with binary protein interactions from experiments and by mining the literature. These not only involve physical interactions but also indirect inference through predication of functional associations between proteins. Protein interactions can also be predicted based on their protein interaction domain structure using databases such as DIMA or PIBASE. HumanNet is another probabilistic human protein interaction network that is based on reported evidences, such as co-immunoprecipitation, co-citation or co-expression among human genes and genes in other organisms (219). This network is constructed by a modified Bayesian integration of 21 types of ‘omics’ data from multiple organisms and each type of data is ranked according to the evidence for each individual protein:protein interaction. This method is used in Chapter 6 to generate protein interaction networks of chromatin-bound proteins, identified by mass spectrometry.

We know much about certain, specific protein:protein interactions which occur in a cell but we still have little understanding of how protein:protein interactions are all connected with each other in a complex biological system. Large scale mapping of protein:protein interactions provides a view of potential complex molecular mechanisms within a cell. However, the prediction of how protein:protein interactions change in a network requires System Biology analyses that utilise a combination of bioinformatics and experimental approaches. Combining and modelling high-throughput analyses and wet-lab experiments will enable us not only to understand the complex biological system better but also to follow the behaviour systematically under different conditions. Systems Biology approaches will not only address those interactions in a normal cell, but also potentially predict how abnormalities in individual proteins could lead to the development of diseases such as cancer.

1.1.4. Protein interaction networks in T cells

T cells can remain quiescent in the peripheral blood for months or years. In response to stimulation *via* CD3/CD28 (3) or with PMA/Ionomycin they undergo defined programmes, which cause cell cycle entry ($G_0 \rightarrow G_1$ transition), initiation of the growth cycle (cell size), suppression of apoptosis programmes and induction of effector functions *e.g.* γ-IFN, IL-2 and CD69. Cellular programmes are normally co-ordinately regulated during entry into the cell cycle from quiescence, but previous work in the laboratory showed that entry into the cell cycle and induction of early effector functions can be uncoupled (218). These programmes are made up of protein:protein interaction networks and recent work in our laboratory has identified chromatin & nuclear matrix (C/NM)-bound networks that change during entry into the cell cycle from a quiescent (G_0) state (290). The project identified an increase in 307 C/NM-bound proteins as T cells progress from $G_0 \rightarrow G_1$. The proteins were identified by mass spectrometry (LCMS/MS) and bioinformatics analyses. Additional data obtained by western blotting were used to validate the induction and chromatin binding of a subset of these proteins. These proteins identified by mass spectrometry were assigned to protein interaction networks by mapping to the current human interactome, using HumanNet (219). Thus, the laboratory identified novel, dynamic sub-networks of identified and predicted C/NM-bound protein:protein interactions of human primary T cells that change during entry into the cell cycle from quiescence, based on wet-lab experiments and bioinformatics analyses.

1.1.5. Optical Proteomics - Förster resonance energy transfer (FRET)-Fluorescence Lifetime Imaging Microscopy (FLIM)

Validation of protein:protein interactions can be performed by diverse biophysical and biochemical methods. In the study reported in Chapter 3, a near-field process, FRET quantified by FLIM, is used to validate protein:protein interactions. As FRET only occurs over very short distances (typically 5-15 nm), this permits the measurement of protein:protein interactions. It is applicable for fixed and living cells and tissue imaging down to single molecule level (141). FRET-FLIM is relatively

non-invasive and enables the study of dynamic spatial changes in protein:protein interactions. The power of this technique lies in the ability to track the localisation of a protein and also its interaction with other molecules (or activity) in a way that is independent of the local concentration of fluorescent molecules and the excitation intensity (124, 224, 400, 408).

The proteins of interest are expressed in the cell with specific fluorophore tags (*e.g.* GFP or RFP) and the fluorescence intensity and fluorescence lifetime of the donor is measured by FLIM. Fluorescence is described as the radiative de-activation of the first electronically excited singlet state and can be characterized by multiple parameters such as intensity, position, wavelength, fluorescence lifetime and polarisation (124, 224). Fluorescence lifetime is the average time a fluorophore remains in the excited state after excitation. Fluorescence lifetime is usually in the order of nanoseconds and strongly depends on the local environment of the molecule, such as the presence of an acceptor fluorophore (124). A way to detect dynamic protein:protein interactions in living cells or dynamic conformational changes with spatio-temporal resolution is to label proteins with appropriate dyes or fluorescent proteins and monitor FRET (141, 224, 400). FRET is a physical phenomenon in which energy absorbed by a fluorophore is transferred to another molecule through a non-radiative pathway (396).

Three specific conditions are required for FRET to occur (Figure 1.1.5 A-D):

- The emission spectrum of donor fluorophore must overlap the acceptor molecule's absorbance spectrum to be able to detect sensitized emission.
- The donor and acceptor must reside within 10nm (100Å) of each other. The FRET efficiency has an inverse sixth power dependence on the separation distance between the donor and acceptor. Therefore the measurement of FRET is strongly dependent on the separation distance between the two interacting molecules.
- The emission dipole of donor and the absorption dipole of acceptor must not be oriented perpendicular to each other. In a perpendicular constellation, no FRET will be possible due to cancellation of the dipole-dipole moment (124, 334, 396).

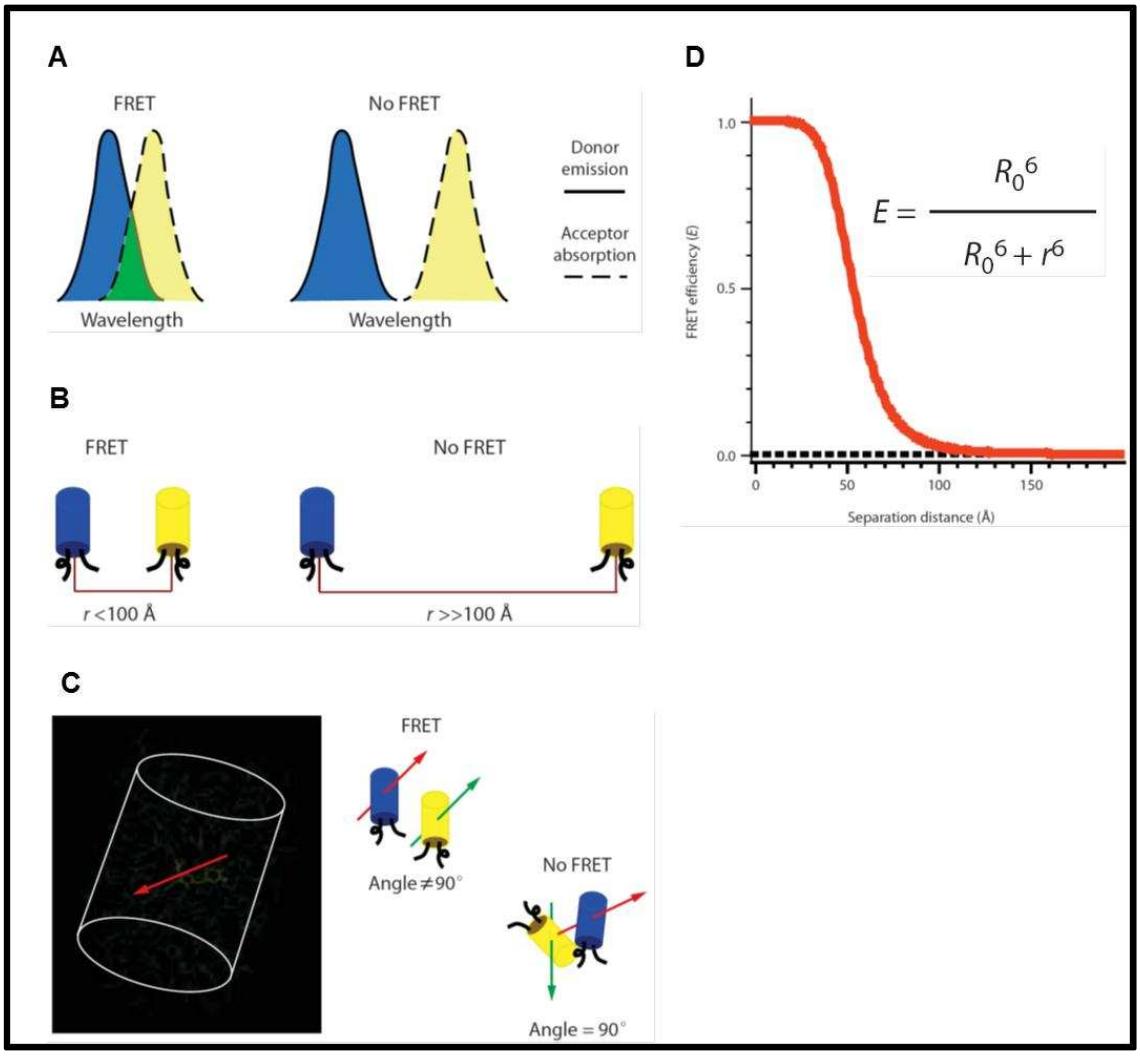

Figure 1.1.5 Requirements for FRET (reproduced from (396)).

A. FRET can occur only if the emission spectrum of the donor overlaps the absorption spectrum of the acceptor. The overlapping region is green. C. The enhanced GFP chromophore is represented as a cylindrical structure. Its dipole moment (red) has a specific orientation. FRET can only occur when the angle of the emission dipole (red arrow) is not 90°to the absorption dipole (green arrow). B. Resonance energy transfer is observed only when the distance between two fluorophores (r) is less than 1.8 x Å Förster distance (R_0), which is typically less than 100. D. FRET efficiency has a 6^{th} power dependence on the separation distance (r).

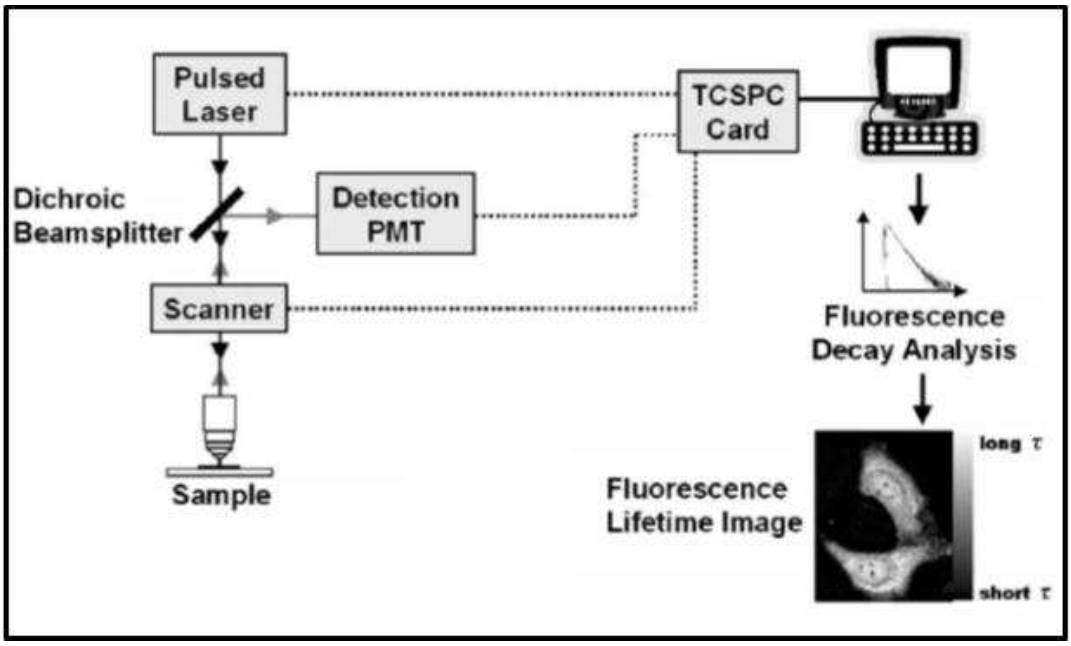

Figure 1.1.5 E. Schematic illustration of a typical confocal or multiphoton FLIM system (Reproduced from (124)).

Fluorophores in fixed or live cell samples are excited by single or multiple photons from a pulsed laser source. Picosecond pulsed lasers such as a Ti: Sapphire laser are typically used for multiphoton excitation with a wavelength from 690nm-1000nm. The fluorescence is detected using a non-descanned detector for multiphoton excitation. The electrical signals transfer to a time-correlated single photon counting (TCSPC) card in the PC. The time delay between the laser excitation pulse and the arrival of the fluorescence photon is measured many times, from which a histogram of photon arrival can be built up for each pixel. Further data analysis allows the extraction of the fluorescence lifetime (τ) from the decay. The precise microscopy set-up used in my studies is described in Figure 1.1.6.

The instrumentation used for FLIM is a confocal microscope or two-photon excitation microscope (Figure 1.1.5 E). For the studies reported in Chapter 3, I used a specific microscope configuration designed and constructed in Prof Ng's laboratory at Guy's.

In my study in Chapter 3, the donor fluorescence lifetime is measured under different experimental conditions. A short pulse of light is used to excite a sample and the intensity of the fluorescence signal is measured as a function of time. The intensities are fitted to an exponential model, which allows the fluorescence lifetime to be calculated. The fluorescence lifetime of the donor is shorter if FRET is occurring. For the analysis of FLIM-FRET, software such TRI2 is used, which uses a curve-fitting algorithm to determine the donor's fluorescent decay constant. The fluorescent decay constant is defined as a variable that provides a parameter of the kinetics of fluorophore decay. A ratio of this time constant is used to calculate the FRET efficiency. One major disadvantage of FLIM-FRET is that it requires the detection of large numbers of emitted photons for accuracy and thus prolonged exposure of the molecule (396). FRET efficiency has an inverse sixth power dependence on the separation distance between the donor and the acceptor. Therefore small errors in accuracy can have large effects on the actual transfer efficiency when, for example, FRET efficiencies of 10% are measured with actual values between 5% and 15% (396).

1.1.6. Multiphoton microscopy

Multiphoton microscopy (MPM) is an advanced imaging technique which allows cells and tissues to be visualised *in vivo* up to a depth of one millimetre by using a pulsed long wavelength laser light to excite fluorophores (108, 157). Traditional optical microscopy techniques such as confocal microscopy use linear one photon excitation/absorption processes to generate contrast in images. Both confocal microscopy and multiphoton microscopy have the capability of optical sectioning, which allow one to produce clear images of a focal plane deep within a thick sample (371). However, confocal (one–photon) microscopy techniques are limited in imaging up to 100μm in the effective depth with high-resolution due to the high

sensitivity to light scattering (157). Multiphoton microscopy allows imaging more deeply into cells and tissues with less toxicity and efficient light detection, as compared with other optical imaging methods (Table 1.1.6) (105). Since MPM is associated with lower cell lethality, imaging can be carried out for longer time periods (108, 299). Multiphoton microscopy is typically combined with the use of a laser scanner (106, 371). These advantages will be explained in the following paragraph.

The concept of multiphoton excitation is based on the idea of non-linear excitation, in which two or more photons of low energy can excite the fluorescent molecule by near-simultaneous absorption. This results in the emission of a photon with much higher energy than either one of the excitation photons. Their combined energies promote the molecule to an excited state, which proceeds along the normal fluorescence –emission pathway (106). Since the probability that several photons are absorbed near simultaneously is extremely low, short pulses of longer wavelength light in femto second ranges are required (299). Typically, the excitation occurs in the near infrared wavelength range 700-1000nm, whereas emission occurs in the in visible range (158).

In confocal microscopy, the fluorophore excitation is directly proportional to the photon flux of the incident light. However, in two-photon or three-photon microscopy the excitation depends on the square or cube of the intensity of the incident light. Since the probability of two or more photons simultaneously exciting a fluorophore is low, in MPM the excitation remains restricted to the focal plane. As a result, the lower energy excitation of molecules outside the focal plane produces less photoinduced toxicity. Compared to confocal microscopy this minimizes the background (108, 353).

Denk and colleagues introduced the first functional instrument for biological applications (105). Figure 1.1.6 shows an image of the MPM used in Prof. Ng's laboratory and the beam path when operated in multi-photon excitation.

Imaging technique	Principle	Spatial resolution	Depth	Advantages	Disadvantages
Positron emission tomography (PET)	Detects high energy γ rays emitted from a radiolabelled probe (typically a metabolically active molecule)	mm	No limit	Non-invasive, 3D imaging	Low spatial resolution
Whole body fluorescence/ Bioluminescence	Detect light emitted from cells expressing a luminescent enzyme/protein	mm	1–2 cm	Non-invasive, high sensitivity	Low spatial resolution, weighted toward 2D imaging
Wide-field epifluorescence	Fluorophore(s) excited with light (UV or visible) resulting in emission of light at a longer wavelength (Stokes shift)	nm-μm	~20 μm	Low cost, single cell resolution, can be integrated with other microscopy techniques	High background, limited imaging depth
Confocal microscopy	Similar to epifluorescence except laser beam passes through an aperture resulting in "optical sectioning" to reduce out of volume signal	nm	~50–100 μm	High spatial and temporal resolution, reduces out of plane fluorescence, can be integrated with other microscopy techniques	Aperture loss, limited imaging depth
Multiphoton microscopy	Optical sectioning occurs when two (or more) low energy (high wavelength) photons excite a fluorophore to produce an emission identical to the corresponding single photon excitation	nm	~400–1,000 μm	High spatial and temporal resolution, limited out of plane fluorescence, produces harmonic generation, can be integrated with other microscopy techniques	High cost, limited imaging depth

Table 1.1.6. Overview of different imaging techniques (Reproduced from (299)).

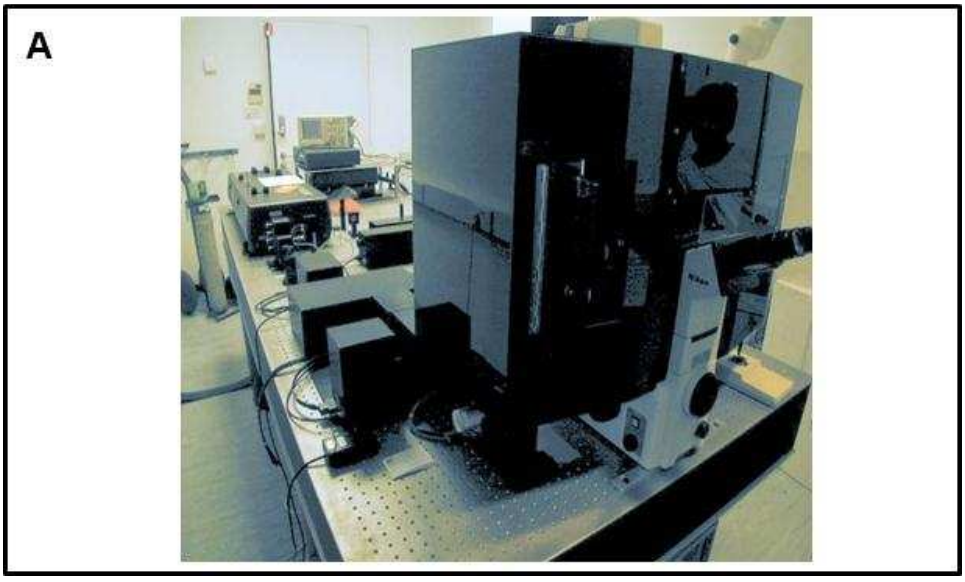
A

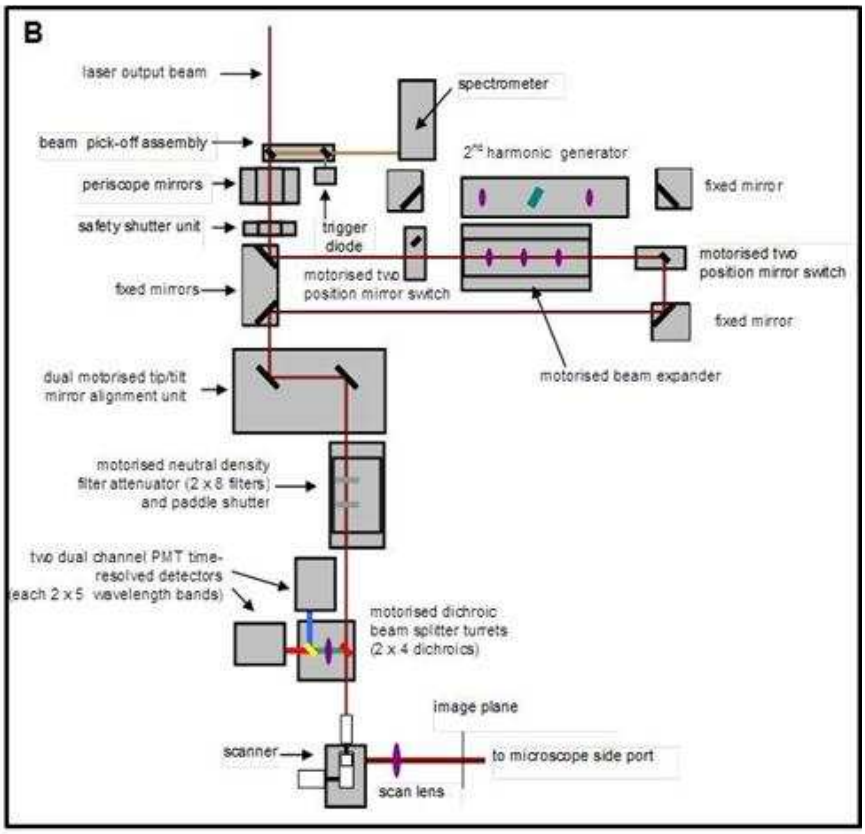
B
laser output beam
spectrometer
beam pick-off assembly
2nd harmonic generator
periscope mirrors
fixed mirror
safety shutter unit
trigger diode
motorised two position mirror switch
fixed mirrors
motorised two position mirror switch
fixed mirror
motorised beam expander
dual motorised tip/tilt mirror alignment unit
motorised neutral density filter attenuator (2 x 8 filters) and paddle shutter
two dual channel PMT time-resolved detectors (each 2 x 5 wavelength bands)
motorised dichroic beam splitter turrets (2 x 4 dichroics)
image plane
scanner
to microscope side port
scan lens

Figure 1.1.6 Multiphoton-microscopy.

A. Set up of the multiphoton-microscope in Prof Ng's Laboratory. B. Beam paths of the multi-photon excitation mode. The input to the system is the output beam from a femtosecond pulse Coherent Mira self-mode locked Ti:Sapphire laser. A wedge (beam pick-off assembly) samples some 5% of the beam and this is further split to provide two beams: one feeds a trigger diode to provide a timing reference; the other is coupled to a spectrometer to monitor the laser wavelength and, by inference, pulse width. The height of the main beam is then reduced with a periscope consisting of two NIR mirrors and the beam then passes through a solenoid-activated safety shutter. At this point, the beam is 'bent' through 90° to make optimum use of the optic al table area. The beam passes through a motorised telescope that determines the beam diameter and optimises this to optimally fill the back aperture of the particular objective used in the microscope. It then enters a motorised beam alignment unit, which houses near-field and far-field tip/tilt mirrors. This arrangement allows accurate alignment of the beam into the scanner/detectors/microscope path. From then on, the beam is passed through a motorised attenuator unit that allows 64 possible combinations of filters to be inserted in the beam path (2 x 8 positions). The second sampler is intended to provide a beam pick-off to be coupled to a quadrant type of photodetector that would maintain beam position through feedback to the aforementioned tip/tilt alignment mirrors. The properly shaped and aligned excitation beam enters a motorised dichroic turret assembly. This consists of two 4-position turret wheels. The first wheel inserts the dichroic filter that separates the excitation light from the emission light. The emission light then passes through the second filter wheel and is split into the detector assembly. The excitation beam continues on into the scanner assembly, which consists of a slow paddle-mounted scanning mirror, used to scan 'down' the image frame and a much faster line-scanning mirror that provides the scan path 'along' the frame. An achromatic scan lens is used to form an image of the scan at the microscope's image plane. (Reproduced from the Handbook of King's College time resolved imaging system).

1.2 Cdc42 in NK cells

1.2.1. Role of NK cells

Natural killer (NK) cells constitute a major component of the innate immune system and they are often defined as large granular lymphocytes. However, NK cells only represent a small fraction of lymphocytes (~2%) in the blood that express the Fc receptor (CD16) and CD56, CD11b/Mac-1, usually also CD8, though the NK cell receptor may differ and they are TCR/CD3 negative (216). They contribute to direct killing of target cells and play a major role in the host defence against viral infections and rejection of cancerous cells (255, 287, 375). The name 'natural killer' originates from the initial hypothesis that NK cells do not need activation in order to kill other cells which are 'missing-self' *i.e.* cells which have a low expression level of major histocompatibility complex (MHC) class-I surface markers (227).

Cytotoxic T lymphocytes (CTL) and NK cells have similar mechanisms for killing target cells, but they recognize different types of target cells. The specificity of the receptors with which NK cells recognize potential targets are not diversified like the αβ and γδ receptors (TCRs) of T cells and the antigen receptors (BCRs) of B cells. According to the missing-self hypothesis, it was assumed that NK cells recognize only host cells that fail to express MHC class-I molecules. However, it is more complicated than first thought and there are many positive and negative receptors, plus some heterogeneity in which MHC is recognized (98, 227). Those host cells are then eliminated through localized delivery of lytic granules (210).

Cytolytic activity of NK cells is induced by diverse signals such as cytokines, interferons (IFN) and immunoglobulins. Molecules such as IFN-α, -β and –γ are released by cells upon viral infection and can stimulate NK cell responses (41, 375). NK cells express a diversity of receptors that enable them to respond effectively to a variety of different pathogens. There are a multitude of activating and inhibitory receptors and the net balance of signals from these receptors enables NK cells to provide effective killing of target cells while maintaining self-tolerance (73).

1.2.2. Natural killer cell activation and its cytotoxic role

The mechanism for target cell killing is tightly regulated. Cytolytic killing is regulated through a number of phases in NK cells. The innate cytolytic effectors, NK cells, and the adaptive cytolytic effectors, CTL, both use the same lytic mechanism and granule release. However, upon forming a tight target cell contact with the target cell the established cytoskeletal polarisation in NK cells is a slow or incomplete stepwise process, which constitutes a series of checkpoints in NK killing. In comparison, the process of cytoskeletal polarisation in CTLs is rapid and robust (419).

NK cells circulating in the periphery contain a high concentration of preformed granules in their cytoplasm (89). The stepwise cytolytic killing is initiated by the integrin-mediated adhesion to target cells, movement of cytolytic granules towards the microtubule organizing center (MTOC) (82) and reorientation of the MTOC towards the target cells. NK cells release the lytic content of their granules at the immunological synapse through a process of exocytosis where these lysosomes or vesicles fuse with the plasma membrane (89). During degranulation, perforin and granzyme B (GrB) become released. Perforin forms pores in the target cell membrane, allowing GrB to enter the target cell (226). In turn, GrB induces death of target cells through caspase-dependent or -independent activation of apoptosis (397).

1.2.3. The immunological synapse in NK cells

NK cell effector function is usually achieved when a direct cell-to cell contact occurs. The binding of an NK cell to a target cell is achieved through the creation of complex structures at the cell-cell interface known as the immunological synapse (IS). Davis *et al.* defined the IS as intercellular contact involving at least one cell of the immune system (*e.g.* NK cell or T cell) at which the encounter causes proteins to segregate into micrometer-scale domains (97, 98, 398). Many different signals are involved in the formation of NK cell-target cell conjugates including the T cell receptor, MHC, LFA-1, ICAM, CD28 and CD80/CD86.

The first observed immunological synapse was reported for T cell interaction with antigen presenting cells (APC). The immunological synapse was originally described by post-fixation imaging of T cells (259) and the synapse was visualized on T cells by live imaging of T cell interactions with supported planar lipid bilayers carrying ligands of activation receptors, presenting ICAM-1 and MHC-peptide complexes (145).

There are important differences between the IS in T and NK cells. For example, NK cells use a variety of activating receptors for signalling as compared with T cells and the localisation of some IS proteins differs significantly. Moreover, within NK cells there are several different types of NK immunological synapse which regulate NK cell activity (210).

Unlike in T cells, the activating NK cell immunological synapse (NKIS) is formed sequentially in distinct stages, which require different phases (287, 419) (Figure 1.2.3). The first step is integrin-mediated contact and adhesion of an NK cell to a target cell. This is followed by receptor ligation and segregation. Then actin cytoskeleton rearrangements occur, which allow further receptor clustering and sustained signalling (signal amplification). The microtubule cytoskeleton rearrangements associated with MTOC polarisation result in granule polarisation toward the immunological synapse. Finally, in the degranulation process cytotoxic molecules kill the target. The IS then disassembles (210). The mature activating NKIS has a characteristic structure and contains a central (c) and peripheral (p) supramolecular activation cluster (SMAC). This structure includes polarized surface receptors, filamentous actin (F-actin) and perforin. It has been shown that in the activated NKIS LFA-3 (CD2), LFA-1(CD11a), Mac-1 (CD11b) and F-actin co-localize in the peripheral SMAC whereas perforin is accumulated in the cSMAC (287). Those three receptors participate in both adhesion and stimulation between NK cells and their target cells. CD2 induces kinase function and extension of lipid raft domain, whereas LFA-1 and CD11b induce phosphorylation-dependent NK cell activation (340).

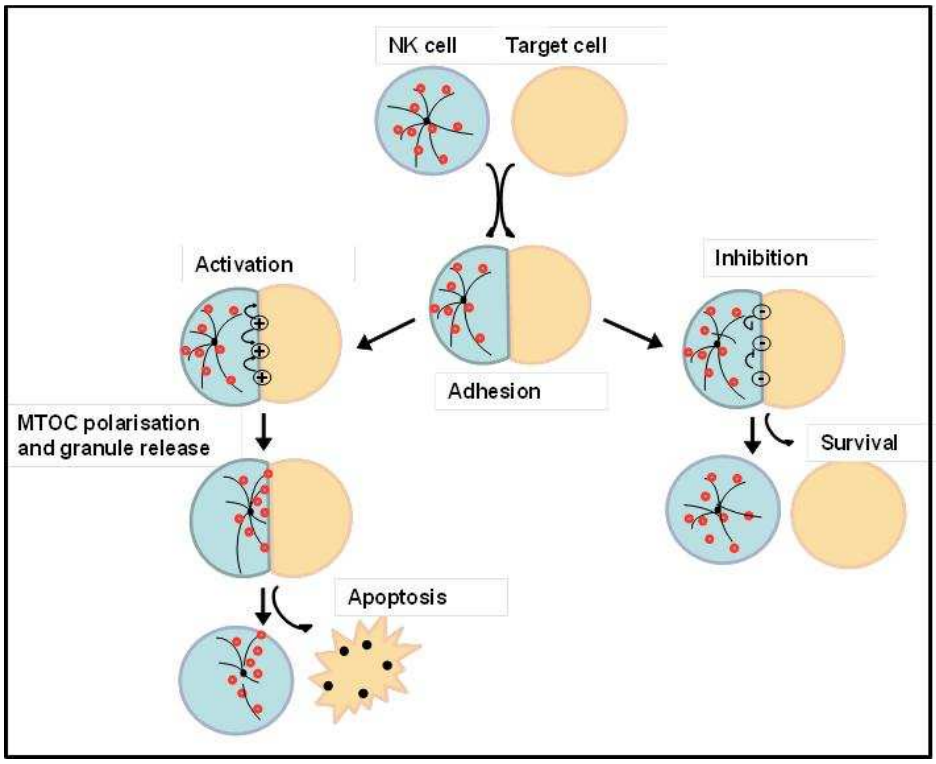

Figure 1.2.3 The NK cell immunological synapse is formed in distinct stages (reproduced from (210)).

The encounter between NK and target cell results in adhesion and conjugate formation (top). The balance between activating and inhibitory receptor signalling on the cell:cell interface decides the outcome of the interaction. The lack of MHC-I molecules on the target cell, caused by viral infection or tumours, favours formation of the activating NKIS (left). Engagement of NK cell activating receptors by their ligands induces an initial wave of actin cytoskeleton rearrangements. This in turn leads to more stable conjugation by creating of an F-actin ring in the pSMAC area and formation of a signalosome comprising many signalling and adaptor molecules in the cSMAC. Thus, a positive feedback loop is generated causing signal amplification and sustained signalling that stimulates robust actin polymerisation of the MTOC to the activating NKIS. Lytic granules, containing perforin and granzymes, are transported along microtubules tracks and with MTOC translocation they are delivered to the cSMAC, where they are subsequently released. Perforin makes pores in the membrane of target cell, allowing granzymes to enter the cell and induce apoptosis. After induction of target cell lysis, the NK cell detaches from its target cell and can search for another target. Conversely, the presence of MHC-I on the surface of the target cell results in preventing actin cytoskeleton rearrangement and inhibits MTOC and lytic granule polarisation, resulting in survival of the target cell.

1.2.4. Stages of the activating NKIS formation

During IS formation critical interactions are formed with the cytoskeleton. In order to induce NK cell cytotoxicity, actin polymerization and accumulation at the NKIS are required. The activating NKIS is a time–dependant structure and accumulates LFA-3, LFA-1, Mac-1, F-actin and perforin. Other important actin-associated proteins like talin and WASP are also found in SMAC (398). WASP contributes to F-actin polymerization (143). Both actin polymerization and WASP function are required to localize the perforin-containing granules to activating NKIS.

When the first contact between target and NK cells is initiated LFA-1 and Mac-1 segregate in the pSMAC. LFA-1 has three main functional roles during IS formation: it is important for phosphorylation of signalling molecules for inducing signals for granule polarisation in a later step and induces signal for actin polymerization (210), which in turn makes F-actin accumulate at pSMAC. Accumulation of those receptors and F-actin is rapid and dependent on WASP-driven actin polymerization (288). Activating receptors accumulate in the central SMAC and are responsible for recruitment of molecules for signal transduction. The signalosome formed at the cSMAC results in cytotoxicity and cytokine secretion as effector function through two main pathways, PI3K-ERK2 and PLCγ-JNK, which lead to MTOC polarisation and delivery of perforin and GrB. Polarisation of perforin is a much slower process than the previous step and requires intact actin, WASP and microtubule function (287). The final step of lytic granule exocytosis is associated with the actin cytoskeleton, which involves the CIP4 protein. This protein links the microtubule and the actin network, thus allowing MTOC polarisation and cytotoxicity.

In resting and non-activated NK cells perforin co-localizes with Lamp-1 and GrB in vesicles within the cell and is therefore not detectable. Upon NK cell activation, for example after encountering a tumour cell, the vesicles fuse with the plasma membrane and allow perforin to temporarily appear at the cell surface (14) (Figure 1.2.4 A).

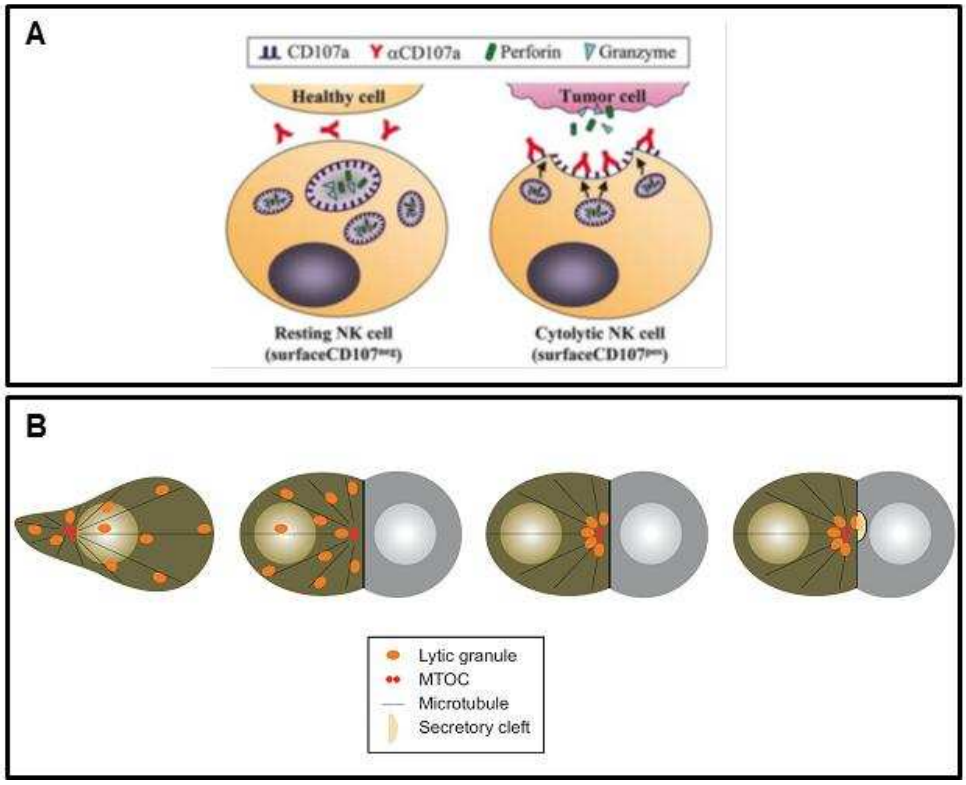

Figure 1.2.4 Polarisation and release of cytotoxic granules in NK cells and cytolytic T cells.

A. Cytolytic response of NK cells (Reproduced from (382)). B. Polarisation in a cytolytic T lymphocyte on conjugation with a target (Reproduced from (358)).

During the process of NK cell and CTL cell activation the MTOC becomes polarized. After conjugation to a target cell the MTOC moves towards the immunological synapse, followed by movement of the granules towards the polarized MTOC. At the cell contact site the content of the granules is released into the secretory cleft (358) (Figure 1.2.4 B).

1.2.5. Rho-GTPases - role and function of Cdc42

Rho-GTPases constitute a distinct family of small GTPases within the superfamily of RAS proteins. Rho GTPases, such as cell division cycle 42 (Cdc42), Rac1 and Rho1 are small signalling G-proteins. Rho GTPases are implicated in many cellular events including cell division motility, cell adhesion, vesicular trafficking, phagocytosis and transcriptional regulation (277, 311, 411). These proteins have many different functions, of which one is to regulate actin dynamics and cytoskeletal changes (Figure 1.2.5). The Cdc42 GTPase plays a central role in the regulatory events controlling the activation of cytotoxic lymphocytes activation such as CTL or NK cells (200).

Upon receptor stimulation of Rho-like GTPases, the activity of Cdc42 is strictly controlled and in turn this causes activation of temporally and locally specific downstream signalling pathways. In general the regulation of the activity of Rho-GTPases like Cdc42 is controlled by three types of proteins: guanine exchange factors (GEFs), GTPase-activating proteins (GAPs) and guanine nucleotide dissociation inhibitors (GDIs). In the resting (inactive) state Cdc42 is bound to guanosine diphosphate (GDP). The activation of Cdc42 requires the GDP dissociation and binding of guanosine triphosphate.

GEF promotes nucleotide exchange and alters the conformation of switch regions of GTPases. Thus, GEFs activate G-proteins and increase the binding affinity of effector proteins leading to downstream signalling (117). One group of GEFs consists of two characteristic catalytically-functional domains. Structurally they contain the catalytic DBl homology (DH) domain and a pleckstrin-homology domain (PH). The PH domain interacts with phospholipids, which activate the catalytic DH

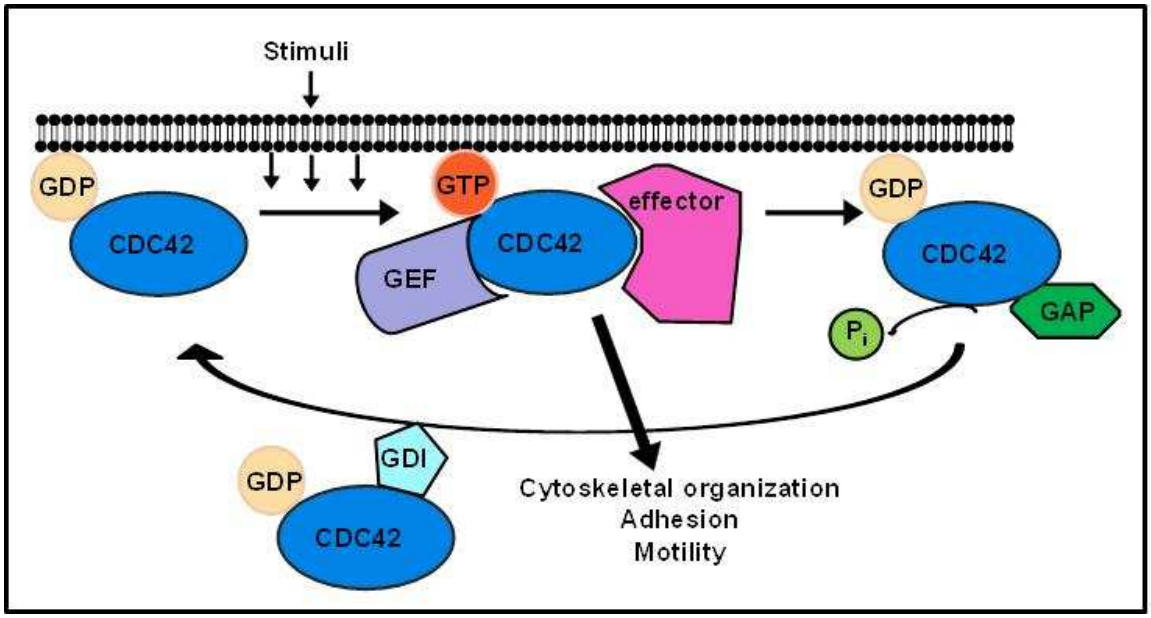

Figure 1.2.5 Regulation of GTPases cycle (Reproduced from (117)).

GDP-bound inactive GTPases are mainly cytoplasmic, maintained there by GDIs which mask the C-terminal tail required for plasma membrane localisation. Upon dissociation of GDI, posttranslational modifications can take place and GTPases translocate to the plasma membrane, where they can be activated by GEFs upon external stimuli from surface ligand-receptor systems such as adhesion receptors GPCR and receptor tyrosine kinases. Upon activation by GEFs, RHO GTPases can bind different effector proteins, the selection of which can be mediated by GEFs. This process induces downstream signalling pathways. GAPs inactivate the Rho-GTPases and switch off the downstream signalling.

domain of GEF and localize the GEF to the plasma membrane. The other group of GEF are Dock180 related proteins. The presence of Dock-homology region-2 (DHR2) makes GEF catalytic functional. Additional domains on GEF determine the signalling route downstream either by direct binding to effector molecules or activation of downstream effectors of signalling pathways (117).

GAPs are regulatory proteins which enhance GTPases to hydrolyse bound GTP to GDP, thus inactivating the active form of GTPases and inhibiting the signalling pathway. Typically the C-terminal sequence in Rho-GTPases ends with a CAAX motif that has post-translational modifications which determine intracellular localisation of the protein and also function as a lipid anchor.

The GDI proteins are located in the cytosol and form complexes with the inactive GDP-bound Rho-GTPases or interact also with the active GTP-bound GTPases and prevent cycling of GTPases between cytosol and plasma membrane. GDI proteins can also bind to the active GTP-bound GTPases, thus inhibit hydrolysis, and inhibit interaction with downstream effectors. GDI keep the Rho-GTPases in the cytoplasm in an inactive state. The Rho-GDI-GTPase complex can be dissociated through phosphorylation. One example is the phosphorylation of GDI by p21-activayted kinase 1 (PAK-1), allowing translocation of Rho-GTPases from the cytoplasm into the plasma membrane, followed by GEF activation.

The regulators GAP, GEF and GDI are in turn strictly controlled. There are far more regulators than Rho-GTPases family members. The activation state is strongly dependent on the output of the activators/regulators as well as on the number active GTP-bound Rho-GTPases. Each Rho-GTPase has the capacity to bind to several effector proteins and the same effector protein can be recognized by different Rho-GTPases. Many of them are serine/threonine kinases and usually phosphorylate downstream targets and multiple signalling cascades regulating different processes in the body.

A well-characterized Rho-GTPase and effector are Cdc42 and PAK-1 proteins. PAK-1 is known to be an important mediator of the organization of the cytoskeleton

(117). Small GTPases like Cdc42 regulate each others' activity *via* cross talk, which provides a tool for fine-tuning signalling events.

One particular function of Rho-GTPases is the regulation of the actin cytoskeleton. Cdc42 regulates the formation of filopodia. The actin dynamics are regulated by coordinated activation of different signalling pathways downstream of small GTPases. Cdc42 can signal to the ARP2/3 complex *via* the effector WASP, which results in actin polymerization and formation of filopodia. Besides this function, they also regulate the microtubule cytoskeleton. Cdc42 can influence microtubule stabilization by mediation of PAK. Cdc42 also has an important role in the reorientation of the Golgi apparatus and MTOC through binding of Cdc42 to the PAR6 protein (122).

1.2.6. Cdc42–Biosensor (Raichu 1054)

The Cdc42 FRET biosensor allows measurement of the activation of Cdc42 in fixed and live cells. The original probe was constructed by Prof. Matsuda and colleagues (178, 427). In Prof. Ng's laboratory the cyan fluorescent protein (CFP)/red fluorescent protein (RFP) was changed to green fluorescent protein (GFP) /RFP to make it more suitable for FLIM. CFP has a complicated multi-exponential lifetime. The probe constructed is a fusion of monomeric RFP at the N-terminus of the *CDC42* gene and the Cdc42/Rac-interactive binding (CRIB) domain of the PAK-1 protein linked on the C-terminus to GFP. The p21-activated kinase (PAK1) is a downstream effector of Cdc42 and is a critical effector that links Rho-GTPases to cytoskeleton reorganization and nuclear signalling (203). Thus, PAK-1 is a target for Cdc42. When Cdc42 activity increases, GFP and RFP are brought into close proximity and GFP is quenched. Thus, FRET efficiency increases and fluorescence lifetime of the GFP decreases (Figure 1.2.6).

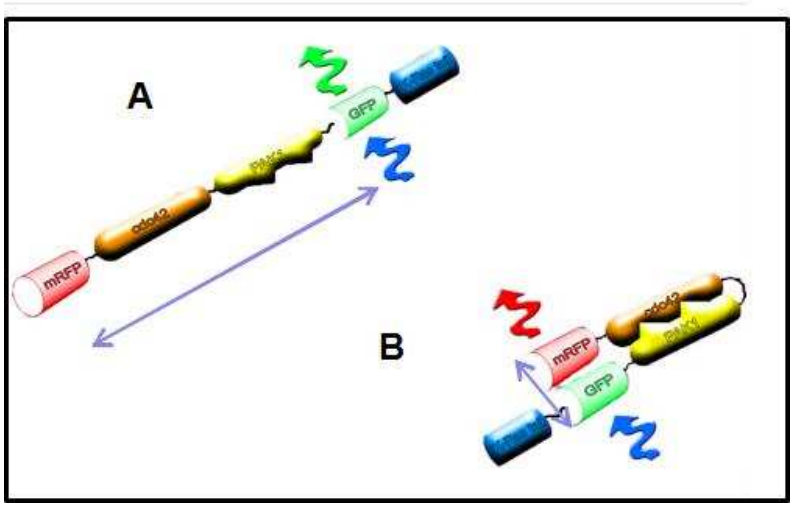

Figure 1.2.6 Design of the Cdc42 Raichu Biosensor (Reproduced from L. Carlin).
A. Raichu probe in an inactive state: low FRET efficiency is detectable due to the large distance between monomeric RFP and GFP. B. Raichu probe RFP and GFP are in close proximity, Cdc42 and PAK1 interact with each other. High FRET efficiency is detectable.

1.3 Aims

The aims of my thesis are:

- To understand complex cellular systems, with the focus on the function of haematological cells.

- To apply systems biology approaches to obtain a better understanding of complex cellular systems.

Specifically:

- To employ a novel bioinformatics/wet-lab microscopy strategy to identify new regulators of NK cells.

- To apply bioinformatics approaches to predict functionally important proteins that are required to maintain genome stability and test predictions.

- To optimise conditions for the identification of the chromatin-bound proteome of activated human primary T cells by high-content LCMS/MS and

- To elucidate the effects of downregulating a DNA replication protein on the chromatin-bound proteome of T cells.

Chapter 2

2. Materials and Methods

2.1 Reagents

2.1.1. General chemicals, consumables and kits

Human AB serum	Invitrogen
Acetonitrile	Sigma
Agar	Sigma
Amaxa human T cell nucelofector kit	Lonza
Amicon Ultra centrifugal filter units 10K 0.5ml	Millipore
Anti-CD3/CD28 immunomagnetic beads	Invitrogen
Anti-mouse IgG immunomagnetic beads (Depletion Dynabeads)	Invitrogen
Aprotinin	Sigma
BCA assay	Pierce
Bovine serum Albumin	Sigma
Bromphenol Blue	Sigma
C18 tips	Thermo
Cell tracker orange 5-(and-6)-(((4-chloromethyl)benzoyl)amino)tetramethylrhodamine (CMTMR)	Invitrogen
Centrifugal Filter units Ambion Ultra	Millipore
Colcemid	Sigma
Coomassie brilliant blue	Thermo
CrypMaxx SF	PAA
Detergent removal spin columns	Pierce
DH5α competent cells	Invitrogen
1,4-diazabicyclo (2.2.2) octane	Sigma
Dithiothreitol (DTT)	Sigma
DNA ladder	Fermentas
ECL Chemiluminescent Western Blot Detection Kit	GE Healthcare
ECL plus Chemiluminescent Western Blot Detection Kit	GE Healthcare

ECL WB Substrate Thermo	Pierce
1.5ml Eppendorf microcentrifuge tubes 0.5ml Eppendorf micocentrifuge tubes	Starlabs
Ethanol	Fisher Scientific
15ml and 50ml Falcon tubes	VWR international
FACS tubes	BD Biosciences
Fluorescein isothiocyanate (FITC)	Sigma
Foetal bovine serum	Sigma or Biosera
Formaldehyde	Sigma
Histopaque 1077	Sigma
Hybond- C extra membrane	GE Healthcare
Hyperfilm ECL	GE Healthcare
Hypersep C18 Columns	Thermo Scientific
IGEPAL-CA-630 (Nonidet P40)	Sigma
Iodoacetamide	Sigma
Lipofectamine2000	Invitrogen
MES SDS running buffer	Invitrogen
MES transfer buffer	Invitrogen
Methanol	Fisher Scientific
Micococcal Nuclease	Roche
Mowiol mounting medium	ICN Biomedicals
Neubauer Improved Haemocytometer	VWR international LTD
Nitrocellulose membrane (Hybond C Extra)	GE healthcare
NK isolation kit	Miltenyi Biotech
Non-essential amino acids	Gibco
Non-fat dried milk (Marvel)	Sainsbury's
Novex sharp protein standards	Invitrogen
Nucleofection system	Lonza
NuPAGE gels	Invitrogen
NUPAGE LDS sample Buffer	Invitrogen
NuPAGE running buffer	Invitrogen

NuPAGE transfer buffer	Invitrogen
OrgoSol DetergentOUT detergent removal kit	G-Biosciences
Paraformaldehyde	Sigma
Penicillin	Sigma
Phenylmethanesulfonylfluoride (PMSF)	Sigma
Phorbol 12-myristate 13-acetate (PMA)	Sigma
Phosphate buffered saline (PBS) tablets	Sigma
Pierce Detergent Removal Spin Columns	Thermo
Platinum Quantitative PCR SuperMixUDG with ROX	Invitrogen
Platinum SYBR Green qPCR SuperMix-UDG with ROX	Invitrogen
Polyacrylamide Bis-Tris gels	Invitrogen
Pre-separation filter, 30µm nylon mesh	Miltenyi
Propodium Iodide (PI)	Sigma
PureLink Hipure plasmid preparation kit	Invitrogen
PVDF (ImmobilonP transfer membrane)	Millipore
RNAse A	Sigma
Rosswell Park Memorial Institute medium (RPMI-1640)	Invitrogen
RNase Out	Invitrogen
siGenome On-Targetplus SMART pool duplex (see section 2.3.2 for sequences used in this Thesis)	Dharmacon
Single donor buffy coats/ cones	National Blood Transfusion Service
siRNA (see section 2.3.1 for sequences used in this Thesis)	Dharmacon or Ambion
SSC	Ambion
Stem Cell Growth Media (SCGM)	CellGro
Streptomycin	Sigma
SuperScript ^{TM} III	Invitrogen

Superscript III first strand synthesis super mix	Invitrogen
Transfection buffer (Nucleofection)	Lonza
Trifluorethanol	Sigma
T cell negative isolation kit	Invitrogen
Trizol	Invitrogen
Trypsin (proteomics grade)	Sigma
Whatman 3MM paper	VWR international LTD
X-ray film (Hyperfilm–ECL)	GE healthcare
X- Vivo 15 cell culture media	Lonza
Zorbax C18 column	Agilent

2.1.2. Buffers and solutions

Cell cycle stain	40µg/ml Propidium Iodide, 5µg/ml Fluorescein isothiocyanate and 1µg/ml of RNase A in PBS
Complete Protease inhibitor cocktail (serine and cysteine protease inhibitor)	The composition is confidential.
CSK extraction buffer	100mM PIPES pH 6.0, 100mM NaCl, 300mM sucrose, 3mM $MgCl_2$,1mM DTT, 1mM EGTA, 0.5% (v/v) Triton X-100, protease inhibitors
DNA loading buffer	30% (v/v) glycerol, 0.25% (w/v) Orange R
Dialysis buffer	1mM Tris-HCl (pH7.5), 0.2mM EDTA, 0.2mM PMSF
Fixing solution	methanol: glacial acetic acid (3:1)
Fluorescein Isothiocyanate (FITC)	1µg/ml in PBS
Hypotonic solution	0.075M KCl in dH_20
10 x Iodoacetamide solution stock	550mM Iodoacetamide in urea buffer
Ionomycin	1µg/ml in dH_20
LB agar	LB broth with 1.5% (w/v) agar; Ampicillin was added to a final concentration of 100µg/ml
Luria-Bertoni (LB) Broth	1% (w/v) bactotryptone 0.5% (w/v) yeast extract,

	0.5% (w/v) NaCl; after autoclaving, Ampicillin was added to final concentration of 100µg/ml
1 x MES SDS running buffer	50mM MES, 50mM Tris, 0.1% (w/v) SDS, 1mM EDTA pH 7.3
Micococcal Nuclease	10 units/µl in 50% (w/v) Glycerol
Micococcal Nuclease digest buffer	0.32M Sucrose, 50mM Tris-HCl pH 7.5, 4mM $MgCl_2$, 1mM $CaCl_2$, 0.1mM PMSF
Micococcal Nulcease stop buffer	20mM EDTA
MS buffer A	100% (v/v) H_20, 0.1% (v/v) formic acid
MS buffer B	100% (v/v) Acetonitrile, 0.1% (v/v) formic acid
MS buffer C	95% (v/v) H_20, 5% (v/v) Acetonitrile, 0.1% (v/v) formic acid
Nuclei Buffer I	0.3M Sucrose, 60mM KCl, 15mM NaCl, 5mM $MgCl_2$, 0.1mM EGTA, 15mM Tris-HCl pH7.5, 0.5mM DTT, 0.1mM PMSF, 3.6ng/ml Aprotinin
Nuclei Buffer II	0.3M Sucrose, 60mM KCl, 15mM NaCl, 5mM $MgCl_2$, 0.1mM EGTA, 15mM Tris-HCl pH 7.5, 0.5mM DTT, 0.1mM PMSF, 3.6ng/ml Aprotinin, 0.4% (v/v) IGEPAL-CA-630 (Nonidet P40)
Nuclei Buffer III	1.2M Sucrose, 60mM KCl, 15mM NaCl, 5mM $MgCl_2$, 0.1mM EGTA, 15mM Tris-HCl pH 7.5, 0.5mM DTT, 0.1mM PMSF, 3.6ng/ml Aprotinin
1 x NuPage transfer buffer	25mM Bicine, 25mM Bis-Tris, 1mM EDTA pH 7.2, 20% (v/v) Methanol
Orgosol DetergentOUT kit	UPPA-I UPPA-II OrgoSol Buffer DO Wash SEED DO Pre Buffer-I DO Prep Buffer-II

Phosphate Buffered Saline	1 tablet (phosphate buffer, potassium chloride 0.02% (w/v), sodium chloride 0.8%(w/v)) dissolved per 100ml of H_2O and autoclaved
Phosphatase inhibitors	2mM β-glycerophosphate, 5mM NaF, 1mM Na_3VO_4, 0.1 µM okadaic acid
2x Platinum SYBR Green qPCR SuperMix-UDG with ROX	Platinum *Taq* DNA polymerase, SYBR Green I dye, Tris-HCl, 6mM $MgCl_2$, 400µM dGTP, 400M dATP, 400M CTP, 800M dUTP, uracil DNA glycosylase (UDG), 1M ROX Reference Dye and stabilizers
PMA	0.1µg/ml in dH_20
Propodium Iodine (PI)	1mg/ml in dH_2O
PureLink HiPure plasmid preparation kit	Resuspension buffer: 50mM Tris-HCl, pH8.0, 10mM EDTA RNase A: 20mg/ml in resuspension buffer Lysis buffer: 0.2M NaOH, 1% (w/v) SDS Precipitation buffer: 3.1M potassium acetate, pH 5.5 Equilibration buffer: 0.1M Sodium acetate, pH 5.0, 0.6M NaCl, 0.15% (v/v) Triton X-100 Wash buffer: 0.1M Sodium Acetate, pH 5.0, 825mM NaCl Elution buffer: 100mM Tris-HCl, pH 8.5, 1.25M NaCl
RNAse A	10mg/ml in dH_2O

10% (w/v) SDS	50g SDS dissolved in 500ml of dH_2O
2x SDS Lysis Buffer	125mM Tris-HCl pH 6.8, 4% (w/v) Sodium Dedocyl Sulphate, 40% (v/v) Glycerol, 200mM DTT and 0.002% (w/v) Bromphenol blue
Secondary antibody incubation buffer	10% (w/v) Non-fat dried milk, PBS, 0.05% (v/v) Tween-20
20 x SSC	3M Sodium Chloride, 0.3 M Sodium Citrate
Stem cell growth media	Salts, sugars, amino acids, vitamins, buffers contains phenol-red (pH indicator), L-glutamine, β-mercaptoethanol
SuperScript ^{TM} III First-Strand Synthesis Super mix for qRT-PCR	Reverse Transcriptase (RT) enzyme mix (Superscript III RT and RNaseOUT), 2x RT reaction mix (2.5µM oligo$(dT)_{20}$, 2.5ng/µl random hexamers, 10mM $MgCl_2$ and dNTPs), *E.coli* RNase H
Triton-based lysis buffer	20mM Tris-HCl pH 8, 1% (v/v) Triton-X100, 130mM NaCl and 5mM EGTA and a protease inhibitor cocktail (16µg/ml Benzamidine HCl, 10µg/ml Phenanthroline, 10µg/ml Aprotinin, 10µg/ml Leupeptin, 10µg/ml Pepstatin A, 1mM PMSF)
Urea Buffer	8M urea in 0.1M Tris-HCl, pH 8.0
Western blot wash buffer	PBS, 0.05% (v/v) Tween-20
Western blot blocking solution (PBST)	10% (w/v) Non-fat dried milk, PBS, 0.05% (v/v) Tween-20

2.1.3. Antibodies

Primary Antibodies	Supplier
AKT1 (C73H10)	Cell Signaling
CDC2 (clone 17; sc-54)	Santa Cruz
CDC6 (sc-9964)	Santa Cruz
CDC7 (C-20; sc-7518)	Santa Cruz
CDT1	A kind gift from Prof J.G. Cook; UNC; Chapel Hill, NC, USA (88)
Cyclin A (BF683; sc-239)	Santa Cruz
Cyclin D3 (C-16)	Santa Cruz
Histone H3 (ChIP grade)	Abcam
LSP-1(L60620)	Transduction Labs
LCK (3A5)	Santa Cruz
mouse anti-human perforin IgG_{2b} (δG9)	BD Biosciences
MCM2 (N-19; sc-9839)	Santa Cruz
MCM4 (#AHP840)	Serotec
MCM7 (sc-9966)	Santa Cruz
Nup160	A kind gift from Prof Farber, USCD, USA
HsORC4 (#611170)	BD Biosciences
PI3K (#06-195)	Upstate Biotechnology
PI3K (#06-497)	Upstate Biotechnology
p85a rabbit monoclonal (#04-403)	Millipore
Phospho-Histone γH2AX (Ser139) (clone JWW)	Millipore
Phospho-pRB ($S^{807/811}$);	Cell Signaling
Rad51 (H-92)	Santa Cruz
pRB (#554136)	BD Pharmingen
Sec13	A kind gift from Prof.

	Hetzer, Salk Institute, Ca, USA
WDHD1	A kind gift from Prof. Dutta, Virginia University, Va, USA
Secondary Antibodies	**Supplier**
goat anti-mouse IgG-Cy5	Jackson Laboratories
HRP-conjugated goat anti rabbit antibody	DACO or GE Healthcare
HRP-conjugated rabbit anti mouse antibody	DACO or GE Healthcare
HRP-conjugated rabbit anti goat antibody	DACO or GE Healthcare
Other Antibodies	**Supplier**
FITC Conjugated anti-human CD3 (Clone Okt3)	Ebiosciences
PE-conjugated anti-human CD69 (Clone FN50)	Ebiosciences
Mouse IgG1 kappa isotype control PE	Pharmingen
Mouse IgG2a kappa isotype	Ebiosciences
CD3/CD28 magnetic beads	Invitrogen

2.2 Cell culture

2.2.1. Culture of cell lines

YTS, is a sub-clone of a human NK cell-like line YT (424) and 721.221 is a human EBV-transformed B cell line which was mutated to express no HLA-A, B or C (342). Both were cultured in RPMI-1640 supplemented with 10% (v/v) heat-inactivated FBS, 1% (w/v) glutamine, 100U/ml penicillin, 100µg/ml streptomycin, 1mM sodium pyruvate, 1x non-essential amino acids at 37℃ in a humidified 5% (v/v) CO_2 atmosphere.

2.2.2. Isolation of primary human T cells from whole blood

All primary T cell were isolated from anonymous normal single donor buffy coats or leukocyte cones obtained from the National Blood Service or from fresh donated human blood. During the first year only buffy coats were used in all experiments. From the second PhD year on, only leukocyte cones were used, due to changes in the isolation method by the National Blood Service. Buffy coats were diluted 1:1 with PBS. Leukocytes cones, fresh blood or diluted buffy coats were layered on top of an equal volume of Histopaque 1077 and then centrifuged at 560 x g_{max} for 30 min without brake. Peripheral blood mononuclear cells (PBMC) were removed with a Pasteur pipette, resuspended in 50ml PBS and centrifuged at 400 x g_{max} for 10 min. Platelets were removed by centrifuging twice in a 50ml of PBS with 2% (v/v) FBS Sigma at 200 x g_{max} for 10 min. T lymphocytes were then purified by negative selection or by adherence of PMBC to plastic ware, as described in 2.2.3 and 2.2.4.

2.2.3. Adherence Method

T cells were enriched from PBMC by depleting monocytes by adhering PBMC to plastic ware. 2 x 10^7 PBMC resuspended in 3ml X-Vivo 15 with 2% (v/v) AB serum were plated in one 6 –well plate and incubated for 2 h at 37ºC. After 2 h adherence, cells were resuspended gently, thereby avoiding dislodging the monocytes, which were attached to the plastic and allowed to adhere overnight. Next day the cell suspension was transferred again to a new well, the cell number was determined and the purity of T cells in this cell suspension was determined by CD3-FITC staining.

2.2.4. Negative selection method

The non-activated T lymphocytes were purified from PBMC by negative selection using a T cell negative isolation kit. This kit contains immunomagnetic beads conjugated to antibodies that will bind to monocytes (CD14), granulocytes (CD15), B cells (CD19), NK cells (CD16 a and b, CD56), erythrocytes (CD235a) and activated T cells (HLA class II DR/DP). The PMBC were resuspended in PBS with

2% (v/v) FBS at 1 x 10^8/ml and incubated with 20µl of antibody mix per 1 x 10^7 cells at 4℃ for 20 min with constant rolling. Unbound antibody was removed by increasing the volume to 20ml with PBS/2% (v/v) FBS and centrifuging at 500 x g_{max} for 8 min. Cells were resuspended at 1 x 10^7/ml in PBS/2% (v/v) FBS with 100µl per 1 x 10^7 cells of anti-mouse IgG immunomagnetic beads. Cells were incubated for 15 min at room temperature with constant rolling to allow binding of the beads to any antibody labelled cells. Bead clumps were dispersed by vigorous pipetting. Cells bound to the beads were removed with a magnet. This was done by placing a 1.5ml Eppendorf containing the mixture on a magnet, and allowing the beads to bind to the magnet for 1min. Thereafter, the unbound supernatant was pipetted off in a clean tube, and cells were collected by centrifugation. The unbound cells in the supernatant are a mixture of $CD4^+$ and $CD8^+$ quiescent T cells. Bead removal was repeated, if residual beads were visible in the supernatant. Each full kit yields 1.25-2.5 x 10^8 cells.

Quiescent T cells were then generally cultured at 1-4 x 10^6/ml in RPMI-1640 with 10% (w/v) FBS or X-Vivo15 with 2% (v/v) AB serum. PMA/Ionomycin- or CD3/CD28- stimulated cells were kept in the range of 5 x 10^5 to 1 x 10^6 by the addition of cell culture medium. The cell number was determined by manual counting in the presence of Trypan Blue, using an improved Neubauer chamber. The purity and activation status was determined by CD3-FITC and CD69-PE staining respectively and flow cytometric analyses.

2.2.5. Cryopreservation of peripheral blood mononuclear cells

Freshly isolated PBMC from whole blood were cryopreserved by freezing the cells in CryoMaxx SF freezing media. Typically 1-2 x 10^6 PBMC/ml are obtained from a healthy individual with 95% viability. Up to 20 x 10^6 pelleted PBMC were resuspended in 1ml of ice-cold serum-free CryoMaxx SF by adding the mix drop-wise with gentle agitation between drops. 1ml of the cell suspension was dispensed into one cryo-vial and placed in a ‘Mr. Frosty’ freezer container, which had been pre-cooled at -4ºC. The cryo-vials in the freezer container were placed first at -80ºC

over-night to allow a stepwise, slow freezing, before they were transferred to liquid nitrogen for long-term storage.

2.2.6. Stimulation of G_0 T cells

T cells cultured in X-Vivo15 with 2% (v/v) AB serum were stimulated with PMA and Ionomycin or with anti-CD3/CD28 magnetic beads (0.5 bead/cell).

2.2.7. Agarose gel analysis of DNA

DNA analysis was performed using standard agarose gel electrophoresis. Typically 1.5% (w/v) agarose was dissolved in TAE buffer by boiling in a microwave. After cooling to 50ºC, ethidium bromide was added to a final concentration of 0.5µg/ml to enable visualisation of the DNA under UV light. The heated solution was then cast in a plastic tray, containing the appropriate size of the comb, and the solution was left to cool to room temperature. DNA samples were loaded on the gel with a loading buffer containing glycerol and Orange R dye. Electrophoresis was carried out at 100V and 70mA. The DNA, separated by this process, was visualized on a UV transilluminator at 254nm. A DNA marker of known sizes were analysed alongside the experimental sample to determine the size of the DNA samples being analysed.

2.2.8. Total RNA extraction

1-10 x 10^6 cells were centrifuged at 300 x g_{max} for 5 min and the supernatant was discarded. The pellet was resuspended in 1ml of Trizol by pipetting and incubated at room temperature for 5 min. The sample was transferred to a 1.5ml micro-centrifuge tube and 200µl of Chloroform was added to the sample for phase separation. The mix was incubated at room temperature for 3 min, followed by centrifugation at 12000 x g_{max} for 15 min at 4ºC. The separated upper aqueous phase was transferred to a fresh micro-centrifuge tube containing 600µl of iso-propanol, mixed well and frozen overnight at -20ºC. Next day the sample was incubated 10 min at room temperature and centrifuged for 15 min in a pre-cooled

centrifuge at 4ºC. The supernatant was discarded and 1 ml of 75% (v/v) ethanol was added to wash the pellet. The sample was centrifuged at 12500 x g_{max} for 15 min at 4ºC. The supernatant was removed until 10µl remained, then centrifuged for an additional 2 min. The remaining ethanol was removed carefully by using small pipette tips. The pellet was air dried at room temperature for 2 min and then dissolved in 20-50µl of RNase-free dH_2O. The quality and concentration of the RNA was determined by Nanodrop, as described in 2.2.9.

2.2.9. Determination of the RNA or DNA concentration

RNA or DNA concentration was determined by Nanodrop spectrophotometry (Thermo Scientific). This method measures the absorbance of DNA or RNA in solution at 260nm and the quality is assessed by determining the 260nm/280nm ratio. The Beer-Lambert equation A= E x b x c is used to calculate the DNA/RNA concentration. A is the absorbance value, E is the wavelength-dependant molar absorptivity coefficient or extinction coefficient with units of $l*mol^{-1}*cm^{-1}$, b is the path length in cm, c is the analyte concentration in mol/l. Typically 1µl of DNA or RNA in dH_2O was placed on the Nanodrop optical fibre and the absorbance was measured against a blank of dH_20. The 260nm/280nm ratio is considered to be a good indicator of protein contamination and the purity of RNA or DNA is sufficiently good at a ratio above 1.5.

2.2.10. Reverse transcription (RT)

Up to 1µg of RNA was reverse transcribed into cDNA in a total volume of 20µl using SuperScript ^{TM} III First- Strand Synthesis Super mix for qRT-PCR. The RT reaction was prepared on ice by combining RT enzyme mix (includes SuperScript ^{TM} III and RNAse OUT) and 2 x RT reaction mix with up to 1µg of total RNA. The volume was made up to a total of 20µl.

The 2 x RTenzyme mix contains as follows:

Reagent	
Oligo $(dT)_{20}$ primer Random hexamers	2.5µM 2.5 ng/µl
RNA	1µg
10mM dNTP Mix	1µl
DEPC-treated water	10µl
Total	10µl

The following cDNA mix was prepared and mixed with the RNA:

Component	**Volume (10µl)**
10x RT buffer	2µl
25mM $MgCl_2$	4µl
0.1M DTT	2µl
RNase OUT (40 U/µl)	1µl
Superscript III RT (200 U/µl)	1µl

The components were gently mixed and incubated at 25ºC for 10 min, followed by incubation at 50ºC for 30 min. The reaction was terminated at 85ºC for 5 min and then chilled on ice. The single stranded cDNA (ss-cDNA) was treated with 2 U RNAse H for 20 min at 37ºC to degrade the RNA template. The cDNA was diluted to 30µl with dH_20 and kept at -20ºC for long term storage.

2.2.11. Analysis of mRNA expression levels by real time PCR (quantitative RT-PCR)

Real time PCR was performed using Platinum SYBR Green qPCR SuperMix-UDG with ROX to determine the mRNA expression levels of the target genes. Platinum *Taq* DNA polymerase is a recombinant *Taq* DNA polymerase complexed with a proprietary antibody that blocks polymerase activity at ambient temperatures. The activity is restored after the denaturation step in PCR cycling, providing an automatic hot start PCR for increased sensitivity, specificity and yield (80, 339).

SYBR green is a fluorescent dye that binds directly to double stranded DNA (dsDNA). In qPCR, as dsDNA accumulates, the dye generates a signal that is proportional to the DNA concentration and that can be detected using real-time qPCR instruments (177, 414). ROX is a reference dye to normalize the fluorescent signals on instruments and adjusts for non-PCR fluctuations in fluorescence between reactions. ROX provides a stable baseline in multiplex reactions. UDG and dUTP in the super mix prevent the re-amplification of PCR products carried over between reactions. The 25µl reaction mixture contains 1 x Platinum SYBR Green qPCR SuperMix-UDG with ROX, 3pmol each of the forward and reverse primers and 3µl of cDNA. Real-time PCR was performed on an ABI PRISM 7900 instrument. Recommended standard reaction conditions were 50ºC for 2 min, 95ºC for 10min, 40 cycles of 95ºC for 15 s and 60ºC for 60 s for all used primers. The comparative CT, also referred as the 2 (–ΔΔC(T)) method was applied to estimate relative transcription levels (331). First, the ΔCT value for each sample is determined by calculating the difference between the CT value of the target gene and the CT value of the endogenous reference gene (calibrator sample). Levels of mRNA encoding Abl1 were used as an endogenous reference to normalize each sample. Next, the ΔΔCT is determined by subtracting the ΔCT value of each calibrator form the ΔCT value of the sample. If the PCR efficiencies of the target gene and the endogenous reference gene are comparable, the normalized level of target mRNA expression is calculated using the formula (303):

Normalized target mRNA expression level in sample = $2^{-\Delta\Delta CT}$

Component	**Volume (25µl)**
Platinum Quantitative PCR super mix-UDG with ROX	12.5µl
Primer Forward	1µl
Primer Reverse	1µl
dH_2O	5.5µl
cDNA	5µl
Total Volume	25µl

Description	Primer	Manufacturer
ARHGAP6 forward	5’-GTCTCGCTGCAGCACCTCCA	Sigma
ARHGAP6 reverse	5’-TGGTGAGAGCGTGGGCCTGT	Sigma
PIK3R1 forward	5’-ACCTGTTGCGAGGGAAGCGA	Sigma
PIK3R1 reverse	5’-GGCTCGGCAAAGCCATAGCCA	Sigma
AKT1 forward	5’-CCCAAGCACCGCGTGACCAT	Sigma
AKT1 reverse	5’-GCGTAGTAGCGGCCTGTGGC	Sigma
MAPK8 forward	5’-TACGGGGGCAGCCCTCTCCT	Sigma
MAPK8 reverse	5’-GCCCAGCTGCTGCTTCTAGACT	Sigma
ITSN1 forward	5’-AACAGTGGGCGACAAGGCCG	Sigma
ITSN1 reverse	5’-GGCCGGTGGCGGTGTATGAG	Sigma
CDGAP forward	5’-TTCACGGAGGCAGTGTCGCA	Sigma
CDGAP reverse	5’-GGCGATATGGGCCAGGTGTCG	Sigma
MAPK9 forward	5’-GCCCGGACAGCGTGCACTA	Sigma
MAPK9 reverse	5’-CCAGCTCTCCCATGATGCAACCC	Sigma
PAK2 forward	5’-CCTCAGGCTGTGCTGGATGTCCT	Sigma
PAK2 reverse	5’-CCCTTGGCATTCAGTGCTGGTGT	Sigma
PAK1 forward	5’-GCCACAGGACAGGAGGTGGC	Sigma
PAK1 reverse	5’-ACCCACAGCTCATCTCCCACGA	Sigma
ARHGEF7 forward	5’-GCTGTGCTTTTCCGGACGC	Sigma
ARHGEF7 reverse	5’-TCCGGCCCTCAGCTGCTCTC	Sigma
ARHGEF6 forward	5’-TCGAAGCCTACTGCACCAGCG	Sigma
ARHGEF6 reverse	5’-TGGTCTGGCCGTTGCTTCTGG	Sigma

2.3 Transfections

2.3.1. Transient transfection of primary T cells with siRNA by Amaxa Nucleofection

Quiescent T cells were transfected with small interfering RNA (siRNA) using the Nucleofection system (Lonza). $5x10^6$ quiescent T cells were harvested by centrifugation at 200 x g_{max} for 5 min. The culture medium was completely removed and the cells were resuspended in 100µl of T cell Nucleofection kit solution (230). 5µl of siRNA (Dharmacon or Ambion) was added to a final concentration of 1-5µM, as indicated in the text. A non–targeting siRNA was used as a control. The cell suspension was then transferred into a Nucleofection cuvette, which was placed into the Nucleofection II device and transfection was carried out using programme U-24, which is specified for primary human unstimulated T cells. The transfected cells were then transferred into one 6 well plate containing 3 ml of X-Vivo15 with 2% (v/v) AB serum. The cells were cultured overnight to recover at 37ºC in a fully humidified atmosphere of 5% CO_2.

siRNA Target	Sequence	Supplier
AND1/WDHD1 #1	GCUUCAAAAACUAAGUGAAtt	Ambion
AND1/WDHD1 #2	GAAGGAAUGAUUCGAUUUAtt	Ambion
AND1/WDHD1 #3	GCACUUAGUCGAACUACAAtt	Ambion
SEC13/ SEH1L #1	CGACCAAAGAUGUGAGAAUtt	Ambion
SEC13/ SEH1L #2	CAGAUGGUAUAGUAAGAAUtt	Ambion
SEC13/ SEH1L #3	GCUCAGUUCGAUAAUCAUAtt	Ambion
MCM7 #1	GAGACAAUGACCUACGGUU	Thermo (siGenome)
MCM7 #2	UGUCAUACAUUGAUCGACU	Thermo (siGenome)
MCM7 #3	GGAGAGAACACAAGGAUUG	Thermo (siGenome)
MCM7 #4	GGAAAUAUCCCUCGUAGUA	Thermo (siGenome)

2.3.2. Electroporation of NK cells with a plasmid encoding the Cdc42-biosensor (1054rg) and/or siRNA

YTS cells were split at a 1:2 dilution the day before electroporation. For each sample, 10^6 cells were resuspended in an appropriate volume of serum-free RPMI-1640 media containing 25mM HEPES to a concentration 4 x 10^6 cells/ml. The Raichu-CDC42 plasmid DNA was prepared using the pure link hipure plasmid preparation kit and stored in dH_2O. For each sample, 40µg plasmid DNA and/or 2.5µl or 6µl of 20µM siRNA (siGenome On-Targetplus SMART pool duplex) (Table 2.3.3 A) or labelled siRNA (Table 2.3.3. B) were used. The YTS cell suspension and plasmid DNA and/ or siRNA were mixed thoroughly in a 1.5ml tube and transferred carefully to a 4mm cuvette to avoid creating bubbles. The cuvette was left for 10 min at room temperature prior to electroporation. Electroporation was performed at 260V/975µF using the Gene Pulser-II electroporation system (BioRad). 10 min after the electroporation, cells were resuspended in supplemented RPMI-1640 media pre-warmed to 37℃ (see section 2.2 .1), and the cells were washed in 15ml media once to remove all debris. The cell pellet was resuspended in 3ml supplemented RPMI-1640 media and transferred to one 6-well plate and incubated for 24 h at 37℃ to allow expression of t he construct before imaging.

siRNA Target	**Antisense Sequence**
Human ARH GAP1	5'- PUCAUAUUUGAGCACUUGGCUU 5'- PAACACAAUGAUCUUCCGCCUU 5'- PGAAAACAACAGCCAGGUUAUU 5'- PUACUUCUGCUGCACUUCCCUU
Human PI3KR1	5'- PUAUGACACAAUGCUUUACUUU 5'- PUUAUUCAUACCGUUGUUGGUU 5'- PCAAGUAUUGGUCUCUCGUCUU 5'- PUUCCCCUACAGCUUCAAUAUU
Human AKT1	5'- PUUGGUCAGGUGGUGUAGAUGUU 5'- PUUAAUGUGCCCGUCCUUGUUU 5'- PCUUGCCGAAAGUGCCCUUGUU 5'- PGAGUACUUCAGGGCUGUGAUU
Human MAPK8	5'- PUACUACUAUAUUACUGGGCUU 5'- PUUUCCUUGUAGCCCAUGCCUU 5'- PUAAGCUGCGCAUACUAUUCUU 5'- PCACUACAUAAGGCGUCAUCUU
Human ITSN1	5'- PUCAAUCGACAUCUGAUAUCUU

	5’- PAUUCUAUGAUCUUUCGUUCUU 5’- PGAAGACUCCGGCCUUGUCGUU 5’- PCUAGUGCCCAUAUCUGUGCUU
Human CDGAP	5’- PUGUUCGAUUGAAAUUUCCCUU 5’- PUCGCCCUCCUGCUUGGUGAUU 5’- PUACUGAAUGGGUUACAUCCUU 5’- PUUACUGAUCUCCGCUGAGGUU
Human MAPK9	5’- PAAAUGCAGCACAAACAAUCUU 5’- PUAACCUAUCAUCGACAGCCUU 5’- PUAAUUCCUCACAGUUGGCUUU 5’- PUAAGAGGACAAGUUCACGAUU
Human PAK2	5’- PUAACGGUUUGGCCAGUUUCUU 5’- PUACUGCGUUUGCUCUGCUCUU 5’- PUAGUAAUCGAGCCCACUGUUU 5’- PUCUCGUUAAUGAUCAGUUCUU
Human PAK1	5’- PUAAUUCACAAUGUUUGGGUUU 5’- PUAUGCUUCGUAAUUUCUCCUU 5’- PUGUCUAGGCCGUUAUUUGAUU 5’- PGACUUAGUGAUAUUUGAUGUU
Human ARHGEF7	5’- PUAUCCGCUCAAUCAUGCUCUU 5’- PUGUUCCGUGAGGACAUUCAUU 5’- PUGAGAAGGAAAGCUCGUCCUU 5’- PAUCUGUAUGAUAAUCCUCCUU
Human ARHGEF6	5’- PUAAGAUUAUAAGACAUCCUCUU 5’- PUAAGAGAAGAGGAACGUCCUU 5’- PUAAUCACAUAUUCCUCCUCUU 5’- PGUGACGUAAAUGAUGUCCUU
ON-Target plus non-targeting pool	Pool of non-targeting siRNA

Labeled siRNA	**Anti-sense sequence**
Accell Green (FAM)non-targeting siRNA (Dharmacon)	5’- GCA GCA CGA CUU CUU CAA GTT- FITC
Negative control siRNA Alexa Fluor 647 (#1027100, Qiagen)	5’- UUC UCC GAA CGU GUC ACG UdT dT-AlexaFluor647

2.4 Analysis of the cell cycle by flow cytometry

The cell cycle status of T cells was determined by analysing the DNA and total protein content, as used for previous studies in our laboratory *e.g.* (218). 2 x 10^5 cells per sample were collected by centrifugation at 200 x g_{max} for 5 min. 2 x 10^5 T cells were taken at the indicated time points and were fixed in 500µl of 70% (v/v) ethanol. The fixed cells were then centrifuged in FACS tubes at 350 x g_{max} for 8 min and the supernatant was removed. The cell pellet was resuspended in 400µl FITC/PI cell cycle stain, which contains DNAase-free RNAase. RNA in the sample was digested for 30 min at 37ºC. Flow cyctometric analysis was then performed using a Becton Dickinson FACS Caliber machine. The WinMDI2.9 or FlowJo program was used for cell cycle data analysis. Cells, which pass the flow cytometer laser as doublets or aggregates were excluded from the analyses because those cells will have 2 x 2n DNA content and will therefore be quantified as having 1 x 4n DNA content. To avoid the artefact that the doublets will be scored as G_2/M cells, a doublet discriminator gate was applied in the flow cytometry analysis. The principle is that total fluorescence detection, which is equivalent to the area under the curve (FL2-A Area), is proportional to the time that a cell needs to pass a detector (FL2-W Width). Doublets will have a much bigger FL2-W, due to their bigger size. Therefore plotting the area (FL2-A) against width (FL2-W) and applying a gate around cells with a correct pulse width corresponding to single cells, excludes the doublets events. PI (FL-2A) was then plotted against FITC (FL-1H), which quantifies total protein content. The percentages of cells in each cell cycle phase were calculated by manually applying gates around populations of cells in G_0, G_1, S phase, G_2/M and apoptosis.

2.5 Determination of the activation state of T cells

Quiescent T cells were stimulated with 1µg/ml PMA and 0.1µg/ml Ionomycin overnight and harvested by centrifugation at 200 x g_{max} for 5 min. Cells were then resuspended in 100 µl PBS at a concentration of 1- 2 x 10^6 cells/ml and stained with anti-human CD69-PE or PE-labelled isotype-matched control at 4ºC for 30min.

Expression of CD69 was determined by flow cytometric analysis using a Becton Dickinson FacsCalibur instrument.

2.6 Protein analysis

2.6.1. Preparation of total cell lysates

1 x 10^6 YTS cells were pelleted by centrifugation at 300 x g_{max} for 5 min and lysed in either an SDS- or Triton- based lysis buffer. Cells were lysed in 2 x SDS-lysis buffer for 5 min at 95℃. In case the protein concentration needed to be determined by BCA assay (see section 2.6.2), DTT and Bromphenol Blue were added to the samples after the protein concentration was determined. Generally 50µl SDS buffer was added per 1 x 10^6 cells. Where indicated, cells were lysed in Triton-buffer on ice for 15 min and centrifuged at 13000 x g_{max} for 8 min. The lysate was centrifuged and the supernatant was removed to a fresh tube. Samples of both supernatant and the pellet were both analysed by Western blotting (see section 2.6.7). After determining the protein concentration by BCA assay, samples were prepared in NUPAGE LDS Sample Buffer (4x) with 100µM DTT. Samples were stored at -20ºC if not needed immediately for western blotting.

2.6.2. BCA assay

To determine the protein concentration, a standard curve with bovine serum albumin (BSA) was prepared by a sequential dilution of 11 samples in the concentration range from 0 to 4.0µg/µl. 5µl of each BSA sample or test sample diluted in lysis buffer was added into a 96-well plate. Each BSA sample was diluted with the lysis buffer and each test sample was diluted with dH_2O up to 10 µl. The BCA reagent A and B were mixed in a ratio of 50:1 and 200µl were added to each sample. The 96-well plate was incubated at 37℃ for 30min and analysed at 562nm using a plate reader spectrophotometer.

2.6.3. Formaldehyde crosslinking of proteins to chromatin

10-25 x 10^6 cells were centrifuged for 5 min at 300 x g_{ave}. The supernatant (XVivo15 medium/2% (v/v) AB serum) was removed, the pellet was washed in 10 ml PBS, centrifuged for 5 min at 300 x g_{max} and the supernatant was removed. Cells were resupsended in 10ml PBS and 270µl of 37% (v/v) formaldehyde was added (final concentration 1% (v/v)). Cells were incubated for not more than 10min at room temperature and agitated by gentle rolling. The precise time was determined experimentally as described in Results 5.2.3. To stop the reaction, 2.5M Glycine was added to a final concentration of 125mM. Cells were centrifuged and the supernatant was discarded. The cells were washed once with 10 ml cold PBS and the supernatant was removed. The cell pellet was transferred to a 1.5 ml microcentrifuge tube by resuspending the pellet in 1ml PBS and further processed by CSK extraction or nucleosome/chromatin isolation.

2.6.4. Isolation of chromatin and nuclear matrix-bound proteins

The method was carried out essentially as described in (218, 290). Cells were centrifuged for 5 min at 300xg and lysed in 20µl of ice cold CSK Buffer per 1 x 10^6 cells. Complete protease inhibitors and phosphatase inhibitors were added to the lysis buffer before use. The cells were lysed on ice for 10 min, and then centrifuged in a pre-chilled centrifuge at 1000 x g_{max} for 5 min at 4°C. The supernatant, which contains unbound proteins, was transferred to a clean tube. Care must be taken at this step not to disturb the pellet, which can be difficult to see, especially if fewer than 1 x 10^6 T cells are used.

The pellet (from 10-50 x 10^6 cells, typically used for mass spectrometry analyses), containing the chromatin/nuclear matrix bound proteins, was resuspended in 200µl of ice cold CSK buffer containing protease and phosphatase inhibitors and centrifuged at 1000 x g_{max} for 5 min at 4°C. The wash step was repeated. A final centrifugation step (10000 x g_{max}, 1 min, 4°C) may be necessary as sometimes the pellet is stuck to the side of the tube.

4x volume of –20°C Acetone was added to the unbound (supernatant) fraction to precipitate the proteins, before centrifugation at 10000 x g_{max} for 10 min. The supernatant was discarded and the dry pellet was left for 15 min in a laminar flow hood with an open lid to allow the residual Acetone to evaporate. All samples were stored at –80°C and sent to Professor Edward Marcotte's laboratory, Univeristy of Texas at Austin, USA for analysis by mass spectrometry (see section 2.12).

For western blotting analysis, parallel CSK-extracted pellet fractions were resuspended in SDS lysis buffer as in 2.6.7. Sufficient SDS buffer was also added to the corresponding unbound, supernatant fractions to make the sample volume the same. Samples were stored at -20ºC until required.

2.6.5. Isolation of chromatin-bound proteins

The method was adapted from the native chromatin immunoprecipitation (NChIP) protocol used by (188, 350). 15 x 10^6 quiescent or stimulated T cells were pelleted by centrifugation at 200 x g_{max} for 10 min in a 50 ml centrifuge tube. After pouring off the supernatant, the cells were resuspended in 2 ml ice-cold nuclei buffer I, followed by addition of 2 ml ice-cold nuclei buffer II (see Table in 2.1.2 for the composition of both buffers). The buffer mix was gently inverted and placed on ice for less than 10 min. After 8min the swelled cells were carefully layered on top of 8 ml of ice-cold nuclei buffer III (sucrose cushion) in two 15ml centrifuge tubes. The tubes were then centrifuged in a pre-chilled 4ºC swing-out rotor at 7000 x g_{max} for 20 min. At this stage the nuclei form a pellet at the bottom along one side of the tube (or at the side of the tube), whereas the cytoplasmic components remain on the top layer. The supernatant was aspirated carefully using a Pasteur pipette. The pellet containing the nuclei was resuspended in 250µl - 500µl per 15 x 10^6 cells in *M.nase* digest buffer (see Table in 2.1.2) and transferred to a 1.5 ml micro centrifuge tube, placed on ice. The presence of un-lysed cells and intact nuclei was determined by staining 10µl of the preparation with Trypan blue. This was viewed with a microscope at 10 x and 100 x magnification under white light. 1µl of *M.nase* (10 units) were added to each tube of resuspended intact nuclei in *M.nase* buffer, and mixed gently before incubation in a 37ºC water bath for 5 -10 min. The

nuclease reaction was stopped by the addition of 5mM EDTA on ice. The sample was centrifuged for 10 min at 4ºC at 10000 x g_{max} and the supernatant (S1) was retained and transferred to a new tube. The pellet was resuspended in dialysis buffer (500µl buffer per 15 x 10^6 cells) and incubated on ice for 10 min. Samples, which were cross-linked with formaldehyde (see section 2.6.3) prior to isolating nuclei were sonicated on ice with a 3mm probe and 80% power with a probe sonicator. The samples were sonicated for 10 sec, and then left on ice for 10 sec to reduce heating. The sonication was repeated 5 times. Following sonication, the samples were centrifuged 4ºC at 10000 x g_{max} for 10 min at and the supernatant (S2) was retained and transferred to a new tube. The remaining pellet (P) was resuspended in 50µl dialysis buffer for DNA gel analysis. At this stage quality control was performed to assess the nucleosome state after *M.nase* treatment. The optical density was measured at 260 nm (Nanodrop) and approximately 0.5 µg of each fraction (S1, S2 and P) was phenol extracted once, mixed with DNA loading dye and analysed by gel electrophoresis through a 1.2% (w/v) agarose gel. The gel was stained with ethidium bromide and visualized under UV illumination. The chromatin preparations were only analysed by mass spectrometry if the DNA was predominantly digested to nucleosomes (see text for details).

2.6.6. Crosslinking reversal and DNA purification

Aliquots of chromatin cross-linked with formaldehyde were incubated with 250mM NaCl and DNAase-free RNase A at 65ºC overnight to reverse the crosslinking and to digest co-purified RNA. Next day, an equal volume of Phenol/Chloroform/Isopropanol mix (25:24:1) was added and vortexed for 30 seconds to extract the DNA. This procedure was carried out for each of the S1, S2 and P fractions. The mix was centrifuged at 15000 x g_{max} for 15 min and the aqueous layer containing DNA was taken off carefully and transferred to a fresh 1.5 ml micro centrifuge tube. 5µl of 5M NaCl was added per 100µl to give a final concentration of 250mM and 3µl of 100% (w/v) glycogen was added as a carrier. An equal volume of isopropanol was added to the mix and the sample was allowed to precipitate at -80ºC for 2 h. The sample was then centrifuged at 13000 x g_{max} for 10 min. The supernatant was removed and the pellet was air dried at room

temperature. When all the remaining alcohol had evaporated, the pellet was resuspended in 10µl of dH_2O. The DNA concentration was determined using the Nanodrop as described in section 2.2.9 and the DNA quality was determined by gel electrophoresis (see section 2.2.7).

2.6.7. Protein electrophoresis and western blotting

Protein lysates were incubated for 5 min at 95°C and these, together with a protein standard were separated on 4–12 % (w/v) polyacrylamide Bis-Tris gels by electrophoresis at 200V for 1 h in MES running buffer (see composition in 2.1.2).

Gels were transferred by electro blotting at 30–40V for 1 h to a PVDF or nitrocellulose membrane in NuPage transfer buffer and 20% (v/v) methanol. Non-specific protein binding sites in the membrane were blocked by incubation in PBST with 10% (w/v) milk (commercially available skimmed milk powder) or with 3-4% (w/v) BSA in PBST for 30 min at room temperature. The blot was washed once with PBST prior to antibody probing. Primary antibodies were typically used at dilutions of 1:1000 in PBST with 3% (w/v) BSA and 0.01% (w/v) NaN_3. Blots were incubated in primary antibodies overnight, then washed 3 x 5 min in PBST and incubated in secondary antibody for 30 min. Blots were washed again three times and protein bands were detected using the ECL-Plus, ECL or ECL WB Substrate Thermo detection systems and exposed to X-ray film for various periods of time. Primary antibodies used in the experiments are listed in Table 2.1.3.

2.7 Immunofluorescence staining at the immunological synapse

1 x 10^6 721.221 cells were resuspended in 1ml RPMI-1640 without serum containing 3µl CellTracker Orange CMTMR stock solution at 37°C for 10-15 min. The excess CMTMR stain was removed by washing the cells twice in RPMI-1640 without serum and centrifugation for 5 min at 250 x g_{ave}, followed by one wash in complete RPMI-1640 media containing serum. The cells were resuspended in 1 ml RPMI-1640 media and incubated for 15-30 min at 37°C , washed 1 x in RPMI-1640 and resuspended in 100µl complete media. 2 x 10^6 YTS cells previously transiently

transfected with a plasmid encoding the CDC42-biosensor (see section 2.3.1) were pelleted by centrifugation at 250 x g for 5 min. The 721.221 cells in 100µl complete media were added in YTS cells, mixed in a conical bottom 15ml centrifuge tube, and incubated for 10 min, 30 min, 1 h or 3 h at 37°C with agitation. Cells were fixed with 4% (v/v) paraformaldehyde in PBS for 12 min at room temperature and washed twice in PBS. Cells were permeabilised with 0.1% (v/v) Triton-X-100 in PBS for 10 min on ice and washed twice with PBS/0.1% (v/v) Tween-20 (PBST). Before staining the cells, cells were blocked for 20–30 min with 10% (v/v) horse serum in PBST at 4℃ and then washed in PBST. Cells were incubated with the primary antibody (mouse anti-human perforin IgG_{2b} (δG9)) at a dilution of 1:50 in blocking solution for 90 min at 4℃. Cells were washed 3 x in PBST and incubated in the secondary antibody (goat anti-mouse IgG-Cy5) at a 1:250 dilution in blocking solution for 40 min at 4℃. Stained cells were washed 3 x in PBST and 1 x with PBS. Cover slips were finally prepared for imaging with Mowiol mounting medium containing 2.5% (w/v) 1,4-diazabicyclo (2.2.2) octane as an anti-fade reagent.

2.8 Multiphoton FLIM measurement and analysis

An in-house multiphoton microscopy system was used to perform time-domain FLIM (see Figure 1.1.6). This system uses a solid-state pumped (8-W Verdi; Coherent), femtosecond self-modelocked Ti:Sapphire (Mira; Coherent) laser system as the light source. It consists of an inverted epifluorescence microscope (Nikon TE2000E) and a scan head developed in-house. Fluorescence lifetime imaging was measured using a time correlated single photon counting (TCSPC) electronics system (Becker & Hickl, SPC700). All images were acquired at a suitable spatial and time resolution to provide enough photon arrival times for accurate fluorescence decay fitting, whilst avoiding detector 'pile-up'. Cells were imaged using a 40 x, 1.4 N.A. oil-immersion objective (Nikon). Epifluorescence images of GFP (FITC filter set), RFP (G-2A filterset) and Cy5 (Cy5 filter set) were acquired in the same image view prior to multiphoton FLIM (mFLIM).

Time resolved analyses were carried out with in-house image analysis software (TRI2) (31). Data were loaded into the software and time resolved analysis was

performed. Pixels with a low intensity were excluded as these are not sufficient for the analysis. The presence/absence of FRET was monitored by the following equation: conventional FRET efficiency ($FRET_{Eff}$) = $1-\tau_{da}/\tau_{control}$, where τ_{da} is the lifetime of GFP-Raichu-RFP and $\tau_{control}$ is GFP-Cdc42 lifetime measured in the absence of acceptor (124, 194). Pixel-by-pixel lifetime determination was achieved using a mono-exponential Levenberg-Marquardt fit using TRI2 (31, 124).

2.9 Interphase fluorescence *in situ* hybridization (I-FISH) with locus-specific probes

For karyotype analysis non-activated, quiescent peripheral blood T cells were transfected with siRNA against proteins of interest (see section 2.3.1) and stimulated for 4 days with PMA and Ionomycin (see section 2.2.6). On day 5, 0.6µM colcemid was added to inhibit mitotic spindle formation and the cells were incubated overnight.

Cells were harvested in a 15 ml centrifuge tube by centrifugation at 300 x g_{max} for 8 min and the media was aspirated. While vortexing, 3-4ml pre-warmed hypotonic solution was added and the cells were incubated at 37ºC for 15 min to allow swelling to occur. The cells were centrifuged at 300 x g_{max} for 5 min and the supernatant was discarded. 1ml of pre-cooled fixing solution was added drop wise to the cells while vortexing, to preserve the cellular morphology. At this point the cells were stored at -20ºC until further processing. The cells were thawed and centrifuged at 300 x g_{max}, the supernatant was removed and the fixation was repeated twice with 5ml of the fixing solution. Cytospin slides were prepared with 40,000 fixed cells per slide. Slides were chemically “aged” by incubation in 100% ethanol for 20 sec at 94ºC, before being washed in 2 x SSC buffer for 20 min. Each slide was dehydrated by dipping slides sequentially for 2 min in 70%, 80% and 100% (v/v) Ethanol. The probes used for the analyses were genetic targets for chromosome 5, Chromosome 9 and chromosome 15. LSI D5S23, D5S721/5Gn/CEP 9SA/CEP15 (Vysis). 3µl of the probe was dropped on the center of the selected area on the slide and incubated at 37ºC for 10min -15 min. Probes were denatured by incubation at 74ºC for 4 min and then the slides were incubated overnight in a humidified hybridisation chamber at 37ºC. After incubation, the slides

were washed in 0.4 x SSC for 2 min at 73ºC, then incubated in 2 x SSC/0.01% (v/v) Tween-20 for 1 min. A Zeiss Axioskop fluorescent microscope equipped with single band-pass filters was used to evaluate the staining. The microscope allows visualization of six fluorochromes: Dapi, Green spectrum, Red spectrum, FarRed Spectrum, Aqua Spectrum and Gold Spectrum. To evaluate the staining, images were captured using a SmartCapture and SmartType imaging system (Digital scientific). 50 cells were scored for the presence of chromosomal abnormalities and re-analysed by Dr D Ladon, Cytogenetics Department, King's College Hospital.

2.10 DNA damage assay

Cells were transfected with control siRNA or with siRNA against SEC13 or AND1 mRNA, as in section 2.4.1. After stimulation for 72 h with PMA/Ionomycin, Cytospin slides were prepared using the Shandon Cytospin 4 (Thermo) using poly-lysine slides with approximately 100,000 cells per slide. Cells were fixed with 4% (w/v) paraformaldehyde in PBS for 15 min at room temperature and washed Slides were blocked in 10% (w/v) BSA and in PBS/0.1% (v/v) Tween-20 for 30 min at room temperature, before incubation with the appropriate primary antibody. Primary antibodies were diluted in blocking solution at 1/50 and slides were incubated overnight at 4℃. Slides were then washed three tim es in 1 % BSA (w/v) /PBS/0.1% (v/v) Tween-20 for 5 min each. Fluorochrome-conjugated secondary antibodies were diluted 1/200 in blocking solution and then added to the slides. Slides were incubated 1 h at room temperature before being washed as above. Cells were counterstained with DNA stain (DAPI) and rinsed in PBS. Slides were mounted using Mowiol and analysed with an fluorescence microscope with DAPI/FITC/TRITC triple pass filters. Between 50-100 cells were examined per sample for the presence of nuclear foci. Cells with more than 5 foci per nucleus were considered to be positively stained.

2.11 Detergent removal for MS analysis

Before analysing the CSK- extracted (section 2.6.4) or chromatin-bound protein samples (section 2.6.5) by mass spectrometry, residual detergents were removed.

Residual detergents carried over from the protein extraction procedures used affect mass spectrometry analyses and decrease the sensitivity of peptide detection. Three different methods (Orgosol DetergentOut, Pierce detergent removal columns, filter-aided sample preparation) were investigated for their efficiency of removing residual detergent.

2.11.1. OrgoSol DetergentOUT detergent removal system

The OrgoSol DetergentOUT Detergent removal kit (G-Biosciences) was used according to the manufacturer's instructions. The entire procedure was performed on ice and all reagents were pre-cooled. The components of the kit are confidential. The OrgoSol buffer was kept at -20℃ for at least 1 h prior to use.

Up to 100µl Hela or T cell lysate samples containing 0.1% (v/v) NP40, 0.1% (w/v) SDS or 1% (w/v) SDS or without detergent were mixed with 300 µl UPPA-I and the mixture was vortexed. 300µl UPPA-II for every 100µl of original protein solution was added and vortexed. The tubes were positioned with the cap-hinge facing outward and centrifuged at 15000 x g_{max} for 5 min to form a tight pellet. Immediately after centrifugation, the entire supernatant was removed carefully and without disturbing the pellet. The centrifuge tube was again positioned with the cap-hinge facing outward and centrifuged for 30 sec at 15000 x g_{max} and the remaining supernatant was removed. 40µl of DO wash was added on the top of the pellet. The pellet was washed 3-4 times by pouring the wash solution over the pellet without disturbing it. The tube was carefully positioned in the centrifuge as before and centrifuged for 5 min at 15000 x g_{max} and the wash solution was discarded. 25µl deionized water was added and vortexed. For every 100µl - 300µl initial protein solution, 1 ml of pre-chilled OrgoSol Buffer and 5µl Seed solution were added. The solution was vortexed to resuspend the pellet. The tube was incubated at -20℃ for 30 min with periodical vortexing. After incubation, the pellet was centrifuged at 15000 x g_{max} for 5min to form a tight pellet. The supernatant was removed and discarded and the visible white pellet in the tube was air-dried until it turned translucent. The dried pellet was resuspended in 40µl of DO Prep-Buffer-I, vortexed to suspend the pellet and incubated for 5min on ice. For each 5 µl DO Prep buffer-I used, 1µl of DO Prep

buffer–II was added and incubated for 5min on ice. After the pellet dissolved, the protein solution was digested with Trypsin as described in 2.12.1 and the samples were analysed by LCMS/MS using the LTQ-Orbitrap mass spectrometer.

2.11.2. Pierce detergent removal spin columns

To equilibrate the Pierce Detergent Removal Spin columns, the bottom closure from each column was removed and the cap was loosened. The column was placed into a 2 ml collection tube. The column was centrifuged at 1500 x g_{max} for 1 min to remove the storage solution. The column was washed by adding 500 µl of MS buffer C and centrifuged at 1500 x g_{max} for 1 min. The buffer was discarded and this step was repeated twice more. After the washes, the column was placed in a new collection tube. The sample solution was slowly applied to the top of the compact resin bed and incubated for 2 min at room temperature. The tube was centrifuged at 1500 x g_{max} for 2 min to collect the eluted sample (detergent-free sample). The column was then discarded. The protein solution was digested with trypsin as described in 2.12.1 and analysed by LCMS/MS.

2.11.3. Filter-Aided Sample Preparation (FASP) detergent removal

Up to 50 µl of protein extract was mixed with 200µl of urea buffer in the Ambion ultra (0.5 ml) centrifugal filter unit with 10kDa cut-off and centrifuged at 14000x g_{max} for 20 min. The flow-through was discarded from the collection tube. 200µl of UB with 10 µl of 10 x Iodoacetamide stock solution was added to the protein solution on the filter unit, mixed by pipetting up and down and centrifuged at 14000 x g_{max} for 20 min. 200µl of UB was added to the filter unit and centrifuged at 14000 x g_{max} for 20min. This step was repeated once more. To recover the sample, the spin column was centrifuged upside down in a clean tube for 2 min at 1000 x g_{max}. The 20µl recovered protein sample was diluted from 8M Urea in 20µl to 1M Urea by adding 120µl of 40mM Tris-HCl, pH 8.0, followed by Trypsin digestion as in 2.12.1. The samples were then analysed by LCMS/MS.

2.12 Mass spectrometry

2.12.1. Trypsin digest for mass spectrometry analysis

Protein extracts to be analysed by mass spectrometry were first prepared as in 2.6.4 or 2.6.5. Detergents were removed from the samples as described in 2.11 before digesting the proteins into peptides with Trypsin.

Protein samples, from which the detergent had been removed using the FASP method (section 2.11.3), were digested with Trypsin by adding 20µl of 0.4µg/µl Trypsin (Proteomics Grade) to 120µl protein solution. The mixture was incubated at 37℃ for 4-5h. To stop the digestion, 1.6µl formic acid was added (1 % (v/v) final concentration). The sample was then frozen at -80℃. Next day, the sample was dried to 10-20µl using a Speed Vac and diluted to 150µl with MS buffer C. The samples were purified from salts and urea using C18 tips prior to analysis of mass spectrometry, as described in section 2.12.2.

Protein samples from which detergent was removed with Orgosol DetergentOut (Chaper 2.11.1) or Pierce spin columns (section 2.11.2) were denatured by adding 50µl Trifluorethanol (TFE) (50% v/v) to 50µl detergent-free protein sample (1-2mg/ml protein concentration) and vortexed. Proteins were reduced by adding 5 µl of 200mM DTT (final concentration 10-15mM) and heating to 56℃ for 45 min. The samples were cooled to room temperature (5 min). Proteins were then alkylated by adding 12µl of 550mM Iodoacetamide (IAA) to a final concentration of 55mM and incubated in the dark at room temperature for 30 min. The samples were diluted 10-fold with digestion buffer by adding 885µl of 50mM Tris-HCl, pH 7.8 and 2mM $CaCl_2$ to reduce the TFE concentration to 5% (v/v). 20µl of 0.1µg/µl Proteomics Grade Trypsin was added (the final concentration of Trypsin: protein is 1:25 – 1:50). The samples were incubated at 37℃ for 4-5 h. To stop the reaction, 10 µl of formic acid (to 1% (v/v) in total) was added and samples were frozen at -80℃. The frozen samples were defrosted to room temperature and dried with a Speed Vac for 4-5 h to a final volume of 10-20µl. The samples were made up to 150µl with MS Buffer C

(95% H_2O, 5% (v/v) Acetonitrile (ACN), 0.1% (v/v) formic acid) and the samples were further prepared as in section 2.12.2.

2.12.2. Sample preparation for mass spectrometry (MS) analysis

Prior to MS analysis, the protein samples digested with Trypsin were purified of contaminants (small molecules, salts) by reverse phase chromatography on Hypersep C18 tips. The C18 resin was washed three times with 50µl of 60% (v/v) Acetonitrile solution (60% of MS Buffer B, 40 % MS Buffer A) followed by three washes with 50% of MS Buffer A. The sample was loaded on the resin. The resin was then washed three times with 50µl of MS Buffer A. The sample was eluted with 50µl of 60% (v/v) Acetonitrile solution in 100µl.

All samples were dried to 10-20µl with a Speed Vac (approximately 20 min) and resuspended in 100µl of MS Buffer C (approximately 120µl in total). The sample was filtered using Microcon 10kDa spin tubes and centrifuged at 14000 x g_{max} for 30 min at 4℃ to filter out undigested proteins. An additional 20µl of MS buffer C was added and the filter was centrifuged for an additional 15 min. The filter was discarded and samples were stored in -20℃ until MS analysis.

2.12.3. Mass spectrometry analysis

Mass spectrometry analyses of the cleaned up peptide samples were carried out using a Surveyor Plus HPLC system connected to an LTQ-Orbitrap or Velos-Orbitrap mass spectrometers (Thermo Scientific). Mass spectrometry runs were performed together with Dr. Daniel Boutz in Prof. Marcotte's laboratory. For the mass spectrometry analyses using the LTQ-Orbitrap, Tryptic peptide mixtures were separated online by reverse phase chromatography on a Zorbax C18 column. The separation of peptides was accomplished by running a 5-38% (v/v) ACN gradient over 230 min. Three injections were carried out per sample. Eluted peptides were directly injected by electrospray ionization into the LTQ-Orbitrap equipped with a nano-spray ion source for analysis. Full parent spectra (MS1) were collected at 60,000 resolution. Ion fragmentation spectra (MS2) were collected in a data-

dependent manner, with ions required to carry +2 or greater charge for MS2 selection. The top 12 most intense qualifying peaks were selected per round, with peaks selected twice within 30 s excluded from selection for 45 s to avoid the detection of only the most abundant peptide in the time period. Data was analysed using the Sequest search algorithm within the Proteome Discoverer 1.3 software package (Thermo). Sequest is a tandem mass spectrometry data analysis program, which allows identification of tandem mass spectra to tryptic peptide sequences that have been generated from databases of protein sequences. The spectra were searched against the non-redundant Ensembl v64 Homo sapiens (NCBI36) protein-coding data set. Results were filtered at 1% false discovery rate by Percolator (53).

Additionally, selected samples were analysed using a Dionex Ultimate 3000 RSLCnano HPLC system connected to an Orbitrap Velos Pro mass spectrometer (Thermo Scientific). Details of the analyses are identical to the LTQ-Orbitrap, with the following exceptions: Tryptic peptide mixtures were separated online by reverse phase chromatography on an Acclaim PepMap RSLC C18 column (Dionex). The separation of peptides was accomplished by running a 5-40% (v/v) ACN gradient over 245 min. The top 20 most intense qualifying peaks were selected per round.

For each biological replicate fraction, LC-MS/MS injections analysed independently were merged, with spectral counts summed within each replicate set. All data sets were aligned, and proteins observed in only one biological replicate fraction were removed. Keratins were also removed from the data set. To account for the occurrence of degenerate peptides assigned to multiple proteins, proteins were grouped using the Proteome Discoverer software. Protein groups consisted of the smallest set of proteins needed to account for non-unique peptide identifications, whereby all group members shared equal evidence of occurrence.

2.12.4. Statistical methods

Statistical analyses used in Chapter 3. FRET histograms were fitted to Gaussians to calculate mean and standard deviation (SD) values for each condition with or without target cells. *P* values are from unpaired, two-tailed Student's *t* tests performed for each condition (siRNA, LFA-1-blocking mAb or inhibitor) to compare NK cells in the presence or absence of target cells with *n* values from each experiment.

Statistical analysis in Chapter 4. The mean percentage of Sec13-or And1-siRNA transfected cells in each cell cycle phase was analysed by calculating the average and standard deviation. The p-values were calculated for control and Sec13- or And1-siRNA transfected cells using a paired, two-tailed Student's *t* test.

Statistical analysis in Chapters 5 and 6. Proteins were quantified by comparison of spectral counts, as described in (233). In summary, frequencies of observations were calculated by comparing the frequencies for control and Mcm7-depleted samples to determine the statistical significance of relative abundance. A *Z*-score of ±1.96, corresponding to a *P*-value <0.05, was used as a determinant of significance in the stringent analyses or a *Z*-score of ±1.65, corresponding to a *P*-value <0.1, was used as a determinant of significance in the relaxed analyses. Composite *Z*-scores for control and Mcm7-depleted samples were then calculated from the individual *Z*-scores for each biological replicate. Fold-change was calculated as a ratio of frequencies of observations for each protein in the control and Mcm7-depleted samples. For each protein, a pseudo-count of 1 was added to each spectral count total prior to frequency calculations in order to adjust for proteins with zero-count.

Chapter 3

3. Application of a novel strategy to identify regulators of NK cells at the immunological synapse

3.1 Introduction

Natural killer cells are of functional importance in the immune system, but our knowledge of the signalling pathways that are involved in immunological responses of NK cells is incomplete. The aim of the study presented in this chapter is to identify new regulators of a signalling pathway in NK cells and to do this by applying a novel strategy, described below.

3.1.1. NK immune surveillance

NK cells are a major component of the innate immune system that play an important role in defences against pathogens, such as viruses and also cancerous cells (60). An important feature of NK cells is their cytotoxic function *via* the formation of an immunological synapse that enables cytolytic activity against target cells (210, 286). In the context of leukaemias, NK cells have been shown to be dysfunctional in acute and chronic myeloid leukaemias (AML and CML) and NK cell inhibition is associated with a poor patient outcome (251, 335). Nevertheless, donor NK cells have a therapeutic application in leukaemias, as demonstrated for instance by studies of allogeneic bone marrow transplantation and new therapies based on manipulating the activation or inhibition of NK cells (87, 176, 335). For example, CD80/Interleukin 2 lentivirus-transduced AML cells promote NK cell activation and cytolytic activity (176). Moreover, there are data from clinical studies of bone marrow transplantation which propose that preventing NK cell inhibition by human leukocyte antigen class I can promote graft-versus-leukaemia effects and reduce graft-versus-host disease in AML and CML (335). In the field of immunology there are a number of examples of the importance of NK cells in the immune system and in NK immune surveillance, such as using modified NK cell receptors to target patients' T cells against their own tumour cells (335). However, to induce an effective response, a number of changes have to occur in the immune system during NK cell:target cell interaction, such as adhesion to the target cell,

polarisation of the microtubule organisation centre and release of cytotoxic granules towards the target cells.

One major and crucial process involved in the NK:target cell interaction is the reorganisation of the cytoskeleton in the NK cells (66, 419). Cdc42 is a protein that is known to be involved in cytoskeleton rearrangements and it is a good candidate for integrating both positive and negative signals to induce an effective response. This protein is a small GTPase (310, 383) and its activation leads to binding of GTP. This activated form is able to induce *de novo* gene transcription, induction of anti-apoptosis pathways, membrane trafficking and changes in cell morphology (117).

3.1.2. An assay for measuring Cdc42 activity

In order to investigate the role of Cdc42 activation in cellular functions, there is a need to be able to analyse the biological activity of Cdc42. Cdc42 activity in cells can be analysed effectively using the Förster resonance energy transfer (FRET) Cdc42-biosensor (178, 427) and quantified by fluorescence lifetime imaging measurement (FLIM). This Cdc42-biosensor was modified in Professor Tony Ng's laboratory to be suitable for FRET quantification (Figure 3.1.2 A) and it has been used recently for imaging Cdc42 biological activity in T cells by FRET-FLIM (236). In the biosensor, Cdc42 is linked to the red fluorescent protein (RFP) and to a fragment of Pak1 that is a target for activated Cdc42 (203). Pak1 is further linked to the green fluorescent protein (GFP). In an inactive Cdc42 state, the biosensor is in an open conformation (inactive biosensor). When Cdc42 becomes activated, it binds to the Pak1 domain, which results in a change in conformation of the fusion protein and enables the two fluorophores to come into close proximity (<10nm (active biosensor)) (Figure 3.1.2 A). Physically, when EGFP is excited with photons of a specific wavelength, the energy absorbed by EGFP is transferred to RFP. This change in the fluorescence intensity of EGFP can be measured as a decrease in the fluorescence lifetime and this is correlated with a higher FRET efficiency (Figure 3.1.2 B). Measurement of the FRET efficiency is therefore a surrogate readout of Cdc42 activity.

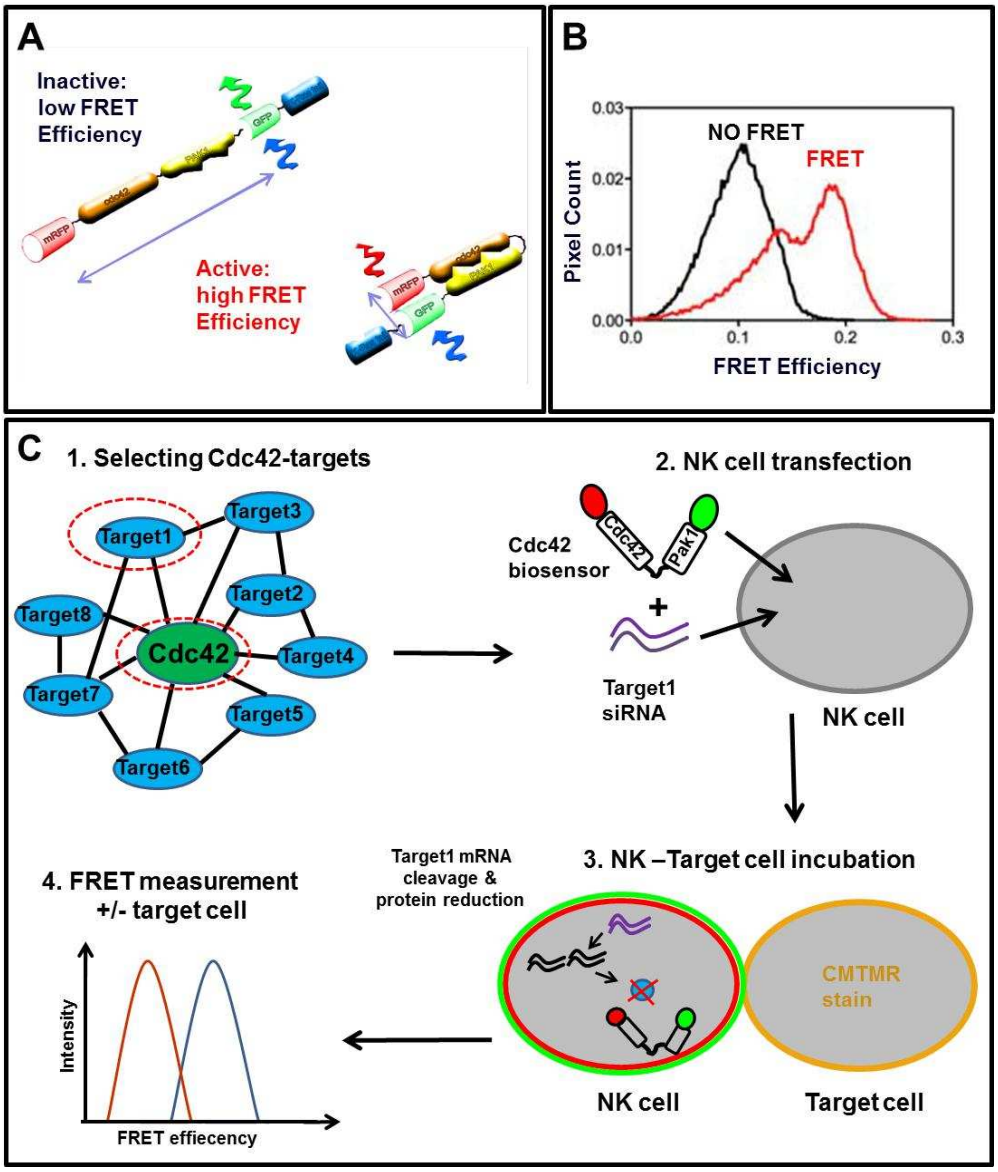

Figure 3.1.2 Experimental approach to measure Cdc42 activity.

A. The Cdc42-biosensor was used to measure Cdc42 activity as described in 3.1.2. B. Cdc42 activity was determined by measuring changes in the FRET efficiency. C. Schematic representation of the experimental approach to investigate predicted targets using an siRNA screen and FLIM-FRET imaging. 1. A specific target from the predicted Cdc42 interaction network was selected for validation. 2. The siRNA against the target, together with the plasmid encoding the Cdc42-biosensor were transfected into NK cells and the cells were cultured for 24 h to allow the downregulation of the target and expression of the encoded biosensor protein. 3. Transfected NK cells were allowed to interact with or without target cells (labeled with CMTMR). 4 The Cdc42 activity was measured in NK:target cell conjugates or NK cells alone by FLIM microscopy.

3.1.3. Experimental approach

The aim of this study is to identify new regulators of the Cdc42 signalling pathway in NK cells using a novel strategy. This strategy involves bioinformatic prediction of targets and a targeted siRNA screen, with a read-out of Cdc42 activity using the Cdc42-biosensor and FRET-FLIM quantification. The experimental approach is represented by the schema in Figure 3.1.2 C.

To predict crucial proteins that regulate Cdc42 activity, protein reference databases (http://www.hprd.org/ and http://ipfam.sanger.ac.uk/) were used to select crucial candidate proteins that were predicted to interact with Cdc42. These predictions were filtered to only include RhoGEFs, RhoGAPs and proteins containing a kinase domain. Based on these filtered predictions, a Cdc42-specific protein:protein interaction network was formed. In it, Cdc42 forms the core of the network and it is predicted to interact with 13 different proteins (Figure 3.1.2 C, step 1). This network formed the basis for selecting targets for an siRNA screen. To validate each of the targets for its potential role in regulating Cdc42, the network was perturbed by downregulating each of the target proteins in the NK cell line YTS and then Cdc42 activity was measured using the Cdc42-biosensor. This was achieved by transfecting the siRNA against a specific target together with the plasmid encoding the Cdc42-biosensor into the YTS cell line (Figure 3.1.2 C, step 2). The transfected YTS cells were left in culture for 24 h to allow the expression of the encoded Cdc42-biosensor protein as well as downregulation of the target protein. NK cells were then incubated with target cells to allow NK:target cell conjugates to form (Figure 3.1.2 C, step 3). Prior to NK:target cell conjugation, the target cells were stained with the CMTMR dye to be able to distinguish between NK and target cells during imaging. After staining the target cells for 5 minutes, the cells were washed and conjugated with NK cells in a 1:1 NK:target cell ratio for 15 minutes. Following conjugation, the cells were fixed on microscopy slides and the FRET efficiency of the Cdc42 biosensor in the NK cells was measured by FLIM. This assay was carried out in the presence or absence of the target cells. (Figure 3.1.2 C, step 4). The objective of this study is to identify which of the predicted proteins affect Cdc42

activity in NK cells during NK:target cell interaction and to determine whether any of these proteins are required for NK cell activity.

3.2 Results

3.2.1. Cdc42 activity oscillates during NK immune surveillance

With the objective of gaining a deeper understanding about the role of Cdc42 in the NK immunological synapse, Cdc42 activity was imaged in human NK cells using the Cdc42-biosensor described in section 3.1.2. and quantified by FLIM. A plasmid encoding the Cdc42-biosensor was transfected into the NK cell line YTS, which were then allowed to interact with the target cell line 721.221. This target cell line is an EBV-transformed B cell line (http://bio.lonza.com/no_cache/extras/cell-transfection-database/cell-details/cell/176/) and is a good killing target for YTS cells used by many research groups (for example (386)). Live cell imaging experiments were carried out previously in Prof. Ng's laboratory with YTS NK cells interacting with 721.221 target cells. It was shown that Cdc42 activity in the YTS NK cell line in contact with a target cell oscillates, after an initial increase in Cdc42 activity (Figure 3.2.1 A, upper panel, + Target Cells). When YTS cells were imaged in the absence of 721.221 cells, there was no increase in Cdc42 activity and no oscillation was observed (Figure 3.2.1 A, upper panel, - Target Cells). The mean periodicity of the Cdc42 activity was calculated to be 300-350 seconds for five independent NK:target cell interactions (Figure 3.2.1 B). The oscillation could occur either throughout the cell or specifically at the site of NK:target cell contact. To investigate this, the analysis was performed on the whole conjugate or at the immunological synapse alone (Figure 3.2.1 A, + Target cells, #1 and #2). When the site of cell:cell contact was analysed in isolation, Cdc42 oscillation was still present at the individual immunological synapse with a periodicity of 304±25 seconds. These data indicate that the Cdc42 activity does not occur throughout the whole cell, but rather occurs specifically at the site of NK:target cell interaction.

Taken together, these results indicate that Cdc42 activity is regulated by upstream and downstream signalling proteins in response to NK:target cell contact, and a

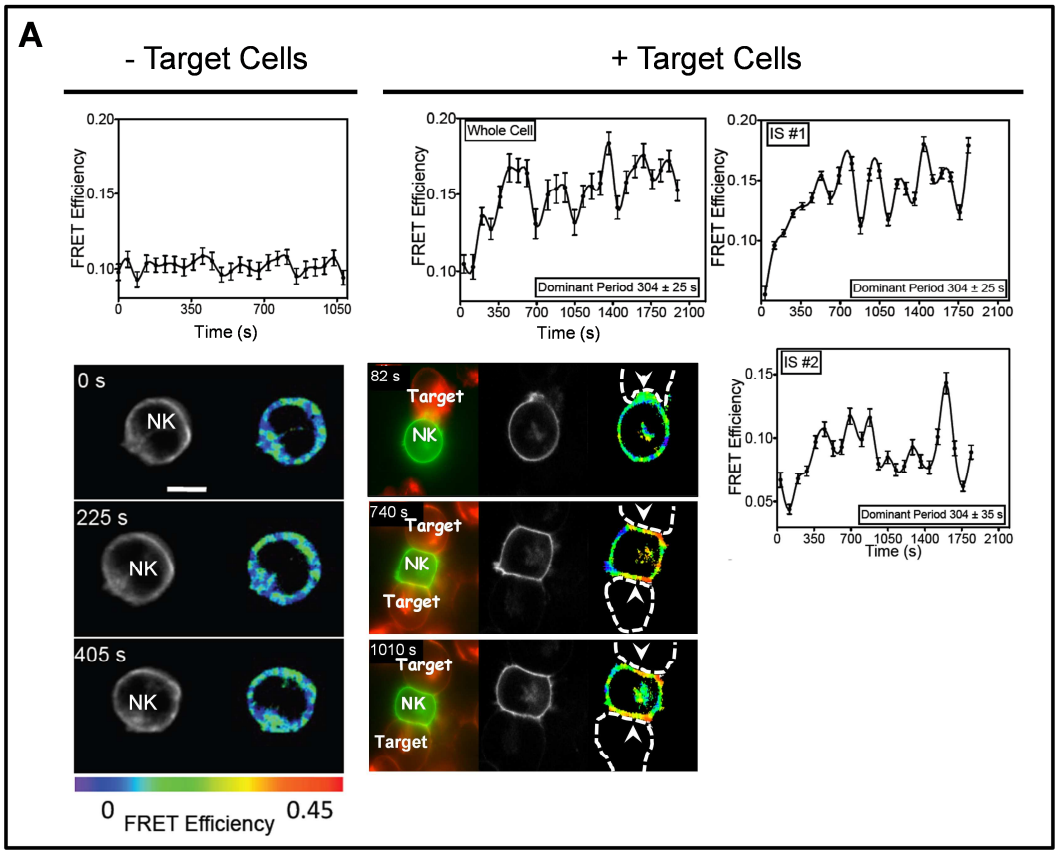
A
- Target Cells
+ Target Cells
FRET Efficiency
Time (s)
Whole Cell
Dominant Period 304 ± 25 s
IS #1
Dominant Period 304 ± 25 s
IS #2
Dominant Period 304 ± 35 s
0 s
225 s
405 s
82 s
740 s
1010 s
NK
Target
0 FRET Efficiency 0.45

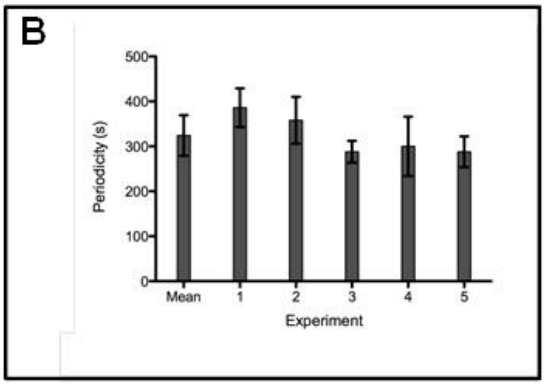
B
Periodicity (s)
Mean
1
2
3
4
5
Experiment

Figure 3.2.1 Cdc42 activity increases and oscillates during NK:target cell interaction. A. Upper panels: The mean FRET efficiency plotted over time from time-lapse FLIM for YTS NK cells expressing the Cdc42-biosensor with or without target cells (upper panels). FRET efficiency plots *versus* time are shown for one whole NK cell or for the immunological synapse alone of two NK cells in contact with a 721.221 target cell (IS#1 and IS#2). Lower panels: Representative snapshots from time-lapse experiments quantified in the upper panels. Left to right: epifluorescence images of EGFP (green) and DiD (red; a membrane dye to identify target cells), multiphoton EGFP intensity image (grey), FLIM map of Cdc42-biosensor FRET efficiency shown in the FRET efficiency scale from 0 - 0.45 at the bottom. White arrows indicate areas where the NK and target cells come into contact. B. The analysis was carried out for five separate Cdc42-biosensor NK:target cell conjugates. The dominant periodicity was determined to be 300-350 seconds. (Data from Dr. Leo Carlin, Randall Division, KCL).

feedback mechanism might be involved in regulating Cdc42 activity. Identifying and characterizing the signalling molecules involved will give a better understanding of the mechanisms involved in Cdc42 regulation at the immunological synapse.

3.2.2. Bioinformatic approach to identify proteins which may regulate Cdc42 activity

Systems Biology approaches were applied to predict which signalling molecules affect Cdc42 activity. The bioinformatics methodology, developed by Dr. Franca Fraternali and Dr. Luis Fernandes, was used to identify proteins which interact with Cdc42 and to select candidates for a small interfering RNA screen. The first general network was generated based on proteins reported to interact with Cdc42 in the human protein reference database (HPRD) and based on prior knowledge about GEF, GAP and Cdc42 interacting proteins (Figure 3.2.2. upper network). The HPRD (195) currently has 36,500 protein-protein interactions annotated for 25,000 human proteins. The protein-protein interactions are broadly grouped in three categories: *in-vitro*, *in-vivo* and yeast-two-hybrid experiments. 60% of the annotated protein interactions are supported by a single experiment and 26% are supported by two or three experiments. This first network is based not only on direct interactors of Cdc42 (nearest neighbours), but also homo-dimeric interactions between the proteins themselves. This information was integrated with data from the PFAM (302) database, which contains information about the architecture of protein interaction domains. Protein-protein interactions can be defined as domain-domain interactions and further information was provided in IPFAM. IPFAM combines information about 3D structures and PFAM domains, whether a certain domain is reported to interact, whether it interacts with other domains or with itself and if this is reported in a 3D structure. In this manner a degree of confidence to each protein in the network can be assigned for the reported interaction. The primary sub-network is shown in Figure 3.2.2. The information from HPRD, iPFAM and PFAM were integrated to assign the interactions a degree of confidence. For example, if the domains of two proteins were likely to interact, according to the

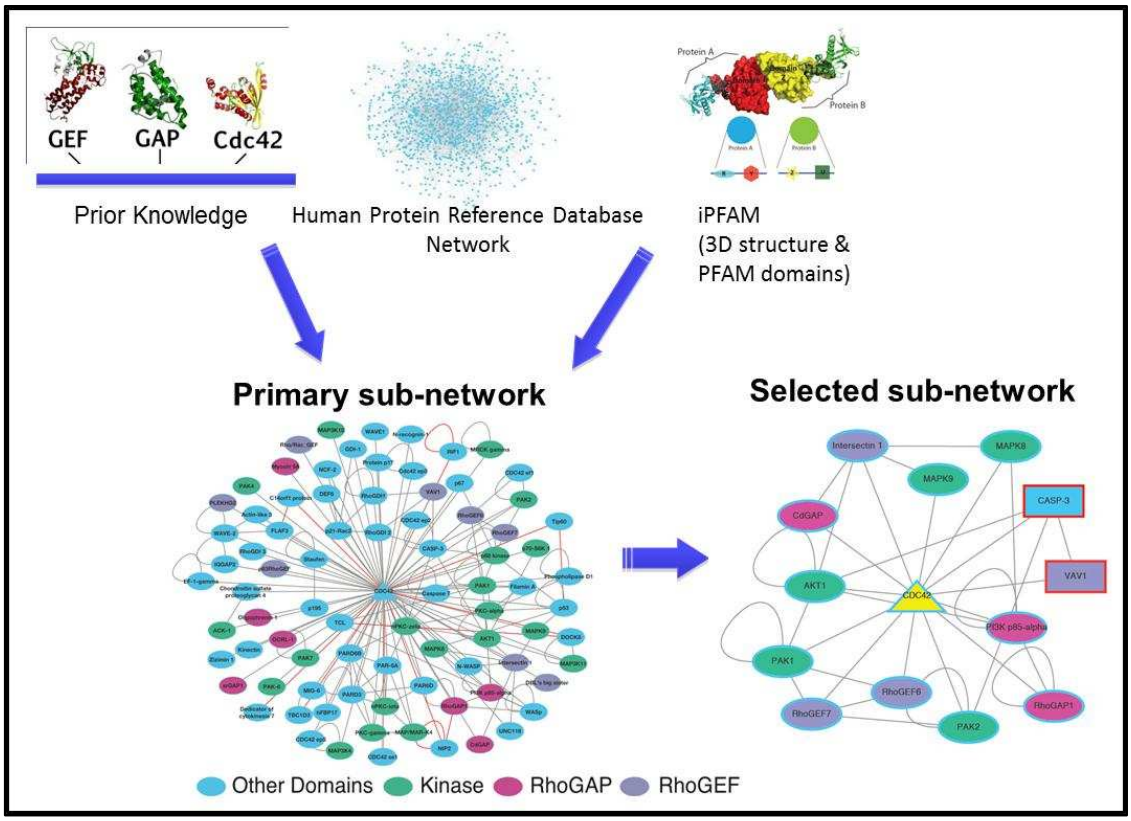

Figure 3.2.2 Generation of a Cdc42 protein interaction network to predict siRNA targets interacting with Cdc42.

First, a network was generated based on prior knowledge of GEF, GAP and Cdc42 interacting molecules using the human protein reference database (HPRD). This was further combined with information about 3D structure and domains from IPFAM. The databases were integrated to assign the interactions a degree of confidence. This master network was further refined to a Cdc42 sub-network by selecting only proteins with RhoGEF, RhoGAP or kinase domains and only those which were involved in a loop with Cdc42 were selected. Based on this approach, Cdc42 was predicted to interact with 13 different proteins. High confidence interactions are connected with black lines. Networks were generated according to methodology developed by Dr. Luis Fernandes and Dr. Franca Fraternali, KCL.

iPFAM, then a higher confidence was assigned to the interaction. However, if interacting proteins were reported without their interacting domains, a lower confidence was assigned to them. This first network was further refined to a Cdc42-specific network based on the assumption that Cdc42 exhibits oscillatory characteristics and that Cdc42 regulators form feed-back loops. Therefore, a Cdc42 specific network was constructed to include first only RhoGEFs, RhoGAPs and proteins containing a kinase domain, secondly, those which directly interact with Cdc42 and thirdly, only those which interact amongst themselves and are therefore in a loop with Cdc42. The evidence for each interaction is summarised in Table 3.2.2. In this network, Cdc42 is predicted to interact with 13 different proteins. Two additional proteins, Vav1 and Caspase1 were also added, even though they did not fulfil the strict criteria. Vav1 is a member of the Dbl family of guanine nucleotide exchange factors (GEF) (4) and Vav1 is important in haematopoiesis as it activates RhoA and Rac (20, 104). There is also evidence that Vav1 is linked to Cdc42 in T cells after CD28 co-stimulation (326). However, applying the stringent criteria described above, Vav1 would not fit into the 3-member loop. Because of the strong evidence for Vav1 interaction with Cdc42, the criteria were relaxed and Caspase1 was integrated into the network as it interacts with Cdc42 and Vav1 directly (163, 377). This network (Figure 3.2.2, network on the right) forms the basis for selecting targets for an siRNA screen. The objective is to identify which of the targets are required to regulate Cdc42 activity in NK cells, using the Cdc42-biosensor as readout.

Interactor A			Interactor B	
Name	**UniProt ID**	**Reference**	**Name**	**UniProt ID**
Akt1	P31749	(17, 96)	Akt1	P31749
Akt1	P31749	(13)	Pak1	Q13153
Akt1	P31749	(368)	p85α	P27986
Cdc42	P60953	(25)	RhoGEF6	Q15052
Cdc42	P60953	(404)	Mapk8	P45984
Cdc42	P60953	(404)	Mapk9	P45985
Cdc42	P60953	(404)	Akt1	P31749
Cdc42	P60953	(25)	RhoGEF7	Q14155
CdGAP	Q2M1Z3	(184)	Intersectin1	Q15811
CdGAP	Q2M1Z3	(213)	Cdc42	P60953
Intersectin1	Q15811	(404)	Mapk9	P45985
Intersectin1	Q15811	(170, 352)	Cdc42	P60953
Intersectin1	Q15811	(404)	Akt1	P31749
Intersectin1	Q15811	(404)	Mapk8	P45984
Mapk8	P45983	(198)	p85α	P27986
Pak1	Q13153	(24, 155, 190, 238, 295, 434)	Pak1	Q13153
Pak1	Q13153	(204, 239, 243)	Cdc2	P60953
Pak1	Q13153	(240)	RhoGEF6	Q15052
Pak2	Q13177	(190, 356)	Cdc42	P60953
Pak2	Q13177	(135, 401)	Pak2	Q13177
p85 α	P27986	(167, 389)	p85α	P27986
p85 α	P23986	(135, 401)	Cdc42	P60953
RhoGAP1	Q07960	(347)	Cdc42	P60953
RhoGAP1	Q07960	(232)	RhoGAP1	Qo7960
RhoGAP1	Q07960	(33)	p85α	P27986
RhoGEF6	Q15052	(315)	RhoGEF7	Q14155
RhoGEF7	Q14155	(343)	Pak2	Q13177
RhoGEF7	Q14155	(211, 264, 380)	Pak1	Q13153

Table 3.2.2. siRNA Targets

The table summarises the evidence for the interaction between the final selection of proteins with Cdc42 and amongst themselves. References are provided for each reported interaction.

3.2.3. Actin polarisation and Cdc42 activity in YTS NK immune surveillance can be reduced by monoclonal antibody blocking LFA-1

Before exploring potential effects of each of the predicted interacting proteins on Cdc42 activity, experiments were performed in Prof. Ng's laboratory to validate the specificity of the Cdc42-biosensor. A negative and a positive control were established for the screen by transfecting NK cells with the Cdc42-biosensor and staining the NK:target cell conjugate for F-actin with fluorescent Phalloidin to reveal actin accumulation at the synapse. Under normal conditions, a functional NK:target cell interaction causes actin accumulation at the synapse (Figure 3.2.3. A, left pair). This correlates with a higher FRET efficiency of the Cdc42-biosensor in an NK:target cell contact than in NK cells without target cells, meaning a higher energy transfer between EGFP and RFP of the Cdc42-biosensor due to activation of Cdc42 and interaction between Cdc42 and the Pak1 domain. Therefore there is an increased Cdc42 activity in an NK:target cell conjugate (Figure 3.2.3. B, left histogram). However, when the NK:target cell interaction was inhibited by blocking the intergrin LFA-1 with a blocking anti-LFA1 monoclonal antibody (mAb) (111), the phalloidin image shows that F-actin does not accumulate at the NK:target cell interface (Figure 3.2.3. A, right pair). This inhibition correlates with a reduction of Cdc42 biosensor FRET efficiency in the NK target cell conjugate to that of an NK cell alone (Figure 3.2.3.B, right histogram). Therefore a physiologically relevant antagonist of NK cell activity, which is known to inhibit Cdc42 causes a reduction of Cdc42-biosensor FRET efficiency. This system was therefore considered to be suitable for investigating whether any of the predicted protein candidates described in section 3.2.2 are required for Cdc42 activity by carrying out an siRNA screen and quantifying Cdc42 activity using the biosensor. The anti-LFA1 blocking antibody was used as a positive control for the primary screen of siRNA targets.

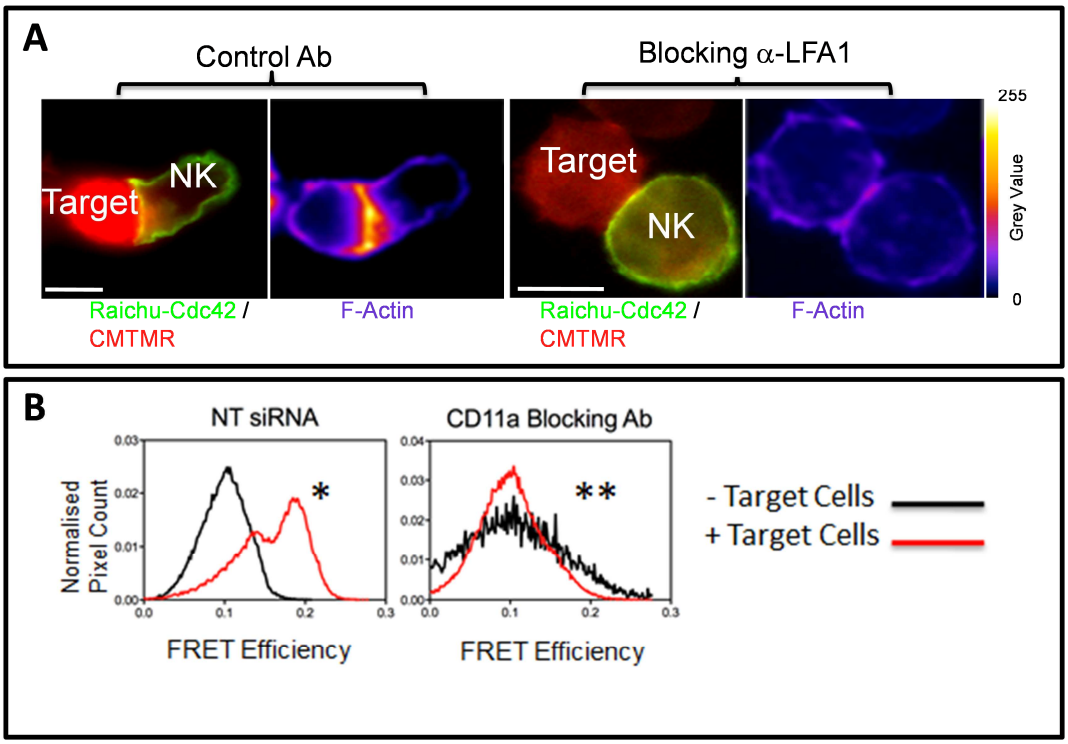

Figure 3.2.3 Anti-LFA1(CD11a)-mediated inhibition of synapse formation blocks Cdc42 activation.

A. Left panel of each pair: Epifluorescence images of EGFP from the Cdc42-biosensor (green) and CMTMR labelled target cells (red). Right panel of each pair: The corresponding Phalloidin images showing F-actin accumulation locally. For this, cells were fixed and stained for F-actin with fluorescent Phalloidin (purple/yellow) in the presence of an anti-LFA-1 antibody or control antibody. B. Pooled Cdc42-FRET efficiency histograms from 7-15 cells. NK:target cell conjugates blocked with LFA-1 monoclonal antibody or incubated with control IgG in the presence or absence of the target cell (*p≤0.005, **p≥0.6) (Experiment performed by Dr. Leo Carlin, KCL).

3.2.4. Analysis of the transfection efficiency of siRNA and the plasmid encoding the Cdc42-biosensor into YTS cells

In order for an siRNA screen of cellular regulators to be feasible, the majority of YTS cells should be transfectable with siRNA, and both siRNA and the plasmid encoding the Cdc42-biosensor need to enter the same cells. To investigate how many YTS cells become transfected with siRNA, FITC-labelled siRNA was used so that the uptake into YTS cells could be analysed by flow cytometry. The method used to transfect YTS cells was electroporation, which had been used previously in the laboratory. 89% of YTS cells transfected with FITC-labelled siRNA were positive (Figure 3.2.4 A). These data indicate that the majority of cells were transfected with siRNA, however the flow cytometry analyses do not prove that the siRNA entered the cells. Evidence for this is provided by depletion of mRNA targets described below in section 3.2.5. Next, it was investigated whether the siRNA concentration affects the transfection efficiency. Therefore, labelled-siRNA (FITC-siRNA or Alexa647-siRNA) was transfected at different concentrations. Viable YTS cells were gated on SSC/FSC and quantified in the FL1 channel for FITC staining. The data suggest increasing FITC-siRNA concentration from 8nM up to 480nM or the Alexa647-siRNA from 480nM to 960nM increases the transfection efficiency to 98% (Figure 3.2.4 B and C). For this reason, a concentration of siRNA of 480nM or more was used in subsequent experiments to validate the reduction of PI3K p85α and Akt1 protein levels by western blotting (section 3.2.7). Apart from this section, 120pmol of siRNA were used for experiments.

Next, I determined the percentage of YTS cells which are transfected with the plasmid encoding the Cdc42-biosensor. Since both siRNA and plasmid need to be co-transfected for the screen, the transfection method was the same as that used for transfecting the siRNA, described above. The YTS cells were transfected with the plasmid encoding the Cdc42 biosensor and cultured for 24 h or 48 h before analysis to allow the biosensor to be expressed. As estimated visually by fluorescence microscopy, fewer than 10% of cells expressed the Cdc42-biosensor. The percentage of cells expressing the Cdc42-biosensor was then quantified by

flow cytometry based on their GFP or/and RFP expression. Gates of forward scatter (FSC) and side scatter (SSC) parameters were set to analyse only the viable cells. The percentage of viable cells expressing the Cdc42-biosensor was determined by simultaneous detection of the 488nm (FITC) and 610nm (PE-Texas Red) detectors. Negative gates were set on non-transfected YTS cells (Figure 3.2.4. D, control). The transfection efficiency of the Cdc42-biosensor into YTS cells was 5-7% (Figure 3.2.4 D, Cdc42-biosensor; n= 2 experiments). No change was observed in the percentage of transfected cells 48 h after transfection as compared with 24 h and very few GFP- and RFP- positive cells were detectable after an additional 5 days in culture. Therefore, cells transiently transfected for 24 h were used in all further studies.

The experiments described above showed that YTS cells could be transfected with the plasmid encoding the Cdc42 biosensor, but at a relatively low efficiency. Therefore, I determined whether the transfected cells could be isolated by flow cytometric sorting. The GFP/RFP cells were sorted for maximum purity (FACS Canto, BD Biosciences) (thanks to Dr David Darling, KCL). Re-analysis of the sorted cells showed that 88% were GFP/RFP positive (Figure 3.2.4 E). Based on these experiments, it was estimated that 1000-4000 cells could be recovered, starting with 1 x 10^6 cells (0.05 Cdc42-biosensor-positive cells x 0.08 viable cells x 10^6 = 4000 cells). Sorting on two parameters simultaneously such as on RFP and GFP facilitates a clearer distinction of transfected from the majority of non-transfected and dead cells, despite the fact that for the Cdc42 biosensor there is no peak evident for the positive population based on either of the single parameters. However, this experiment also showed that it is not reasonable to sort sufficient cells for routine western blotting or RT-PCR experiments as sorting >1 x 10^5 cells would require too many starting cells and transfection reagents.

If 89% or more of the cells were transfected with targeting siRNA it ought to be possible to detect a change in the Cdc42-biosensor if the plasmid and siRNA enter the same cells, without having to isolate the transfected cells by sorting. To determine whether this is the case, the transfection efficiency of Alexa647-siRNA was determined when co-transfected with the Cdc42-biosensor plasmid. YTS cells

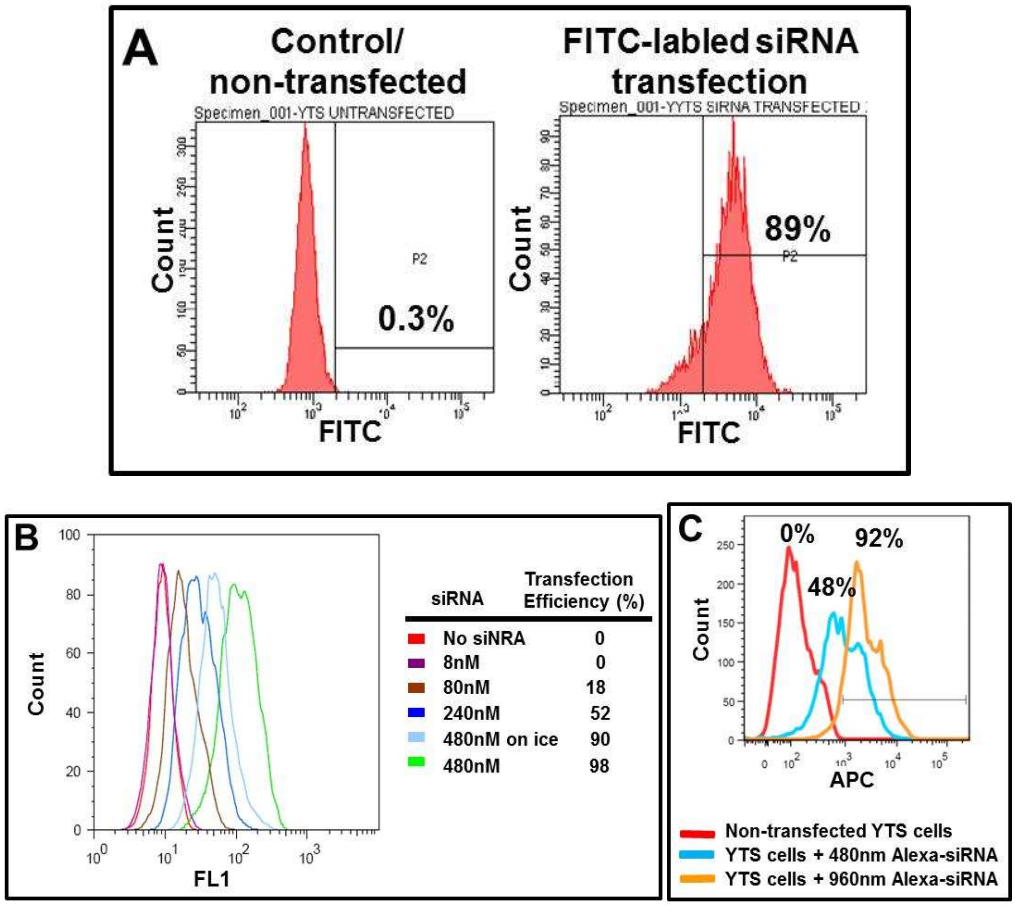

Figure 3.2.4 A-C Transfection efficiencies of labelled siRNA into YTS cells.

YTS cells were transfected with FITC-siRNA (FL1) (A and B) or Alexa647-siRNA (C). Non-transfected YTS cells were used as the control. 24 h post transfection, viable YTS cells were analysed by gating on FSC/SSC and the percentage of cells positive for FITC or Alexa647 was determined. A. YTS cells were transfected with FITC-labelled siRNA or not transfected. B FITC-siRNA titration from 8nM up to 480nM. C. Alexa647-siRNA transfection efficiencies at 480nM and 960nM.

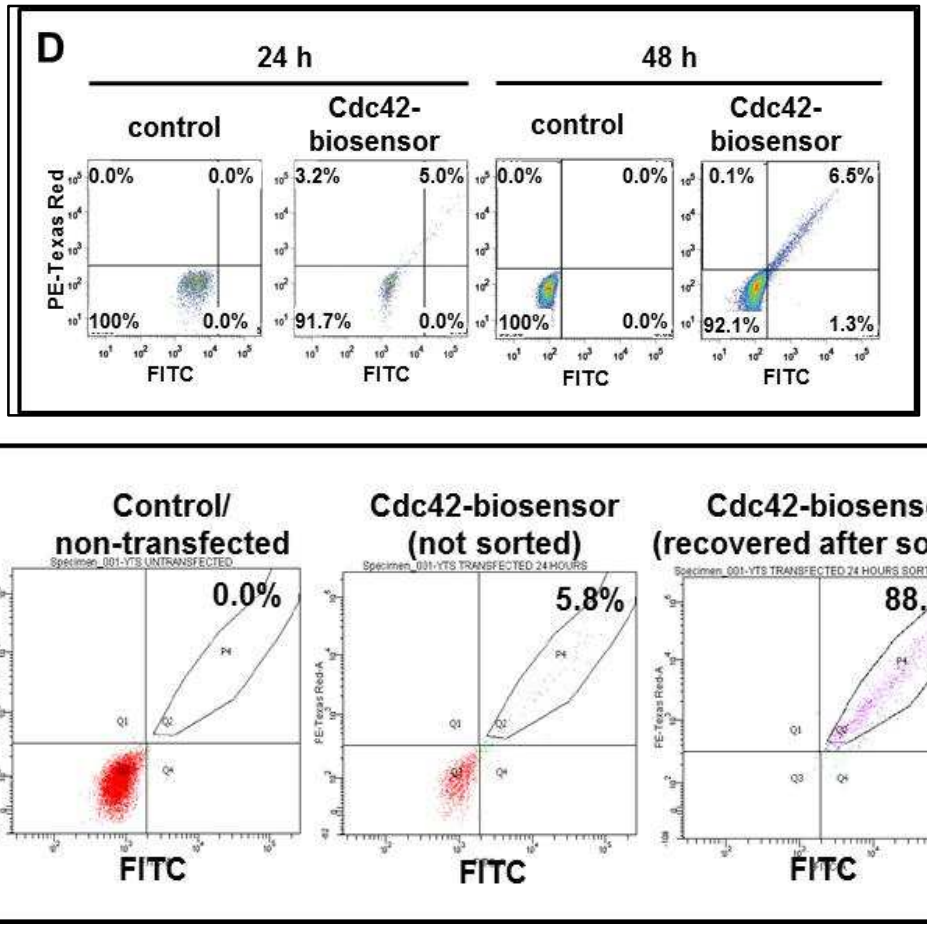

Figure 3.2.4 D-E Cdc42-biosensor transfection efficiencies into YTS cells.

YTS cells were transfected with the GFP-RFP-Cdc42-biosensor and analysed 24 h or 48 h after the transfection by flow cytometry. YTS cells were analysed by gating on FSC/SSC and the percentage of cells which were positive for GFP (FITC) and RFP (PE) was determined at the indicated time points. Non-transfected YTS cells were used as the control. D. Transfection efficiencies of the Cdc42-biosensor into YTS cells after 24 h or 48 h. E. YTS cells were cultured for 24 h after transfection with the plasmid encoding the Cdc42-biosensor and the cells were sorted based on GFP/RFP. The purity of the cells expressing the Cdc42-biosensor after sorting was determined.

were electroporated with Alexa647-labelled siRNA alone or together with the Cdc42-biosensor plasmid (used at the same concentrations as in previous experiments). In these series of experiments, 14% of YTS cells were Red3-positive (Figure 3.2.4. F; n= 3 experiments) and this was the same when the siRNA was co-transfected with the plasmid encoding the RFP-GFP-Cdc42-biosensor (Figure 3.2.4 F). This suggests that the transfection of the siRNA (Red3) together with the plasmid encoding the Cdc42-biosensor (FITC/TexasRed-PE) is the same as transfection of the siRNA alone and therefore that the transfection efficiency of the siRNA is not reduced in the presence of a plasmid encoding the Cdc42-biosensor. Furthermore, of the 15% siRNA-positive cells, 16% contained the Cdc42-biosensor. On the other hand, 8% of the cells express the plasmid encoding the Cdc42-biosensor and of those Cdc42-biosensor positive cells 40% contain Alexa647-siRNA (Figure 3.2.4 F).

The experiments in this section suggest that near 100% of YTS cells may be transfected with siRNA under the appropriate conditions. Furthermore, although only a small proportion of YTS cells are transfectable with a plasmid encoding the Cdc42-biosensor, 40% of these cells are also transfected with siRNA, as judged by flow cytometry. Because of the difficulty in detecting a discrete population of cells expressing the biosensor by flow cytometry, these experiments were not pursued further and it was decided to test whether co-transfection of any of the siRNA against the eleven targets identified in section 3.2.2 had a functional effect in the Cdc42-biosensor (see section 3.2.6).

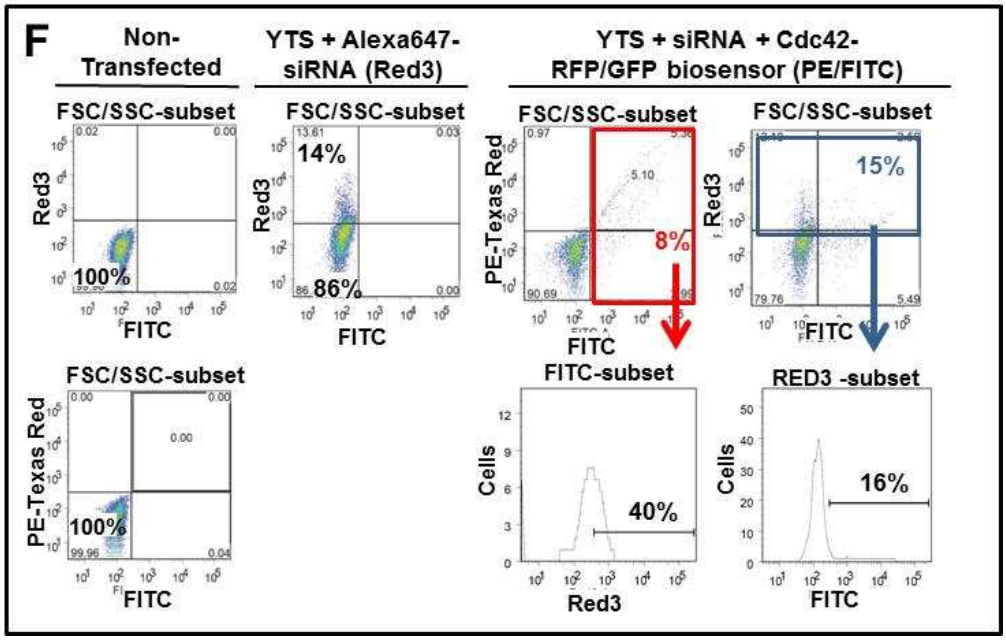

Figure 3.2.4 F Transfection efficiencies of the Cdc42-biosensor with the labeled siRNA into YTS cells.

YTS cells were transfected with just the Alexa647 siRNA (Red3) or with the Alexa647-siRNA (Red3) plus the plasmid encoding the Cdc42-GFP-RFP–biosensor (PE-Texas/FITC). Non-transfected YTS cells were used as the control. 24 h post-transfection, viable YTS cells were analysed by gating on FSC/SSC and the percentage of cells which were positive for siRNA (Red3) and Cdc42-biosensor (PE-Texas/FITC) was determined. PE-Texas Red-positive cells were gated (red line) and the percentage expressing siRNA (Red3) was determined. siRNA-positive cells were gated (blue line) and the percentage of FITC-siRNA transfected cells was determined; n = 3 experiments.

3.2.5. Investigation of mRNA down regulation of the 11 siRNA targets by quantitative real time PCR

The data in the previous section shows that FITC-siRNA might be taken up by the majority of YTS cells. The siRNA could either be inside the cells, bound to the plasma membrane or both. To determine whether an siRNA screen was feasible, YTS cells were transfected with siRNA to each of the eleven targets identified in section 3.2.2 and the mRNAs targeted were quantified by quantitative RT-PCR. YTS cells were transfected with the appropriate siRNA (siGenome On-Targetplus SMART pool, Dharmacon - see 2.4.3) as described above. The cells were then cultured for 24 h, total RNA was extracted, the RNA was reverse transcribed to cDNA, which was then used for real time PCR with either Taqman probes or Sybr green as a means of detection. The mRNA encoding Abl1 was also quantified as the endogenous control. Abl1 mRNA detection is established in the diagnostics laboratory in our Haematology Department using accredited primers and is used on a regular basis as a control for diagnosis assays of patients with leukaemias. It was used as the endogenous control to normalise signals obtained for each specific mRNA. The cDNA was amplified for a total of 40 cycles and a relative quantification analysis was performed for each mRNA compared with expression of mRNA encoding Abl1 using the CT method. First, the ΔCT value for each sample was determined by calculating the difference between the CT value of the target mRNA and the CT value of the endogenous reference (Abl1 mRNA). Next, the levels of each specific mRNA in siRNA-treated cells were compared with those in cells transfected with non-targeting siRNA by calculating the ΔΔCT. ΔΔCT was determined by subtracting the ΔCT value of each calibrator (non-targeting siRNA transfected cells) from the ΔCT value of the sample (siRNA transfected cells) and the normalized level of target mRNA expression was calculated using the formula described in chapter 2.3.6. In the analyses, the data were normalized to 1 for samples from cells transfected with the non-targeting siRNA.

Of the 11 siRNA tested, 9 caused a reduction of the corresponding mRNA target by 50% or more (Figure 3.2.5). The expression of mRNA encoding ITSN1 and CdGAP were not reduced by the siRNA and so these targets were excluded from further

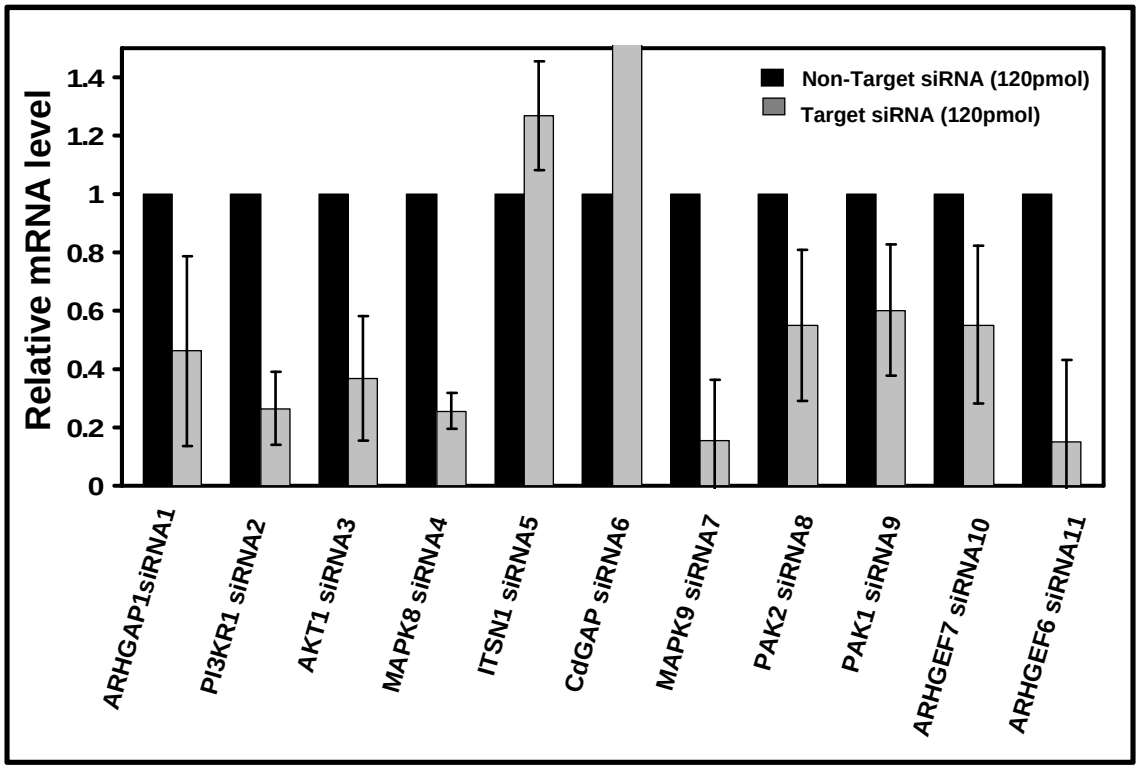

Figure 3.2.5 Quantitative real-time RT-PCR analyses of mRNA levels of each of the siRNA targets.

mRNA levels of siRNA-transfected YTS NK cells were normalised to the expression of Abl1 mRNA and the data for each specific mRNA were compared with that in cells transfected with non-targeting siRNA (normalised to 1). The relative mRNA level of the CdGAP mRNA is 10.1. The values plotted are mean±STDEV of triplicate analyses of a representative experiment from n=3 (quantitative RT-PCR; two with Taqman probes and one with Sybr Green).

analyses. The reasons for the relative increase in expression of their mRNA was not investigated further, but might be due to the design of the PCR primers or to relative changes in Abl1 mRNA.

3.2.6. FRET-FLIM analyses of Cdc42 activity after target protein downregulation by siRNA

The data in section 3.2.5 showed that mRNA for 9 of the 11 siRNA targets could be reduced by transfecting YTS cells with the appropriate siRNA. The flow cytometric analyses of YTS cells transfected with fluorochrome conjugated siRNA and the plasmid encoding the Cdc42-biosensor showed that siRNA was associated with or entered some of the cells expressing the Cdc42-biosensor (section 3.2.4). I investigated whether the reduction of mRNA encoding each of the siRNA targets resulted in a change in Cdc42-biosensor activity. YTS cells were co-transfected with the target-specific siRNA (siGenome On-*Targetplus* SMART pool, as for 3.2.5) or control (non-targeting) siRNA and a plasmid encoding the Cdc42-biosensor. After 24 h in culture, the transfected YTS cells were incubated for 15 min with or without 721.221 target cells that had previously been stained with CMTMR. The NK:target cell conjugates were fixed and imaged using FRET-FLIM. Based on the EGFP expressing YTS cells and CMTMR stained 721.221, cell conjugates were selected and epifluorescence images were recorded and analysed in ImageJ, as shown in Figure 3.2.6 A. Transfected YTS cells were visualised in the green channel for the expression of EGFP, whereas the 721.221 target cells stained with CMTMR were imaged in the red (G2A) filter channel. YTS-721.221 cells which formed tight conjugates were selected and multiphoton time-resolved EGFP images were acquired (middle column). TRI2 software (32) was used to generate the Cdc42-biosensor fluorescence lifetime histogram of thresholded area in the cell and the same scale for the lifetime was set for all cells measured (right column). For each cell imaged, an average Cdc42-biosensor lifetime histogram was determined for >5 cells per target sample. TRI2 data was extracted to Excel and the average lifetime for each cell is displayed as a histogram (Figure 3.2.6 B). In order to be able to compare the same Cdc42-biosensor lifetime ranges between different cells, Pixel intensities of different cells were normalised to the highest and lowest lifetime.

The individual histograms of several NK:target cell conjugates were then pooled to produce one averaged FRET histogram for each NK cell transfected with siRNA against the same target or with non-targeting siRNA. The same processing was performed for transfected YTS cells in the absence of 721.221 cells. This was done in order to be able to compare the average lifetime of NK cells alone or of an NK:target cell conjugate for each siRNA target (Figure 3.2.6 B). The lifetimes determined were used to convert them to FRET efficiency using the formula, E = 1-(tau da/tau d) where E is efficiency, tau is lifetime, d is EGFP alone and da is EGFP/RFP (*i.e.* Cdc42-biosensor). The average control GFP lifetime was 2.25 ns in the absence of RFP. Those values were multiplied by 100 to obtain the FRET percentages.

The final pooled histograms of FRET efficiencies were generated for YTS cells alone transfected with non-targeting or targeting siRNA and compared with FRET efficiencies of transfected YTS cells conjugated with 721.221 cells (Figure 3.2.6 C). The Cdc42-biosensor is known to exhibit a baseline FRET due to indefinite separation of the two fluorescent proteins when the biosensor is in an open conformation (178), and therefore the FRET efficiency will always be > 0 %, even if there is no Cdc42 activity. Treatment of YTS cells with blocking LFA-1 antibody in the presence of target cells was associated with a decrease in Cdc42 activity to the baseline established by imaging YTS cells alone. Therefore, the blocking LFA-1 mAb (described in section 3.2.3) served as a 'positive' control for the primary screen of siRNA targets. YTS cells alone transfected without siRNA had lower FRET efficiencies than YTS:target cell conjugates and were used as a negative control for the screen (*i.e*. YTS cells transfected without siRNA did not affect the increase in Cdc42-biosenor activity). An siRNA-reduced candidate was considered as a potentially important regulator of Cdc42 when the Cdc42 activity was reduced in a YTS:721.221 conjugate to be comparable with YTS cells alone. As described in 3.2.5, siRNA against CdGAP and ITSN were not included in the siRNA screen. Furthermore, because Vav1 and Caspase1 do not fulfill the strict criteria set out in section 3.2.2, it was decided that they should not be analysed further.

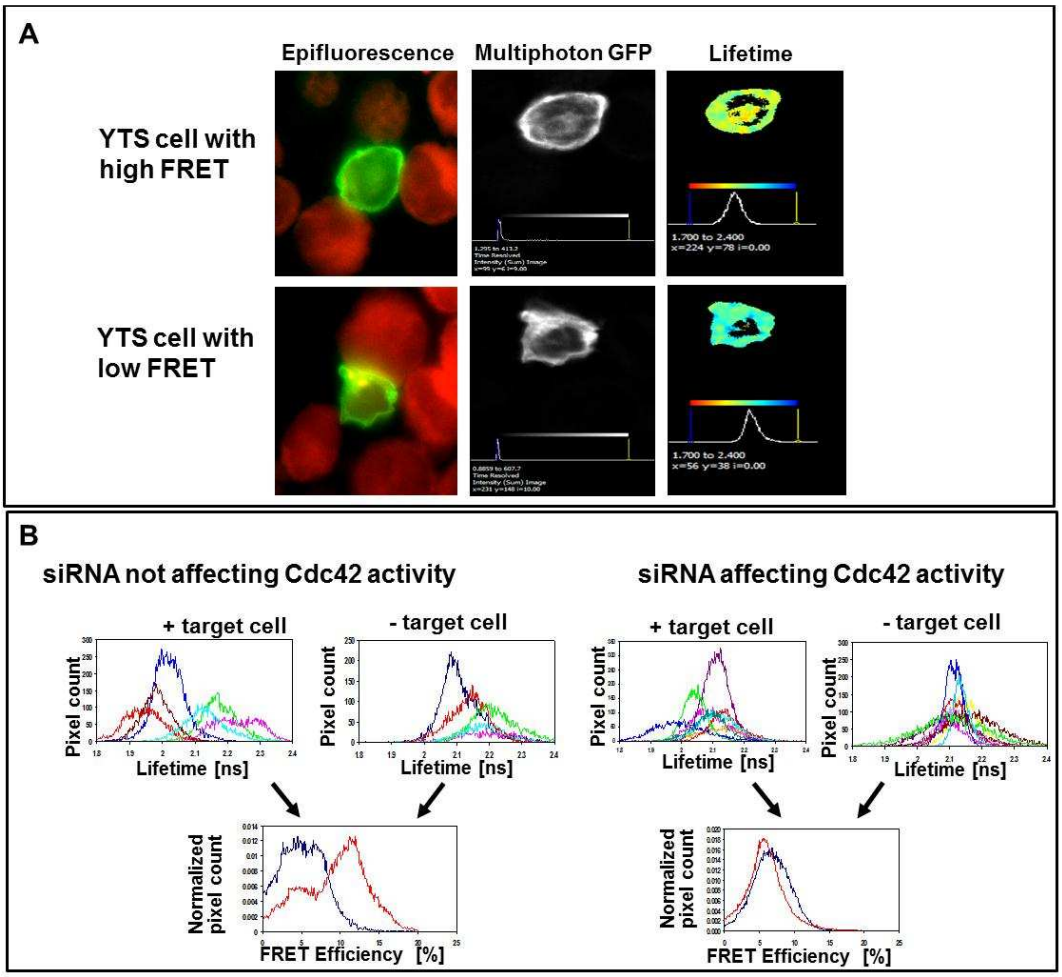

Figure 3.2.6 A and B FRET analysis of the Cdc42-biosensor after knockdown of targets by siRNA.

YTS cells were co-transfected with the plasmid encoding the Cdc42-biosensor together with targeting or non-targeting siRNA and YTS-target cell conjugates were analysed using multiphoton FLIM. A. Epifluorescence images of CMTMR-stained target cells (red) and Cdc42-biosensor expressing cells (green) (left column). Multiphoton EGFP images of selected cell-cell conjugates (middle column) and acquired lifetime images (right column) using TRI2 software. B. Acquired lifetime images were adjusted to the same lifetime scale and raw data was extracted for each cell measured and displayed in one histogram. Lifetime data from >5 cells in the presence or absence of target cells was averaged and normalized to the lowest and highest pixel intensity, resulting in one pooled histogram per siRNA in the presence or absence of target cells. In the final histogram, the lifetime was converted to percentage FRET efficiencies. Left panel: siRNA not affecting Cdc42 activity. Right panel: siRNA affecting Cdc42 activity. C. Resulting pooled histograms for different siRNA targeting mRNA in the presence or absence of target cells.

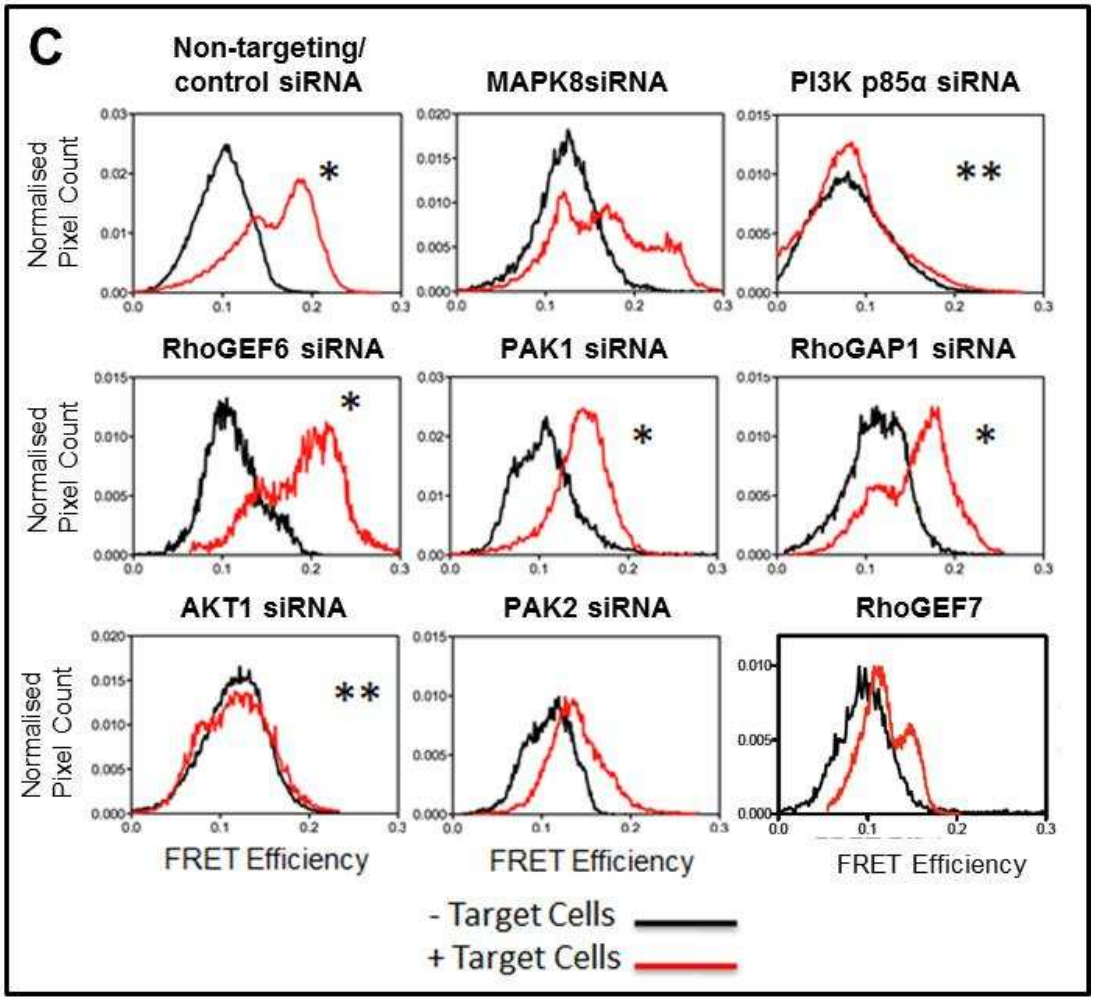

Figure 3.2.6 C Pooled Cdc42-biosensor FRET efficiency histograms.

Cells were fixed after 15 min of interaction with and without 721.221 target cells from 3 independent experiments, approximately 7-15 cells were analysed for each siRNA target. *p≤ 0.05 there is a significant difference in FRET efficiency between the NK cells with or without target cells in the presence of the siRNA. **p>0.6 there is no significant difference in FRET efficiency between the NK cells with or without target cells in the presence of the siRNA (unpaired two-tailed Student's *t* test).

Many of the targets of the different siRNA tested did not abrogate Cdc42 activity. However, transfection of siRNA against two putative candidates reduced the FRET efficiency of the Cdc42-biosensor to control levels. The siRNA against RhoGEF6, RhoGAP1 or Pak1 had little effect on Cdc42 activity, while siRNA against MAPK8 and RhoGEF7 had a heterogeneous effect. This heterogeneity in response might be explained by variable gene knockdown in different cells in the population, leading to an inconsistent reduction of the proteins and therefore to a non-significant statistical response. Alternatively, this heterogeneity in response might also be explained by interactions not directly related to Cdc42. Of all the potential targets, PI3KR1 and Akt1 were taken forward for further investigation and validation.

3.2.7. Validation of the reduction of PI3K p85α and Akt1 protein levels by western blotting

The data in section 3.2.6 show that transfecting YTS NK cells with siRNA targeting the mRNA encoding PI3K p85α or Akt1 had functional effects on the Cdc42-biosensor. Furthermore, work in section 3.2.5 showed that the mRNA encoding PI3K p85α and Akt1 were reduced in YTS NK cells transfected which each siRNA.

To investigate whether the PI3K p85α and Akt1 proteins are also reduced in YTS NK cells transfected with each specific siRNA, the protein levels were analysed by western blotting (WB). 1-2 x 10^6 YTS cells were transfected with targeting or non-targeting siRNA at a concentration of 250nM, 480nM or 960nM. After 24 h or 72 h cells were lysed and Western blotting analyses were carried out. Initially, a Triton lysis buffer was used, but since not all proteins are solubilised by this method, SDS- or LDS-lysis buffers were used in subsequent experiments. Proteins in each of the samples were separated by electrophoresis through polyacrylamide gels under denaturing conditions in the presence of DTT. The separated proteins were transferred to nitrocellulose membranes and probed with antibodies against Akt1 and PI3K p85 as well as high and low molecular weight loading controls, such as pRb and Cdc2.

The best and most clear knockdown of Akt1 protein was observed after YTS cells transfected with 480nM or 960nM siRNA were lysed in LDS-lysis buffer after 72 h in culture (Figure 3.2.7, two right panels). The reduction in Akt1 was observed in at least three independent experiments. A difference in the levels of PI3K p85α expressed in cells transfected with PI3K p85α siRNA was visible as compared with the control (Figure 3.2.7, two left panels), but the data obtained in several independent experiments were not as consistent as the reduction in Akt1. This occurred when fresh siRNA or different lysis buffers (Triton or SDS) were used as well as increasing the siRNA concentration up to 960nM. An explanation for the lack of detecting consistent knockdown of PI3K p85α might be due to detection of different p85 isoforms. PI3K is a heterodimer comprised of a catalytic p110 and a regulatory p85 subunit. Five different isoforms of the regulatory subunit can be used (384, 385): p85α, p55α, p50α, p85β or p55γ. I tested three different antibodies to detect p85α. The p85α antibody form Millipore did not give a clear signal and the other commercial antibodies used (p85 Upstate # 06-195, p85 Upstate # 06-497) detect other isoforms of p85, such as p85β or p85γ in addition to PI3K p85α. p55γ has a molecular weight of 55kDa, whereas p85α and β have similar molecular weights of 83-85kDa. Therefore, the overlapping detection of both p85 α and β isoforms cannot be excluded and if so would impede the detection of changes in p85α. Alignment of the human p85α amino acid sequence against the other isoforms using UniProt showed that there was 59% identity of the protein sequence with the human p85β isoform (http://services.uniprot.org/blast/blast-20100510-1645225534). However, the antibodies bind to conserved sequences, which would explain the lack of detection of only the p85α isoform.

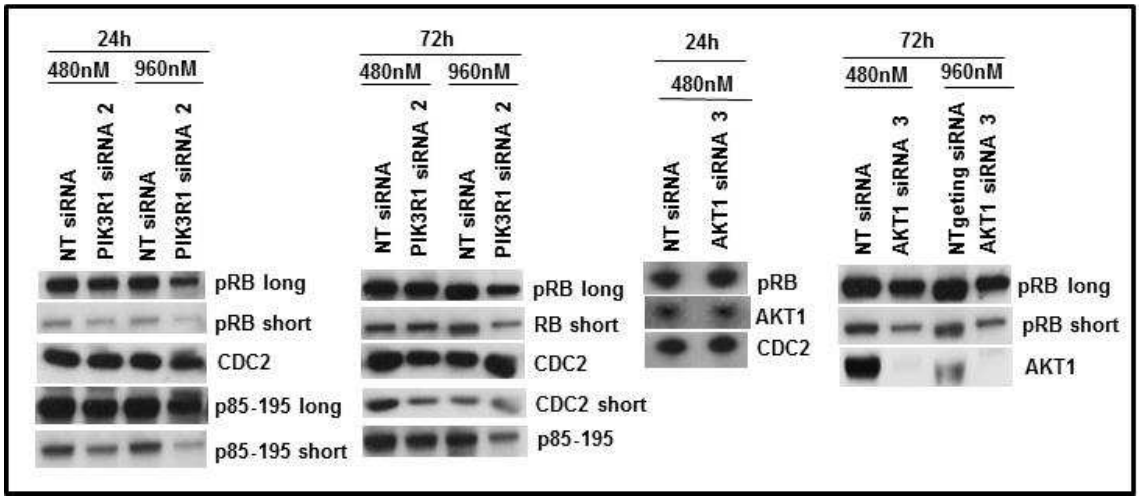

Figure 3.2.7 Western blotting analysis of Akt1 and PI3K p85α protein in YTS cells transfected with siRNA.

1-2 x 10^6 cells were lysed 24 h or 72 h after transfection with AKT1 or PI3KR1 siRNA in LDS-lysis sample. Western blots were probed with antibodies against Akt1 or PI3K p85 (# 06-195 from Upstate Biotechnology). Blots were also probed for Cdc2 and pRb as loading controls.

3.2.8. Inhibitors of PI3K and AKT reduce Cdc42 activity

The siRNA screen in section 3.2.5 and Cdc42 biosensor analyses in 3.2.6 showed that Akt1 or PI3K p85α downregulation impair Cdc42 activity. The data suggest that both these proteins are required for Cdc42 activation during NK:target cell contact. To investigate whether this effect on Cdc42 not only occurs as a result of siRNA transfection and that the same pathways can be perturbed by other means, a second approach was used. Akt1 or PI3K p85α activities were inhibited with small molecule inhibitors. The PI3K inhibitor LY-294002 abolishes PI3 kinase activity, but does not inhibit other lipid and protein kinases investigated, which include PI4 kinase, Pkc, Mapk or c-Src (392). The Akt inhibitor VIII inhibits Akt1, Akt2 and Akt3 and the inhibition is PH domain dependent (61). The compound does not inhibit Akt proteins lacking a PH domain or other closely related AGC family kinases, such as Pka, Pkc and Sgk, even at concentrations as high as 50μM. YTS NK cells were transfected with a plasmid expressing the Cdc42-biosensor and after 24 h in culture, the cells were pre-incubated with the VIII Akt inhibitor (34, 103) or the LYw-294002 PI3K inhibitor (304) for 1 h, before mixing them with target cells for 15 min. The presence of the PI3K or Akt1 inhibitors reduced Cdc42 activity to background levels (Figure 3.2.8). Therefore, the inhibitors have an effect which is similar to that obtained by transfecting the cells with the target-specific siRNA. These data strengthen the conclusions that Akt1 and PI3K are regulators of Cdc42.

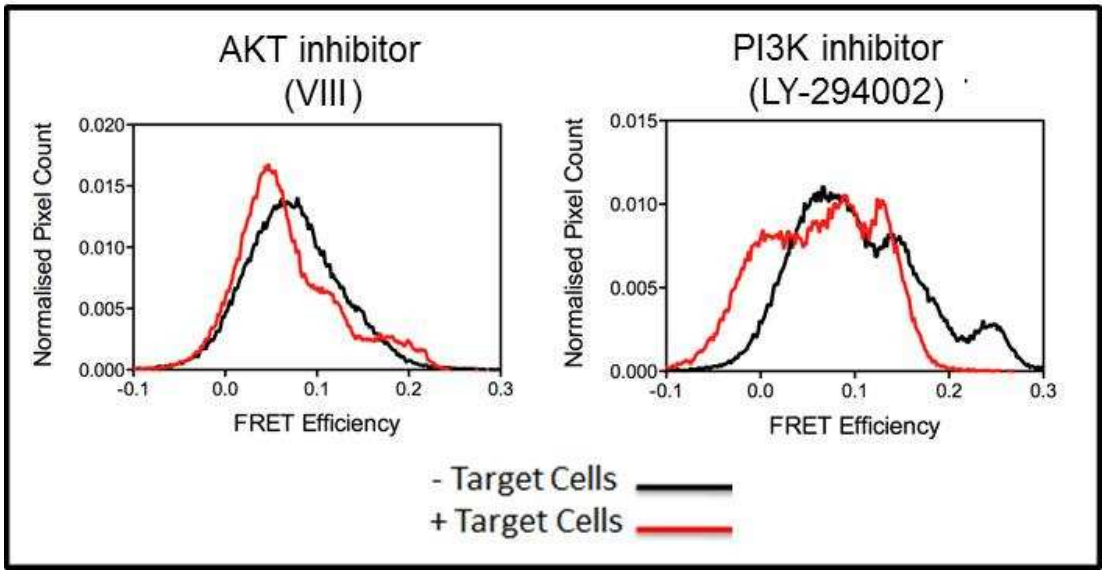

Figure 3.2.8 Inhibitors of PI3K and Akt reduce Cdc42 activity.

Pooled FRET efficiency data for YTS cells expressing the Cdc42-biosensor incubated with or without target cells in the presence of PI3K (LY-294002) or Akt (Akt inhibitor VIII) inhibitors. The experiment was performed by Dr. Rachel Evans, KCL.

3.2.9. Cytotoxic granule polarisation during target protein knockdown

The data in section 3.2.6 showed that the transfection of siRNA against Akt1 or PI3K p85α reduced FRET efficiency of the Cdc42-biosensor, indicating that both are necessary for Cdc42 activity that is induced during NK:target cell contact. Furthermore, inhibiting Akt1 or PI3K p85α with small molecule inhibitors also inhibited Cdc42 activation. Taken together, the data suggest that Akt1 and PI3K p85α are important regulators of Cdc42 during NK:target cell interaction. To investigate downstream effects of Cdc42, I tested whether reduction of these proteins has a functional effect on NK cells and whether downregulation of PI3K p85α or Akt1 impairs the cytotoxic function of NK cells. The formation of the NK:target cell conjugate induces processes that result in killing of the target cell (210). A well described process involved in the cytotoxic response of NK cells is cytotoxic vesicle polarisation towards the immunological synapse (54). Thus, if PI3K p85α and Akt1 are required for the activation of endogenous Cdc42, reducing either PI3K or Akt1 with siRNA should reduce granule polarisation after NK:target cell conjugate formation. To investigate whether either has a functional effect, NK cells were co-transfected with the siRNA against PI3K or Akt1, together with the plasmid encoding the Cdc42-biosensor. The biosensor was not used to measure Cdc42 activity in this approach, but it was co-transfected so that experimental conditions were similar to those used in section 3.2.6 and 3.2.8. After transfection, the cells were cultured for 24 h. NK cells were then incubated with the 721.221 target cells for 30 min, fixed with paraformaldehyde and stained with an Alexa647-conjugated anti-perforin antibody. NK cells were evaluated visually to determine whether cytotoxic granules were polarized towards the synapse (Figure 3.2.9).

To induce a cytotoxic response of NK cells towards target cells, it is necessary that the cytotoxic vesicles in NK cells polarise towards the immunological synapse at the site of the NK:target cell interface. In order to investigate whether a cytotoxic response is induced at the NK:target cell interface, the localisation of perforin was determined within NK cells. To do this, confocal z-stacks were acquired using a Cy3-labelled anti-perforin antibody. These were assessed manually to determine whether perforin was localised across the whole cell or specifically at the cell:cell

interaction interface. No staining was observed after probing with an isotype-matched control antibody (Figure 3.2.9 A). The z-stacks acquired showed perforin polarisation only at the point of cell:cell contact (Figure 3.2.9 A) for a ‘polarised’ cell. Epifluorescence images were then acquired and more than 10 cells per siRNA tested were analysed in two independent experiments (Figure 3.2.9 B). In the siRNA experiment, 55% of the NK:target cell conjugates that were transfected with control siRNA (non-targeting) polarised vesicles towards the target cell after the 30 min incubation (Figure 3.2.9 D). Reducing either PI3K p85α or Akt1 by transfecting the appropriate siRNA caused a significant reduction of the polarized granules towards the synapse to 20% or 30% respectively (Figure 3.2.9 D). These data indicate that PI3K p85α and Akt1 have a strong effect in reducing conjugation triggered by Cdc42 activity and that reducing either of these proteins affects granule polarisation (Figure 3.2.9 D).

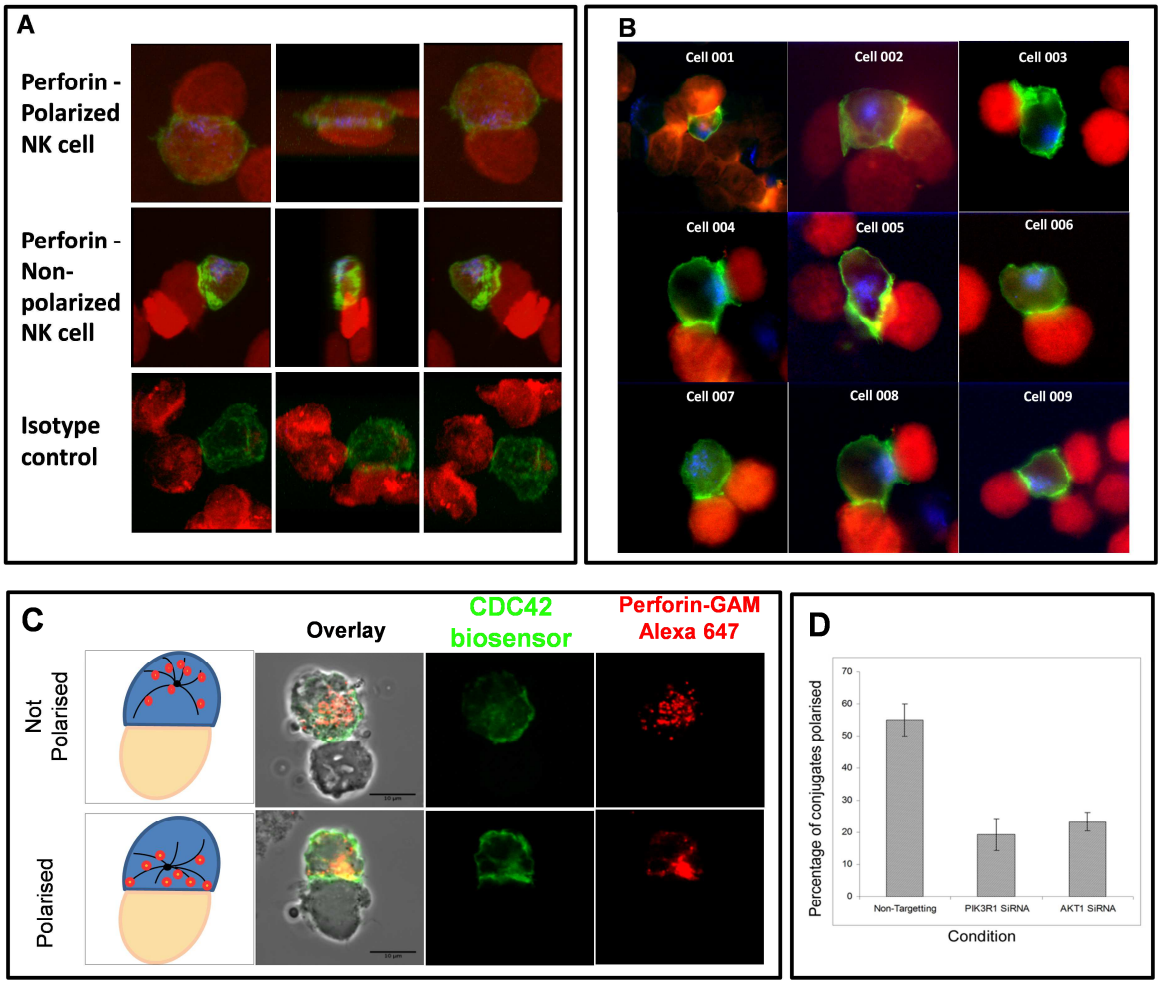

Figure 3.2.9 Cytotoxic granule polarisation and the effects of Akt1 or PI3K p85α reduction.

A. An example of Cdc42-biosensor NK cells (green) in a conjugate with target cells (red), stained with anti-perforin antibody (blue) by confocal (z-stacks) microscopy. Images are shown of perfoin staining that is either polarised or not polarised toward the immunological synapse. Isotype-matched control shows no specific staining. B. The polarisation of perforin was visually estimated in 5-10 cells per siRNA target. A representative example showing that five out of nine cells transfected with siRNA against PI3KR1 are not polarised. C. Schematic and experimental representation of polarised or non-polarised cytotoxic granules. D. Pooled data from multiple siRNA knockdown experiments. Bar chart showing the percentage of cells with granules polarised towards the synapse (mean±STD).

3.3 Discussion

In this study, a new strategy was applied to identify novel regulators of a signalling pathway of functional importance. The strategy was tested by using it to identify regulators of a key protein, Cdc42, which is required for the activation of human NK cells and enables NK cell cytotoxicity (26). It was shown for the first time that Cdc42 activity not only increases but also oscillates during NK:target cell interaction. This result indicated that there is likely to be a feed-back loop regulating Cdc42 activity. To identify the proteins required for Cdc42 to be activated in NK cells in response to NK:target cell interaction I used a Systems Biology approach and predicted proteins that interact with and may regulate Cdc42. Several databases, including the Human Protein Reference Database (HPRD), IPFAM and PFAM were integrated by using information about GEF, GAP and Cdc42 interacting molecules as well as 3-D structure and protein domain:domain interactions to predict proteins which interact with Cdc42 and assign the interactions a degree of confidence. All but two of the predicted targets were downregulated by siRNA in NK cells, which were also co-transfected with a plasmid encoding the Cdc42-biosensor, a surrogate readout of Cdc42 activity. The Cdc42 activity was quantified in the presence or absence of the NK:target cell contact using the Cdc42-biosensor, measured by FLIM. This screen identified PI3K p85α and Akt1 as potential novel regulators of Cdc42. Reducing the levels of Akt1 or PI3K p85 α by transfecting specific siRNA caused a decrease in Cdc42 activity. Small molecule inhibitors of PI3K and Akt also reduced Cdc42 activity to the same extent as the target-specific siRNA. Downregulation of PI3K p85α and Akt1 proteins not only reduces Cdc42 activity, but it has also functional consequences for the NK:target cell interaction. Reduction of either of these proteins decreased cytotoxic granule polarisation, thus each is required for NK cells to become functionally active. This is a proof of principle study and demonstrates the potential of a Systems Biology approach to predict biological targets of a signalling pathway and the strength of advanced FRET imaging to detect changes in protein activity, in this instance using the Cdc42-biosensor.

Small RhoGTPases such as Cdc42 are very well characterized molecules that regulate cell motility, cell cycle progression and actin dynamics (310, 312, 391).

Cdc42 is a plasma membrane bound protein (312), but there is also evidence that it is localised in the Golgi apparatus (120). It has been shown that the Cdc42/Wasp pathway plays a crucial role in regulating NK cell migration. NK cells derived from patients with Wiskott-Aldrich syndrome carrying mutations in the *WASP* gene have a reduction in NK cell migration (354). Furthermore, Sinai *et al.* have shown the importance of Cdc42 in NK cells, in which Cdc42 controls the transient polarisation of cytolytic effectors to induce efficient target cell killing (348). Apart from the role of Cdc42 in NK cells, Cdc42 has been reported to be an important regulator of neuronal morphology and is a positive regulator promoting neurite outgrowth and growth cone protrusion (74). This protein is also crucial for the development of an adequate immune response. Rho GTPases such as Cdc42 control T cell function as the key signal transducer proteins from chemokine and antigen receptors, which lead to T cell activation and motility (317). Taken together, Cdc42 has several biological functions in different cells, but it is particularly a regulator of changes involved in the cytoskeleton in many cell types, including NK cells.

To measure the biological activity of Cdc42 in live NK cells during immune surveillance, a FRET-Cdc42-biosensor was used in this study and live imaging was performed with an in-house multiphoton microscopy system (see section 1.1.6). It is not unexpected that Cdc42 activity increases after contact with a target cell, but surprisingly the activation resulted in a periodic oscillation after an initial increase of Cdc42 activity. Oscillatory behaviour has been observed in other proteins, such as the transcription factor nuclear factor kappa B (NFκB). Single-cell time-lapse imaging and computational modelling of NFκB localisation showed an asynchronous oscillation following cell stimulation that controls gene expression (271). Another oscillation of proteins was described for ROP GTPases, leading to polarized growth of pollen tubes in plants (172, 173). Further, spreading of lamellipodia in NK cells has been demonstrated in response to NKG2D ligation to LFA1 on NK cells that occurred in waves, but Cdc42 was not measured in the context (94). Very recent data showed that Cdc42 activity is increased upon cross-linking of the activating receptor NKG2D in NK cells. Inhibition of Cdc42 activity using RNA interference impaired NKG2D-mediated NK cell migration, but no oscillation of Cdc42 was reported (336). Our study is the first to describe that

oscillation in Cdc42 activity occurs at the immunological synapse. In 2012, oscillatory dynamics of Cdc42 were reported during growth in fission yeast in which Cdc42 controls polarized growth. Similar to our study, the data indicate delayed negative feedback loops involving competition of regulators (95).

The oscillation in Cdc42 activity observed by the Ng laboratory led to the hypothesis that Cdc42 activity is regulated by one or more proteins, which are in a signalling feed-back loop. The oscillation can be explained if Cdc42 is activated not only by one but rather by several proteins. Because those proteins can send signals to inhibit specific protein interactions, they may have negative feed-back effects on activated Cdc42. This study differs from the traditional thinking that a single protein activates another protein in a linear pathway. The study shows evidence of an interplay between positive and negative signals from interacting (nearest neighbour) proteins. This indicates that the regulatory network is a complex and dynamic system and the interactions are non-linear and comprise a multi-directional network. Therefore, there is a need to study complex protein interactions in whole biological systems. Systems Biology allows the study of protein interactions using a holistic approach, including bioinformatics combined with experimental methodologies, rather than a reductionist approach in which the study is minimised to a single protein/component of a network in order to understand the connections between individual proteins.

To identify critical regulators of Cdc42, several publically available databases were integrated to generate a Cdc42-specific protein interaction network. The information from the HPRD, PFAM and iPFAM was merged to identify direct Cdc42-interactors and to minimise false positives from different biological experiments from the HPRD. The difficulty is that protein interactions reported in a database differ in the type of experiments which were carried out and in the number of publications from which the evidence for a particular protein interaction is derived. The number of random matches can be avoided by combining several databases and by using stringent criteria to assign a higher degree of confidence to the interactions. Therefore, adding information about domain-domain interactions increases the confidence of the reported interactions. Since the purpose of the screen was to

predict which signalling molecules might be involved in the formation of a feedback loop, a very stringent screen was performed. The criteria were that not only the direct partners of Cdc42 were considered, but those had also to be in a loop with other proteins. Moreover, only protein categories such as GAP, GEF and kinases were analysed due to the fact that Cdc42 is a Rho GTPase and it needs to interact with GEFs, GAPs and kinases to become activated. Rho GDP dissociation inhibitor (GDI) proteins represent a different class of Rho GTPases and are also reported to interact with Cdc42 (162). Those were excluded from the analyses as they have the ability to extract Rho proteins from membranes and keep them in an inactive cytosolic complex (374). Cdc42 is only active at the membrane and the aim of the study was to identify candidates that perturb Cdc42 activity. Moreover, the Cdc42 network does not contain all direct effectors of Cdc42, such as Mrck (406), Wasp (186) and Dbl (406). There is strong evidence of the interaction between of Wasp and Cdc42 and Wasp is also a critical regulator of actin cytoskeleton remodelling controlling NK cell migration (354). These proteins however were excluded from the Cdc42 network, as they do not fulfil the stringent criteria of being in a loop with Cdc42.

Conventional high-throughput studies start from large-scale biological experiments, such as a high-throughput-screening (HTS) to identify RNAi or small molecules that abrogate a particular cellular phenotype. This screening results in many hits, which are then connected using bioinformatics approaches to find interactions between proteins. A large European consortium carried out an integrative research project to study the regulation of mitosis in human cells, called MitoCheck (http://www.mitocheck.org/). An automated platform for high-content RNAi screening was developed and analysed by time-lapse fluorescence microscopy of live HeLa cells expressing histone-GFP to identify genes involved in chromosome segregation and structure (272). In another example, a global analysis of the yeast proteome was carried out by cloning 5,800 open reading frames and overexpression and screening of the proteins using microchips to identify global protein activities (285). The strength of the intelligently designed screen described in this chapter is that the selection of candidates for siRNA screening is very conservative. The final network resulted in fewer than twenty proteins predicted to

regulate Cdc42. This more targeted approach reduced the number of experiments and the cost of testing the predictions experimentally, compared with hundreds or even thousands of targets that need to be analysed based on high-throughput analyses.

The candidate proteins predicated to regulate Cdc42 were tested by siRNA knockdown followed by FRET imaging of the Cdc42-biosensor. The screen identified p85α subunit of phosphatidylinositol 3-kinase (PI3K1) and Akt1 as novel regulators of Cdc42. PI3K has been shown to be of importance in NK-cell development and cytokine secretion as well as being required for glycosylation of NKG2D in NK cells (37, 202) and the glycosylation levels regulate effector function in NK cells through the PI3K pathway. The PI3K regulatory subunit also has a role in controlling PDGF receptor-induced cytoskeletal changes and cell migration (186). The NK cell activating receptor NKG2D mediates cytotoxicity and is linked to PI3K in NK cell adhesion, polarity and granule secretion (332). It has been shown that stimulation of NK cells with soluble NKG2D ligands causes activation of PI3K and Akt signalling pathways (361). When the gene encoding PI3K p85α was deleted in mice, the lineage commitment and cytotoxicity of NK cells was impaired (22). Taken together, the studies cited above indicate the importance of PI3K in NK cell function, but no direct connection to Cdc42 has been reported.

There are many studies analysing large data sets and employing high-throughput technologies to identify novel biological components of a network. One example of applying Systems Biology methods uncovered a new function for Cyclin D1 in DNA repair by protein interactome analyses. In this study, a proteomic screen was performed for Cyclin D1 to identify protein partners in several types of human tumours in which Cyclin D1 is overexpressed. For the screen, Cyclin D1 containing complexes were purified using double immuno-affinity purification and Cyclin D1 interactors were identified by repeated rounds of liquid chromatography and high-throughput mass spectrometry. Apart from its known role in the cell cycle, analyses of Cyclin D1 interactors revealed a network of DNA repair proteins (187). The importance of the study is that Systems Biology approaches can help to discover new functional roles of proteins.

A second example is the novel, ground-breaking ‘Phenolog’ method that predicts new human genes of functional importance and that is used in Chapter 4. The method is based on the fact that essential proteins encoded by orthologous genes in different species are commonly used in the same networks (pathways), but not necessarily for the same functions (248). The study suggests a yeast model for angiogenesis defects and a worm model for breast cancer. Therefore, predictive biology is a novel tool and of increasing value to understand complex biological systems.

Chapter 4

4. The Phenolog approach predicts that And1 and Sec13 are involved in maintaining genome stability

4.1 Introduction

4.1.1. Mapping between phenotypes and genotypes

Predicting the function of genes in particular diseases is difficult. The aim of the work described in this chapter is to determine whether a new predictive approach can be used to identify genes that are involved in genomic instability in cancers.

Each gene correlates in general with a particular phenotype. However, mapping between genotypes and phenotypes is not obvious. Through the course of evolution, only some genes have been conserved between organisms and involved in the same phenotype. For example the *CDK1* gene, which encodes the master regulator of mitosis, is functionally conserved across species (Figure 4.1.1 A, Example 1). The human gene compensates for the loss of the homologue in fission yeast (221) and is the only Cdk required for cell division in mouse embryos (328). There are several other proteins, including ribosomal proteins and DNA polymerase that are conserved across all species and perform the same function. However, even conserved genes can be involved in two completely different phenotypes in different organisms. For instance, in *C. elegans* genes encoding proteins involved in cilia formation, such as *IFT20*, are important for motility (129). In contrast, in human T cells that lack primary cilia, the same proteins are involved in T cell receptor trafficking and downregulation of *IFT20* leads to impaired T cell receptor signalling (127) (Figure 4.1.1 A, Example 2). In *C. elegans*, the retinoblastoma gene is involved in vulval development, but in mice, depletion of *RB1* causes placental abnormalities (220) and pRb is involved in cellular mechanisms, including cell cycle regulation (84), apoptosis (166), differentiation (209) and maintenance of genomic stability (57, 160, 237, 262).

Genetic screens show that in many cases deletion of orthologous genes often does not produce the same phenotype in different organisms as they do in humans. There is an accumulation of scientific knowledge in databases of genes and their

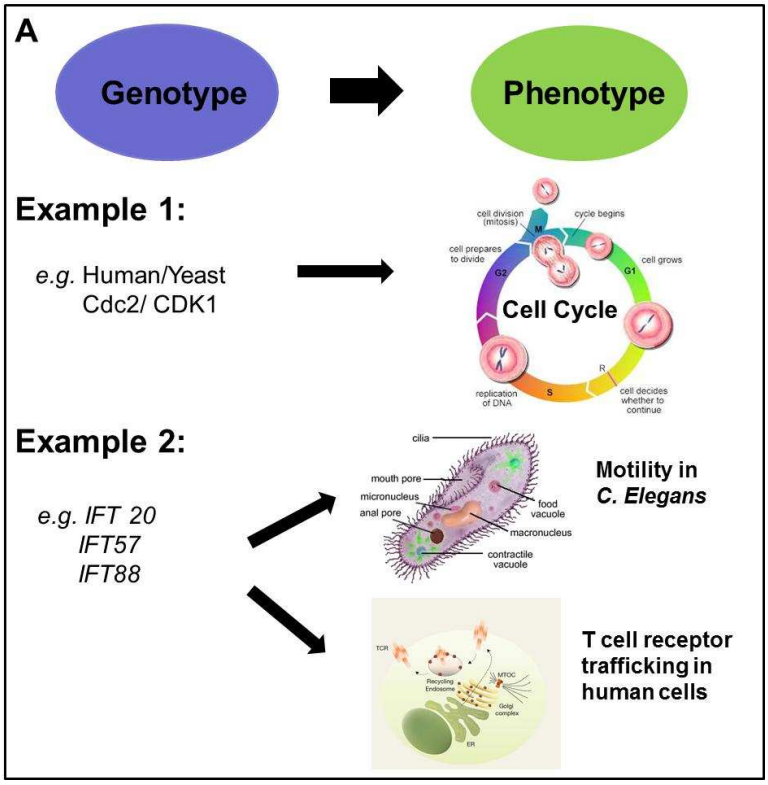

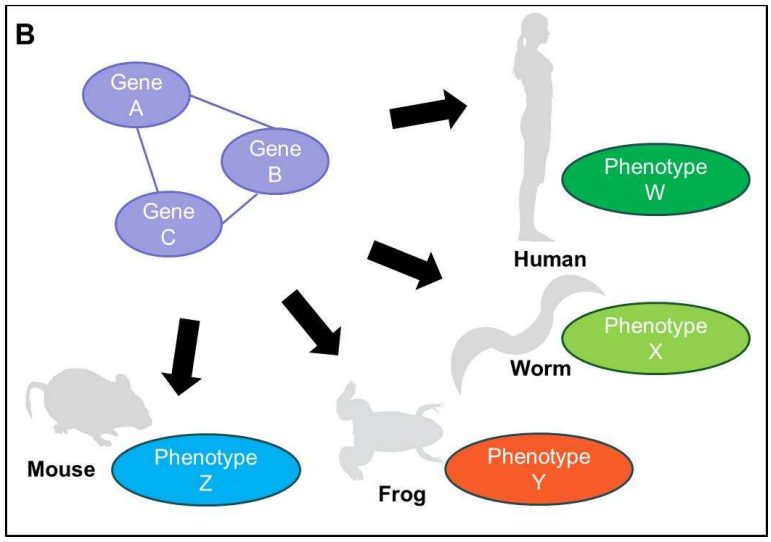

Figure 4.1.1 Mapping between genotype and phenotype (adapted from Marcotte).
A. The master regulator gene of mitosis, *CDK1*, is conserved between species and gives the same cell cycle phenotype in human and yeast (example1). However, many conserved clusters of genes can give rise to two completely different phenotypes (Example 2) Adapted from (127) (http://learninglab.co.uk/headstart/images/cycle1a.jpg and http://www.biologycorner.com/resources/paramecium.gif.) B. Genes encoding proteins involved in the same pathways often result in different phenotypes in different organisms.

correlated functions in many different species. For instance, the McKusick's Online Mendelian Inheritance in Man (OMIM) database contains information from the published biomedical literature and reports over 18,000 human genes and phenotype associations (15). Species-specific databases also exist for the nematode worm (www.functionalnet.org/wormnet/), the plant A*rabidopsis thaliana* (www.arabidopsis.org/) and others. However, even if orthologous genes in different species such as nematodes, yeast, mouse and humans are commonly used in the same networks (pathways), the genetic concordance between humans and other organisms such as nematode worms is poor. Therefore, mapping between genotype and phenotype is often non-obvious and it is difficult to predict the phenotype (Figure 4.1.1 B).

Our collaborator, Professor Marcotte from the University of Texas at Austin has made use of information about genes that are conserved between many different species and which are functionally important in humans. He termed the methodology, the "Phenolog approach''. Phenologs can be defined as mapping of orthologous genes between species such that the deletion of orthologues leads to completely un-related phenotypes in each organism (www.phenologs.org/). "Orthologues" are genes in different species that are descended from a single gene in an ancestral organism (128), whereas "homologues" refer to genes that are related to a second gene by descent from a common ancestral DNA sequence (206). There are publically available databases of gene homologues, such as HOVERGEN, which is devoted to homologous vertebrate genes (http://pbil.univ-lyon1.fr/databases/hovergen.php), or HOGENOM, which is a database of homologous genes from fully sequenced organisms (http://pbil.univ-lyon1.fr/databases/hogenom.php). In the Phenolog approach, conserved groups of genes may still work together, but lead to completely different phenotypes in diverse species (Figure 4.1.1 B). The breakthrough of this study was reported in the New York Times (www.nytimes.com/2010/04/27/science/27gene.html?pagewanted=all) and the research is reported in McGary *et al*. (248). The method has enabled Prof. Marcotte to identify a number of genes involved in human disorders. This approach for example predicts a yeast model for mammalian angiogenesis based on the

knowledge of mouse genes, deletions of which cause angiogenesis defects, and yeast genes that are involved in drug-sensitive growth. Apart from the orthologous genes between mice and yeast, additional worm genes were identified whose depletion leads to drug sensitivity. The mouse orthologues of these predicted worm gens have been shown to be important in angiogenesis, as validated in a *Xenopus laevis* embryo model (248). Simple organisms like yeast do not have a haematopoietic system and they do not make blood. However, this approach still has the power to predict unique angiogenesis genes for higher eukaryotes from a yeast model. Therefore, this novel approach is applicable to any human disorder to discover non-obvious genes involved in human diseases through analyses of orthologous phenotypes. As an example, the Phenolog approach leads to predictions of novel genes that are involved in breast and ovarian cancer and associated with DNA repair and genomic instability (see 4.3.1) that are validated by wet-lab experiments in chapter 4.2.2 - 4.2.8.

4.1.2. Assaying proteins required to maintain genome instability

A previous study from our laboratory showed that genomic instability is induced by reducing the level of the DNA replication proteins Mcm7 or Mcm4 and this occurs within one cell cycle (291). In this study, it was shown that MCM protein levels are induced during the $G_0 \rightarrow G_1$ transition in primary T lymphocytes. Reduction of the levels by even 50 % leads to increased centromere separation, premature chromatid separation and gross chromosomal abnormalities. It was also observed that reducing the levels of Mcm7 or Mcm4 caused DNA damage, involving activation of Atr, Atm, Chek1 and Chek2 and other DNA repair proteins.

In order to test the Phenolog predictions, I used the primary T cell system employed in (291). These primary cells have a normal genotype and cellular mechanisms are normal. In comparison, cell lines have a number of genetic abnormalities, which deregulate processes such as cell proliferation (373). Additionally, cell lines may already be genomically unstable (51, 137, 138, 306). Another advantage of carrying out genomic instability studies with peripheral blood T cells is their availability and that near 100% of quiescent T cells can be transfected with siRNA (290, 291).

4.2 Results

4.2.1. And1 and Sec13 are predicted to be involved in DNA damage responses in breast cancer

Using the Phenolog approach, Professor Marcotte's laboratory predicted worm genes associated with a change in the percentage of male progeny in *C. elegans*, which predicted human genes that are linked to breast and ovarian cancer. The approach is based on the knowledge of gene-phenotype associations for the two organisms (Figure 4.2.1 A). In the primary step, 4,649 orthologues were mapped between human and worm genes based on literature searches. A set of 12 genes are associated with breast/ovarian cancer in humans, including *ATM*, *BRIP1*, *KRAS*, *PHB*, *PIK3CA*, *RAD51*, *RAD54*, *SLC22A*, *TCG101*, *BARD1*, *BRCA1* and *CHEK2*. Three of the genes, namely *BRCA1*, *BARD1* and *CHEK2*, however are also known to be associated with a different phenotype in worms. Downregulation of these or 13 other worm genes (16 worm genes total), are linked to a higher percentage of male progeny and thus their human orthologues may be involved in breast cancer (Figure 4.2.1 B). The 13 worm gens identified are: *BARD1*, *BRCA1*, *CHEK2*, *FAM82B*, *GCC2*, *HMG20A*, *HORMAD2*, *KIF15*, *MRE*, *PIHA*, *RAD1*, *RAD21*, *SEH1L*, *SVIL*, *TSPO* and *WDHD1* (Figure 4.2.1 C).

Abnormalities in the three overlapping, orthologous genes in worms and humans, *BRCA1*, *BARD1* and *CHEK2* (Figure 4.2.1 C) are involved in human breast/ovarian cancers. Germline mutations of *BRCA1* are responsible for many breast and ovarian cancers and *BRCA1* is identified as a tumour suppressor (416). *BRCA1* mutations were identified either as frame-shift or nonsense mutations (69, 253), and *BRCA1* gene abnormalities are one of the prognostic markers for breast cancers (215). The Brca1 protein is involved in DNA repair and maintaining genomic stability (169). Brca1 is known to exist in a heterodimeric complex with Bard1 (417) and is involved in homology-directed repair (HDR) of double-strand DNA breaks (265, 388). The Chek2 protein activates DNA repair in the presence of DNA double-strand breaks and *CHEK2* gene is also mutated in breast cancers (273). Proteins encoded by *CHEK2* together with *BRCA1* and *BARD1* with other

breast cancer susceptibility genes such as *ATM* are involved in DNA damage response pathways (242).

Based on the overlapping set of genes, *BARD1*, *BRCA1* and *CHEK2*, it was then determined whether there are worm genes whose depletion changes the ratio from female to male worms (Figure 4.2.1 A), and therefore their orthologues in humans may be involved in breast/ovarian cancer, linked to chromosomal instabilities. Of the 13 predicted worm genes, 9 have been reported in the literature to be involved in breast cancer (Table 4.2.1). A number of abnormalities of these genes have been reported to occur in breast cancers, including copy number variation, missense mutations and overexpression of the encoded protein. Many of those genes are linked, or the proteins they encode are in complexes. For example, the Hmg20A protein binds to Brca2 and a germline mutation in the *BRCA2* gene causes DNA damage and chromosomal aberrations (241). However, 4 of the 13 genes are novel predictions for breast/ovarian cancer: *GCC2*, *PIGA*, *SEH1L*/*SEC13* and *WDHD1*/*AND1*/*CTF4*.

And1 is an important component of the DNA replication complex. The protein is required for unwinding the DNA for DNA replication initiation and it is crucial for coupling Mcm2-7 to DNA polymerase α (133). In contrast, Sec13 is a multifunctional protein with roles in the nuclear pore complex, which is required for transport of molecules into and out of the nucleus (119), in chromosome segregation during mitosis (171) and it is part of the COPII-complex, which transports proteins from the ER to the Golgi apparatus (274). And1 and Sec13 were selected for further investigation.

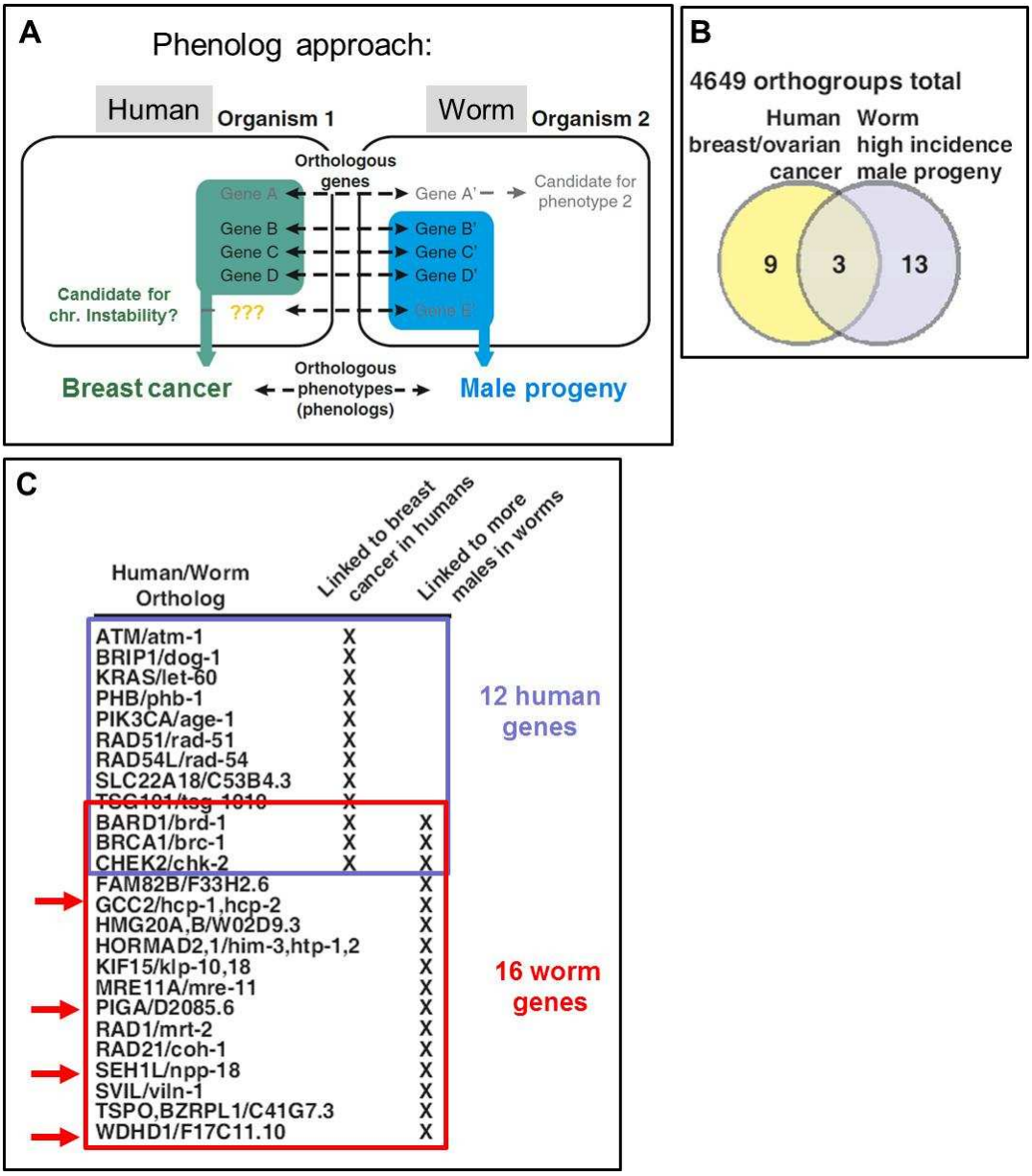

Figure 4.2.1 A high incidence of male progeny in worms maps to breast/ovarian cancer and chromosomal instability in humans (Modified from (248)).

A. Simplified schema of the Phenolog approach. A seed set of orthologous genes between the two organisms forms the basis for predicting novel genes involved in breast cancer. B. From a total of 4,649 *C. elegans*-human orthologues, 12 genes were identified to be linked to human breast/ovarian cancer and 16 genes to a high incidence of male progeny in worms. Three of the genes overlap between the two species. C. From 13 uniquely identified worm genes, 4 are novel predictions: *GCC2*, *PIGA*, *SEH1L* and *WDHD1* (arrowed) that may be involved in breast/ovarian cancer.

Gene	Reference	Comment
FAM82B	(78)	Copy number alteration and aberrant gene expression in breast cancer
HMG20A, B/BRAF35	(241)	DNA binding protein in complex with Brca2
HORMAD2,1	(5)	Copy number variation and aberrant gene expression in basal breast cancer
KIF15/NY-BR-62	(329)	Overexpression in breast cancer
MRE11A	(131)	Missense mutation in breast cancer
RAD1	(72)	Overexpression/Phosphorylation of Rad1-Rad9-Hus1 complex in breast cancer
RAD21	(333)	Polymorphisms of *RAD21* associated with breast cancer
SVIL	(276)	Deregulated in metastases of brain cancer
TSPO/BZRPL(PBR)	(152)	Overexpression in highly aggressive breast tumours

Table 4.2.1 9 of 13 predicted genes involved in breast cancer are supported in the literature

The table summarizes the evidence that 9 of 13 genes that are predicted by the Phenolog approach are associated with breast cancer.

4.2.2. Sec13 and And1 are expressed in primary T cells during cell cycle entry

Human primary peripheral blood T cells were used previously in the laboratory to investigate whether the level of Mcm7 and Mcm4 induction during the $G_0 \rightarrow G_1$ transition was necessary for maintaining genome stability during the subsequent S-phase (291). To determine whether the same T cell system could be used for analysing Sec13 and And1, their expression was analysed by preparing total protein lysates of human peripheral blood T cells during cell cycle entry and progression from $G_0 \rightarrow G_1 \rightarrow S \rightarrow G_2/M$. Western blot analysis shows that And1 and Sec13 are not expressed in G_0 (Figure 4.2.2). And1 becomes expressed in G_1 by 24 h, and Sec13 in late G_1/early S phase by 48 h post CD3/CD28 stimulation. Since Sec13 has a major role as a nuclear pore complex protein, the expression of another nuclear pore complex protein was analysed. The nuclear pore complex protein Nup160 is also induced at 48 h, at the same time as Sec13. The blot was also probed for Lck (189, 395) and for Histone H3 as controls for loading (Figure 4.2.2).

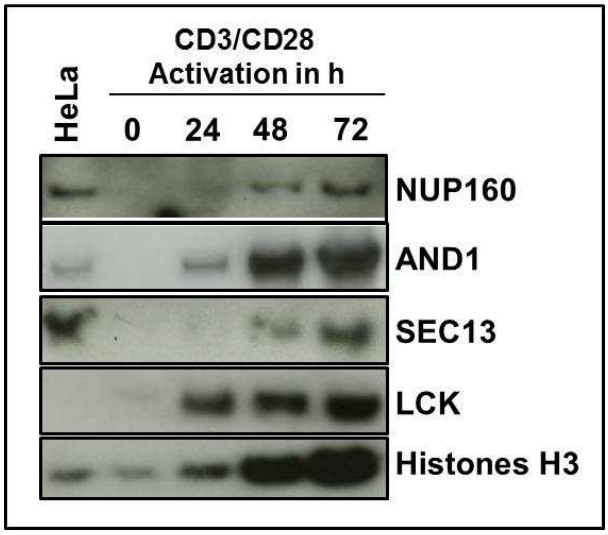

Figure 4.2.2 Sec13 and And1 are expressed during cell cycle entry.

Human primary peripheral blood T cells were isolated by negative selection and stimulated with CD3/CD28 beads. Whole cell protein extracts were prepared at the times shown and the expression of And1, Sec13, Nup160, Lck and Histone H3 were analysed by western blotting. HeLa lysate is used as a positive control.

4.2.3. Experimental approach to analyse DNA damage and chromosomal abnormalities

To investigate whether the expression of And1 or Sec13 are required to maintain genome stability, an experimental approach was applied and optimised that has been validated previously in the laboratory by Dr. Steve Orr (291). PBMC were obtained either from fresh blood or from a leukocyte cone from the National Blood Service. T cells were then purified by adhering the cells overnight on plastic plates or by using a negative T cell isolation kit (see 2.2.3 and 2.2.4 respectively for methods and purity). The experimental strategy is shown in Figure 4.2.3. In initial experiments, quiescent T cells were transfected with a pool of three siRNA against Sec13 or And1, or with a non-targeting control siRNA. The T cells were transfected by Nucleofection (Lonza) and this method transfects near 100% of the quiescent T (290, 291). After transfection, the cells were allowed to recover overnight and then stimulated for up to 96 h with PMA/Ionomycin or CD3/CD28 beads, which causes the cells to enter the cell cycle. T cells were then prepared for further analyses, including karyotyping or DNA damage assays.

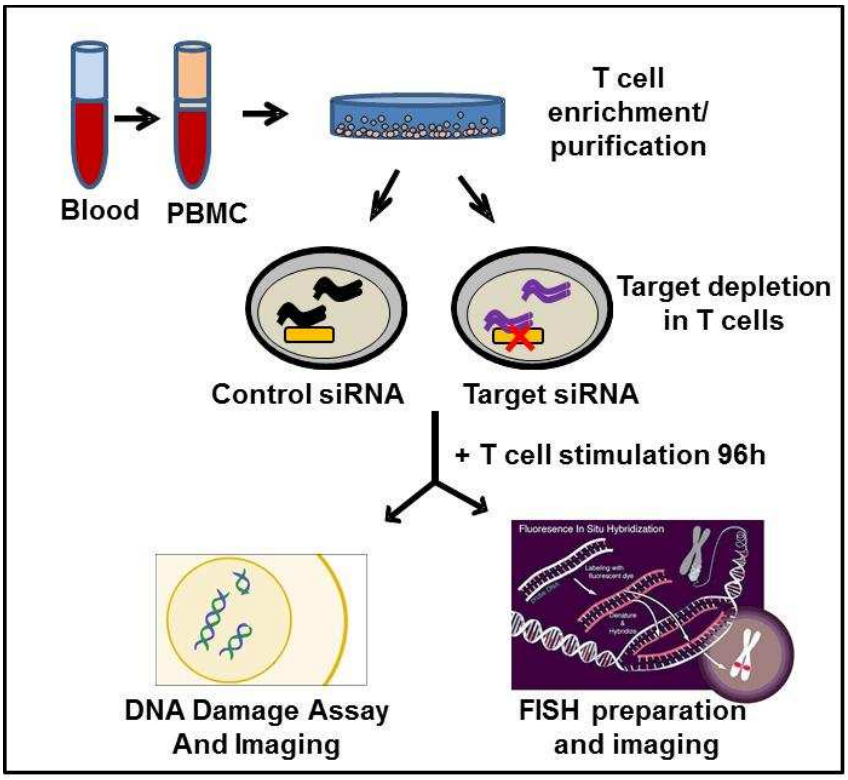

Figure 4.2.3 Schematic representation of the experimental workflow.

T cells were enriched or purified from fresh blood or from a leukocyte cone. The T cells were transfected with siRNA against the specific target or with non-targeting control siRNA. The cells were stimulated with CD3/CD28 beads or PMA/Ionomycin up to 96 h to allow them to enter the cell cycle and proliferate. Samples of the cells were then taken for western blotting, analysis of the cell cycle and to carry out DNA damage or fluorescence *in situ* hybridisation (FISH) analyses.

4.2.4. Optimisation of the condition for karyotype analyses

In order to be able to determine whether siRNA depletion of one of the predicted targets, Sec13 or And1 causes chromosomal abnormalities, the experimental conditions were optimised. In order to perform Metaphase FISH (M-Fish) analysis, sufficient numbers of cells are required to progress through to Metaphase of the cell cycle for chromosome spreads to be analysed. Therefore, different conditions and timing of CD3/CD28 activation were tested. In the workflow, T cells isolated from defrosted PBMCs by adherence to plastic were transfected on day 0 and cultured without stimulation for 24 h to allow them to recover. On day 1, the cells were stimulated with CD3/CD28 beads for up to 94 h. Colcemid was then added to arrest the cells in Metaphase and the cells were incubated for an additional 48 h to allow sufficient numbers to complete the cell cycle. They were then analysed by cell cycle analysis and chromosome spreads were prepared (Schema: Figure 4.2.4 A).

In the study, T cells transfected with control siRNA or MCM7 siRNA as well as non-transfected T cells were analysed. Previous analysis of Mcm7 knockdown in T cells has been shown to cause chromosomal abnormalities (291) and was therefore used as a positive control. Flow cytometry analyses were performed to determine the percentage of cells in each phase of the cell cycle by analysing the DNA content on day 1, 2, 3, 4 and 6. On day 1, 24 h after transfection there is no difference in the percentage of cells in G_0 between transfected and non- transfected cells. Stimulation of the cells with CD3/CD28 for 72 h caused a consistent increase in the percentage of cells in S and G_2/M phases (12-14% in G_2/M). Incubation of the cells after Colcemid treatment from day 4 to day 6 caused a further increase in G_2/M and an increase in cells with sub-G_1 DNA staining, consistent with an induction of apoptosis. However, whereas the percentage of non-transfected cells in G_2/M doubled to 24%, in the cells transfected with control or MCM7 siRNA there was only a small increase in G_2/M to 17% (Figure 4.2.4 B). This could be due to cells taking longer to progress through the cell cycle or increased cell death. An increase in the percentage of cells with sub-G_1 DNA content (up to 24%) was observed in cells transfected with control siRNA or MCM7 siRNA, consistent with an induction of apoptosis. This increase in cells with sub-G_1 DNA content occurred

after the addition of Colcemid and was not observed here at day 4 before the addition of Colcemid or in previous studies in the laboratory with T cells, which were cultured with Colcemid for less than 48 h (291).

Next, I determined whether T cells isolated by an adherence method from defrosted PBMCs behave differently from freshly isolated T cells and if the quality of T cells used affects progression through the cell cycle. At the same time, I investigated whether the duration of the stimulation for either 72 h or 96 h and Colcemid treatment for 24 h or 48 h increases the percentage of cells in G_2/M or with sub-G_1 DNA content.

The results show that the percentage of cells in each cell cycle phase were similar for freshly isolated T cells and T cells isolated from defrosted PBMCs, when transfected with the control siRNA or non-transfected (Figure 4.2.4 C). In addition, treatment with Colcemid for 24 h or 48 h also had similar effects. Therefore, treatment with Colcemid for 24 h is sufficient and this is consistent with the protocol used by our clinical cytogenetics laboratory and that used in a previous study (291). Control siRNA-transfected T cells either isolated by adherence from defrosted PBMCs or from fresh blood had the highest percentage of cells in G_2/M when stimulated for 96 h and then treated for 24 h with Colcemid (Figure 4.2.4 C). This condition was chosen for further experiments aimed at preparing sufficient metaphase spreads for M-FISH analyses.

To prepare Metaphase spreads, T cells isolated by adherence from defrosted PBMCs or from fresh blood were transfected with control siRNA or not-transfected. After transfection, the cells were allowed to recover overnight and then stimulated for 96 h with CD3/CD28 beads, followed by Colcemid treatment for 24 h. The cells were incubated in a hypotonic solution to cause swelling and rupture of the nucleus, followed by fixing the cells on a glass microscope slide and the percentage of Metaphases were analysed by manual counting. The results show that each of the samples had none or only a few Metaphases, and the number of Metaphases observed was insufficient to be able to carry out M-FISH and quantify the karyotypes obtained in a statistically significant manner (n=3). The M-FISH method

had been used successfully in a previous project and it is unclear why too few metaphases were obtained in the current study. Because small changes in the percentage of metaphases obtained could significantly affect the experimental results, it was decided to carry out Interphase FISH (I-FISH) instead. Typically, fewer chromosomes are analysed by I-FISH, but cells in all cell cycle phases are analysed and the method does not require cells to be blocked in Metaphase. Before carrying out the DNA damage and I-FISH assays, the reduction of Sec13 and And1 expression by the siRNA approach was analysed.

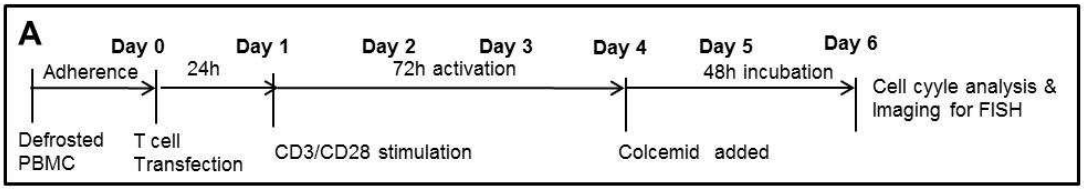

B

Non Transfected Cells

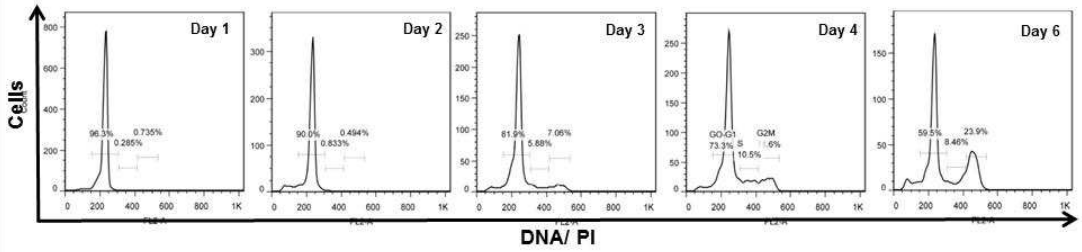

	Day1 %	Day2 %	Day3 %	Day4 %	Day6 %
Sub-G1	3	8	5	4	7
G0/G1	96	90	82	73	60
S	0	1	6	11	9
G2/M	1	0	7	12	24

Transfected with non-targeting, control siRNA

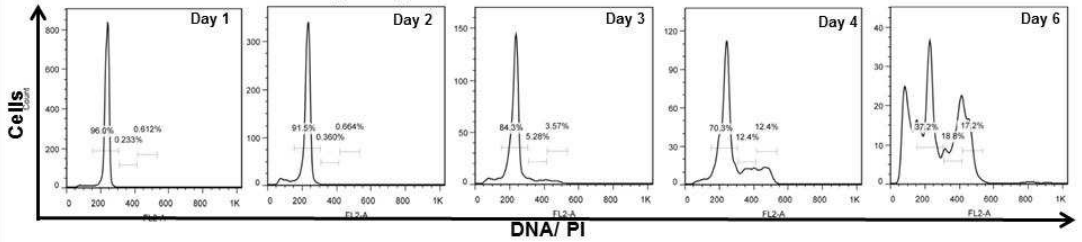

	Day1 %	Day2 %	Day3 %	Day4 %	Day6 %
Sub-G1	3	7	6	4	24
G0/G1	96	92	84	70	37
S	0	0	5	12	19
G2/M	1	1	4	12	17

Transfected with MCM7 siRNA

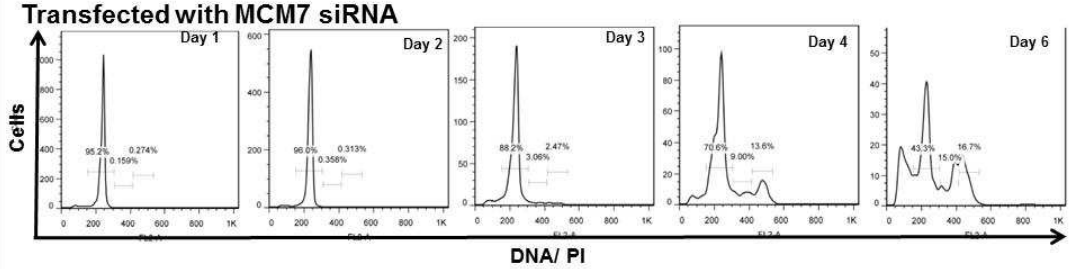

	Day1 %	Day2 %	Day3 %	Day4 %	Day6 %
Sub-G1	4	3	6	6	22
G0/G1	96	96	88	71	43
S	0	0	3	9	15
G2/M	0	0	2	14	17

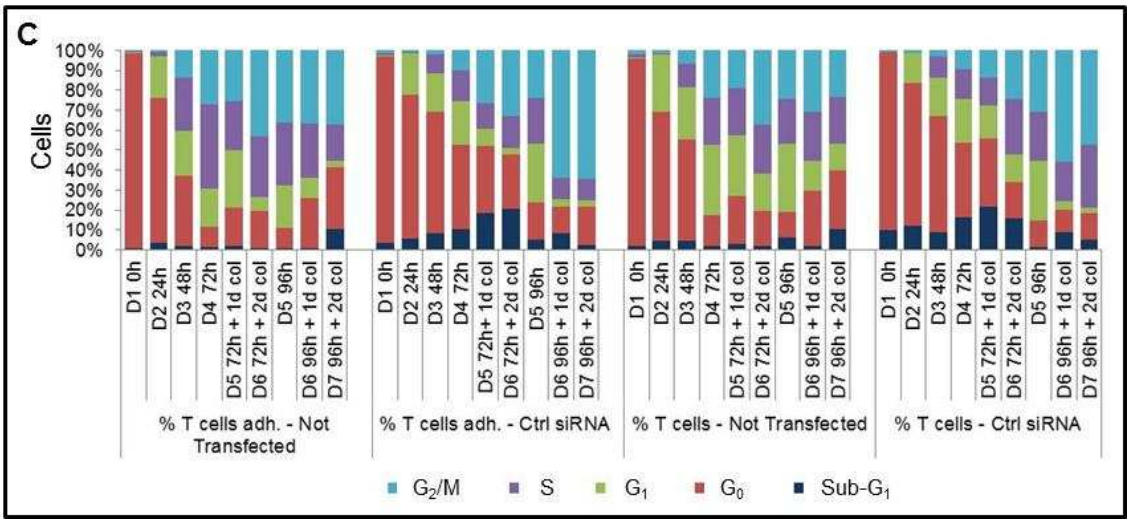

Figure 4.2.4 Optimisation of the siRNA knockdown for FISH analysis.

A. Experimental workflow to analyse the cell cycle status from day 1 up to day 6. T cells isolated from defrosted PBMCs by an adherence method were transfected with control siRNA, stimulated for 72 h (day 2 to day 4) with CD3/CD28 beads, Colcemid was added on day 4 and cultured to day 6 to arrest cells in M-phase. B. Cell cycle analyses of PI-stained DNA of non-, control- or MCM7-siRNA-transfected T cells at the time points indicated. C. Graphs of the percentage of cells in G_0, G_1, S and G_2/M phases or with sub-G_1 DNA content of either freshly purified T cells or T cells isolated from PBMCs by the adherence method under the following conditions: stimulation with CD3/CD28 beads up to day 5, with samples taken each day for analysis; Colcemid (col) was added either at 72 h or 96 h and samples were taken one or two days later. (Colcemid (col); T cells isolated from PBMC by an adherence method (T cells adh.); freshly isolated T cells (T cells); control, non-targeting siRNA (ctrl siRNA)).

4.2.5. Reduction of Sec13 and And1 expression with siRNA

To investigate the effects of reducing the levels of And1 or Sec13 during cell cycle entry, the induction of these proteins that occurs during G_1 (Figure 4.2.2) was inhibited using siRNA. Three different siRNA (Figure 4.2.5 A and B) were used for each target, which were initially pooled and transfected by Nucleofection into quiescent T cells, freshly isolated from leukocyte cones. Non-targeting siRNA was also transfected as a control. After being left to recover overnight, these cells were stimulated with CD3/CD28 beads for 72 h and the expression of Sec13 and And1 were analysed by western blotting (Figure 4.2.5 C and D). These data show that the targeting siRNA reduced the expression of And1 and Sec13 proteins respectively, as compared with T cells transfected with control, non-targeting siRNA.

To control for off-target effects of the siRNA, T cells were also transfected with each of the individual siRNA prior to stimulation. Each of the siRNA targets a different sequence of the mRNA encoding Sec13 and And1. The *SEC13* gene lies on chromosome 18 and consists of 3,503 bp and 9 exons (Figure 4.2.5 A). The siRNA #1, #2 and #3 bind to mRNA sequences encoded by exon 6, exon 4 and exon 7 respectively. Each of these individual siRNA reduced expression of the Sec13 protein, as shown by the Western blot analysis (Figure 4.2.5 E). These data indicate that Sec13 depletion is unlikely to be due to off-target effects as the sequences of each of the siRNA are different (see Table 2.4.2 in Materials and Methods). When individual siRNA against *AND1* mRNA were transfected, an efficient knockdown was observed with siRNA #1 and #3 (Figure 4.2.5 F). All three siRNA sequences however bind to mRNA sequences encoded by separate regions of chromosome 14 (exons 19, 23 and 25) (Figure 4.2.5 B), and each has a different sequence (Table 2.4.2). Because two of the three siRNA caused a reduction of And1, again it is unlikely that the effects of the siRNA are due to off-target binding.

When the percentage of Sec13-siRNA transfected cells in each cell cycle phase was analysed, there was an apparent increase in the percentage of cells in G_1 phase and a decrease in cells in $S/G_2/M$ phases in comparison with control-siRNA

transfected cells. 48% (48%±19; mean±SD) of cells transfected with Sec13-siRNA were in G_1 phase and 23% (23%±1%) of the cells were in S/G_2/M phase of the cell cycle, as compared with 36% (36%±23%) and 26% (26%±1%) respectively for cells transfected with control siRNA (n=3; two with 3 individual siRNA and one with pooled siRNA) (Figure 4.2.5 G). However, the increase in G_1 (p=0.08) and decrease in S/G_2/M (p=0.09) is not statistically significant. Transfection with And1-siRNA did not change the percentages of cells in any phase of the cell cycle in comparison with control siRNA. However, a delay in cell cycle entry was observed for the control- and And1-siRNA transfected cells in comparison with non-transfected cells. This delay in cell cycle entry caused by the transfection was observed previously in the laboratory (Orr, personal communication). Similar results were obtained with pooled or individual siRNA against *SEC13* or *AND1* (Figure 4.2.5 H).

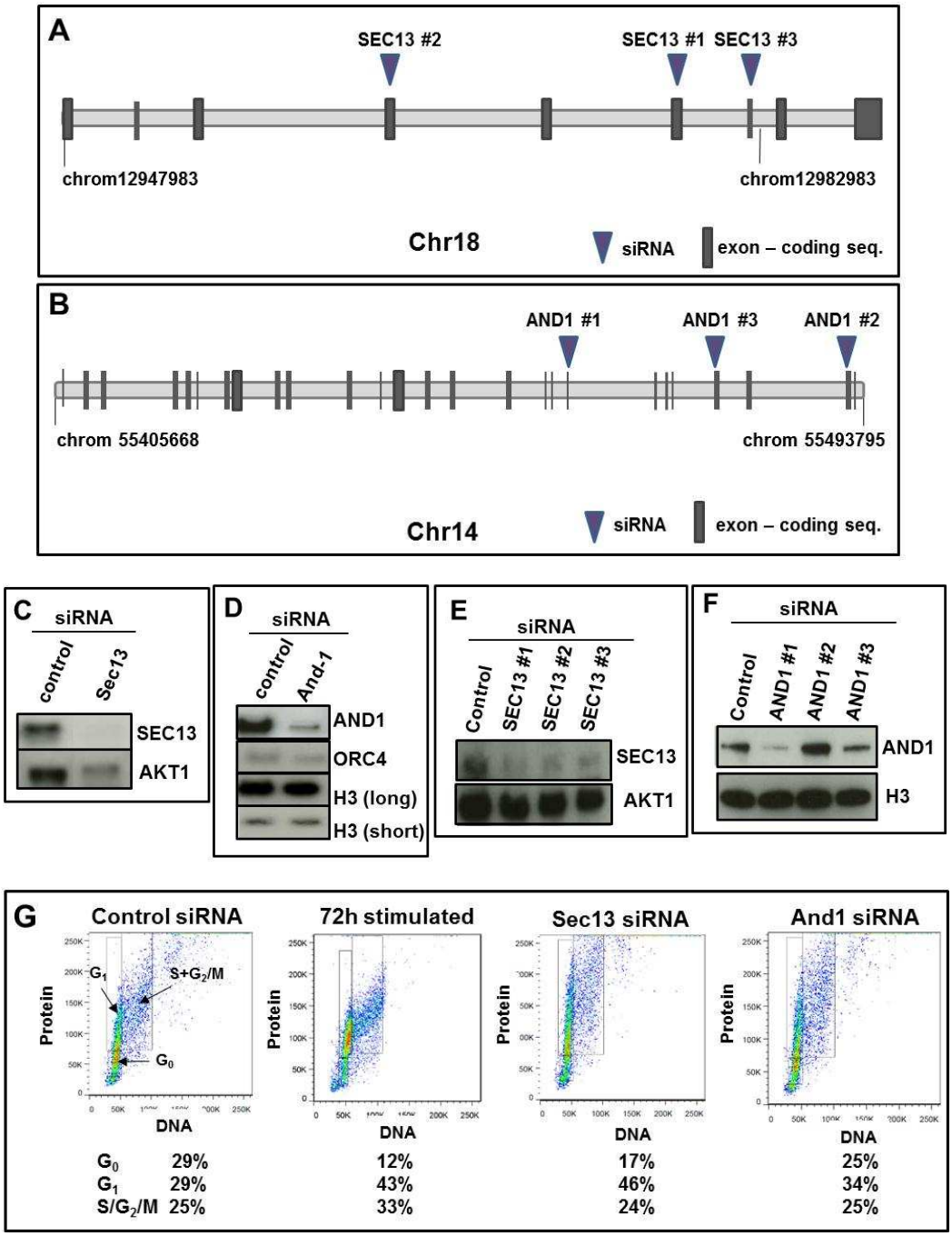
A
SEC13 #2
SEC13 #1
SEC13 #3
chrom12947983
chrom12982983
Chr18
siRNA
exon – coding seq.
B
AND1 #1
AND1 #3
AND1 #2
chrom 55405668
chrom 55493795
Chr14
siRNA
exon – coding seq.
C
siRNA
control
Sec13
SEC13
AKT1
D
siRNA
control
And-1
AND1
ORC4
H3 (long)
H3 (short)
E
siRNA
Control
SEC13 #1
SEC13 #2
SEC13 #3
SEC13
AKT1
F
siRNA
Control
AND1 #1
AND1 #2
AND1 #3
AND1
H3
G
Control siRNA
72h stimulated
Sec13 siRNA
And1 siRNA
Protein
DNA
G1
S+G2/M
G0
G0 29% 12% 17% 25%
G1 29% 43% 46% 34%
S/G2/M 25% 33% 24% 25%

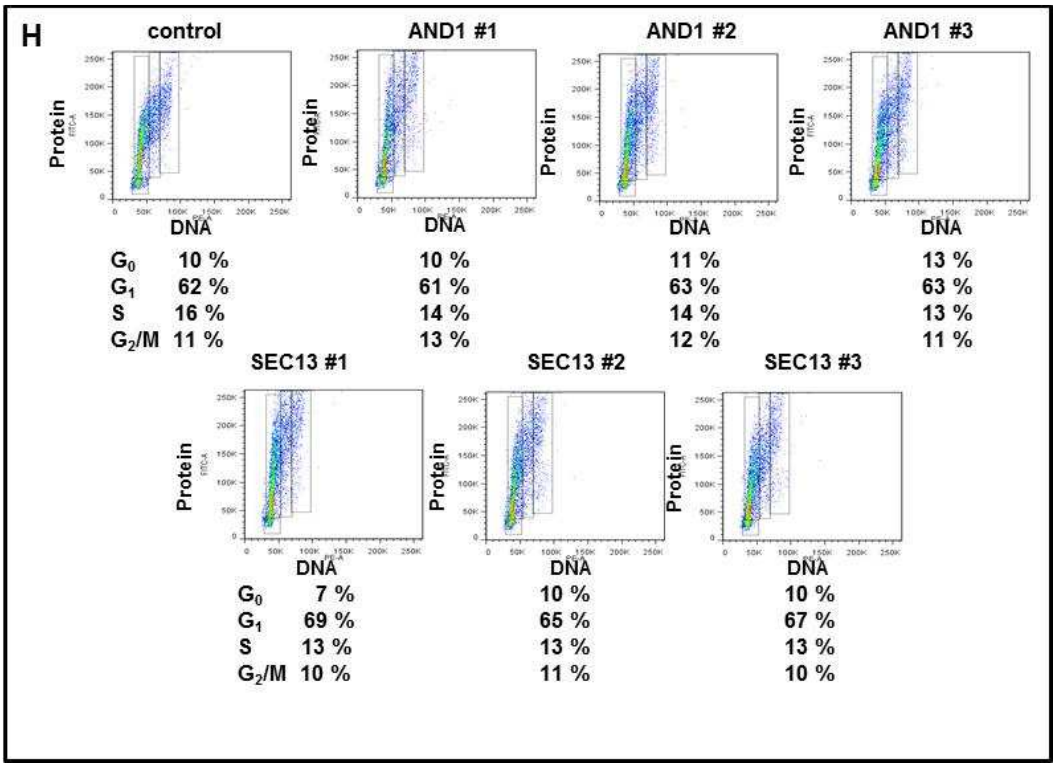

Figure 4.2.5 Reduction of And1 and Sec13 protein expression with siRNA and the effect on the cell cycle.

A. and B. Schematic representation of the chromosome map with the location of targeting and binding of the individual siRNA for exons encoding Sec13 (A.) and for And1 mRNA (B.). Quiescent T cells were transfected with pooled or three individual siRNA against mRNA encoding And1 or Sec13 or control/non-targeting siRNA. The transfected cells were cultured overnight and then stimulated with CD3/CD28 or PMA/Ionomycin for 72 h. The expression of Sec13 or And1 proteins was detected by western blotting for pooled (C. and D. respectively) or individual siRNA (E. and F. respectively). The blots were also probed for Histone H3, Orc4 or Akt1 as loading controls. G. and H. Effects of depleting And1 or Sec13 on the cell cycle using pooled (G.) or individual (H.) siRNA. The cells were fixed with Ethanol and stained with PI (DNA content) and FITC (protein content). The percentage of cells in each cell cycle phase was determined by flow cytometry.

4.2.6. Reduction of And1 or Sec13 levels cause DNA damage

The Phenolog approach predicts that And1 and Sec13 are involved in DNA damage and they may cause chromosomal instabilities, based on the seed set genes *BRCA1*, *BARD1* and *CHEK2*. Therefore, I investigated whether DNA damage is observed in cells in which And1 or Sec13 have been depleted. To do this, the T cell system was used, which was optimised in sections 4.2.4 and 4.2.5 and has been used previously to analyse the initiation of DNA damage and chromosomal abnormalities caused by depleting Mcm7 or Mcm4 (291). Human primary, quiescent, non-activated T cells were transfected with pooled siRNA against mRNA encoding And1 or Sec13 or control/non-targeting siRNA. After a 24 h recovery, the cells were stimulated with CD3/CD28 for 72 h to allow them to enter the cell cycle and to divide. The DNA damage assay was carried out by immunofluorescence staining of DNA damage proteins and scoring the number of cells containing >5 nuclear foci. The CD3/CD28 stimulatory beads were not removed prior to the assay as there can be a significant loss of cells if the beads are not completely dissociated prior to their removal using a magnet. Furthermore, the cells being stimulated would be lost, skewing the results. First, the percentage of foci of phospho-γH2AX (p-γH2AX) was determined. Double strand breaks (DSB) induce histone H2AX phosphorylation on serine 139, which is one of the first responses to such DNA damage (296, 314). Both And1- and Sec13- depleted cells had an increase in p-γH2AX foci *versus* cells transfected with the siRNA control (Figure 4.2.6 A and B). These responses also occurred in T cells cultured with the chemotherapy drugs Etoposide or Bleomycin, which were used as controls in the assay. Bleomycin causes DSB by inhibiting thymidine incorporation into DNA (247), whereas Etoposide is a topoisomerase inhibitor (114) and results in DNA cleavage and chromosome breaks. Note that the CD3/CD28 beads appear as small, round fluorescent spots on all slides, even when the primary antibody is omitted. No foci were observed in assays of Bleomycin- or Etoposide-treated T cells in which no primary antibody was added (Figure 4.2.6 A and B).

Rad51 is a crucial protein for DNA repair through homologous recombination (183, 289). Rad51 is present throughout the nucleus, but upon induction of DNA damage

it relocates specifically to sites of damage, which appear as nuclear foci (77). DNA damage occurs mainly in S phase of the cell cycle and Rad51 co-localizes with p-γH2AX after DNA damage (296). The percentage of cells containing >5 Rad51 foci was determined and whereas foci of Rad51 were observed in 15% of And1-depleted cells, this did not occur in cells in which Sec13 was depleted (Figure 4.2.6 B and D).

Although preliminary, the data described above are indicative of DNA damage caused by depleting And1 or Sec13. Both p-γH2AX as well as Rad51 target DSB, but there is a difference in the percentage of foci for each. This might be due to the fact that γH2AX phosphorylation at sites of DSB occurs within minutes after the initiation of DNA damage, whereas Rad51 and other proteins involved in the DNA repair mechanisms are recruited later. p-γH2AX is responsible for recruitment of other DNA damage proteins (296) and this might explain the difference in the percentages of Rad51 and p-γH2AX observed in this study in response to depletion of And1. Similar differences in the percentage of cells with Rad51 foci was observed in another study from our laboratory (291) and in other work (139).

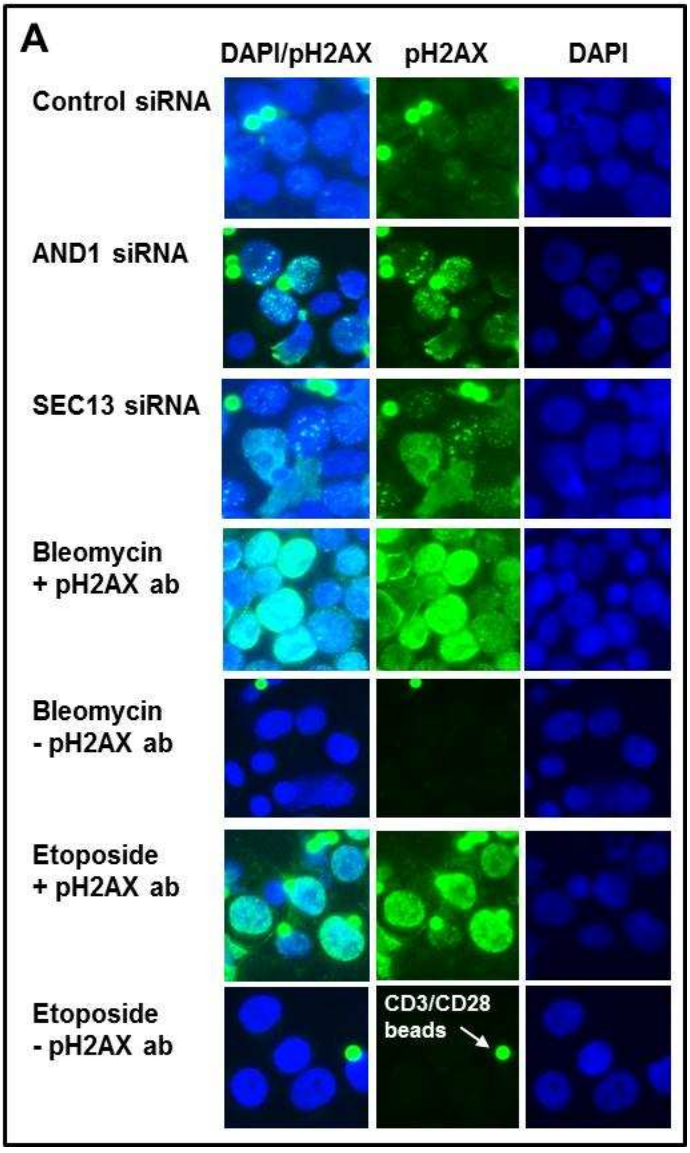
A
DAPI/pH2AX
pH2AX
DAPI
Control siRNA
AND1 siRNA
SEC13 siRNA
Bleomycin
+ pH2AX ab
Bleomycin
- pH2AX ab
Etoposide
+ pH2AX ab
Etoposide
- pH2AX ab
CD3/CD28
beads

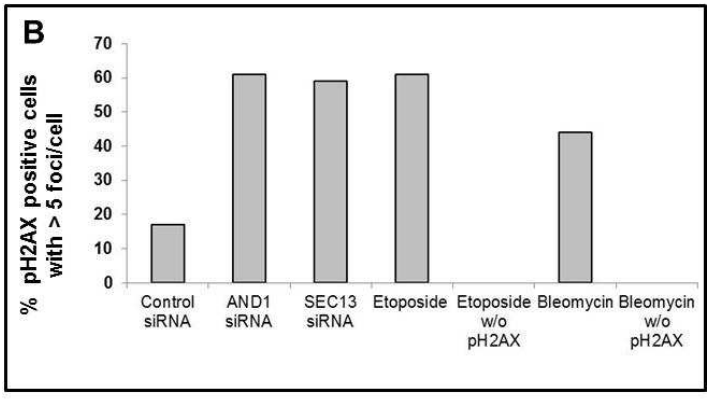
B
% pH2AX positive cells
with > 5 foci/cell
70
60
50
40
30
20
10
0
Control siRNA
AND1 siRNA
SEC13 siRNA
Etoposide
Etoposide w/o pH2AX
Bleomycin
Bleomycin w/o pH2AX

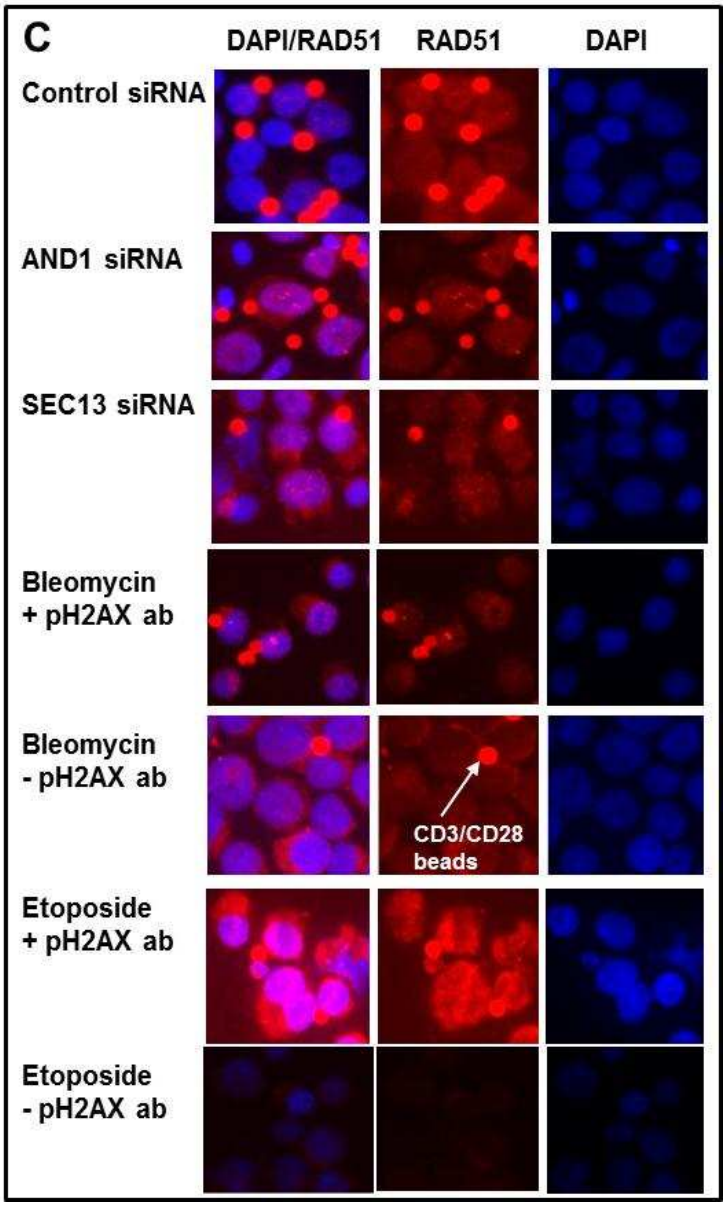
C
DAPI/RAD51
RAD51
DAPI
Control siRNA
AND1 siRNA
SEC13 siRNA
Bleomycin
+ pH2AX ab
Bleomycin
- pH2AX ab
CD3/CD28
beads
Etoposide
+ pH2AX ab
Etoposide
- pH2AX ab

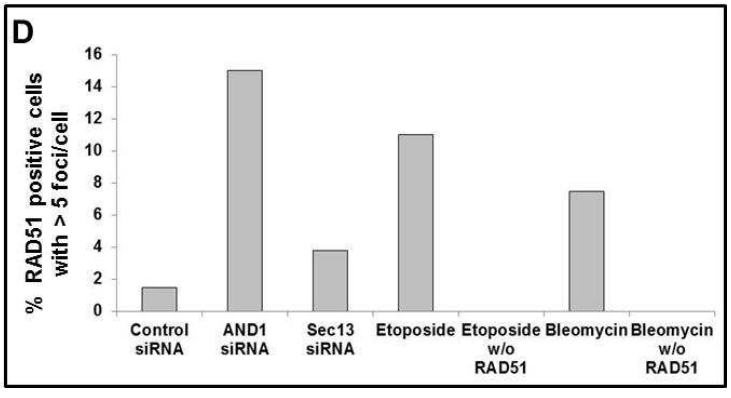
D
% RAD51 positive cells
with > 5 foci/cell
16
14
12
10
8
6
4
2
0
Control
siRNA
AND1
siRNA
Sec13
siRNA
Etoposide
Etoposide
w/o
RAD51
Bleomycin
Bleomycin
w/o
RAD51

Figure 4.2.6 Reduction of And1 or Sec13 levels induce DNA damage.

T cells transfected with siRNA against And1 or Sec13 mRNA, or control siRNA were cultured overnight to recover and then stimulated for 72 h with CD3/CD28 beads. The cells were fixed with paraformaldehyde and immobilised on poly-L-lysine-coated slides by cytocentrifugation. Immunostaining was carried out using an anti-p-γH2AX (A. and B.) or anti-Rad51 (C. and D.) antibody and the number of foci per nucleus was quantified manually by immunofluorescent imaging (B. and D.). As a positive control, T cells stimulated for 72 h with CD3/CD28 beads were treated with Bleomycin or Etoposide for 1 h to induce DNA damage. Bleomycin- or Etoposide-treated cells were also stained with the secondary antibody only (w/o p-γH2AX or w/o Rad51). These are preliminary results; n=1.

4.2.7. Reduction of And1 or Sec13 expression leads to chromosomal instability

The data in the section 4.3.6 show that inhibiting the induction of And1 or Sec13 in T cells causes DNA damage. Genomic instability can result from impaired cell division and DNA damage that is not correctly repaired (182). To investigate whether genomic instability occurs as a consequence of And1 or Sec13 depletion, I-FISH analyses were carried out using fluorescent probes to analyse the integrity of chromosomes 5, 9 and 15. Primary human quiescent non-activated T cells were transfected with pooled siRNA against And1 or Sec13 mRNA or control/non-targeting siRNA and the cells were stimulated with CD3/CD28 for 72 h. To analyse the karyotype, the cells were prepared for I-FISH by incubating the cells in a hypotonic solution to allow swelling, followed by fixation. Hybridisation was carried out with fluorescent DNA probes that bind to chromosomes 5, 9 and 15 and the cells were stained with DAPI to visualise the nuclei. The karyotype was analysed by fluorescence microscopy and the number of each of the chromosomes in at least 50 cells was scored manually for each sample.

Sec13- and And1-depleted cells had abnormal karyotypes, with losses or gains of each of the chromosomes. A variety of abnormalities was observed and representative examples of abnormalities are shown in Figure 4.2.7 A. Cells in which And1 or Sec13 were depleted have >48% and >37% of total chromosomal abnormalities respectively in comparison with the non-targeting siRNA control in at least 3 independent experiments (2 experiments with pooled siRNA and 1 experiment with 3 individual siRNA) (Figure 4.2.7 B). Furthermore, 8%-27% of And1 depleted cells had chromosomal losses and 16%-35% gains of chromosomes (Figure 4.2.7 C and D). When Sec13 was downregulated, 12%-29% of cells had chromosome losses and chromosome gains were detected in 11%-37% of cells (Figure 4.2.7 C and D).

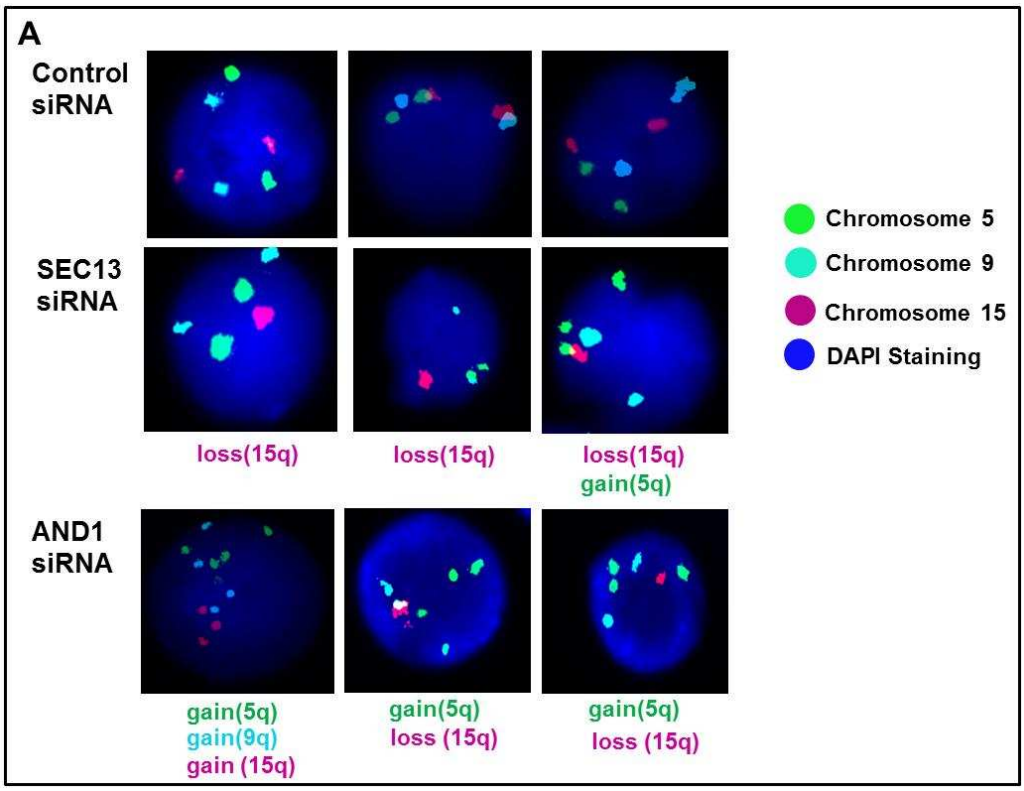
A
Control siRNA
SEC13 siRNA
AND1 siRNA
Chromosome 5
Chromosome 9
Chromosome 15
DAPI Staining
loss(15q)
loss(15q)
loss(15q)
gain(5q)
gain(5q)
gain(9q)
gain (15q)
gain(5q)
loss (15q)
gain(5q)
loss (15q)

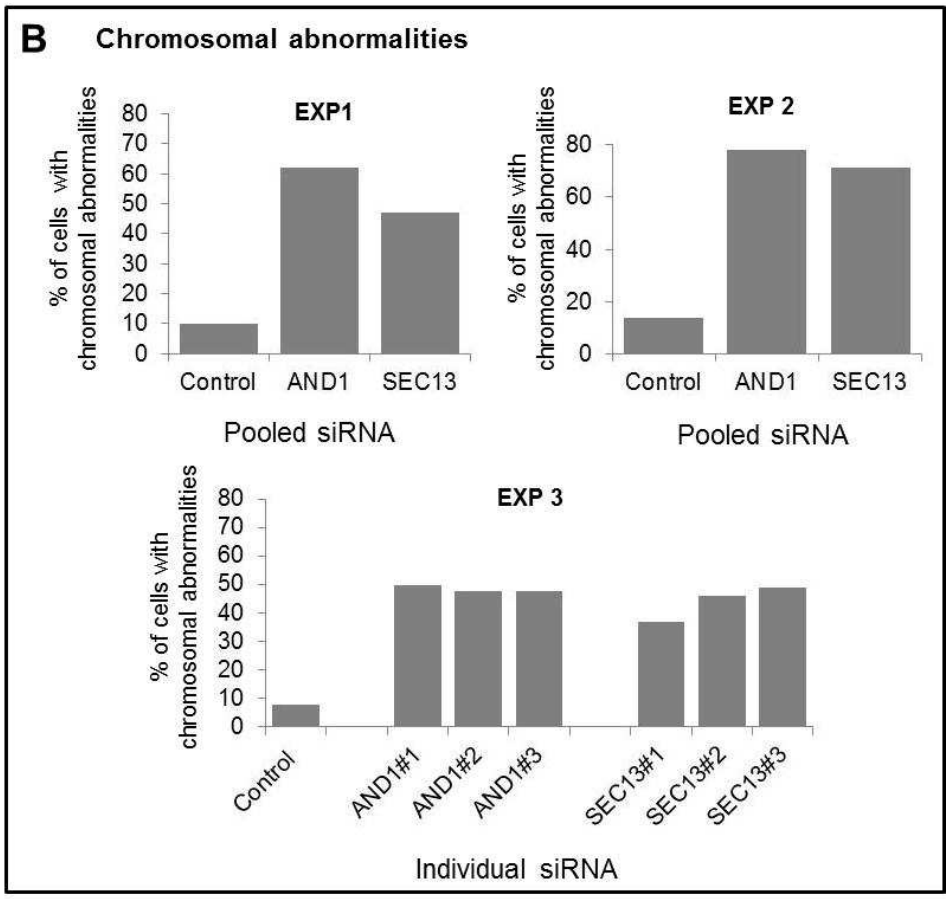
B
Chromosomal abnormalities
EXP1
% of cells with chromosomal abnormalities
Control
AND1
SEC13
Pooled siRNA
EXP 2
% of cells with chromosomal abnormalities
Control
AND1
SEC13
Pooled siRNA
EXP 3
% of cells with chromosomal abnormalities
Control
AND1#1
AND1#2
AND1#3
SEC13#1
SEC13#2
SEC13#3
Individual siRNA

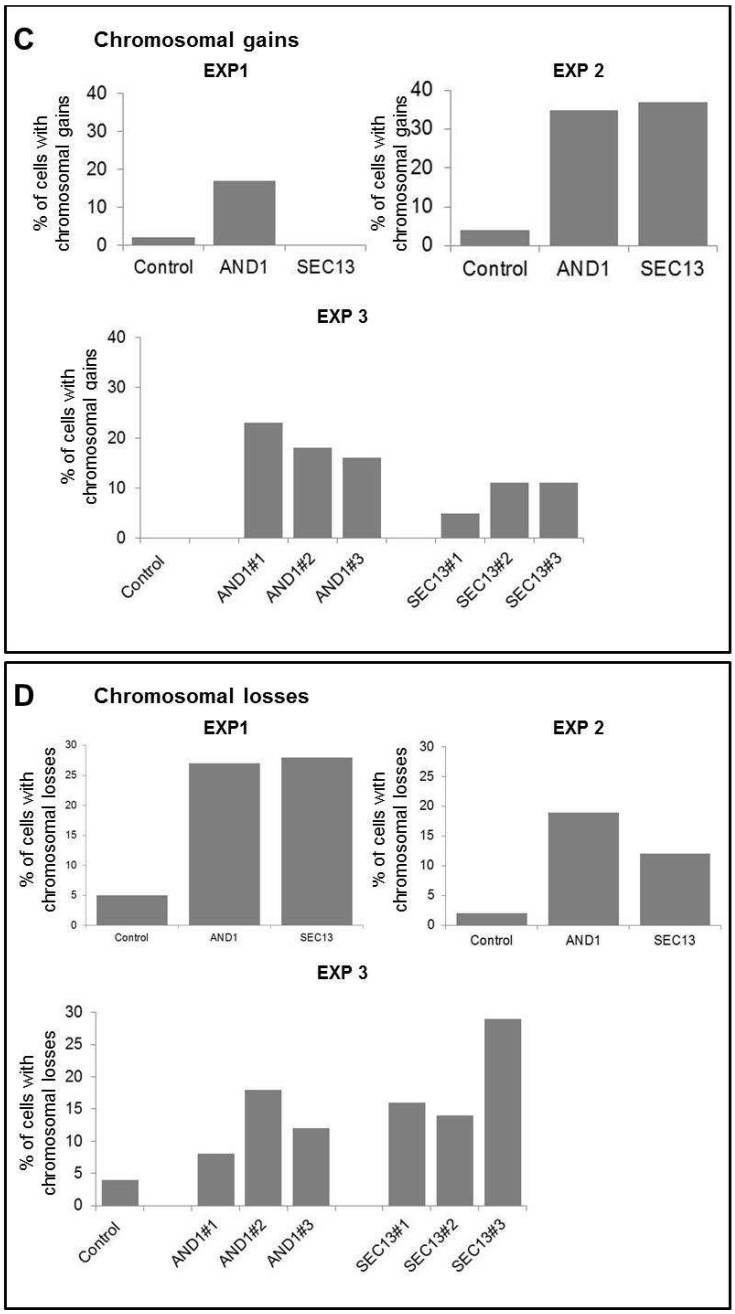

Figure 4.2.7 Depletion of And1 or Sec13 results in abnormal karyotypes.

The induction of And1 or Sec13 was reduced in primary human T cells with siRNA as described for Figure 4.2.6 and I-FISH analyses were carried out using probes for Chromosome 5, 9 and 15. A. Examples of I-FISH analyses of T cells transfected with control siRNA and in T cells transfected with And1 or Sec13 siRNA. B. Percentage of cells with total chromosomal abnormalities, n=3 independent experiments (two with pooled siRNA, one with 3 individual siRNA). C. Percentage of cells with chromosome gains and D. chromosome losses for the same experiments analysed in B.

4.2.8. Quantification of proteins bound to chromatin/nuclear matrix after depletion of Sec13 or And1

The results show that reducing the induction of And1 or Sec13 during entry into the cell cycle from quiescence cause DNA damage and chromosomal instabilities during the first cell cycle. This might occur by several mechanisms. Sec13 is an important component of the nuclear pore complex and one of its' major functions is the transport of molecules between the cytoplasm and nucleus (119, 318). Thus, reducing Sec13 levels will affect the transport of proteins between the cytoplasm and nucleus. This could result in a reduced nuclear localisation of proteins involved in DNA replication and/or DNA damage, such as Mcm2-7, PCNA and DNA polymerase proteins and/or Rad51/XRCC4. On the other hand, And1 is a DNA replication initiation factor (133) and so its' nuclear localisation is crucial for DNA synthesis to occur. Reducing And1 will therefore cause replication fork collapse, consequent DNA strand-breaks, leading to genomic instability, a mechanism similar to that proposed when Mcm7 or Mcm4 are reduced (291).

In order to investigate whether inhibiting the induction of Sec13 affects the nuclear localisation of specific proteins, chromatin/nuclear matrix (C/NM) and free proteins of target-depleted T cells were extracted as previously described (125, 208, 218) (see section 2.6.4). T cells transfected with control or Sec13 siRNA were recovered overnight and stimulated using CD3/CD28 beads for 72 h. C/NM and free fractions were then prepared. The lysates were analysed by Western blotting for proteins involved in DNA replication. The data show that reducing Sec13 causes a reduction in DNA polymerase α (PolA1) but not in the DNA replication protein Orc4 (Figure 4.2.8). Thus, the amount of PolA1 in the cell is decreased, which would be expected to impair DNA replication and cause replication fork collapse.

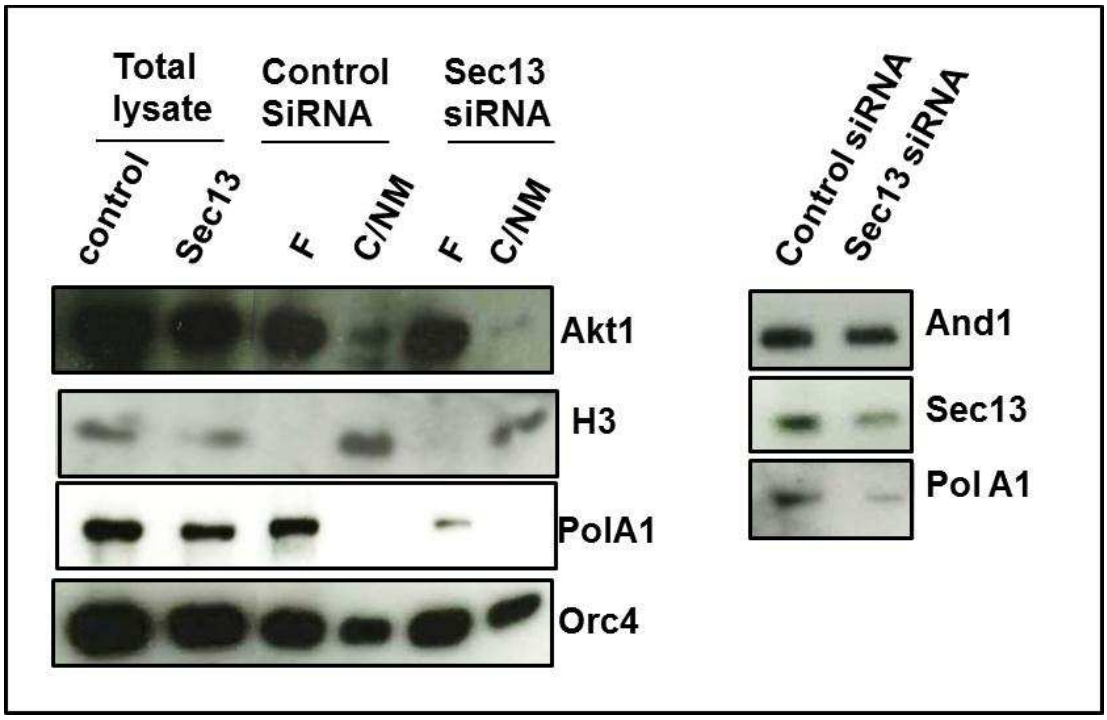

Figure 4.2.8 Western blot analyses of chromatin/nuclear matrix (C/NM)-bound and free proteins extracts.

Quiescent T cells were transfected with siRNA and stimulated as described for Figure 4.2.6. Chromatin/nuclear-matrix (C/NM) and free (F) proteins were extracted from the control- or *SEC13*-siRNA transfected cells and the expression of the proteins shown was analysed by western blotting. The blot was probed for Histone H3 for the extraction of chromatin bound proteins and Akt1 as a control for free proteins.

4.3 Discussion

4.3.1. Validation of the Phenolog predictions

The data presented here show that the proteins encoded by the genes *AND1* and *SEC13* predicted by the Phenolog approach are required to maintain genomic stability. These predictions are based on associations with genes known to be abnormal in breast cancer, but they can be applied to any cancer or disorder in which some genetic or epigenetic abnormalities are known (248). This novel approach is founded on genetic information from many different species and is a very powerful tool for systematically predicting non-obvious genes that are functionally important in a range of human diseases.

4.3.2. AND1

The results of experiments described in this Chapter demonstrate that reducing the induction of And1, which normally occurs during entry into the cell cycle from quiescence, causes chromosomal abnormalities. I investigated the consequences of reducing And1 expression using a human primary T cell system that was used previously in the laboratory to investigate what occurs when the expression of the DNA replication proteins, Mcm4 and Mcm7 are reduced (291). And1 is a protein associated with the DNA replication complex and it sits between the MCM helicase that unwinds the DNA and DNA polymerase α (437) (Figure 4.3.2). And1 recruits DNA polymerase α to chromatin to initiate DNA replication at licensed replication forks and is involved in establishing sister chromatid cohesion (39, 121).

Reducing the induction of And1 has been shown here to cause DNA damage. Analysis of proteins which interact with And1 using HumanNet, a probabilistic human protein interaction network (www.functionalnet.org/humannet/) (219), suggest that And1 interacts with Atr, which is a protein required for DNA repair in response to DNA damage (269). Phosphorylation of And1 is induced by replication arrest and depends on Atm/Atr (428). There is also evidence that Atr interacts with Brca1 (405), which is again one of the 3 seed set proteins of the Phenolog

predictions. This indicates that there is a link between And1, Brca1 and the response to DNA damage. Formation of Rad51 foci observed when And1 is depleted indicates further that the HR repair pathway is involved (183). The HR pathway is one of the DNA repair pathways which operates during S-phase (291). Reduction of And1 and a consequent reduction in the recruitment of DNA polymerase α would lead to replication fork collapse and DNA damage, which was observed here by the formation of phospho-γH2AX nuclear foci.

The consequences of downregulating DNA replication proteins has been studied previously in the laboratory (291). Reducing Mcm4 or Mcm7 causes DNA damage, consistent with stalling of the replication fork. Assays were also carried out in this study which showed that reducing components of the MCM helicase led to premature chromatid separation and genome instability. A similar mechanism may also occur when And1 is depleted, but this would be due directly to a failure to recruit DNA polymerase α rather than to reducing the binding of the MCM proteins.

The role of And1 has been studied in other species apart from humans. Mcl1, an And1 homolog in the fission yeast *Schizosaccharomyces pombe*, has been reported to be essential for viability, maintenance of genome integrity and regulation of telomere replication (376).

Depletion of And1 in HeLa cells is reported to cause G_1/S phase arrest (39). Downregulation of And1 increases DNA damage, delayed progression through S phase, leading to accumulation of cells in late S and/or G_2/M phases and induction of cell death. It has been proposed that And1 coordinates S and G_2 phase processes, such as checkpoint activation, sister chromatid cohesion and DNA damage repair and it plays a pivotal role in maintaining genomic integrity (428). However, the percentage of cells in the G_1/S phases of the cell cycle were not altered in And1-depleted T cells in my study. This observation may be due to the fact that in the studies by Bermudez *et al.* (39) and Yoshizawa Sugata and Masai (428) cancer cell lines were used (HeLa and U2OS cells). These cells have abnormal karyotypes (www.lgcstandards-atcc.org/LGCAdvancedCatalogueSearch/tabid/961/Default.aspx?CollectionID=106)

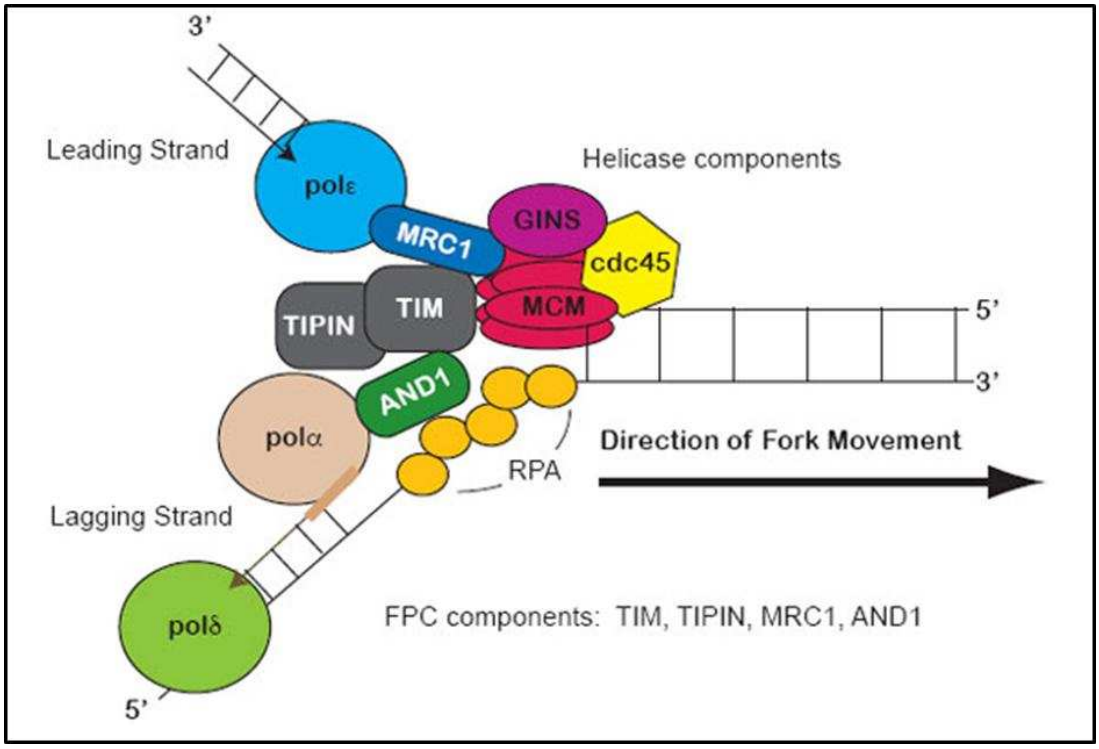

Figure 4.3.2 Schematic representation of the localisation of And1 at the replication fork.

The And1 protein binds to chromatin and is located at the DNA replication fork between DNA polymerase α and the Mcm2-7 helicase complex (Adapted from (325), http://www.nature.com/scitable/content/replication-fork-components-14463312).

and it is known that the p53 and pRb pathways are dysfunctional. The major advantage of using primary T cells is that these cells have a normal genetic background and so all cellular mechanisms are intact.

And1 is also associated with centromeres in a cell cycle-dependent manner in mid to late S phase (165). Centromeres are chromosomal elements to which the kinetochores anchor during mitosis. The effects of And1 downregulation are a failure to recruit epigenetics modifiers Kdm2A and Suv39h1, resulting in defective centromeres and defects in mitosis (165). This mechanism may also cause chromosomal abnormalities, but it was not investigated here.

Finally, genomic instability is a hallmark of cancer (150) and there is evidence for abnormalities in *AND1* in cancers. Mutations of *AND1* have been reported at a low-frequency in ovarian and skin cancer (www.sanger.ac.uk/genetics/CGP/cosmic/). *AND1* has also been shown to be overexpressed in a large proportion of lung and oesophageal carcinomas (327), suggesting that this gene is a crucial player in these cancers. It would be interesting to investigate whether the recruitment of any other DNA replication proteins to DNA is affected by And1 overexpression or *AND1* mutations.

4.3.3. SEC13

I show here that reducing the levels of Sec13 in primary T cells also causes DNA damage and an abnormal karyotype. There is evidence that reducing Sec13 expression causes genomic instability in U2OS cells, assayed by treatment of GFP-Sec13-transfected U2OS cells with nocodazole and analysing the DNA content by flow cytometry (346). However, U2OS is an osteosarcoma cell line and 2% of the cells have multipolar mitoses and are therefore prone to chromosomal variation (275), whereas primary T cells have a normal karyotype.

Sec13 is a multifunctional protein and protein:protein interactions with Sec13 can affect many different processes in the nucleus, such as DNA damage, gene expression or cell cycle progression (Figure 4.3.3 C). Therefore, the mechanisms

involved in causing genomic instability are less obvious than they are for And1 and there are several possibilities how this might occur. Sec13 is a component of the nuclear pore complex that transports macromolecules between the cytoplasm and nucleus (9, 116, 161) (Figure 4.3.3 A). Depletion of a single nucleoporin, Npc107, prevents the assembly of a subset of nucleoporins into the nuclear pore complex. However, Nup96 and Sec13 were unaffected and assembled into Nup107/Nup133-deficient NPCs (47). Sec13 is a component of the core of the nuclear pore complex (119) and is required for the transport of different molecules, such as transcription factors into the nucleus and RNA from the nucleus to the cytoplasm (65, 318, 323).

In order to elucidate the mechanism by which reducing Sec13 causes DNA damage, I investigated whether reducing Sec13 affects the levels of DNA replication proteins. The data indicate that reduction of Sec13 causes a reduction in Pol1A but not Orc4. It is not clear why PolA1 is reduced when Sec13 is depleted, but reducing the level of this polymerase would be expected to impair DNA replication, cause replication fork collapse and lead to genomic instability.

There are several possible mechanisms by which PolA1 could be depleted when Sec13 levels are reduced. Nuclear export of mRNA also occurs through the nuclear pore complex and is closely linked to transcription and RNA processing (357). Nuclear pore proteins have also been shown to be involved in gene activation and regulation (7, 63). Sec13 and other nuclear pore proteins, such as Nup98, bind to the *Drosophila* genome, specifically at transcriptionally active sites (64). Thus, reducing Sec13 levels may also selectively impair transcription of a sub-set of genes in human T cells, such as *POLA1*, but this requires further study. Sec13 is tightly bound to the Nup107-160 complex, but Sec13 is also more loosely associated with the Nup107-160 complex (229), suggesting that it has other functional roles. It has been shown that nucleoporin levels are regulated during cell cycle progression (305) and that during mitosis some proteins of the NPC, such as Nup96 are downregulated (71). Furthermore, changing nuclear pore expression can affect cell cycle progression (71). NPCs, including Sec13, have also been shown to have important roles in kinetochore and spindle assembly functions in mitosis (93, 229). Thus, another possibility is that reducing Sec13 affects

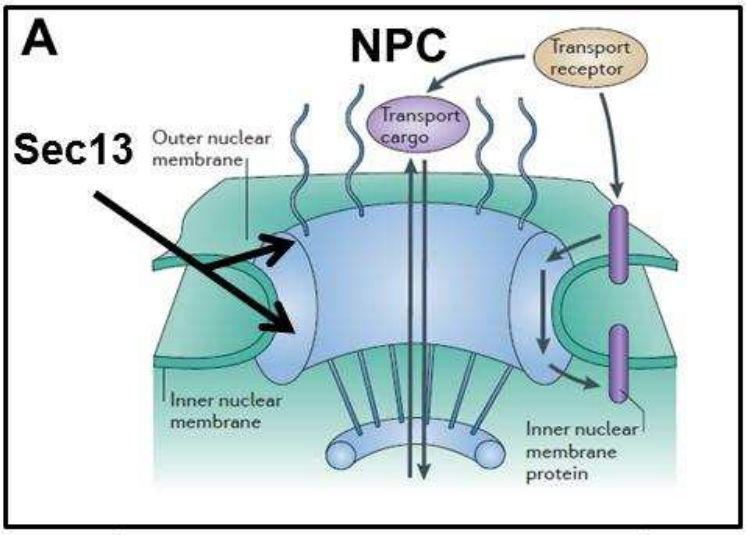
A
NPC
Transport receptor
Transport cargo
Sec13
Outer nuclear membrane
Inner nuclear membrane
Inner nuclear membrane protein

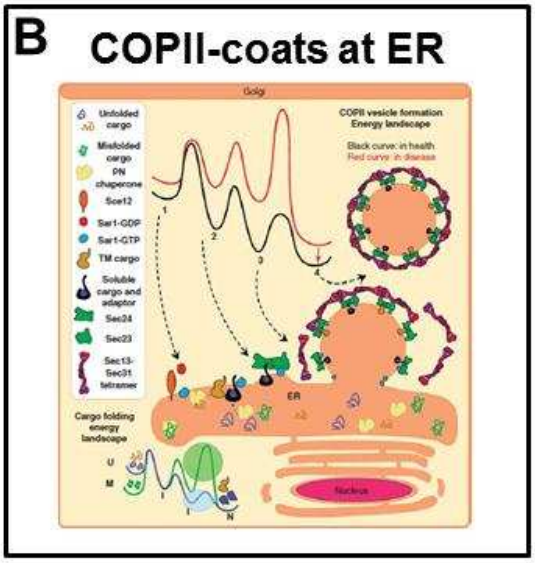
B
COPII-coats at ER
Golgi
COPII vesicle formation Energy landscape
Black curve: in health
Red curve: in disease
Unfolded cargo
Misfolded cargo
PN chuperone
Sce12
Sar1-GDP
Sar1-GTP
TM cargo
Soluble cargo and adaptor
Sec24
Sec23
Sec13-Sec31 tetramer
ER
Cargo folding energy landscape
Nucleus

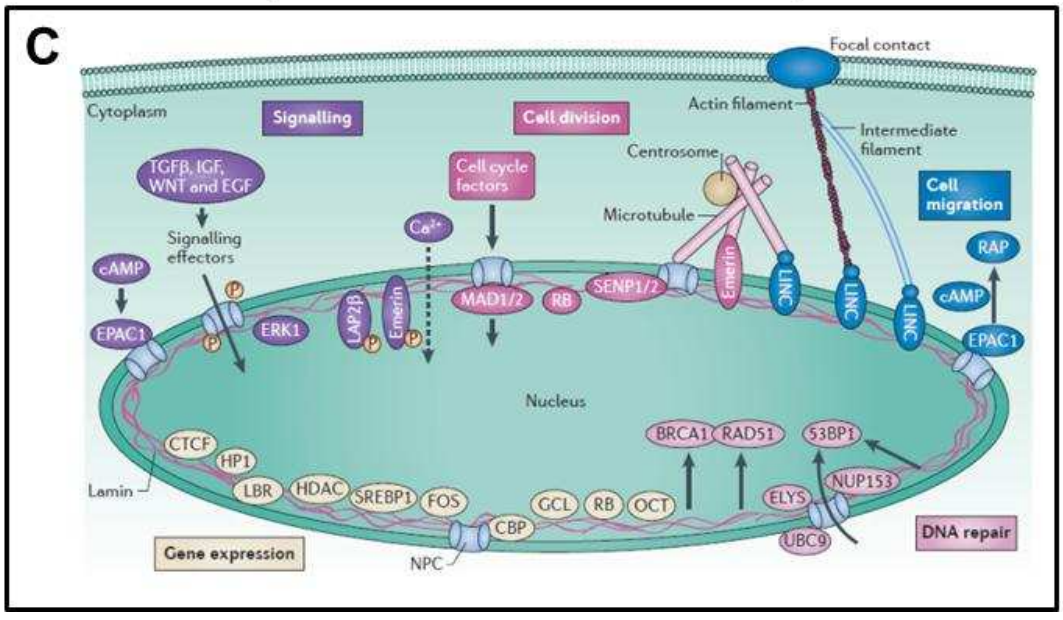
C
Focal contact
Cytoplasm
Signalling
Cell division
Actin filament
Intermediate filament
Centrosome
Microtubule
Cell migration
TGFβ, IGF, WNT and EGF
Signalling effectors
Cell cycle factors
Ca2+
cAMP
RAP
EPAC1
ERK1
LAP2β
Emerin
MAD1/2
RB
SENP1/2
LINC
Nucleus
CTCF
HP1
Lamin
LBR
HDAC
SREBP1
FOS
GCL
RB
OCT
CBP
BRCA1
RAD51
53BP1
ELYS
NUP153
UBC9
NPC
Gene expression
DNA repair

Figure 4.3.3 Potential mechanisms explaining the cause of chromosomal instabilities in Sec13-depleted cells.

Sec13 is a multifunctional protein: it is reported to be involved in transporting molecules into and out of the nucleus (A), it is a part of the COPII complex required for the transport of proteins out of the ER (B) and it is involved in nuclear processes including DNA repair, gene expression, cell division, cell cycle and cell migration (C). The schema in A. and C. are from (81) and B. from (319).

chromosome segregation, thereby causing chromosome abnormalities. However, this is not likely to be the main mechanism in the study presented here, since the chromosomal abnormalities were observed in approximately 50% of cells and fewer than 11% of the cells were in G_2/M.

Sec13 is also a part of the COPII complex required for the transport of proteins out of the endoplasmic reticulum to downstream compartments of the secretory pathway and for delivery of receptors to the cell surface (319) (Figure 4.3.3 B). Sec13 is part of the COPII coat (355), which shares architectural and mechanistic principles with the cylindrical coat of the nuclear pore, including the nucleoporin pair Sec13-Nup145C (101). A role for this function of Sec13 in the induction of chromosomal instabilities has not been reported by others and I did not investigate this mechanism in my studies.

Nucleoporins are linked to cancers, either through higher expression in tumours or through their involvement in gene fusions (205, 421). Chromosomal translocations of *NPC* have been found in leukaemias and produce fusion proteins, such as *NUP98-NSDI* that impair normal transcription (402). *NUP98*–translocations for example have been implicated in causing acute myeloid leukaemia. *NUP98-HOXA10HD* significantly increases the self-renewal capacity of haematopoietic stem cells (430). Moreover, Nup88 has been proposed as a tumour marker and the protein, together with the oncogene *NUP214*, are implicated in leukaemia (154, 421). Normal expression of these proteins is crucial to prevent aneuploidy (154). It would be interesting to determine to what extent such abnormalities affect the normal function of the nuclear pore complex and if so, whether this contributes to the induction of chromosomal instability in these cells, in addition to the roles of the fusion proteins.

Chapter 5

5. Proteome analyses of chromatin-bound proteins in activated primary human T cells by LCMS/MS, using four different extraction methods

5.1 Introduction

T cells can remain in a quiescent state for months or years in the peripheral blood before they become activated and enter the cell cycle. Progression through the cell cycle requires coordination of many cellular programmes that lead to huge changes at protein levels (218). Our knowledge of which proteins interact with each other and how they take part in cellular processes is very incomplete. Studying the changes in protein levels and predicting how they interact will give a better understanding of how cellular processes may be controlled and coordinated. The complexity of protein expression at different times and their sub-cellular localisations however makes a comprehensive understanding difficult.

There is a world-wide interest in understanding the cell at the genome level and genomes of humans and other organisms have been sequenced. Furthermore, microarray and RNA-seq methods have been used to analyse mRNA expression programmes. However, the concordance between mRNA and protein expression is poor and the contribution of mRNA concentration to protein abundance was only 27% in a human cell line (393). Furthermore, protein abundances are conserved more highly across seven different species than the abundance of their corresponding mRNA. These data indicate that there is strong evolutionary pressure to maintain protein rather than mRNA abundances (217). Analysing the proteome directly has the advantage of focusing on the biological effector molecules and at the same time providing information about the subcellular localisation (149). The difficulty is that the proteome is much more complex than the primary sequence of the genome. Currently, analysing the whole proteome, including all potential post-translation modifications, is not feasible. Thus, limiting the analysis of proteins to a particular organelle or investigating changes that occur, for instance during entry into the cell cycle or in response to UV irradiation, can usefully limit the number of proteins that need to be analysed (see (16, 261) for examples).

Previous work in the laboratory was carried out to analyse chromatin/nuclear matrix (C/NM)-bound proteins of primary human T cells during entry into the cell cycle from quiescence (290). This study used a rapid, mild CSK extraction method to enrich the C/NM-bound proteins (described previously in (218, 291); modified from (208)). When quiescent non-activated T cells were stimulated with PMA/Ionomycin for 40 h to enter the first cell cycle, thousands of proteins became induced and these were identified by analysing their Tryptic peptides by liquid-chromatography coupled to tandem mass spectrometry (LCMS/MS). Quantification of the mass spectrometry (MS) analyses of 0h *vs.* 40h stimulated T cells showed that there are many significant changes in C/NM-bound proteins which occur during cell cycle entry. This lead to the generation of a protein-protein interaction network of such changes, in effect a dynamic "wiring diagram" of the T cell.

Since two fundamental biological processes, DNA replication and gene transcription take place at the chromatin level, there is a particular interest in the identification of chromatin-associated proteins (341). However, chromatin proteins are often expressed at very low levels and are potentially difficult to extract from the nucleus (341). A commonly applied method to maintain the structure of chromatin-bound proteins for further analyses is to crosslink proteins to DNA with formaldehyde. This method has been used extensively for chromatin immunoprecipitation (ChIP)-PCR and ChIP-sequencing protocols, including analysing the localisation of E2F and other transcription factors (*e.g.* (188, 291, 350)). Since many methods may selectively extract proteins that are associated with DNA (*e.g.* different phosphorylated forms of the retinoblastoma protein (258)), crosslinking may therefore help to maintain the binding of weak proteins to DNA. Native ChIP protocols isolate chromatin using a mild NP40 extraction by first isolating nuclei, followed by micrococcal nuclease treatment (*M.nase*), which releases mono-, di- and poly- nucleosomes (used in a previous study by our laboratory (350)).

In the study presented in this Chapter, the chromatin proteome obtained by a native, non-cross-linked chromatin extraction method is compared with that

obtained after formaldehyde crosslinking. In addition, the methodology is compared with the CSK extraction method that was used previously in (290). In Chapter 6 I describe the use of methods optimised here to analyse changes in the chromatin-bound proteome which occur when DNA replication is perturbed by depleting the DNA helicase, Mcm7 (291).

5.2 Results

5.2.1. Isolation of quiescent T cells from peripheral blood and induction to enter the cell cycle with PMA and Ionomycin

Primary peripheral blood T lymphocytes were chosen for this study as their cell cycle and other cellular control mechanisms are normal and they have been shown to be a good model for analysing events during cell cycle entry (218). Non-activated T cells were isolated by negative selection from a leukocyte cone or from fresh blood, as described in Chapter 2.2.2 and 2.2.3 The purity of these cells was determined by flow cytometry of CD3 (T cell receptor expression) and these data showed that the T cell preparations were >99% pure (Figure 5.2.1 A). Quiescent cells are in a non-dividing state but they still maintain the ability to divide in response to a stimulus such as PMA/Ionomycin and they induce effector (activation) functions, such as the expression of a number of cell surface proteins *e.g.* CD69 (Figure 5.2.1 B) (see (218)). The quiescent T cells were stimulated with PMA/Ionomycin overnight and stained the next day with a CD69-PE antibody or PE-isotype-matched control IgG. As a negative control, non-stimulated T cells were also stained with each antibody. The analyses of the non-stimulated T cells revealed that >92% of the cells were non-activated, quiescent cells. The quiescent cells do not express CD69 and have a 2n DNA content when stained with propodium iodide (PI) (Figure 5.2.1 C). Staining with FITC (a non-specific protein stain) showed that these cells also had low protein content as compared with the same cells stimulated for 40 h with PMA/ionomycin. Western blotting analyses revealed little or no expression of proteins required for DNA replication such as MCM proteins, Cdc7, Cdt1 and Orc4, whereas the expression of the leukocyte-specific protein LSP1, which is expressed by quiescent T cells (290), is high (Figure 5.2.1 E). Analyses of DNA content and cellular protein content of the T cells stimulated with PMA/Ionomycin for various time periods showed that the cells were responsive to PMA/Ionomycin and they enter the cell cycle (Figure 5.2.1 C). Primary T cells need to be stimulated for 2-5 h to be committed to entering the cell cycle and progress through the G_1 commitment point (218). An increase in protein content, indicative of an increase in cell size (218) is detectable by 16 h and at 32 h 30% of the cells have a 2nDNA content and a higher protein content than the

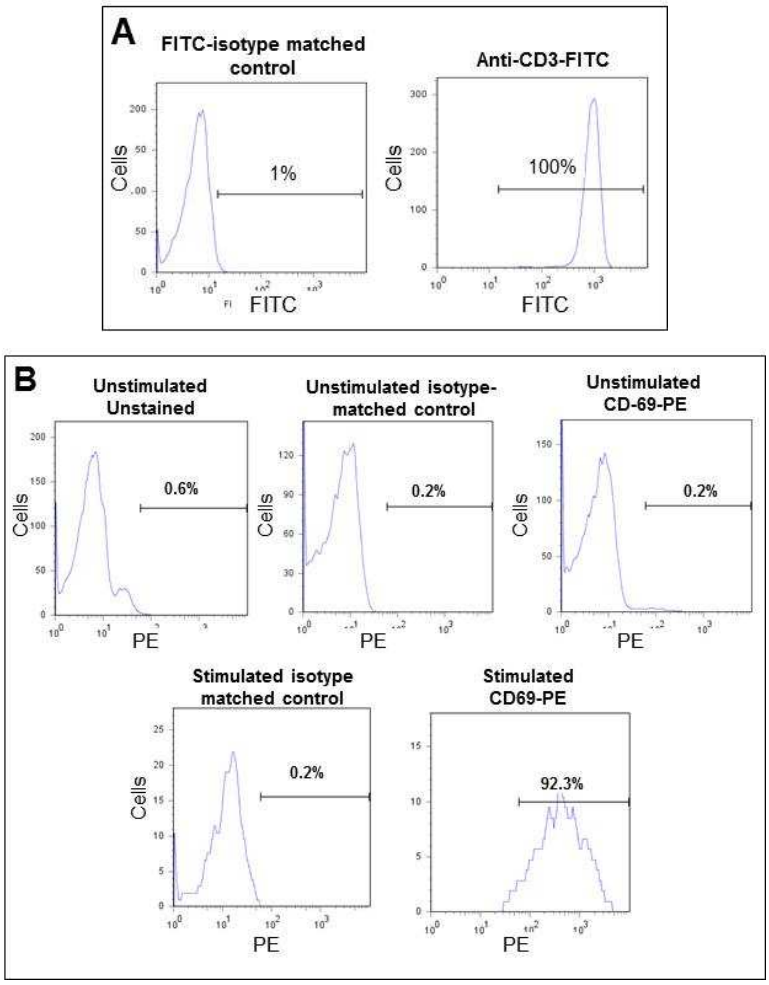

Figure 5.2.1 Isolated T cells are predominantly quiescent and not activated.

A. The purity of primary, peripheral blood T cells isolated by negative selection from a leukocyte cone was determined by quantifying CD3-positive cells (CD3-FITC) or FITC-isotype matched control by flow cytometry. B. The percentage of activated, CD69-positive cells was determined for unstimulated T cells and for T cells stimulated with PMA/Ionomycin overnight. Each preparation was fixed and stained with CD69-PE antibody or PE-isotype-matched control IgG.

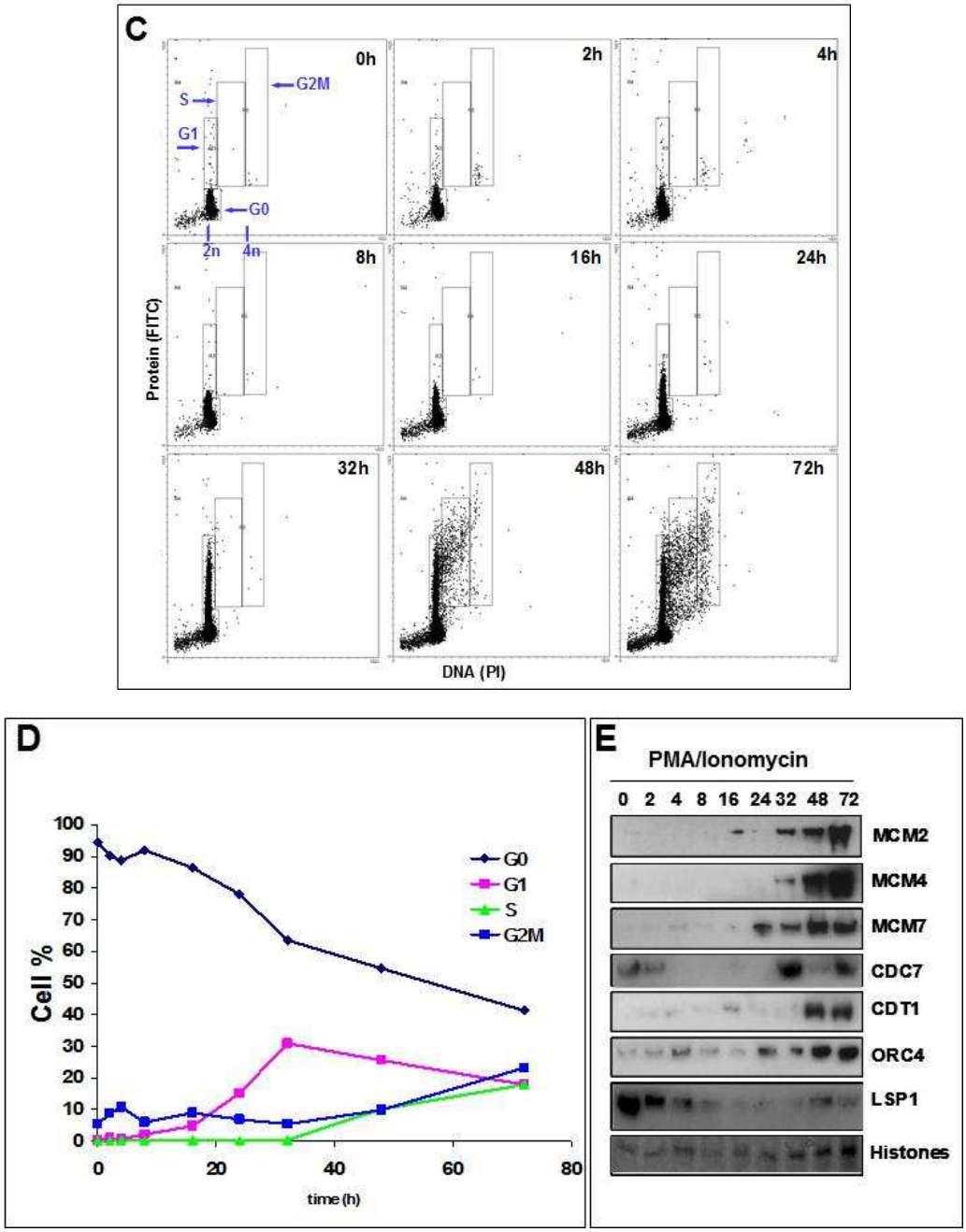

Figure 5.2.1 Kinetics of cell cycle entry.

C. Quiescent T cells were stimulated with PMA/Ionomycin to enter the cell cycle. Flow cytometry analyses of cells stained with PI (DNA content) and free FITC (protein content) were used to quantify the number of cells in each phase of the cell cycle. D. Percentages of cells in different stages of the cell cycle measured by the flow cytometry described for panel C. E. Western blot analysis of the DNA replication proteins shown. LSP1 is highly expressed only in G_0 (290). The blot was also probed for Histone H3 as a control for loading.

quiescent cells, consistent with entering G_1.

Between 32 and 48 h they enter the S-phase, when DNA is synthesised and by 72 h the cells are proliferating. Previous data has shown that 36% of cells divide once and <1% twice when stimulated for 72 h (218) and the kinetics of cell cycle entry for the T cells used for experiments in this Chapter (Figure 5.2.1 D) are consistent with previous studies in the laboratory (218, 290). Analyses of the expression of proteins required for DNA replication show that several of these proteins, such as Mcm2, Mcm4, Mcm7, Cdt1 and Cdc7 are induced between 24 h and 32 h post stimulation (Figure 5.2.1 E). These data are consistent with "licensing" of DNA replication (79), which occurs in late G_1 and these data are again consistent with a previous study by our group (291). Therefore, the T cells, which will be analysed below in section 5.2.3 onwards, respond to stimulation with the expected kinetics and enter the cell cycle, as analysed by a number of criteria.

5.2.2. Detergent removal optimisation prior MS analysis

The nuclear and/or the chromatin-bound proteome of T cells will be analysed in 5.2.3 *et seq* by liquid chromatography (LC) coupled to tandem mass spectrometry (LCMS/MS). The common strategy to convert proteins extracted from biological samples to peptides that are analysed by MS consists of several steps. This includes solubilisation and denaturation of proteins, followed by reduction of disulphide bonds, then alkylation of reduced cysteins and finally Trypsin digestion of proteins to peptides (see sections 2.13.1 and 2.13.2). Overall, each of the steps during sample preparation is crucial and determines the quality of the MS data. For example, the presence of detergents in samples analysed by MS causes severe problems such as signal suppression, formation of adducts with peptides and proteins as well as shape distortion of protein signals (132, 231, 321). Depending on the concentration of detergents, this leads to apparent changes in mass values, increasing the MS complexity and causing a noisy background (19, 62), which significantly reduces the number of proteins identified. Therefore, it is important to remove the detergents in the most efficient manner before MS analyses.

In previous studies carried out in the laboratory, the fractionation of cell lysates using CSK extraction buffer involves the use of 0.5% (v/v) Triton X-100 (290). It was observed that even extensive washing does not remove all of the detergent and this leads eventually to clogging of the LC stages and to a decreased number of peptides detected for specific proteins. Furthermore, the detergent removal method used at that time (Extracti-Gel D, Pierce) caused a selective loss of certain proteins, including MCM complex proteins such as Mcm7, which might partition into micelles ((290)-Supplementary).

To investigate first whether preparation of cell lysates using different detergents has an impact on the MS analysis, two different cell lysate methods were tested, which will be used later. For this, primary quiescent T cells were prepared and stimulated with PMA/Ionomycin for 40 h. The cells were formaldehyde-cross-linked (w XL) for 8 min or not (w/o XL, native). Then, either a CSK extraction method (see section 2.6.4) or chromatin isolation (see section 2.6.5) was carried out. The samples were prepared and analysed by LCMS/MS, as described in 2.13 and illustrated in Diagram 5.2.2. The analyses were carried out in collaboration with Dr. Daniel Boutz while I was in the Marcotte laboratory at the University of Texas at Austin, USA. The LCMS/MS data show that all samples which did not undergo a detergent removal method have a high abundance peak at a very late elution time in the LC chromatograms (Figure 5.2.2 A, upper graphs). This peak correlates in elution time with a very characteristic polymer pattern of peptide adducts in the m/z histogram (Figure 5.2.2 A, lower graphs). The peptides analysed are eluted as adducts with the detergents. The adducts are hydrophilic polyethylene oxide groups from the detergent that shift the m/z ratio by +44. This observation was made regardless of the sample preparation method and which detergent was used (CSK extraction or chromatin isolation). The consequence is that the proteins from which the peptides are derived cannot be identified in such a complex mixture.

In order to remove the detergents efficiently and to decrease the signal suppression by detergents, three alternative methods were investigated to remove detergents prior to MS analysis. In the first method an OrgoSol DetOut detergent removal system (GBiosciences) was used prior to denaturation (see section 2.12.1),

followed by the established MS sample preparation method. The detergent removal kit is a column-based method in which the protein is precipitated with a proprietary mix of organic solvents (similar to acetone precipitation), followed by washes to remove the detergents. The second method, described by Wisniewski, *et al*. (413) is a filter-aided sample preparation (FASP) detergent removal method (see section 2.12.3). This method is based on the observation that membrane proteins can be fully depleted from detergents by gel filtration in 8M urea and then analysed efficiently by MS. Urea is a chaotrope that is commonly used for denaturation by disruption of non-covalent bonds between atoms (38). In this approach, the proteins are solubilized in SDS in the presence of DTT, denatured in 8M Urea and the detergent is removed by gel filtration using a centrifugal filter untit (Ambion). The filter unit acts as 'proteomic reactor' for detergent removal and buffer exchange. The advantage of the method is that the approach can be applied to strong detergents, such as SDS that can be efficiently cleaned up before digestion using an ultra-centrifugation device (413). The disadvantage is that this method is very time consuming, is expensive, has a poor reproducibility and causes a high sample loss (38). In the third method investigated, proteins are digested in the presence of 0.1% (w/v) SDS, and the SDS is removed prior LCMS/MS using a modified commercial detergent removal spin column (Pierce) (38) (see section 2.12.2).

To investigate each of the methods for the capacity to remove detergents, lysates of a HeLa cell line were used to which each different detergent (0.1% (v/v) NP40, 0.1% (w/v) SDS or 1% (w/v) SDS) or no detergent was added. A cell line was used as multiple samples could be prepared as necessary and the effects of the detergents on proteins and their identification by the LCMS/MS methods illustrated in Diagram 5.2.2 are not dependent on the cell of origin. The chromatograms with the corresponding m/z histograms are shown for the different detergents using the OrgoSol DetOut method, as an example (Figure 5.2.2 B). Analysis of peptide spectra after using each of the three detergent removal methods (OrgoSol DetOut, FASP detergent removal or Pierce spin columns) shows that they are all able to remove the detergent effectively. In each case, the characteristic adduct peak is not observed, as indicated by the red arrows in Figure 5.2.2 B.

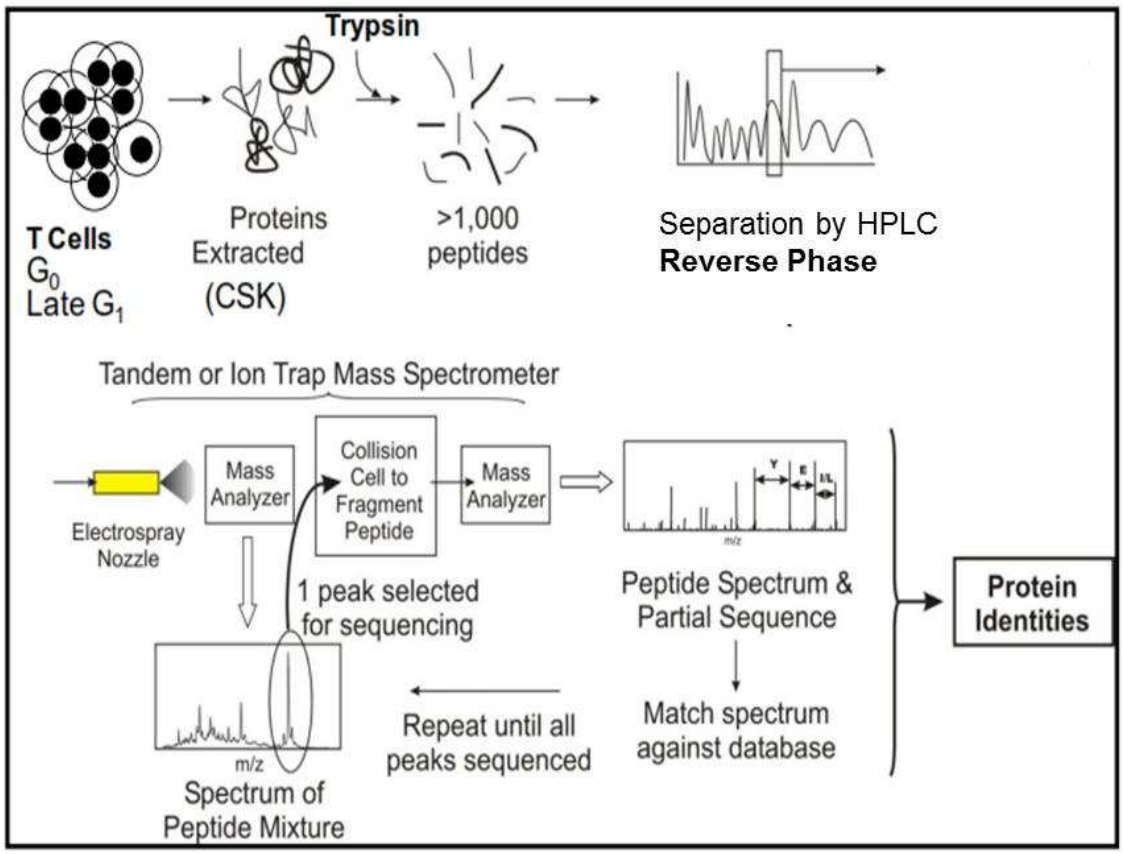

Diagram 5.2.2. Representation of the LCMS/MS workflow (adapted from Marcotte).

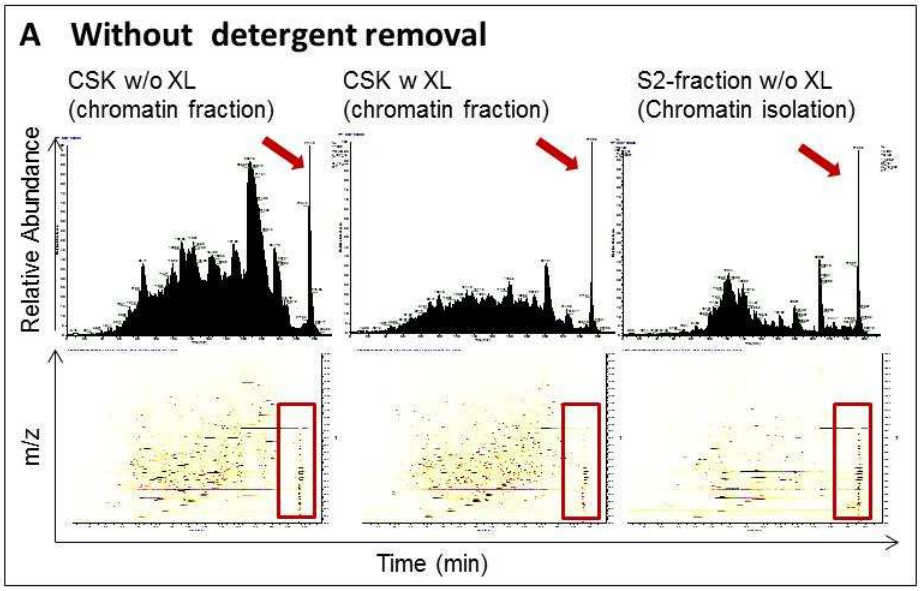
A Without detergent removal
CSK w/o XL
(chromatin fraction)
CSK w XL
(chromatin fraction)
S2-fraction w/o XL
(Chromatin isolation)
Relative Abundance
m/z
Time (min)

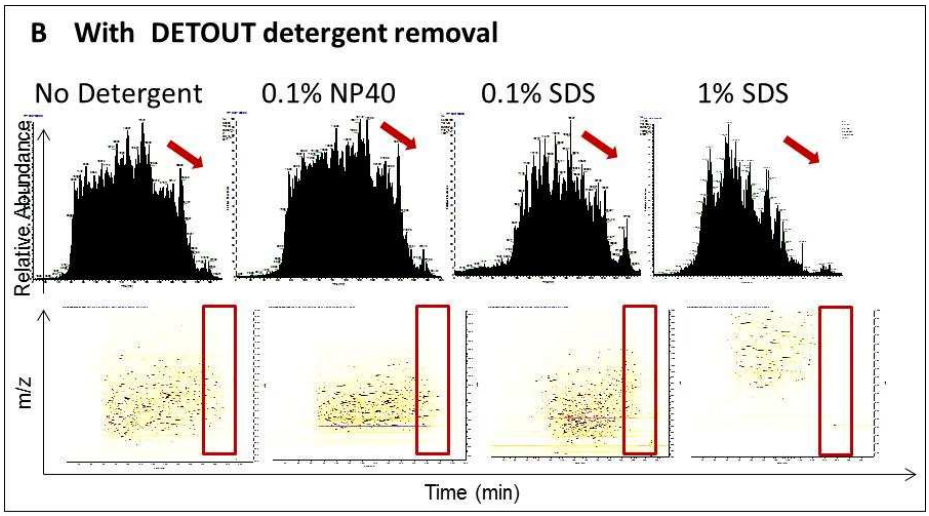
B With DETOUT detergent removal
No Detergent
0.1% NP40
0.1% SDS
1% SDS
Relative Abundance
m/z
Time (min)

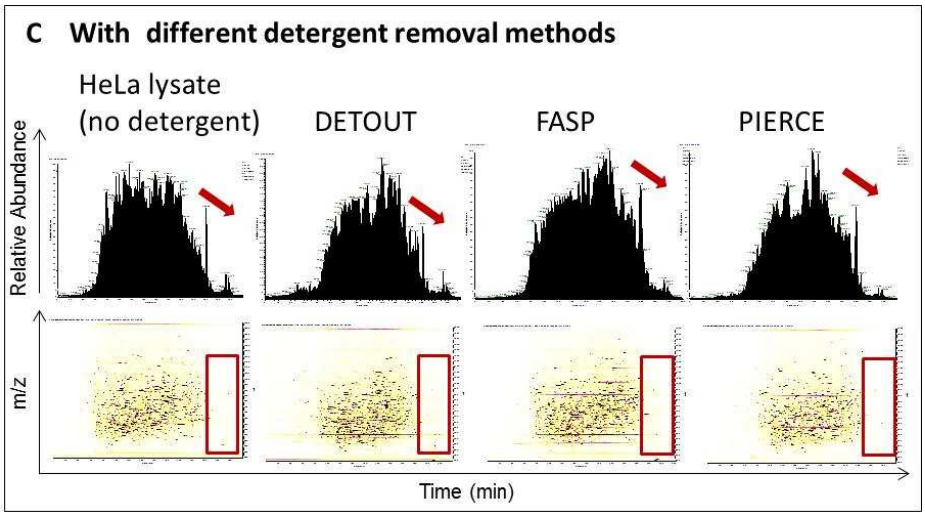
C With different detergent removal methods
HeLa lysate
(no detergent)
DETOUT
FASP
PIERCE
Relative Abundance
m/z
Time (min)

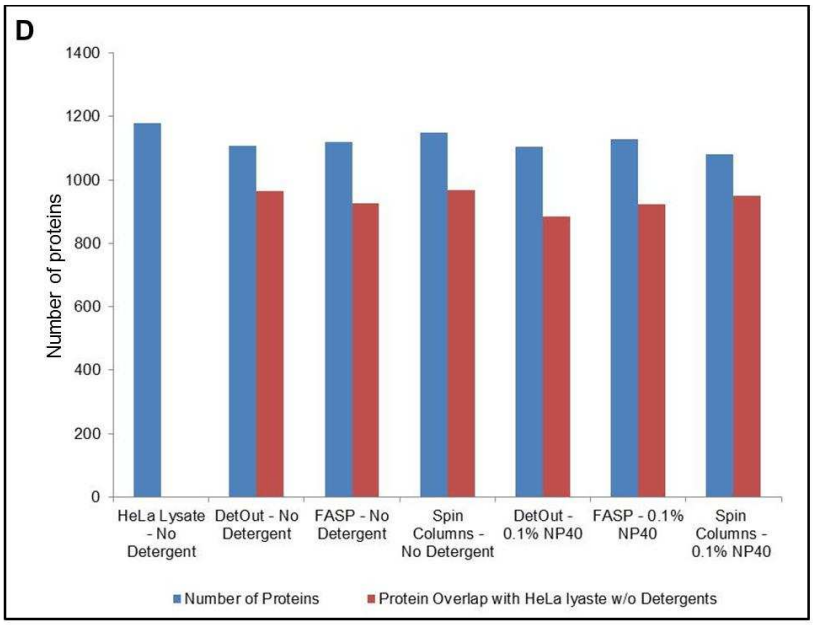

Figure 5.2.2 Optimising the detergent removal method for MS analyses.

A. Primary human quiescent T cells were stimulated for 40 h with PMA/Ionomycin. Proteins were isolated by the CSK extraction method (see section 2.6.4) or by the chromatin isolation (S2-fraction) (see section 2.6.5) that has been previously cross-linked (w XL) using formaldehyde or not (native, w/o XL). Protein samples were analysed by LCMS/MS without removing the detergent. B HeLa lysates without detergents or with 0.1% (w/v) NP40, 0.1% (v/v) SDS or 1% (v/v) SDS were analysed by MS prior to detergent removal using the DetOut kit. C. HeLa lysates containing 0.1% (w/v) NP40 treated with three different detergent removal methods (DetOut, spin columns or FASP). HeLa lysates without any detergent were used as a control. D. Number of proteins identified in HeLa lysates with 0.1% (w/v) NP40 or without any detergent after different detergent removal methods were used. HeLa lysates without any detergents were used as a control. A., B., C. and D. Upper panels: LCMS/MS chromatograms. Lower panels: m/z histograms.

In order to distinguish whether one or the other detergent removal method is more suitable for the purposes of the project, HeLa lysates were used to which only 0.1% (w/v) NP40 was added. Secondly, the HeLa lysates were diluted 5 x to be able to separate the peptides better by LC. HeLa cells without any added detergent were used as a control. The MS analyses of the 0.1% (w/v) NP40-containing HeLa lysate samples that has been prepared using one of the three detergent removal methods showed that the detergent was removed with the same efficacy, as determined by the LCMS chromatograms and m/z histograms (Figure 5.2.2 C). Next, the number of proteins identified was determined for each sample to investigate whether the number of proteins detected is dependent on the detergent removal method used. The number of proteins detected in each sample was compared with the number of proteins detected in the HeLa lysate without detergent. However, the sample underwent the same procedure as samples with detergents. Overall, the number of the proteins was very similar (Figure 5.2.2 D). The identified proteins are in S 5.2.2 on the CD in the back of this Thesis. A total of 1,179 proteins were identified in the HeLa lysate that does not contain any detergent, whereas 1,104, 1,128 and 1,079 proteins were detected in the HeLa lysates containing 0.1% (w/v) NP40 prepared with the DetOut, FASP and spin columns respectively. Thus the number of proteins detected after any of the three detergent removed methods was used is lower as compared with the untreated HeLa lysate, but there is no significant difference between the samples prepared by the different methods. Similar protein numbers were obtained in the samples without detergent as in samples with NP40. The overlap in the proteins is >884 proteins in all samples. Tables showing the proteins detected in each case are appended in Table S 5.2.2 in the CD attached to this Thesis. For all MS analyses in this and the next chapter, the detergents were removed using the spin column method prior to MS analysis. This method was chosen since the proteins prepared with the spin columns and identified by LCMS/MS have the highest overlap with proteins identified in the HeLa lysate without detergents. In addition, this method is the easiest and quickest to perform.

5.2.3. Proteome analyses of the C/NM-bound proteins with or without crosslinking in T cells by LCMS/MS, using CSK extraction

To investigate the impact of crosslinking of proteins to DNA with formaldehyde on the nuclear proteome, samples were prepared from quiescent human peripheral blood primary T cells that were stimulated with PMA/Ionomycin for 40 h. Prior to the extraction, 25 x 10^6 T cells were either cross-linked with formaldehyde for 8 min (XL) or not (Native). C/NM-bound proteins were then isolated by CSK extraction (see 2.6.4). Approximately 10% of the cells were also lysesd in SDS-lysis buffer and analysed by western blotting. The western blot analysis of the C/NM and free/unbound (F) proteins was carried out to test the extraction method. Blots were probed for free/unbound proteins (Cdk6 and phospho-pRb($S^{807/811}$)) and C/NM-bound proteins (Histone H3 and Mcm7) (Figure 5.2.3 B). The data show that Histone H3, which is tightly bound to DNA, is present not only in the cross-linked, but also in the native C/NM-fraction. In comparison, Mcm7 proteins that are involved in DNA replication are not bound tightly to the chromatin in the native fraction (as has been observed previously in the laboratory (291) and a higher proportion of these proteins are detectable in this fraction when the proteins are cross-linked. Cdk6 and pRb phosphorylated on $S^{807/811}$ are present in the free fraction under native conditions. However, a small fraction is C/NM-bound due to crosslinking. A small amount of Cdk6 has been reported previously in the nuclear fraction (349). Human pRb is phosphorylated on 15 different sites and although hyper-phosphorylated pRb would not be expected to be chromatin-bound (258), further work is required to determine which $S^{807/811}$ phosphorylated form(s) of pRb are being detected here. The time of crosslinking is crucial to avoid non-specific binding, but reducing the crosslinking time to 2 or 5 minutes did not affect the results (Figure 5.2.3 A).

The western blotting analyses showed that the extraction of proteins into C/NM-bound and free fractions by the CSK method worked. It was then investigated whether the crosslinking of proteins changes the proteome of the C/NM fractions by MS. The protein extracts were prepared for MS analysis by removing detergents using OrgoSol DetOut kit and one sample was analysed by LCMS/MS. A total of

784 proteins were identified in the non-cross-linked C/NM-fraction (native CSK), whereas 1,187 were identified in the cross-linked C/NM-faction (XL CSK). Of the proteins identified, 44 histones, proteins encoded by 5 pseudogenes and 3 haemoglobins identified in the native CSK protein extract, and 46, 6 and 5 respectively identified in the XL CSK protein extract were removed from the analyses. Histones were removed as they exist is in many variants, which can differ by only a few amino acids (21). It is difficult to identify such variants unequivocally and it is not the intent here to analyse histone variants which are bound to T cell chromatin under different conditions. Haemoglobin proteins are very likely to be contaminants in the analyses from a very small number of red cells and were also removed from the analyses. The identification of proteins encoded by pseudogenes and whether read-through transcripts may encode proteins is problematic and, although they are noted, I removed this group from my analyses. A total of 732 and 1,130 proteins in the native and XL CSK extract respectively were taken for further analysis of subcellular classification. Previous work in the laboratory detected a similar number of proteins (502 in total) in the C/NM-bound, non-cross-linked fraction of T cells stimulated with PMA/Ionomycin for 40 h (Steve Orr Thesis, (290)).

To determine the cellular localisation of the proteins identified in my study, the HumanNet, database (http://www.functionalnet.org/HumanNet/about.html) was used as the reference (219). HumanNet enables the classification of proteins based on their major sub-cellular localisation and gives an indication of which cellular compartment the proteins are localised. In order to be able to classify proteins by the subcellular localisation, the Entrez Gene ID of each protein was required. The Entrez Gene ID was generated for the identified proteins by converting the Ensemble Gene ID using the GO ontology database (www.genontology.org). Proteins that did not have an Entrez Gene ID were removed from the analysis (65 proteins in Native CSK and 61 proteins in XL CSK). Although the sub-cellular localisation was determined primarily using HumanNet, in cases in which the proteins were classified to a complex of proteins that were not defined as a class, the sub-cellular location was determined using either GeneCards (http://www.GeneCards.org/) or NCBI (http://www.ncbi.nlm.nih.gov/) annotations. The proteins identified and their sub-cellular location is in S 5.2.3 on the CD in the

back of this Thesis. Of 667 proteins, 46.5% were nuclear, 6.1% nucleolar (giving a total of 52.6%) and 6.3% cytoplasmic in the native CSK extract (Figure 5.2.2 C). These data correlated with previous data obtained in the laboratory, in which 46% nuclear proteins were identified in the C/NM-bound extract, but it is not clear why a higher number of nucleolar proteins (29.0%) were detected. In the XL CSK extract, 38.6% were nuclear, 3.6% nucleolar (giving a total of 42.2%) and 13.9% cytoplasmic of the 1,069 proteins identified (Figure 5.2.2 D). Thus, although the data show that more proteins were detected in the cross-linked C/NM-fraction extract than in the native fraction of the CSK extract, the percentages classified as nuclear or nucleolar are similar. The HumanNet database however underestimates the number of nuclear proteins, as many proteins are annotated to a different cellular location, such as the cytoplasm, but they also occur in the nucleus. For example nucleoporins, such as Nup188 and Nup85 are classified as 'integral to membrane' according to HumanNet, but they are also known to be localised in or associated with the nuclear envelope as part of the nuclear pore complex (196, 229). Arp2/3 promotes actin cytoskeleton assembly in the cytoplasm, but the Arp2/3 complex is also localized in the nucleus and plays an essential role in mediating nuclear actin polymerization (425). There is also evidence that several ribosomal proteins such as RPS14 have functions in the nucleus. RPS14 has been found to directly interact with and is a critical regulator of p53 and Mdm2 (435). Ribosomal proteins will also be detected because the pre-ribosome is assembled in the nucleolus and ribosomes are exported to the cytoplasm through the nucleus (discussed in (290)). There is also evidence that nuclear forms of actins, MSN and IL16 exist (30, 282). Cherp is mainly known as an endoplasmic reticulum membrane protein, but it has also been observed to be perinuclear (279). Similarly, Ezr is localised in the cytoskeleton but it is also present in the nucleolus (30). Therefore the HumanNet database, as well as other automated methods of functional classification such as GO, are very useful to obtain an initial classification of protein localisation, but care must be taken as other nuclear forms of many proteins may exist.

The analyses also showed that some unique nuclear proteins that are not detected in the crosslinked extract are detected in the non-crosslinked, native fraction, such

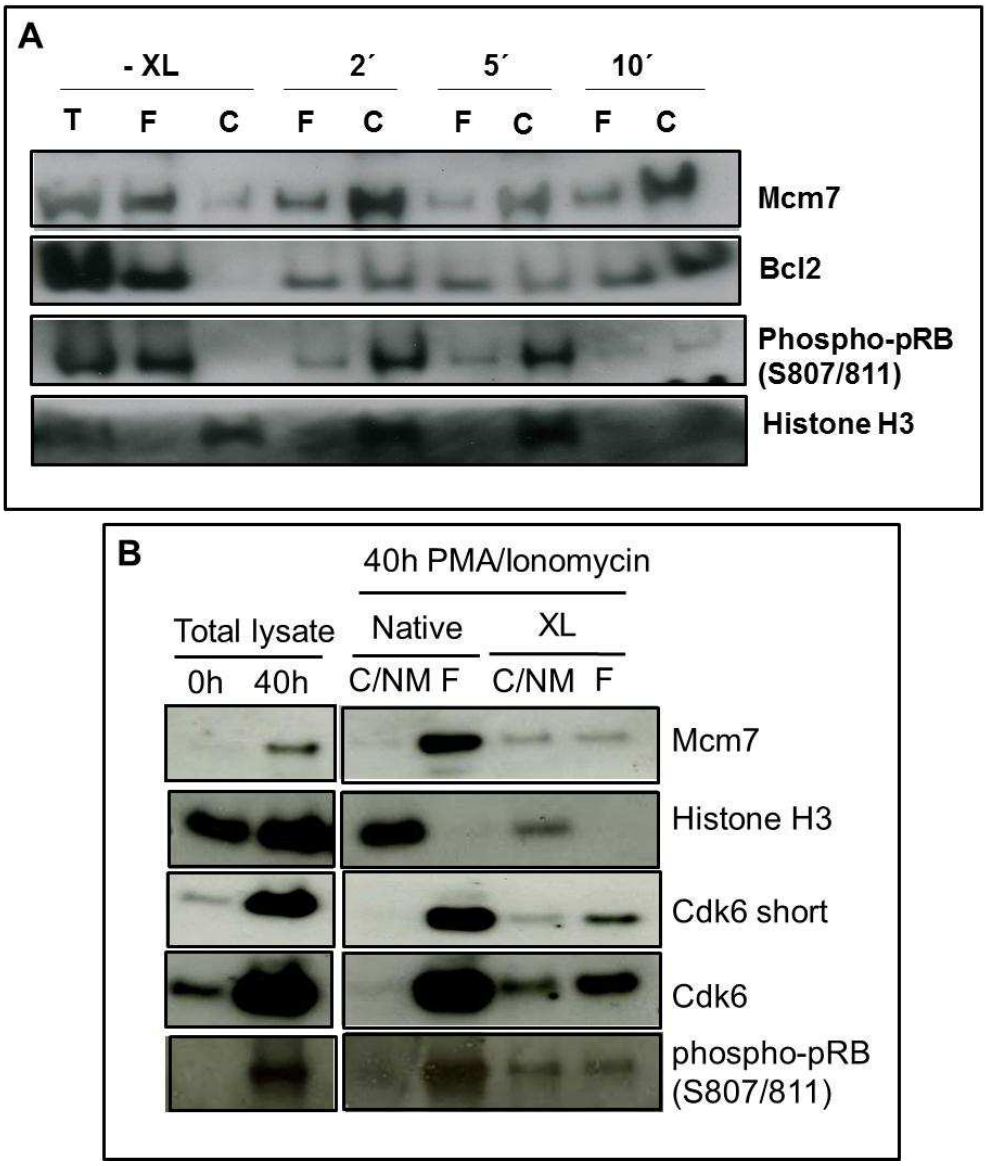

Figure 5.2.3 Western blot analysis of CSK protein extracts.

A. T cells were stimulated for 72 h with PMA/Ionomycin and were either crosslinked with formaldehyde for 2´, 5' or 10' min or not crosslinkled (-XL) and CSK extraction was carried out. Proteins in the C/NM-bound (C) and free (F) fractions as well as in the total lysate was analysed by western blotting.

B. Quiescent primary T cells were left unstimulated or stimulated for 40 h with PMA/Ionomycin and the total lysates were analysed by western blotting. Proteins of 40 h stimulated T cells were crosslinked with formaldehyde (XL) for 8min or not (Native) and extracted using CSK buffer. Analyses of samples of C/NM–bound (C/NM) and free/unbound (F) extracts are shown and these CSK extracts were analysed by mass spectrometry.

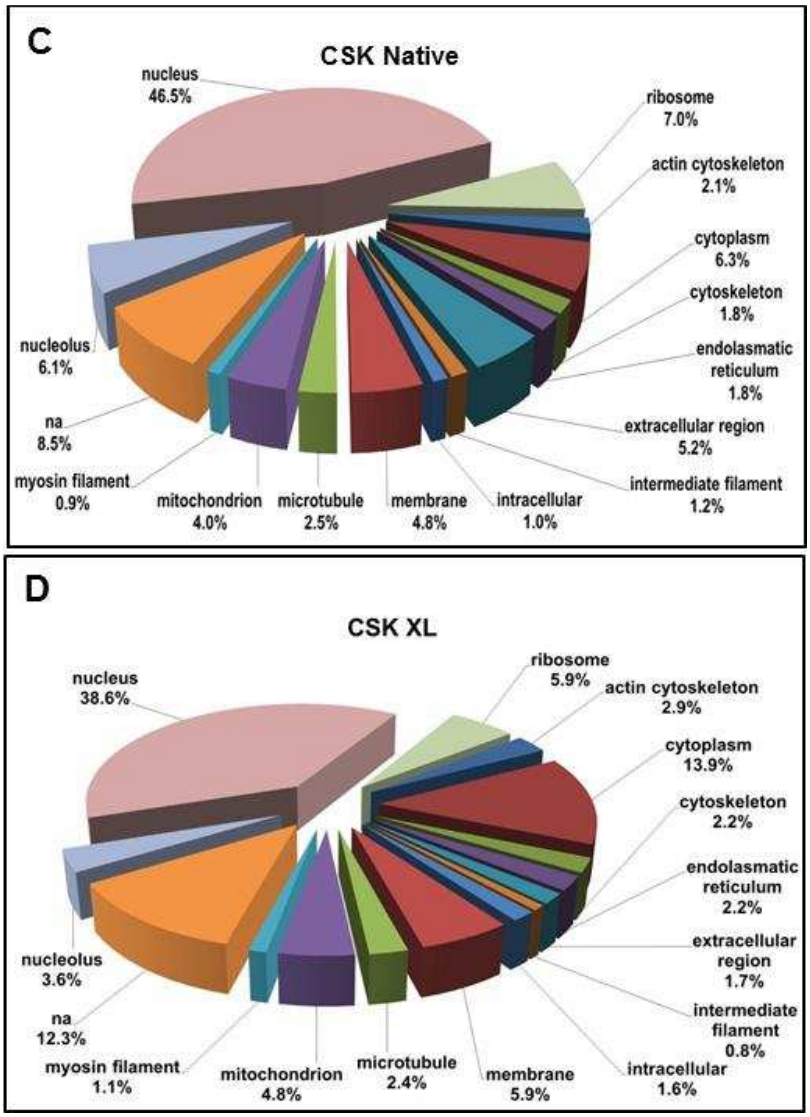

Figure 5.2.3 Subcellular locations of nuclear proteins identified by LCMS/MS.

T cells were simulated for 40 h with PMA/Ionomycin. C/NM-bound proteins were isolated using CSK extraction with prior formaldehyde crosslinking (D.) or without (native) (C.) and are the same as those analysed in Figure 5.2.3 B. The subcellular locations of proteins identified using LCMS/MS were determined first using the HumanNet database (http://www.functionalnet.org/HumanNet/about.html) and secondly using the NCBI (http://www.ncbi.nlm.nih.gov/) or GeneCards (http://www.GeneCards.org/) databases. The percentages in each group are shown.

as the nuclear pore complex proteins Nup107, Nup210 and Nup214. However, unique nuclear proteins are detected more frequently in the crosslinked sample. For instance, nuclear forms of IL16, Mcm3, Mcm4 and Mcm7 were detected in the crosslinked, but not in the native CSK extract.

Taken together, the data show first that proteins that had been crosslinked with formaldehyde can be detected readily by MS. Secondly, crosslinking increases the number of proteins identified, but not necessarily the percentage of nuclear-bound proteins. Each of the methods identifies a number of unique nuclear proteins that are not detected in the other extract, but because of the increase in the numbers of proteins identified and the potential for stabilising loosely-bound chromatin proteins, the effect of crosslinking on the proteome of chromatin identified by LCMS/MS was then analysed.

5.2.4. Proteome analyses by LCMS/MS of chromatin-bound proteins in T cells with or without crosslinking, using a nucleosome extraction method

A total of 667 and 1,069 proteins respectively were identified by native and crosslinked CSK extraction methods and subsequent LCMS/MS analyses, of which 52.6% and 42.2% respectively were annotated as nuclear/nucleolar. In order to increase the number and diversity of proteins strictly associated with chromatin, proteins were isolated by a method typically used for isolating chromatin for ChIP analyses, which has been used previously in our laboratory (350). It has also been shown that isolation of nucleosomes from *Drosophila melanogaster* by digestion with micrococcal nuclease (*M.nase*), identified proteins that are associated with the chromatin state (148). The extraction as described in 2.6.5 allows the isolation of poly-nucleosomes, which bind DNA-associated proteins, such as transcription factors in addition to histones. This potentially removes nuclear matrix- and nuclear envelope-associated proteins, such as nucleoporins or actins, from the analyses.
To compare chromatin-bound proteins isolated by CSK extraction with proteins isolated by chromatin extraction, 15 x 10^6 T cells were stimulated with PMA/Ionomycin and crosslinked with formaldehyde (XL) or not (native). Nuclei were isolated by hypotonic lysis with 0.4% (v/v) NP40 and purified by centrifugation

through a sucrose cushion. The chromatin was then digested with *M.nase* to produce predominantly mono- di- and poly-nucleosomes, which were released from the nuclei (S1 and S2 fractions). Under the conditions used, the *M.nase* cuts every 147bp of the DNA at the linker region between nucleosomes. In order to test whether the *M.nase* had digested correctly, samples of DNA from the S1 and S2 fractions were purified and analysed by agarose gel electrophoresis. The data show that both native and crosslinked S2 fractions (native S2 and XL S2) contain predominantly di- and poly-nucleosomes, whereas the corresponding S1 fractions predominantly contain mono-nucleosomes (Figure 5.2.4 A). Some DNA was recovered in the residual pellet, but far less than in the S2 fraction.

Analyses of the proteome of native and crosslinked chromatin-extracted proteins from the S2 fraction by LCMS/MS showed that 190 native and 319 crosslinked proteins were identified respectively, which have a valid Entrez Gene ID. The proteins identified as well as the analyses of each of the datasets are in S 5.2.3 on the CD in the back of this Thesis. The sub-cellular localisations of each of these proteins were identified first by HumanNet, as described above for the CSK-extracted samples. Of the 190 proteins identified in the native S2 fraction, 54.7% were nuclear, 4.2% were nucleolar and 3.7% cytoplasmic. Of 319 crosslinked S2 proteins, 37.9% were nuclear, 3.1% nucleolar and 8.5% cytoplasmic. The increase in the percentage of mitochondrial proteins identified from 2.6% in non-crosslinked to 6.9% in the formaldehyde crosslinked samples could either be due to non-specific co-isolation of mitochondria or mitochondrial protein complexes with nuclei or to a specific increase in the isolation of perinuclear mitochondria (8). As is the case for proteins identified in the CSK extracted samples, there are a number of examples of proteins classified by HumanNet with a non-nuclear localisation, for which there is evidence that nuclear/nucleolar forms exist. For example, Nesprin3/C14orf49 is classified as a membrane protein, but it is also known to be localised at the nuclear envelope (196). Tubb is a protein that governs the dynamic state and organization of microtubules within cells. However, it is reported to have a role in odontoblast differentiation where it localises at the nuclear envelope (245). Stratifin/SFN has been classified as a cytoplasmic protein, but it was observed in the nucleus as well as the cytoplasm and of epithelial cells (431).

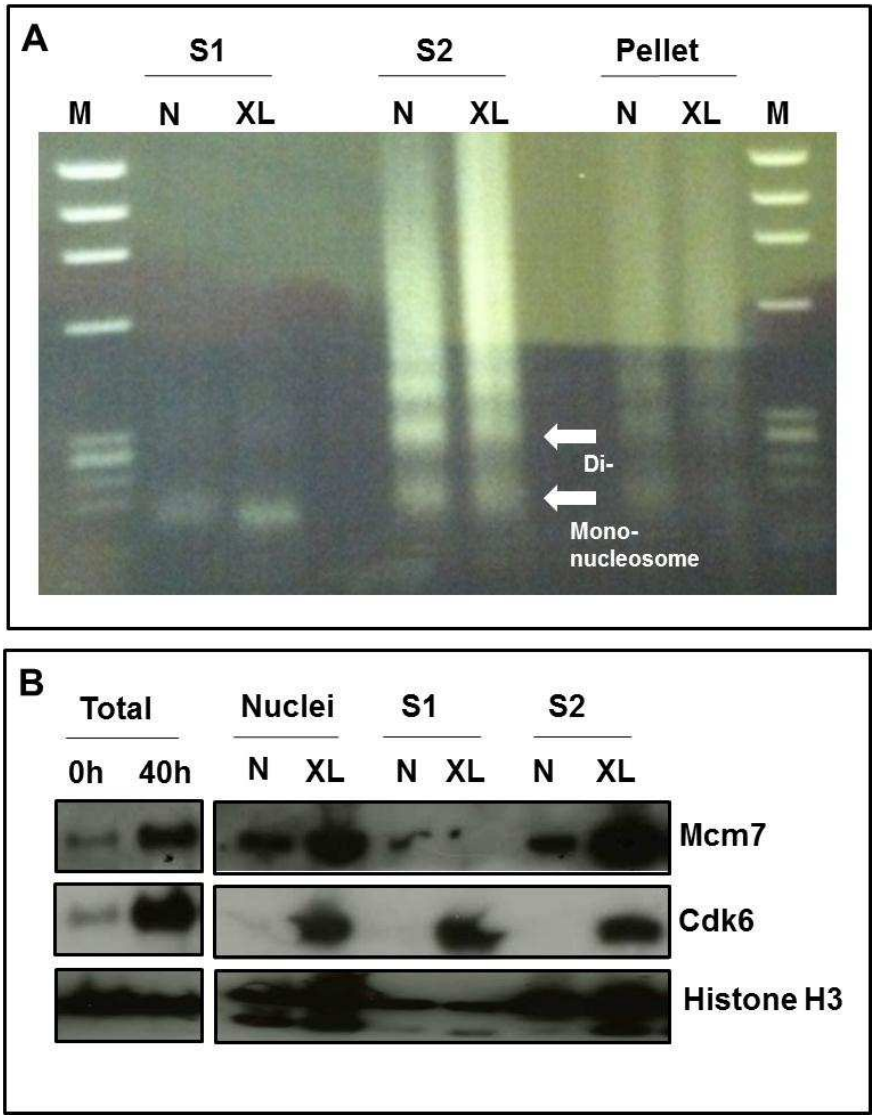

Figure 5.2.4 Isolation of nuclear proteins from stimulated T cells.

40 h post-stimulation with PMA/Ionomycin, T cells were crosslinked with formaldehyde (XL) or not (Native, N). Nuclei were isolated and chromatin was digested to mono-, di-and poly-nucleosomes with *M.nase* and two fractions post-digestion (pre-dialysis S1 and post-dialysis S2) were isolated. The DNA isolated from an aliquot of the S1 and S2 samples as well as the residual pellet were analysed by agarose gel electrophoresis (A). S1 and S2 fractions were lysed in SDS buffer and these, together with the total cell lysates were analysed by western blotting (B).

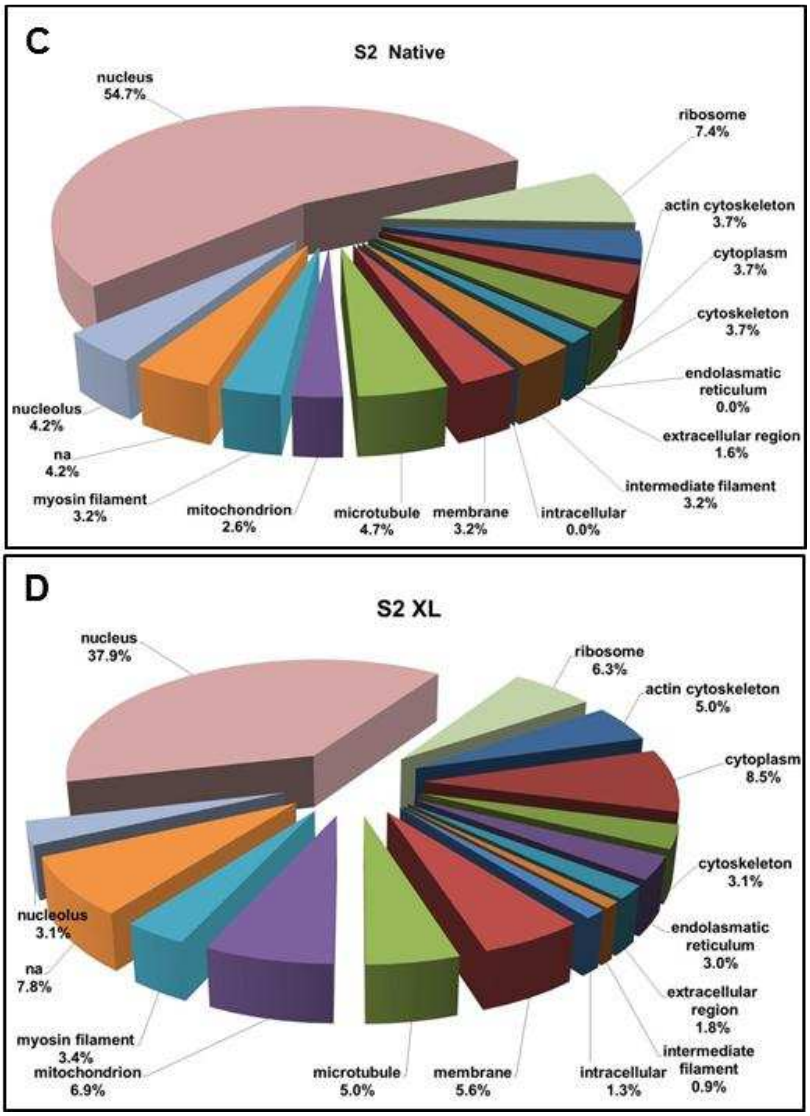

Figure 5.2.4 Subcellular locations of chromatin-bound proteins identified by LCMS/MS.

T cells were simulated for 40 h with PMA/Ionomycin and chromatin-bound proteins were isolated with prior crosslinking (D) or without (native) (C). The subcellular locations of proteins identified using LCMS/MS were determined first by reference using the HumanNet database (http://www.functionalnet.org/HumanNet/about.html) and secondly using NCBI (http://www.ncbi.nlm.nih.gov/) or GeneCards (http://www.GeneCards.org/). The percentages in each group are shown.

A number of nuclear proteins were identified in both native and crosslinked S2 samples, but several unique nuclear proteins were also identified in each fraction. The nucleoporin protein Ahnak that is involved in neuronal cell differentiation was detected with 207 peptide counts in the crosslinked S2 sample, but not in all in native fraction. On the other hand, the nuclear high-motility group protein A1 (HmgA1) that binds to double-stranded DNA was only detected in the native fraction. Similarly, Mcm5 was only detected in native nuclear fraction. These examples highlight that the detection of some nuclear proteins is dependent on the chromatin-bound protein extraction method used.

5.2.5. Protein interaction network of native and crosslinked proteins of S2 fractions

In addition to assigning the cellular localisation of chromatin-associated proteins, the relationships between these proteins may shed light on differences in the nuclear proteome of native and crosslinked proteins. Because more higher-order poly-nucleosomes are present in the S2 as compared with the S1 fraction, I concentrated my analyses on the S2 fractions. A protein interaction network of chromatin-bound proteins from the native and crosslinked S2 fractions was generated using HumanNet,which allows a maximum of 250 seed proteins for the analysis. All 190 proteins from the native S2 extraction that were included in analyses of sub-cellular localisation were used to map protein interactions using HumanNet. Of 320 proteins from the crosslinked S2 fraction, 71 proteins were removed prior to HumanNet analysis, including ribosomal proteins, mitochondrial, intracellular (Rac1, Rac3, Arf3 and Gmip) and proteins to which no localisation was assigned. The analyses showed that of the 249 proteins in the crosslinked S2 extract that were analysed, 244 proteins were connected with each other, whereas in the native S2 extract, 184 of 190 were connected with each other. The data were mapped with Cytoscape software to visualise the connections between the proteins. In Cytoscape, the proteins are represented as nodes with edges representing the interaction between the proteins. A layout was generated using the y-files organic layout tool. This method produces one large network of 184 and 244 connected proteins for the native and crosslinked S2 extracts, with indicative

clusters of proteins that have the same cellular localisation. The most inter-connected sub-networks were identified by analysing the network using the MCODE plugin for Cytoscape (http://baderlab.org/Software/MCODE) with a Kcore of 2, minimum number of edges and a node score cut off of 0.2. The top three subnet-works in the native S2 fraction form clusters of nuclear and ribosomal proteins, of which the top network consists of 29 proteins, mainly heterogeneous nuclear ribonucleoproteins (hnRNP), small nuclear ribonucleoproteins (snRNP) and splicing factors (SF3 and SFRS complexes). The proteins in each of these sub-networks are listed in Table 5.2.5. Nuclear, cytoplasmic/microtubule and myosin clusters formed the top three sub-networks of proteins identified in the crosslinked S2 fraction. The top sub-network, with 32 proteins is very similar to the top sub-network of the S2 native fraction and also consists of hnRNP and snRNP proteins as well as SF3 and SFRS splicing factors. Most of the microtubule/cytoplasmic proteins are different subunits of α- or β-tubulin, β- or γ-actin, heat-shock (Hsp) proteins and the translational elongation EEF1 proteins. It is not clear why these are detected, but they could have a role in nuclear mechano-transduction and EEF1 has a role in nuclear/cytoplasmic shuttling (130, 244). The proteins in each of the sub-networks are in Table 5.2.5. The detection of a number of proteins that are highly interconnected in the same sample and in well characterised protein complexes, such as hnRNPs and SF3 and SFRS splicing factors, is indicative that the methods are effective.

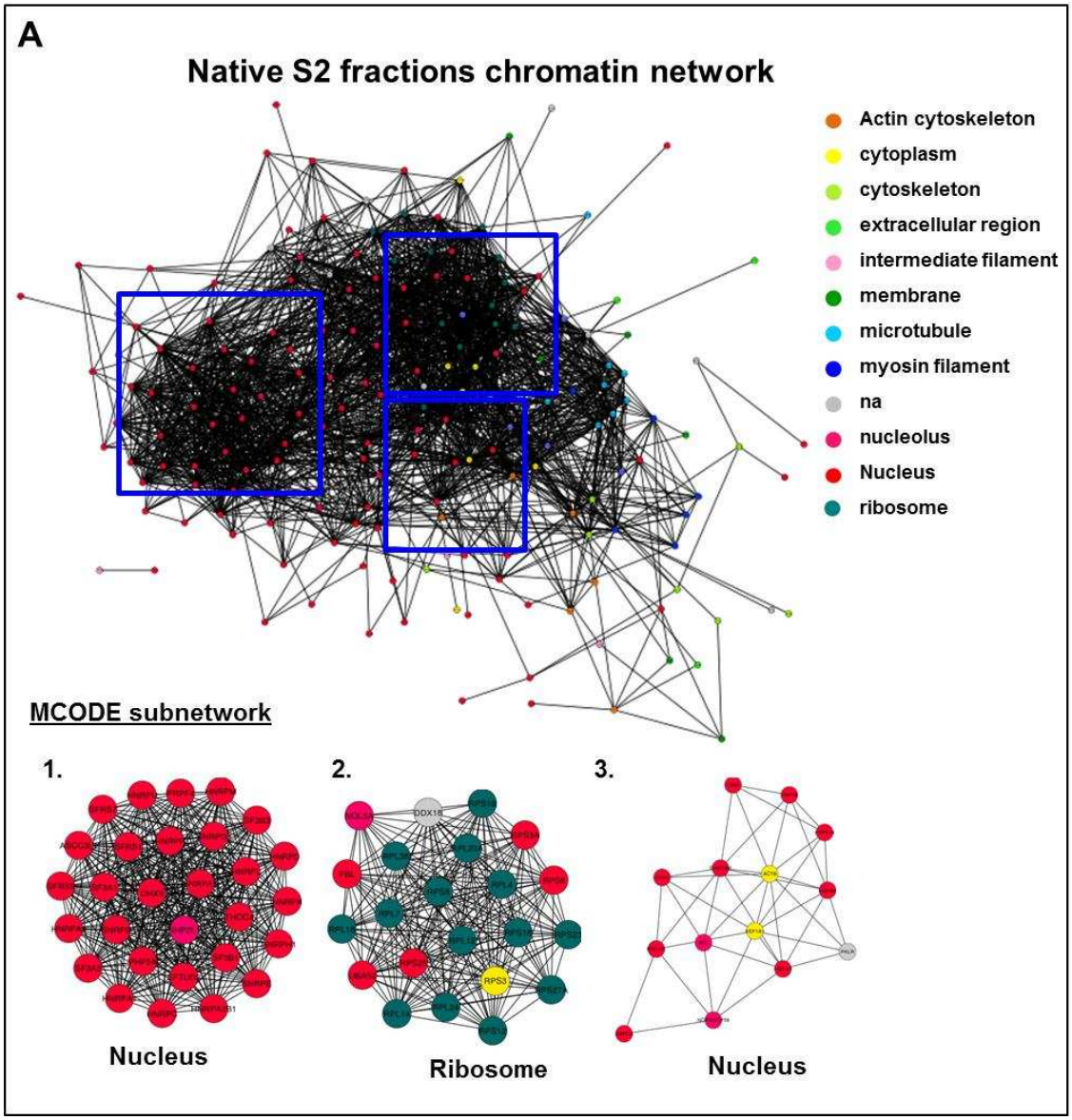
A
Native S2 fractions chromatin network
Actin cytoskeleton
cytoplasm
cytoskeleton
extracellular region
intermediate filament
membrane
microtubule
myosin filament
na
nucleolus
Nucleus
ribosome
MCODE subnetwork
1.
2.
3.
Nucleus
Ribosome
Nucleus

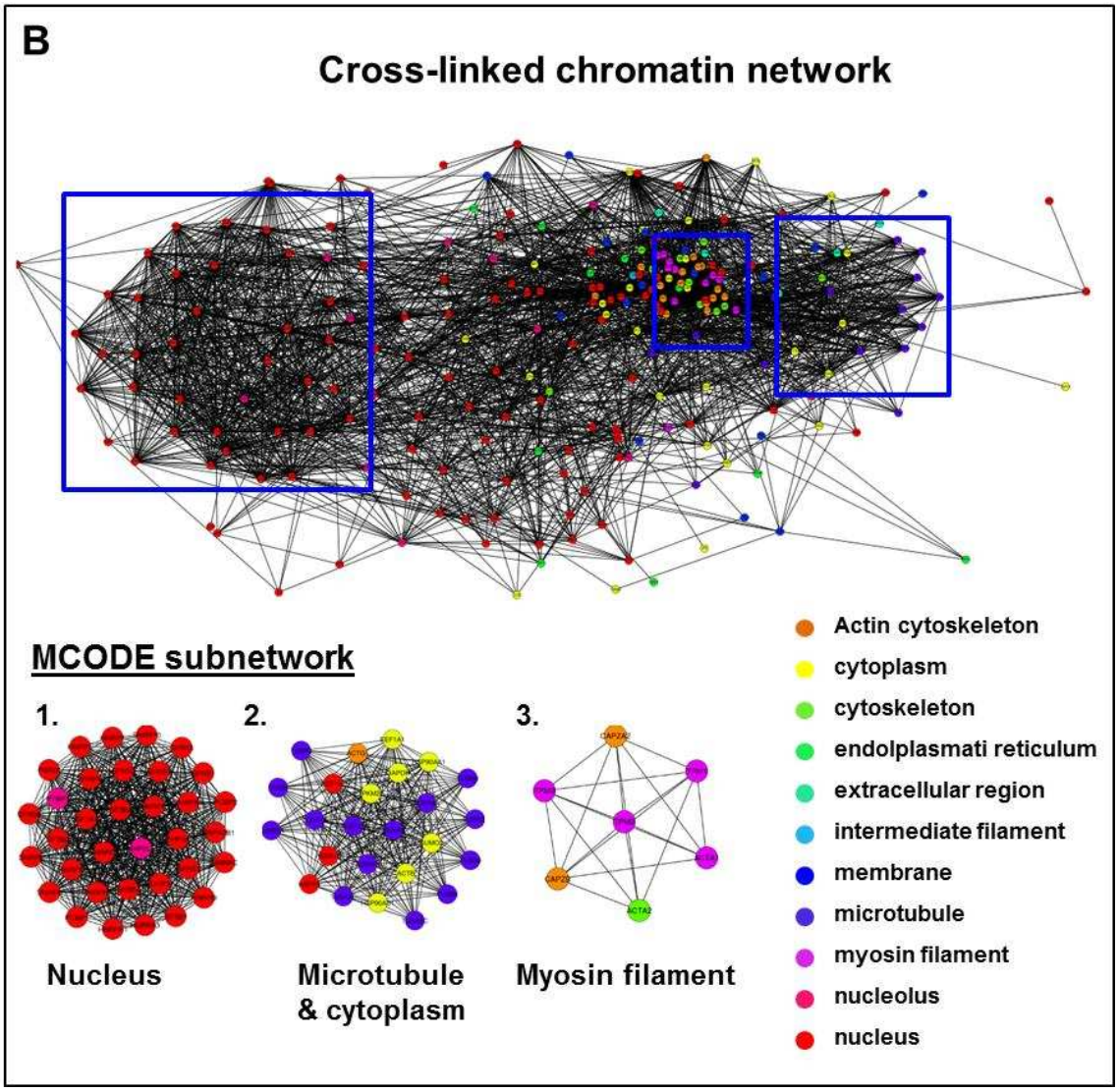

Figure 5.2.5 Protein interaction map of native and crosslinked S2 fractions in chromatin extracts

Proteins identified from the native (A) and crosslinked (B) S2 fractions of chromatin extracts by mass spectrometry were mapped using HumanNet. Interactions between proteins were visualised using Cytoscape and sub-networks were extracted using MCODE. The top three sub-networks are shown. In B. ribosomal, mitochondrial, intracellular proteins and proteins without any location were excluded from the analysis. High-resolution images of these networks are in the CD at the end of this Thesis. The proteins in the MCODE sub-networks are listed in Table 5.2.5.

S2 Crosslinked			S2 Native		
sub-network 1	**sub-network 2**	**sub-network 3**	**sub-network 1**	**sub-network 2**	**sub-network 3**
Entrez Gene ID	Entrez Gene ID	Entrez Gene ID	Entrez Gene ID	Entrez Gene ID	Entrez Gene ID
DHX9	ACTB	ACTA2	ASCC3L	DDX18	ACTB
HNRPA1	ACTG1	CAPZA2	DHX9	FBL	DDX5
HNRPA2B1	EEF1A1	CAPZB	EFTUD2	NOL5A	DIMT1L
HNRPA3	EEF1A2	TPM1	HNRPA1	RPL12	EEF1A1
HNRPC	GAPDH	TPM2	HNRPA2B1	RPL14	HSPA5
HNRPD	HSP90AA1	TPM3	HNRPA3	RPL18	HSPA8
HNRPF	HSP90AB1		HNRPC	RPL23A	LSM4
HNRPH1	HSPA1B		HNRPD	RPL24	NCL
HNRPL	HSPA5		HNRPH1	RPL38	NOP5/NOP58
HNRPM	PKM2		HNRPK	RPL4	PKLR
HNRPR	SUMO3		HNRPL	RPL7	PRPF19
HNRPU	TUBA1A		HNRPM	RPS12	PRPF8
NHP2L1	TUBA1B		HNRPR	RPS16	RSL1D1
PCBP1	TUBA1C		HNRPU	RPS18	SYNCRIP
PCBP2	TUBA3E		NHP2L1	RPS23	
PHF5A	TUBA4A		PHF5A	RPS25	
PTBP1	TUBA8		PRPF4	RPS27A	
RBMX	TUBB		SF3A1	RPS27A	
SF3A1	TUBB2A		SF3A3	RPS3	
SF3B1	TUBB2B		SF3B1	RPS3A	
SF3B2	TUBB2C		SF3B3	RPS6	
SF3B4	TUBB3		SFRS1	RPS8	
SFRS1	TUBB4		SFRS7	UBA52	
SFRS2	TUBB6		SFRS9		
SFRS3	TUBB8		SNRPA		
SFRS4			SNRPB		
SFRS5			SNRPD		
SFRS6			SNRPE		
SFRS7			THOC4		
SNRP70					
SNRPA1					
SNRPB					
SNRPD3					
SNRPE					

Table 5.2.5 List of proteins of native and crosslinked S2 fractions in chromatin extracts identified by MCODE analysis.

5.3 Discussion

The data presented here and in previous studies from our laboratory have investigated changes in individual proteins or in the C/NM-bound proteome that occur when human T cells enter the cell cycle from a quiescent state (218, 290, 350, 372). Nuclear proteins play an important role in the regulation of gene expression, DNA replication and other processes; therefore the analysis of the proteome from a particular compartment of the cell, such as the chromatin-bound proteome is of particular interest. Importantly, advances in mass spectrometry-based proteomics and down-stream analyses of the data enable us to quantify changes in the abundance of thousands of individual proteins (147).

The removal of detergents used in the extraction buffers is crucial for good LCMS/MS analyses. I compared three different detergent removal methodologies, which include Pierce Detergent Removal Spin columns, OrgoSol DetergentOut kit and the FASP method. The data showed that all three methods remove detergents efficiently and I decided to use spin columns for further studies in this and in Chapter 6 due to their ease of use.

Previous work in the laboratory identified changes in chromatin and nuclear matrix-bound proteins of primary human T cells that occur during the transition from $G_0 \rightarrow G_1$ using a CSK extraction method (290). A wide range of C/NM-associated proteins were identified in T cells in G_0 and after stimulation for 40 h with PMA/Ionomycin. In addition to CSK extraction, other methods can be used to identify the chromatin-bound proteome. In the study presented here, I investigated different methodologies for isolating and investigating chromatin-bound proteins. The aim of my study was to carry out a comparison of the chromatin proteome obtained using four different extraction methods, all using T cells stimulated for 40 h with PMA/Ionomycin and analysed by LCMS/MS.

First, I investigated the effect of crosslinking proteins with formaldehyde before carrying out the CSK extraction. The data were compared with the proteome obtained from a native, non-crosslinked CSK extract. Formaldehyde permeates

living cells and the crosslinking stabilizes protein:DNA interactions by crosslinking the primary amino group in proteins with cytosine group in DNA (360). The use of formaldehyde for cross-linking and mass spectrometry has a number of advantages in studying DNA-bound proteins (360). When the native CSK extraction was carried out, 667 proteins were identified, whereas 1,069 proteins were identified in the crosslinked CSK extract. The data indicate that crosslinked samples can be analysed by MS and crosslinking increases the number of proteins identified. In agreement with the data presented here, work from other groups has shown that proteins can be identified by LCMS/MS after formalin (formaldehyde) fixation (293).

The proteins identified were assigned a subcellular localisation using HumanNet, which gives an indication of where in the cell the proteins are localised. The analyses revealed that 52.6% of proteins were nuclear/nucleolar in the native CSK extract, whereas 42.2% proteins were nuclear/nucleolar in the crosslinked extract. Previous work in the laboratory identified 502 proteins in T cells stimulated for 40 h with PMA/ionomycin that underwent a native CSK isolation (Steve Orr Thesis; (290)). Of those, 46% were identified to be nuclear and 29% nucleolar. Interestingly, apart from nuclear proteins that were identified in my study in both the native and crosslinked CSK extracts, additional proteins were uniquely identified in both. 351 proteins were identified in the native and 451 in the crosslinked dataset by HumanNet to be nuclear/nucleolar. Proteins uniquely identified in the native dataset include Brx1, which is involved in the biogenesis of ribosomes, the nuclear protein Ahnak and DNA replication protein 2. Mcm3 and 4 (DNA replication), prefoldin subunits PFDN2, 5 and 6 (involved in folding RNA Polymerases (discussed in Chapter 6)), annexin A7 (translocates to the nucleus during brain development (309)) and A11 were all uniquely identified in the crosslinked samples. None of the selected examples of proteins were found in the list of proteins identified in the native CSK extract carried out previously in the laboratory (Thesis, Steve Orr). Similar to the native CSK dataset presented here, no MCM helicase proteins were detected in the previous study. There are a number of proteins identified both in the previous study (290) and the dataset presented here, such as components of the nuclear pore complex (Nup107, Nup153, Nup155 and Nup205)

and DEAD box helicases (DDX5, DDX18, DDX24, DDX27, DDX47, DDX50, DDX52 and DDX56).

Next, protein extracts were prepared from isolated chromatin and the proteome was analysed again by LCMS/MS. The isolation method was based on a protocol commonly used for ChIP (290), which was used in a ChIP-chip epigenetic study by our laboratory (350). It was shown by Tchapyjnikov *et al*. that LCMS/MS based proteomic profiling can be carried out using nuclei isolated from human cells, which allows the identification of a number of transcription factors (369). In a different study, to identify chromatin-bound proteins, a modified ChIP method was carried out with subsequent MS analysis that consists of an affinity purification of TAP-tagged histone H2A and other histone variants. In this approach *Saccharomyces cerevisiae* cells, expressing TAP-tagged histone H2A or other histone variants were mildly sonicated and isolated using magnetic beads coated with antibodies (214). I took this work further to identify chromatin-bound proteins by LCMS/MS. The first step in this method involves the isolation of nuclei that were then digested with *M.nase* to produce mono-, di- and poly-nucleosomes. The chromatin-bound proteins in both the S1 and the S2 fractions were then analysed by LCMS/MS. However, I expanded the method and also prepared samples in which the proteins were crosslinked with formaldehyde before nucleosome extraction. Similar to the CSK extraction, the proteome of the native S2 fraction was compared with that of the S2 fraction isolated from formaldehyde crosslinked T cells. The analyses showed that 190 proteins were identified in the native and 319 proteins in the crosslinked S2 samples respectively. When the proteins were classified by their sub-cellular localisation, 58.9% were nuclear/nucleolar in the native and 42% nuclear/nucleolar in the crosslinked S2 fraction.

The relationships between the proteins identified were investigated for both the native and crosslinked S2 fractions. To do this, a protein-protein interaction network was generated in HumanNet and visualised using Cytoscape. The colour of the nodes was assigned by the sub-cellular location. 244 proteins were connected in the network of the formaldehyde crosslinked S2 fraction, whereas in the native S2 fraction 184 proteins were connected. Each of the networks was further analysed

using the MCODE plugin that identifies clusters in which proteins are highly connected. The top three most interconnected sub-networks are shown in the text. The top sub-network in both native and crosslinked S2 fractions consists of nuclear proteins, such as hnRNP and snRNP proteins and splicing factors. Proteins were identified in common in the top sub-networks of the native and crosslinked S2 samples, including HNRPA3, HNRPC, HNRPD, HNRPH1, HNRPL, HNRPL, HNRPM, HNRPR and HNRPU, but additionally HNRPF, HNRPA2B1 and HNRPA1 were identified in the crosslinked S2 fraction. Aside from SF3A1 and SF3B1 that were identified in both data sets, additional unique components of the splicing factor SF3A were identified in each data set. Furthermore, the splicing factors SFRS1 and SFRS7 were identified in both, but several more were detected in the crosslinked top sub-network (SFRS1, SFRS2, SFRS3, SFRS4, SFRS5 and SFRS6).

The study presented here highlights differences and similarities between preparation methods for the identification of the C/NM- and chromatin-bound proteome. Crosslinking with formaldehyde has an impact on the identification of nuclear proteins by mass spectrometry. Overall, crosslinking of proteins before the CSK extraction or chromatin isolation increases the number of proteins identified as well as the frequency of peptides detected for each protein. Unlike the CSK extraction, isolation of chromatin is more time-consuming, involves multiple steps and is associated with protein losses during the preparation. However, this method leads to the identification of a distinct nuclear proteome and the ability to identify chromatin-bound proteins that are not identified in the CSK-bound dataset. For instance, Sumo2, Sumo4, Smt3, Rpsa, Atp1A3, Lsm6 and Sec31B are identified only within the native or crosslinked S2, but not in the CSK extracted fraction. Therefore, I decided to use the chromatin preparation method for further studies in Chapter 6, in which proteins are crosslinked with formaldehyde and the S1 and S2 fractions are analysed by LCMS/MS.

Chapter 6

6. Systematic analyses of changes in the chromatin-bound proteome network in activated T cells after depleting the DNA replication factor Mcm7

6.1 Introduction

One of several hallmarks of cancer (151) is the abrogation of cell cycle controls, which perturbs fundamental biological processes. For instance, disruption of the pRB pathway releases E2F transcription factors (76, 159, 257, 365). For E2F1, this leads to uncontrolled cell proliferation, which correlates with insensitivity to anti-growth factors (151), apoptotic cell death in response to DNA damage as well as invasion and metastasis (42, 118, 415, 418). Loss of cell cycle checkpoint control also promotes genomic instability (412). It has been observed that deregulation of the expression of G_1-cyclins induces genomic instability by preventing efficient pre-replication complex formation (PRC), as demonstrated for budding yeast (366).

A major component of the PRC is the MCM helicase, which includes the proteins Mcm2-Mcm7. The MCM helicase, together with other proteins of the PRC, is required to bind to the replication fork and is essential for initiating DNA synthesis during S-phase of the cell cycle and thus is crucial for cell cycle progression (364). First, Orc4 protein is bound to the sites of DNA replication. After the binding of Cdt1 and Cdc6 to Orc4, the MCM helicase is then recruited to unwind the DNA. This induces the wrapping of the Mcm2-7 complex on both sides of the double stranded DNA, which results in replication licensing (Figure 6.1) (45, 107). However, inhibition of one of the PRC components, for instance by downregulating Mcm7 with siRNA, can lead to replication fork collapse and genomic instability. Previous studies in our laboratory showed that MCM protein levels are induced during the $G_0 \rightarrow G_1$ transition in primary T lymphocytes (291). In that study it was shown that genomic instability is induced by reducing the induction of the DNA replication proteins Mcm7 or Mcm4. Furthermore, reduction of Mcm7 protein levels with siRNA by even 50% leads to increased centromere separation, premature chromatid separation during mitosis and gross chromosomal abnormalities. Reducing the levels of Mcm7 or Mcm4 induced DNA damage pathways, involving activation of Atr, Atm, Chek1 and Chek2 and other DNA repair proteins (291). Misregulation

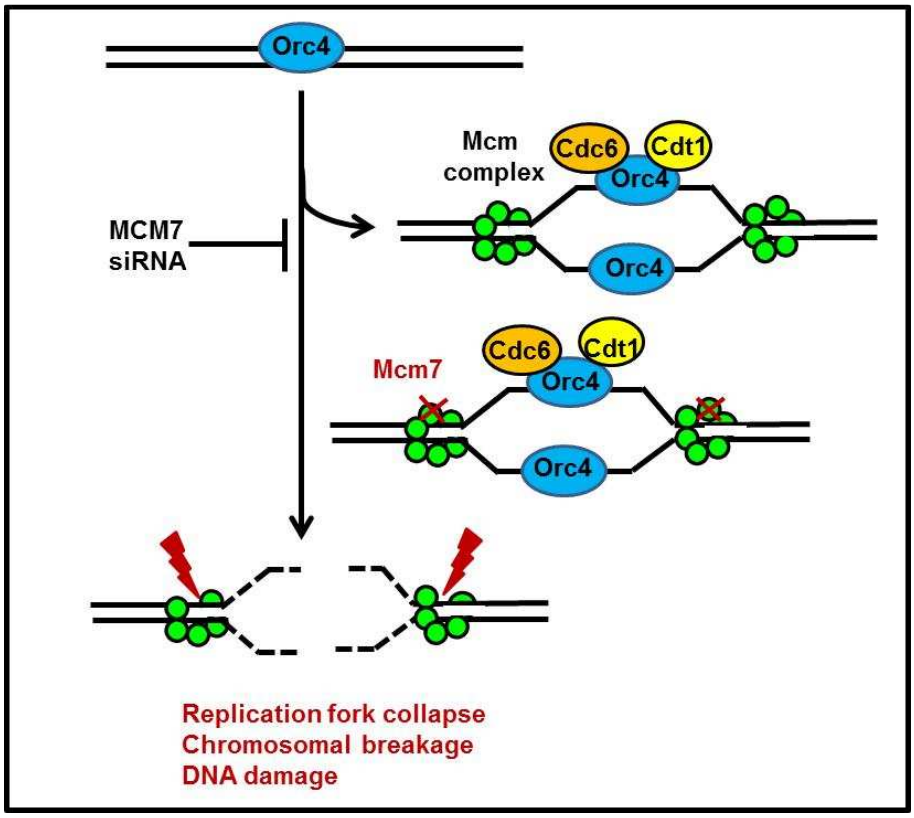

Figure 6.1 Mechanism of Mcm7 expression and the effects of reduction.

Replication licensing occurs in the presence of all components involved in the pre-replication complex (PRC), including Orc4, Cdc6, Cdt1 and Mcm2-7. Inhibition of Mcm7 expression by transfection of siRNA against Mcm7 leads the collapse of replication forks, which results in chromosomal breaks and DNA damage responses. Adapted from (234).

of DNA replication licensing occurs in many cancers, perhaps as a consequence of oncogene-induced cell proliferation and may play an important role in causing genomic instability (46).

The reduction of Mcm7 with siRNA in human primary T cells induces a phenotype that includes a number of significant cellular changes that occur in many cancers (see (291) and references therein). To obtain a better understanding of how these occur, I investigated the chromatin-bound proteome of T cells transfected with either Mcm7 or non-targeting control siRNA by applying the methods described in 5.2.4 for the isolation and subsequent analysis of chromatin-bound proteins by mass spectrometry.

6.2 Results

6.2.1. Experimental approach to investigate changes in the chromatin-bound proteome caused by depleting Mcm7

To study the changes in the chromatin-bound proteome caused by Mcm7 downregulation, peripheral blood mononuclear cells (PBMC) were isolated from three healthy human donors and T cells were enriched by adhering the PBMCs overnight to plastic culture dishes, as described in 2.2.3. Enriched T cells were transfected the next day with pooled siRNA against Mcm7 or control, non-targeting siRNA with a final siRNA concentration of 5µM (1.25µM of each of the four siRNA) (Figure 6.2.1 step 1). The transfected T cells were allowed to recover by culturing overnight without stimulation and then stimulated with PMA/Ionomycin for 72 h. This time-point was chosen based on conditions established in (291). Prior to isolation of the chromatin–bound proteins, the proteins were crosslinked to DNA with formaldehyde (see section 2.6.3). Nuclei were isolated and chromatin was digested with *M.nase* to produce mono-, di- and poly-nucleosomes, according to conditions established in section 2.6.5 (S1 and S2 fractions) (Figure 6.2.1 step 2). The crosslinking was then reversed by heating at 65^{o}C overnight. The digestion pattern obtained in the S1 and S2 fractions was checked by removing 10% of each sample, digesting RNA with DNAase-free RNAseA and the size of the DNA was analysed by agarose gel electrophoresis. The data are shown in section 6.2.3. The proteins in the remaining 90% of the sample were then prepared for LCMS/MS analysis (Figure 6.2.1 step 3). This involves removal of detergents using spin columns, as described in section 2.12.2, followed by denaturation and digestion with Trypsin to produce peptides. The peptides produced from the S1 and S2 fractions of the Mcm7-depleted or control cells were analysed by LC-MS/MS, using LTQ-Orbitrap and Velos-Orbitrap machines, as indicated. The peptides were separated by a reverse phase column (C18), prior to ionisation of the peptides in the MS (Figure 6.2.1 step 4). Selected peptides were then fragmented to obtain an MS/MS pattern. The data were analysed using the Sequest search algorithm within the Proteome Discoverer 1.3 software package (Thermo) for identification of proteins (see 2.13.3).

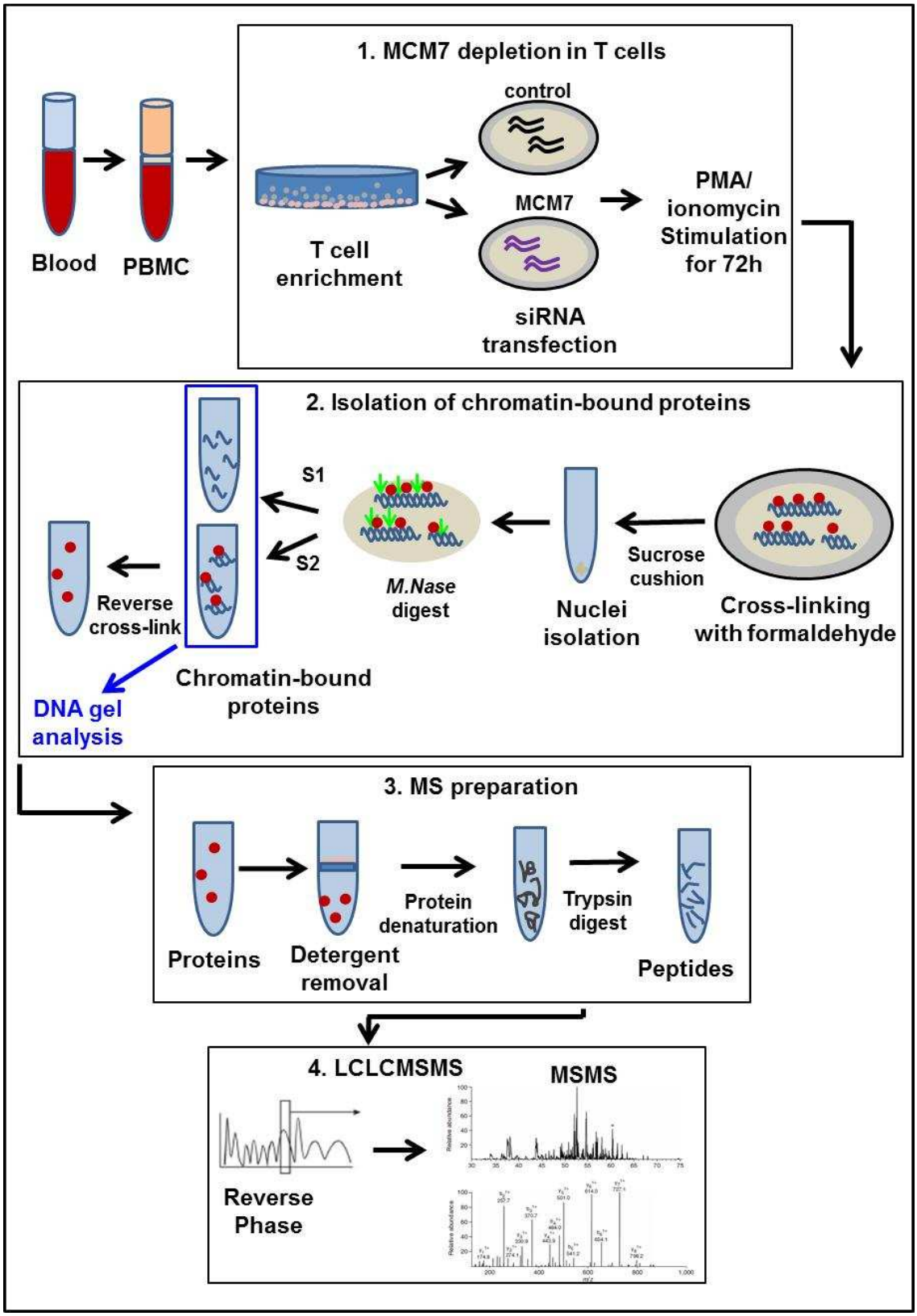
1. MCM7 depletion in T cells
Blood
PBMC
T cell enrichment
control
MCM7
siRNA transfection
PMA/ ionomycin Stimulation for 72h
2. Isolation of chromatin-bound proteins
S1
S2
M.Nase digest
Nuclei isolation
Sucrose cushion
Cross-linking with formaldehyde
Reverse cross-link
Chromatin-bound proteins
DNA gel analysis
3. MS preparation
Proteins
Detergent removal
Protein denaturation
Trypsin digest
Peptides
4. LCLCMSMS
MSMS
Reverse Phase

Figure 6.2.1 Outline of the experimental approach.

Human PBMC were isolated from blood of three healthy donors. T cells in each sample were enriched by adhering PBMC to plastic dishes overnight. 1. T cells were transfected with siRNA against Mcm7 or control siRNA and stimulated for 72 h with PMA/Ionomycin. 2. Proteins were crosslinked to DNA with formaldehyde and the nuclei were isolated by centrifugation through a sucrose cushion. The chromatin was digested with *M.nase* to release mono-, di- and poly-nucleosomes and the S1 and S2 fractions, containing chromatin-bound proteins, were collected. The crosslinking was reversed and the DNA in 10% of each sample was analysed by electrophoresis through an agarose gel. 3. The proteins in the remaining 90% were prepared for LCMS/MS by removing the detergents using spin columns. The proteins were then denatured, followed by Trypsin digestion to produce peptides. 4. The peptides were separated on a C18 reverse phase column and analysed by mass spectrometry (LCMS/MS) using either an LTQ-Orbitrap or a Velos-Orbitrap machine.

6.2.2. Validation of T cells used for Mcm7 downregulation and proteomics analyses

Human T cells were isolated from fresh blood (Donor 3 and 4) or a leukocyte cone (Donor 1) by adhering PBMCs to culture dishes at a concentration of 2 x 10^7 cells in 3 ml media in one 6–well tissue-culture plate. The technique to enrich T cells by adherence to plastic ware was used originally to isolate a highly enriched population of monocytes from PBMC (10) and is described in chapter 2.2.3. Two hours post-adherence, cells were transferred to new culture dishes and cultured overnight to allow further monocyte adherence. The T cell number was determined the following day by counting viable cells and the purity of T cells was determined by staining with CD3-FITC. Adhered T cells from all three donors were >83% $CD3^+$ (Figure 6.1.A). To identify the activation state, a small fraction of the cells (approximately 1 x 10^6) were stained with CD69-PE and analysed by flow cytometry. The data obtained were compared with that obtained for the same cells after stimulation 4 h with PMA/Ionomycin. CD69 is a T cell activation marker, which is induced before the Commitment Point (see (218)). Four hours post-stimulation, the cells expressed between 45-67% CD69 on the cell surface, whereas non-stimulated cells did not express CD69 (Figure 6.1.B). The data indicate that the T cells to be used in the study were predominantly in a non-activated state.

To reduce Mcm7 levels in T cells, 40-50 x 10^6 of the non-activated T cells were transfected with pooled siRNA against Mcm7 (Dharmacon, SmartPool) or control, non-targeting siRNA at a final concentration of 5µM (1.25µM of each siRNA). The transfections were carried out using single Nucleofection cuvettes (Lonza), each cuvette containing 10 x 10^6 T cells. The transfected cells were cultured over night

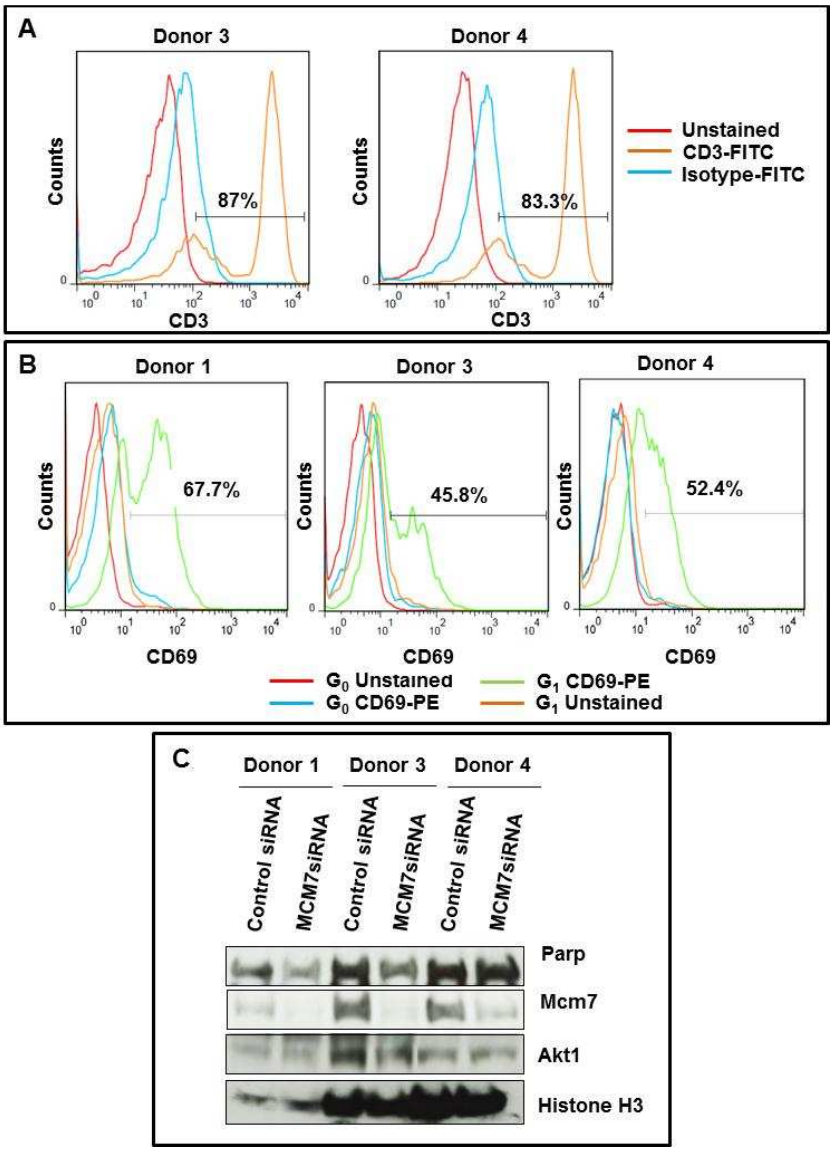

Figure 6.2.2 Purity and activation state of T cells isolated from three healthy blood donors and used for Mcm7 downregulation.

The purity of T cells enriched from PBMCs was determined by staining the cells with CD3-FITC and analysing them by flow cytometry. B. To determine their state of activation, the enriched T cells were stained for CD69-PE and analysed by flow cytometry. These data were compared with the same T cells activated for 4 h with PMA/Ionomycin (labelled as G_1). C. Expression levels of Mcm7 after transfecting T cells with siRNA against Mcm7 or control siRNA, followed by stimulation of T cells for 72 h with PMA/Ionomycin were determined by western blotting. The blots were also probed with antibodies to Parp, Akt and Histone H3, which served as loading controls.

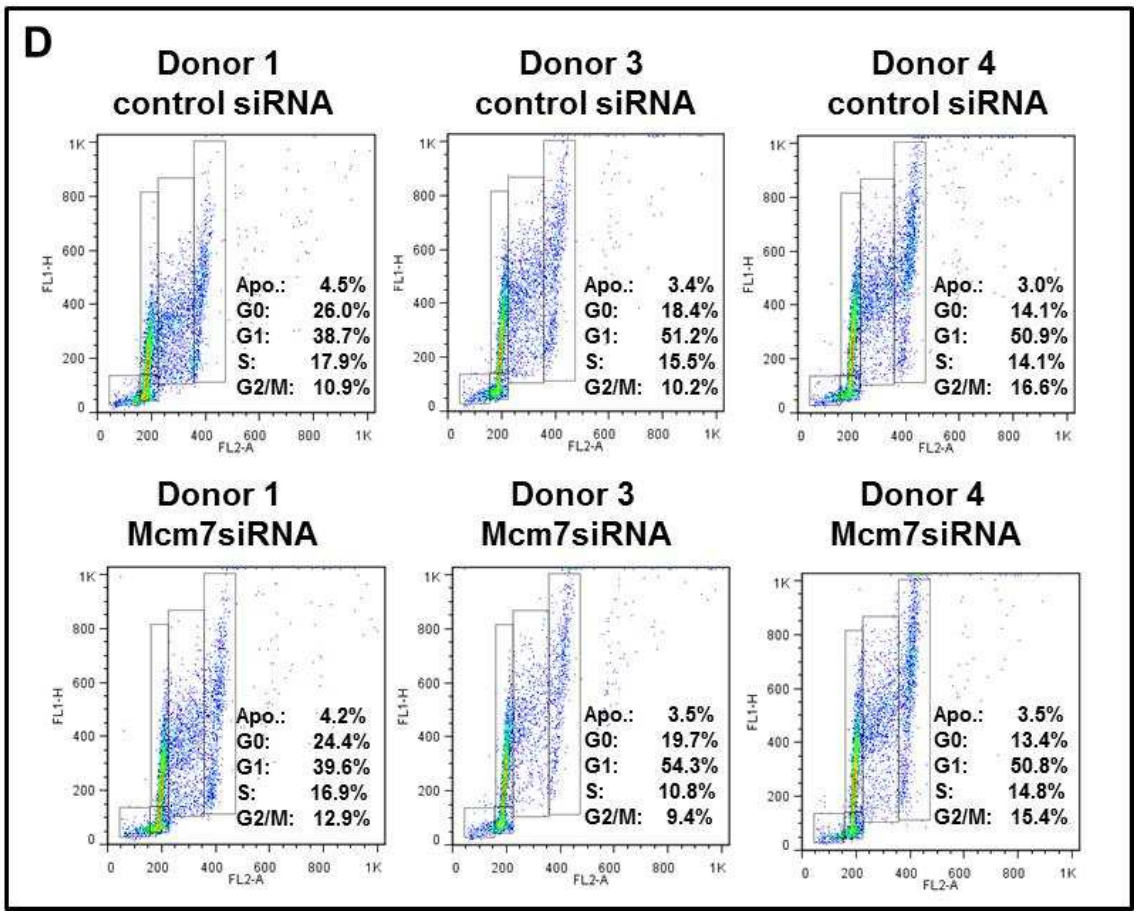

Figure 6.2.2 Cell cycle analysis of transfected T cells.

T cells from three independent donors were transfected with pooled Mcm7 siRNA or control/non-targeting siRNA. 72 h post-stimulation with PMA/Ionomycin, T cells were fixed, stained with FITC (total cell protein content) and PI (DNA content) and analysed by flow cytometry.

without stimulation and the following day the number of viable cells was determined by manual counting in the presence of Trypan blue. On average, half of the cells survived the transfection, which is consistent with the experience of others in the laboratory for other projects (290, 291). The cells were then stimulated with PMA/Ionomycin for 72 h. At this point, 1 x 10^6 T cells were lysed in SDS-lysis buffer and the Mcm7 expression in each sample was investigated by Western blotting. The blots were also probed with antibodies against Parp, Histone H3 or Akt as controls for loading. The western blot analyses show that Mcm7 proteins were markedly reduced by the Mcm7 siRNA in all three biological replicates (Figure 6.1.C).

To determine the percentage of cells in each phase of the cell cycle, transfected cells were fixed with ethanol, stained with free FITC (protein content) and PI (DNA content) and then analysed by flow cytometry. The data show that both control and Mcm7 transfected cells were cycling. 15.8%±1.9% (mean±SD)of the cells were in S-phase and 12.6%±3.5% of the cells were in G_2/M-phase of the cell cycle in the control, whereas 14.2%±3.1% of the cells were in S-phase and 12.6%±3.0% of the cells were in G_2/M-phase of the cell cycle in the Mcm7 transfected cells (Figure 6.2.4 D). These data agree with the previous study from our laboratory (291) that cells enter the cell cycle even when Mcm7 is reduced, but in that study more cells were observed in S-phase (26%) of the cell cycle and fewer cells in G_2M-phase (11%) of the cell cycle in the control cells than in cells transfected with Mcm7 siRNA. However, differences between T cells from different donors were observed in that study (S. Orr- personal communication) and such differences may also be dependent on culture conditions.

6.2.3. Nucleosomal composition of the S1 and S2 fractions

The data in 6.2.2 shows that the isolated T cells were not activated, but entered the cell cycle after transfection with Mcm7- or control-siRNA and stimulation for 72 h with PMA/Ionomycin. In order to isolate chromatin-bound proteins for carrying out high content mass spectrometry, each T cell preparation was crosslinked for up to 10 min with 1% (w/v) formaldehyde, lysed in a buffer containing 0.4% (v/v) Nonidet

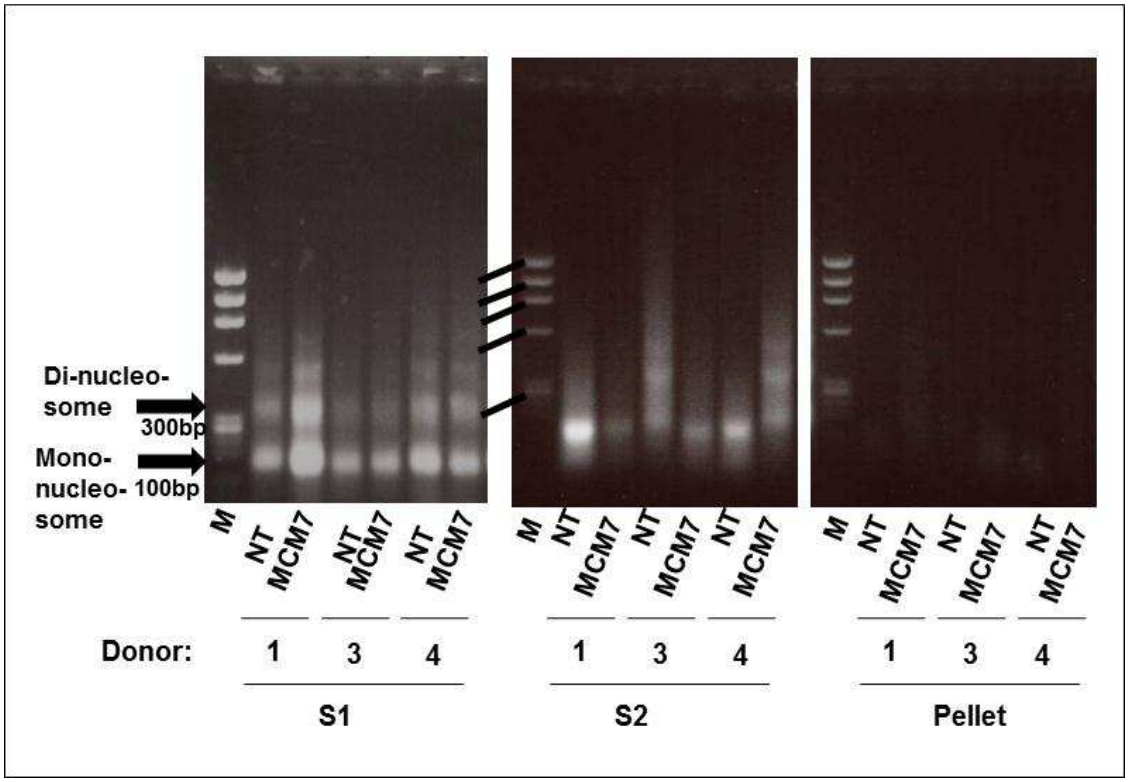

Figure 6.2.3 *M.nase*-digested chromatin isolated from T cells of three biological donors transfected with Mcm7- or control-siRNA.

Mcm7-depleted or control siRNA transfected T cells were crosslinked with formaldehyde and nuclei were isolated. Chromatin was digested with *M.nase* and the S1, S2 fractions and the residual pellet from Donor 1, Donor 3 and Donor 4 were collected. The crosslinking was reversed by heating and DNA present in each sample was analysed by agarose gel electrophoresis. M = DNA ladder marker; NT = non-targeting, control siRNA transfected cells; MCM7= cells transfected with Mcm7 siRNA.

P40 followed by a sucrose cushion to isolate the nuclei. The chromatin in the isolated nuclei was digested for a maximum of 5 minutes with *M.nase* to release mono-, di- and tri-nucleosomes. The nuclei were centrifuged gently after stopping the digestion reaction with 5mM EDTA. The sample was centrifuged for 10 min at 4ºC at 10000 x g_{max} and the supernatant was collected as the S1 fraction. The pellet was resuspended in dialysis buffer and sonicated 5 times on ice for 10 sec each. The samples were then centrifuged at 4ºC at 10000 x g_{max} for 10 min and the supernatant was again collected as the S2 fraction. Since 147bp DNA wraps around each nucleosome, the nucleosomal composition of each fraction can be determined by analysing the DNA. Crosslinking was reversed and contaminating RNA was digested with DNAase-free RNAseA. The DNA of the S1, S2 fractions and the residual pellet were analysed on an agarose gel. The data shows that the S1 fractions of each sample contain DNA lengths consistent with the presence of mono-, di- and some poly-nucleosomes, whereas the S2 fractions predominantly contained mono-nucleosomes (Figure 6.2.3). Because of the differences in the nucleosomal composition of the S1 and S2 samples, proteins present in both the S2 and the S1 fractions of each sample were analysed by mass spectrometry. As expected, very little chromatin was detected in the pellet after the S1 and S2 fractions were collected (Figure 6.2.3). The S1 and S2 fractions were frozen at -80℃ for subsequent proteomics analyses.

6.2.4. Chromatin-bound proteome analyses of human T lymphocytes: the effects of depleting Mcm7

Chromatin-bound protein extracts from the Mcm7- or control-siRNA transfected T cells were prepared from both the S1 and S2 fractions of the three biological replicates, as described in section 6.2.3. The extracts were prepared for LCMS/MS analysis by removing the detergents using spin columns (see section 2.12.2), followed by digesting the proteins into peptides with Trypsin. The peptides were separated by C18 reverse phase columns and analysed by LCMS/MS using the LTQ-Orbitrap or Velos-Orbitrap mass spectrometers, as indicated below. The LC and mass spectrometer conditions are detailed in section 2.13.3. The analyses were carried out in collaboration with Dr. Daniel Boutz in Professor Marcotte's

laboratory at the University of Texas at Austin, USA. Each biological replicate was analysed at least three times (three technical injections). The MS/MS data were analysed by the Sequest search algorithm within the Proteome Discoverer suite and proteins were identified using Percolator as part of Mascot. The criteria set were that each protein required two or more independent Tryptic peptides to be identified and proteins were only included in further analyses if they were detected in two or more technical injections. Secondly, proteins were only included that had a false discovery rate <1% at the spectral count level (see 2.13.3). The S2 fractions of 3 biological replicates were analysed using an LTQ-Orbitrap mass spectrometer (LTQ). The S1 fractions were analysed using both LTQ-Orbitrap and Velos-Orbitrap (Velos) mass spectrometers.

The chromatin-bound proteins identified in each case were analysed using "relaxed" and "stringent" criteria to identify those which change when Mcm7 is depleted. The complete list of proteins identified as well the analyses of each of the datasets are in S 6.2.4 on the CD at the back of this Thesis. The MS data were quantified by identifying differences in protein expression levels using spectral counting methods developed by our collaborators (52, 233). A combined Z-score was calculated by summing the individual Z-scores of the three biological replicates and samples transfected with Mcm7- and control-siRNA. Proteins were included with a statistically significant combined Z-score (combined Z-core >1.65 and <-1.65), meaning there is a statistically significant difference between the Mcm7-depleted cells and control cells with a 90% confidence interval. A combined fold change (FC-combined) in protein expression was calculated for the three biological replicates and proteins were included with a combined FC >2 or <-2. Of those, proteins were only included in the analysis that had an individual FC >2 or <-2 in two of the three biological replicates and, in addition, the third biological replicate had to have a similar trend in fold change, if present. In cases, in which the proteins were detected only in two biological replicates, both replicates had to have a FC >2 or <-2. These data represent the "relaxed" dataset, listed in Table 6.2.4 A. In the relaxed analyses, 95, 87 and 171 proteins were identified in the S2 LTQ, S1 LTQ and S1 Velos datasets respectively (Table 6.2.4 A). For the "stringent" dataset, proteins with a 95% confidence interval were identified by selecting those with a Z-

combined >1.95 and <-1.95. In addition, proteins were only included if at least two of the three biological replicates had a fold change >2 or <-2 and the 3rd value a similar trend. This “stringent” analysis identified 50, 54 and 58 proteins in S2 LTQ, S1 LTQ and S1 Velos datasets respectively (Table 6.2.4 A). Note that the proteins in these relaxed and stringent analyses are those which change in chromatin binding by two-fold or more in response to reducing Mcm7.

A larger number of total proteins were identified using the Velos-Orbitrap compared with the number of proteins identified using an LTQ-Orbitrap and this is consistent with other samples analysed by the Marcotte laboratory using these instruments. More proteins were also identified in the “relaxed” dataset using this instrument. However, no significant difference was observed in the number of proteins in the S1 and S2 samples analysed on an LTQ- or Velos-Orbitrap mass spectrometers when stringent criteria are applied. There was no significant difference in the number of proteins identified in each of the 3 biological replicates. To investigate whether there are qualitative differences in each of the data sets, the proteins identified were classified by their sub-cellular localisation (Figure 6.2.4 A and Table 6.2.4 B) and the overlap of proteins between the data sets was investigated (Figure 6.2.4 B). The sub-cellular localisation was assigned to each of the proteins by using HumanNet (see 5.2.3). As HumanNet underestimates the nuclear forms of proteins and many have more than one sub-cellular location (see 5.2.3), a protein was designated “nuclear” if it was reported to be present in the nucleus in the primary literature. For example, Actr1b/Arp1 is a dynactin complex protein involved in cell wall remodelling before mitosis, but it is also required for nuclear migration (175). Its known major function is as part of the cytoskeleton, but it is also known to have a nuclear form and it has been classified here as a nuclear protein. Similarly, Ptk2b is a multifunctional protein associated with cell polarisation, migration, apoptosis and immune responses. However a nuclear form of this protein, as well as many others, was reported in human cells in a large scale antibody study to define sub-cellular localisation of hundreds of proteins (30). For instance, Zyxin is a zinc-binding phosphoprotein that localises at focal adhesions and along the actin cytoskeleton. However, it is also a crucial nuclear regulator of the apoptotic HIPK2-

	S2 LTQ	S1 LTQ	S1 Velos
Total proteins	1682	1170	3235
Z-combined (>1.65 and<-1.65)	513	495	1148
FC-combined (>2 or <-2)	467	459	1074
Relaxed analyses (FC-individual: FC>2 or <-2 in at least 2 biological replicates; 3rd value must have same trend, if present)	95	87	171
Stringent analyses (Z-combined >1.95 or <-1.95; FC-individual: FC>2 or <-2 in at least 2 of 3 replicates; 3rd value same trend)	**50**	**54**	**58**
Interconnected proteins	32	39	28

Table 6.2.4 A. Analyses of the chromatin-bound proteins identified by mass spectrometry in the S1 and S2 fraction which change in abundance after depleting Mcm7.

S1 and S2 fractions of the Mcm7-depleted and control T cells were analysed using an LTQ- or Velos-Orbitrap mass spectrometer. Of the proteins identified, proteins were selected with a Z-combined >1.65 and <-1.65. Of those, proteins with >2 and <-2 FC-combined were selected. This identified proteins that had a FC-individual in at least 2 biological replicates >2 or <-2 and, in addition, the third biological replicate had at least the same trend in FC, if present. These proteins comprise the “relaxed” dataset. The analysis was further refined to a 95% confidence interval by selecting proteins with Z-combined >1.95 or <-1.95 and with >2 and <-2 FC in in at least 2 of 3 biological replicates and the 3rd replicate must have a same trend in FC. These proteins comprise the “stringent” dataset.

S1 VELOS

EntrezGene ID	HGNC symbol	Localisation	FC-combined
10209	EIF1	cytoplasm	20.83
1977	EIF4E	cytoplasm	12.15
1982	EIF4G2	cytoplasm	8.33
200081	TXLNA	cytoplasm	7.23
9380	GRHPR	cytoplasm	7.20
5707	PSMD1	cytoplasm	6.50
170954	PPP1R18	cytoskeleton	16.86
5033	P4HA1	endoplasmic reticulum	15.51
5627	PROS1	extracellular region	20.11
718	C3	extracellular region	6.89
26578	OSTF1	intracellular	11.99
51123	ZNF706	intracellular	-8.13
5551	PRF1	membrane	9.80
925	CD8A	membrane	6.68
10672	GNA13	membrane	-8.63
2209	FCGR1A	membrane	-25.01
2778	GNAS	membrane	-33.86
1678	TIMM8A	mitochondrion	7.25
56616	DIABLO	mitochondrion	6.61
23215	PRRC2C	na	10.90
5636	PRPSAP2	na	6.53
11333	PDAP1	na	5.90
51386	EIF3L	nucleolus	21.30
6201	RPS7	nucleolus	20.85
39	ACAT2	nucleolus	8.07
6711	SPTBN1	nucleolus	6.45
92140	MTDH	nucleolus	-6.29
8666	EIF3G	nucleus	25.84
4176	MCM7	nucleus	18.90
51637	C14orf166	nucleus	16.29
6741	SSB	nucleus	14.11
10409	BASP1	nucleus	13.78
9126	SMC3	nucleus	13.06
1212	CLTB	nucleus	12.70
3094	HINT1	nucleus	12.30
54931	RG9MTD1	nucleus	10.72
1211	CLTA	nucleus	10.27
8615	USO1	nucleus	9.82
310	ANXA7	nucleus	8.93
3315	HSPB1	nucleus	7.16
29109	FHOD1	nucleus	7.05
5611	DNAJC3	nucleus	6.91
8531	CSDA	nucleus	6.87
3098	HK1	nucleus	6.78
4790	NFKB1	nucleus	6.75
4175	MCM6	nucleus	6.53
4678	NASP	nucleus	6.43
5965	RECQL	nucleus	6.43
9255	AIMP1	nucleus	6.38
4738	NEDD8	nucleus	5.90
2773	GNAI3	nucleus	-7.32
6426	SRSF1	nucleus	-7.86
2079	ERH	nucleus	-14.46
10726	NUDC	nucleus	-14.96
55291	PPP6R3	nucleus	8.80
165904	XIRP1	nucleus	8.55
1329	COX5B	nucleus	-7.28
81027	TUBB1	nucleus	-7.52

S1 LTQ

EntrezGene ID	HGNC symbol	Localisation	FC-combined
10471	PFDN6	cytoplasm	18.47
10606	PAICS	cytoplasm	17.06
2194	FASN	cytoplasm	10.87
16	AARS	cytoplasm	10.71
5214	PFKP	cytoplasm	10.11
6888	TALDO1	cytoplasm	6.57
9322	TRIP10	cytoskeleton	7.40
79767	ELMO3	cytoskeleton	-9.66
9632	SEC24C	endoplasmic reticulum	9.65
462	SERPINC1	extracellular region	16.94
350	APOH	extracellular region	11.71
7448	VTN	extracellular region	-24.36
26578	OSTF1	intracellular	9.40
9525	VPS4B	membrane	6.26
5832	ALDH18A1	mitochondrion	17.21
1371	CPOX	mitochondrion	12.22
51004	COQ6	mitochondrion	11.78
2109	ETFB	mitochondrion	9.16
85476	GFM1	mitochondrion	7.55
9141	PDCD5	na	19.96
3615	IMPDH2	na	9.80
57095	PITHD1	na	9.74
348262	FAM195B	na	8.06
142	PARP1	nucleolus	5.95
311	ANXA11	nucleus	21.70
3662	IRF4	nucleus	21.53
25824	PRDX5	nucleus	17.63
4673	NAP1L1	nucleus	17.28
81892	SLIRP	nucleus	14.17
23157	SEPT6	nucleus	12.26
5905	RANGAP1	nucleus	12.13
3603	IL16	nucleus	12.10
5901	RAN	nucleus	11.96
54205	CYCS	nucleus	11.20
4171	MCM2	nucleus	11.05
10128	LRPPRC	nucleus	9.87
4666	NACA	nucleus	9.67
10120	ACTR1B	nucleus	9.51
10963	STIP1	nucleus	8.06
3842	TNPO1	nucleus	7.34
5594	MAPK1	nucleus	7.32
5931	RBBP7	nucleus	7.14
8498	RANBP3	nucleus	6.95
27101	CACYBP	nucleus	6.31
5928	RBBP4	nucleus	5.91
2288	FKBP4	nucleus	5.74
345651	ACTBL2	nucleus	-7.96
54386	TERF2IP	nucleus	-12.60
3921	RPSA	nucleus	-18.98
6170	RPL39	ribosome	18.53
6137	RPL13	ribosome	16.97
8664	EIF3D	ribosome	12.28
6235	RPS29	ribosome	8.74
6217	RPS16	ribosome	6.53

S2 LTQ

EntrezGene ID	HGNC symbol	Localisation	FC-combined
4144	MAT2A	cytoplasm	7.96
6301	SARS	cytoplasm	-7.35
56926	NCLN	endoplasmic reticulum	11.58
93380	MMGT1	endoplasmic reticulum	11.50
6734	SRPR	endoplasmic reticulum	10.64
4905	NSF	endoplasmic reticulum	9.72
6786	STIM1	endoplasmic reticulum	8.97
11231	SEC63	endoplasmic reticulum	8.61
6513	SLC2A1	membrane	11.50
57488	ESYT2	membrane	9.57
58505	OSTC	membrane	7.82
5018	OXA1L	mitochondrion	10.58
1537	CYC1	mitochondrion	7.99
146206	RLTPR	na	12.17
4288	MKI67	nucleolus	10.06
4176	MCM7	nucleus	33.58
4174	MCM5	nucleus	23.58
27292	DIMT1	nucleus	17.67
55720	TSR1	nucleus	14.86
6728	SRP19	nucleus	14.85
5690	PSMB2	nucleus	14.11
23352	UBR4	nucleus	13.80
4172	MCM3	nucleus	12.06
83939	EIF2A	nucleus	10.80
11331	PHB2	nucleus	10.24
4666	NACA	nucleus	10.02
22870	PPP6R1	nucleus	9.86
51663	ZFR	nucleus	9.70
4926	NUMA1	nucleus	9.67
23223	RRP12	nucleus	9.52
51637	C14orf166	nucleus	8.84
51575	ESF1	nucleus	8.83
79577	CDC73	nucleus	8.65
201161	CENPV	nucleus	8.32
23378	RRP8	nucleus	8.30
4175	MCM6	nucleus	7.36
8189	SYMPK	nucleus	7.18
151246	SGOL2	nucleus	6.78
57805	KIAA1967	nucleus	5.46
6119	RPA3	nucleus	-7.61
9129	PRPF3	nucleus	-7.70
4204	MECP2	nucleus	-7.96
8565	YARS	nucleus	-8.92
10856	RUVBL2	nucleus	-9.08
10120	ACTR1B	nucleus	-19.41
10390	CEPT1	nucleus	13.25
10982	MAPRE2	nucleus	8.66
2783	GNB2	nucleus	8.24
6144	RPL21	ribosome	-15.11
6132	RPL8	ribosome	-39.67

Table 6.2.4 B. Sub-cellular location of chromatin-bound proteins identified in the S1 and S2 fractions by LTQ-Orbitrap or Velos-Orbitrap mass spectrometer analyses that change most significantly when Mcm7 is depleted. Stringent data was analysed.

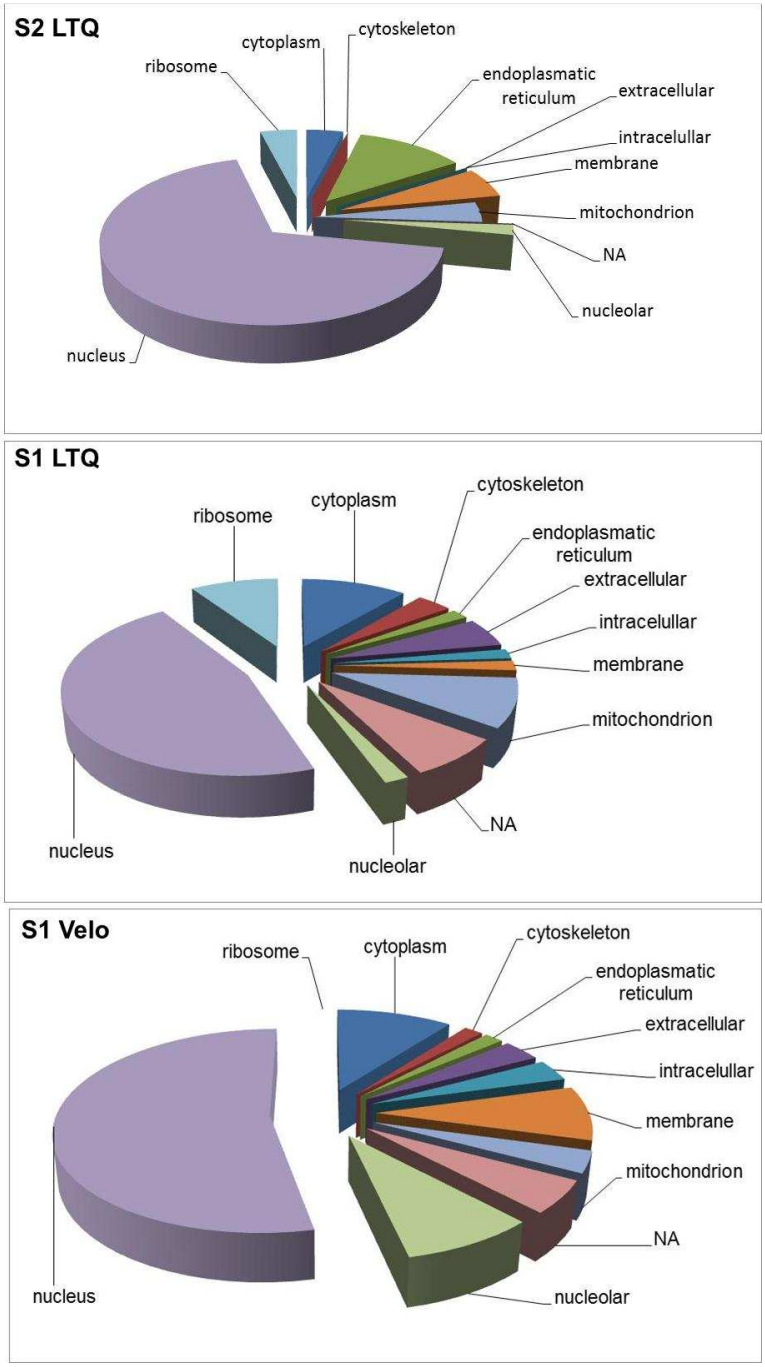

Figure. 6.2.4 A. Classification of the sub-cellular distribution of proteins identified by LTQ-Orbitrap or Velos-Orbitrap in the stringent analysis, which change significantly due to depletion of Mcm7.

The sub-cellular localization was determined using HumanNet and reading the primary literature.

p53 signalling axis in response to DNA damage (91). Furthermore, the ubiquitin ligase protein UBR4 interacts with clathrin in the cytoplasm contributing to cytoskeletal organisation, but it also interacts with the retinoblastoma protein in the nucleus, where it acts as chromatin scaffold (267).

The analyses showed that the S2 LTQ data contain the most nuclear proteins (Table 6.2.4 B). Of all those identified, most chromatin-bound proteins that change due to down regulation of Mcm7 are underrepresented and only a few proteins are overrepresented when Mcm7 is depleted (Figure 6.2.4 A). I investigated the number of proteins that overlap between the three data sets. There is a very small overlap between the data sets, but most of the proteins are unique (Figure 6.2.4 B). The same S1 fractions were analysed using both the LTQ- and Velos-Orbitrap machines and it is unclear why only one protein in the stringent analysis (Ostf1) of chromatin-bound proteins that change in Mcm7 depleted cells was identified by each machine. The limited overlap between the different MS/MS platforms might be due to the fact that the overlap was only determined for the proteins identified in the stringent analysis. 12 proteins overlap in total between the datasets in the relaxed analysis, and thus the overlap of proteins is higher. Moreover, there is a possibility that proteins extracted in S1 or S2 fractions might be different. Since the overlap of proteins amongst three technical replicates is higher than 72% for all the S2 LTQ, S1 Velos and S1 LTQ data (84.4%±7.5% and 81.8%±5% for Velos-Orbitrap and LTQ-Orbitrap respectively; mean±SD), the limited overlap of proteins between the three datasets cannot be explained by undersampling. Three proteins, Mcm6, Mcm7 and C14orf166, overlap between the stringent analyses of S1 Velos and the S2 LTQ data and less of each is detected in the chromatin-bound fraction when Mcm7 is depleted. In the stringent analysis of the S2 LTQ data, Mcm3, Mcm5 and Mcm6 were underrepresented in addition to Mcm7. As described above, the Mcm7 protein is a component of the MCM helicase (Mcm2-7) and downregulation of Mcm7 would be expected to decrease the levels of the other MCM proteins bound to chromatin. These data are consistent with that reported previously by our laboratory (see Figure 2B in (291)). In addition, in the S1 LTQ data, Mcm2 is

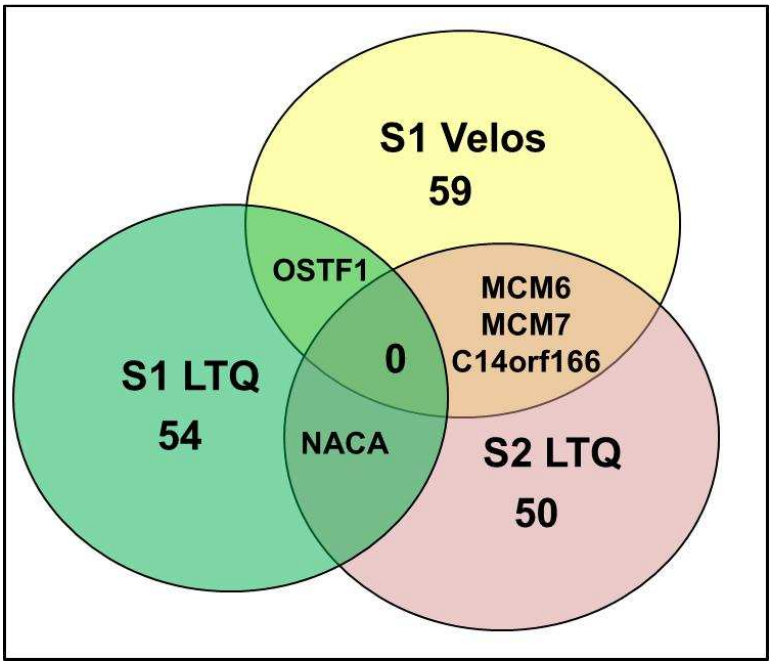

Figure 6.2.4 B. Venn diagram depicting overlap between the three data sets.
The overlap of proteins between each of the chromatin-bound datasets that change due to Mcm7 depletion was identified. Mass spectrometry analyses of data obtained from the S1 and S2 fractions analysed by LTQ- Orbitrap and from the S1 fraction analysed by Velos-Orbitrap. The data show little overlap between the 3 datasets.

significantly underrepresented. Thus, these data validate the experimental approach, since the chromatin-bound levels of five of the six MCM proteins are reduced significantly in response to Mcm7 depletion. These proteins have a FC combined in my analyses of -11, -12, -24, -7 and -34 for Mcm2, Mcm3, Mcm5, Mcm6 and Mcm7.

The only protein shared between the S2 LTQ and S1 LTQ data is Naca. Naca is co-activator of the c-Jun transcription factor in osteoblasts (429) and it is suggested to be involved in proliferative processes during haematopoiesis (23). Surprisingly, only one protein, called Ostf1, overlaps between the same S1 fraction analysed by LTQ and Velos mass spectrometers. Ostf1 is an intracellular protein required for osteoclast formation and bone resorption (307). Since this is the only protein that overlaps between the same S1 samples analysed by two different mass spectrometers, the data suggest that there are clearly differences in the proteins identified by the stringent analysis and the identification of proteins strongly depends on the technical instrument used. Because of this, I chose to combine the S1 and S2 data and data from LTQ-Orbitrap and Orbitrap-Velos machines to identify a master list of proteins bound to chromatin and which change when Mcm7 is depleted.

Based on the stringent analysis, including the S1 LTQ, S2 LTQ and S1 Velos datasets, proteins were identified that had a FC>2 or FC<-2 for each of the 3 biological replicates. All datasets were combined and 38 chromatin-bound proteins were identified, of which 33 were under- and 5 overrepresented (Table 6.2.4 C). These data show that reduction of Mcm7 affects proteins involved in a number of biological processes, including other MCM proteins involved in DNA replication, transcription, translation factors with nuclear functions (discussed below) and DNA damage. Some of the proteins, such as Prf1, Oxa1l or Cpox have not been reported to have a nuclear/nucleolar forms, but as they are all identified by this analysis in three replicate biological experiments they may have as yet unidentified nuclear functions. Most of the proteins I identified are clearly characterised as nuclear proteins, for instance Cdc73, Mcm3, Mcm5, Mcm7 and Cenpv. Cenpv/p30

is a nuclear protein associated with nucleoporins (92) and mitosis, specifically involved in cytokinesis and chromosome condensation (362).

A number of the proteins are classified by GO ontology without a nuclear localisation or biological function. However, there is still supporting evidence for nuclear forms of these proteins. For example, Aldh18 is a mitochondrial enzyme required for arginine biosynthesis and critical for $NAD(P)^+$-dependent oxidation of endogenous and exogenous aldehydes (43), however nuclear activity of Aldh has been reported (252). Pros1 is a cofactor for activated plasma protein C, required for the proteolysis of coagulation factors Va and VIIIa (134), but in addition there is some suggestive evidence that it could also be a component of the nuclear membrane, as indicated by immunostaining (http://www.proteinatlas.org/ENSG00000184500/subcellular). Similarly, Esyt2 plays an important role in calcium-dependent signalling in the cytoplasm, but it has been shown to have nuclear forms by immunostaining (http://www.proteinatlas.org/ENSG00000117868). These data for Esyt2 and Pros1 are not definitive and would require further investigation. There is no evidence for a nuclear form of prefoldin 6/Pfdn6, which is a cytosolic protein that binds chaperonin (C-CPN) (153) and which was also identified in Chapter 5. However, prefoldins were isolated as components of nuclear RNA Polymerase complexes (83) and Pfdn2 and Pfdn6 have also been implicated in the cytosolic assembly of the 12-subunit RNA Pol II complex (50, 90). Pfdn2 and Pfdn6 are also components of the R2TP complex, consisting of Rvn1-Rvb2-Tah1-Pih1 that is involved in chromatin remodelling, telomerase assembly, snoRNP biogenesis as well as RNA polymerase assembly (191). Prefoldin 5/Pfdn5/MM1 has been detected in the nucleus and is involved in the Wnt-pathway and transcription of *WNT4* (426). Therefore, a nuclear form of Pfdn6 cannot be excluded. Prf1/Perforin 1 is involved in cellular responses that lead to apoptosis. It has been shown that the nuclear localisation of granzyme B is Prf1-dependent, leading to a cytotoxic response and apoptosis (44). However, it is not clear whether Prf1 enters the nucleus as part of this process. Rpl39 is transported from the nucleolus through the nucleus as part of the pre-ribosome and it has been reported that Rpl39L has a strong nuclear and cytoplasmic immunostaining (http://www.proteinatlas.org/ENSG00000163923). This and other

EntrezID	HGNC	Description	Localisation	Biological function	Ref
5832	ALDH18A1	aldehyde dehydrogenase	mitochondrion ; nucleus	amino acid biosynthesis ; redox potential regulation	(252)
5551	PRF1	perforin 1	cytoplasm; membrane	apoptosis; cellular defence response	(44)
57488	ESYT2	extended synaptotagmin-like protein	cytoplasm; nucleus	Ca-dependent signalling	
79577	CDC73	cell division cycle 73	nucleus	cell cycle; negative regulation of progression through cell cycle; histone modification	(363, 423, 432)
5627	PROS1	protein S (alpha)	cytoplasm; nucleus	cofactor for the anticoagulant protease; blood coagulation	
170954	PPP1R18	KIAA1949	cytoplasm; nucleus	de-phosphorylation; actin dynamics (elongation and depolymerisation rates of actin filament)	(36) (171)
22870	PPP6R1	protein phosphatase 6	cytoplasm; nucleus	DNA damage; Nfkb component	(30, 110)
4172	MCM3	minichromosome maintenance complex component 3	nucleus	DNA replication; regulation of transcription; cell cycle; cell proliferation	(49)
4174	MCM5	minichromosome maintenance complex component 5	nucleus	DNA replication; regulation of transcription; cell cycle; cell proliferation	(49)
4176	MCM7	minichromosome maintenance complex component 7	nucleus	DNA replication; regulation of transcription; cell cycle; cell proliferation	(49)
5594	MAPK1	mitogen-activated protein kinase 1	cytoplasm; nucleus	MAPKKK cascade signalling; cell proliferation; induction of apoptosis;	(70)
5018	OXA1L	oxidase (cytochrome c) assembly 1-like	mitochondrion	mitochondrial oxoreductase activity; electron transport	
1371	CPOX	coproporphyringen oxidase	mitochondrion	mitochondrial decarboxylation	
201161	CENPV	centromere protein V	nucleus	mitosis (cytokinesis, chromosome condensation); nuceloporin associated protein	(92, 362)
146206	RLTPR	RGD motif, leucine rich repeats, tropomodulin domain and proline-rich containing	cytoplasm	Na	
10471	PFDN6	prefoldin subunit 6	cytoplasm	protein folding	
9632	SEC24C	SEC24 family, member C	cytoplasm; nucleus	protein transport from ER to Golgi;	(30)
11231	SEC63	SEC63 homolog	endoplasmic reticulum	protein transport to ER	
1678	TIMM8A	translocase of inner mitochondrial membrane 8 homolog A	mitochondrion	protein transport; protein import into mitochondrial inner membrane	
1211	CLTA	clathrin, light chain A	cytoplasm; nucleus	protein transport; regulatory element; mitosis	(99, 320)
1212	CLTB	clathrin, light chain B	cytoplasm; nucleus	protein transport; regulatory element; mitosis	(99, 320)
56926	NCLN	Nicalin	nucleus	proteolytic cleavage	(30)
55720	TSR1	20S rRNA accumulation, homolog	nucleus	ribosome biogenesis; translation	(68)
6201	RPS7	ribosomal protein S7	cytoplasm; nucleus	ribosome biogenesis; translation	(180)
6170	RPL39	ribosomal protein L39	ribosome	ribosome biogenesis; translation	
51637	C14orf166	chromosome 14 open reading frame 166	nucleus	transcription (regulation of transcription, regulation of RNA pol2)	(30, 297)
10409	BASP1	brain abundant, membrane attached signal protein 1	nucleus	transcription (transcriptional co-suppressor for WT1)	(67)
10209	EIF1	eukaryotic translation initiation factor 1	cytoplasm; nucleus	translation (regulation of translational initiation); response to stress	(156)
9255	AIMP1	aminoacyl tRNA synthetase complex-interacting multifunctional protein 1	cytoplasm; nucleus	translation (tRNA aminoacylation for protein translation); apoptosis induction; inflammatory response;	(156)
6513	SLC2A1	solute carrier family 2	cytoplasm; nucleus	transport of glucose	(156)
6786	STIM1	stromal interaction molecule 1	membrane; nucleus	transport of calcium; nuclear complex with SFO1	(156)
93380	MMGT1	membrane magnesium transporter 1	cytoplasm; nucleus	transport of magnesium	(156)

Table 6.2.4 C. Identification of chromatin-bound proteins that are most underrepresented in each of the 3 biological replicates. Based on the stringent analysis criteria, proteins were selected from the S1 LTQ, S2 LTQ and S1 Velos datasets that show a FC>2 or FC<-2 in each of the three biological replicates. The sub-cellular localisation and biological function was defined for each protein by reading the primary literature.

ribosome proteins identified in my study are discussed below. Stim1 has been shown to form a nuclear complex with splicing factor 1/Sfo1 (156). The major function of Mmgt1 is to transport magnesium ions in the cytoplasm, but it also forms a nuclear complex with the RNA splicing factor, Dhx15 (156). Both clathrin light chain A and B were also detected in my data. Clathrin plays a major role in the formation of coated vesicles, but it also internalises epidermal growth factor for transport to the nucleus (99) and clathrins coat and stabilize fibres of the mitotic spindle (320). Clathrin light chain A has also been shown to interact directly with the mitotic protein, MAD2B (250) and its role in mediating chromosomal instability caused by reducing Mcm7 is discussed below. Cdc73/parafibromin is a multifunctional protein involved in several biological processes, including cell cycle regulation (432), histone H2B ubiquitination and transcriptional pathways (436). This protein interacts with nuclear proteins, such as RNA Pol II, cyclin D1, C-myc and Wnt-signalling proteins (263, 363, 423). Mapk1/ERK2 is a key signalling protein mediating cell growth and survival, but it is also translocates to the nucleus (70) and phosphorylates many nuclear proteins involved in transcription, including Ets, Elk-1, c-Myc and c-Fos (316, 379). Taken together, most of the proteins reported here that change in response to depleting Mcm7 in the chromatin-bound proteome and are mainly characterised as a non-nuclear/cytoplasmic proteins have evidence for nuclear forms, discussed below.

6.2.5. Protein interaction networks of chromatin-associated proteins that change due to depletion of Mcm7

Downregulation of Mcm7 in T cells followed by analyses of chromatin-bound proteins by LTQ- or Velos-Orbitrap machines showed that the chromatin-bound levels of more than 50 proteins change significantly, as compared with data obtained from control cells. In order to obtain a better understanding of the pathways and protein functions affected by reducing Mcm7 levels and to pinpoint the most crucial proteins, protein interaction networks were generated. HumanNet analyses were carried out to derive protein interaction networks (248). Stringent analyses of chromatin-bound protein levels identified in the S2 LTQ, S1 LTQ and S1 Velos datasets (6.2.4) were used. Cytoscape (www.cytoscape.org) was used to

visualise the interactions identified between the proteins in each dataset as well as from all three combined datasets. The localisation is annotated by using different node colours and the under- or overrepresented proteins are indicated by using different node shapes (circle and triangle respectively). 32, 39 and 28 proteins were connected in the S2 LTQ, S1 LTQ and S1 Velos analyses respectively (Table 6.2.5 A) and the networks are shown in Figure 6.2.5 and their component proteins in Table 6.2.5 A. 121 proteins were connected with each other in the combined data set (total of 157 proteins) (Figure 6.2.5 and Table 6.2.5 A, Combined). MCODE analyses were then performed on the networks to define the most interconnected proteins (top sub-networks). The top three sub-networks are shown in Figure 6.2.5 and the proteins identified are listed in Table 6.2.5 B. The most interconnected sub-network consists of MCM and RPA3 proteins involved in DNA replication. As the MCM helicase works together in a complex, this analysis again validates the strength of the methodology. The first sub-network in the S2 LTQ data set consists of MCM helicases and Rpa3. Rpa3 binds to single stranded DNA to stabilize the structure and assemble other replication proteins. Specifically, it has been reported that Rpa1-3 interacts with Mcm3-7 and plays an important role in regulating the progression of the DNA replication fork (268). In addition, this protein interacts with Rad52 to induce DNA repair. Consistent with this, a previous study in the laboratory showed that inhibiting the induction of Mcm7 causes DNA damage (291). The S2 LTQ data shows that downregulation of Mcm7 increases the levels of Rpa3 bound to chromatin by 7.6-fold. This could be explained by the need to induce a DNA damage response and increased DNA binding of Rpa3 could mediate the recruitment of Rad52 to repair DNA damage caused by replication fork collapse (12, 146). Together with the MCM proteins, the chromatin binding of other proteins such as Dimt1l, Tsr1 and Esf1 are reduced. DIM1 was initially characterised as a protein required for entry into and progression through M-phase and cell cycle (40), but later it was shown that it functions in pre-mRNA splicing and therefore has an indirect role in cell cycle (433). Esf1/Abtap is a conserved nuclear protein that represses transcriptional activation by Abt1 (281). Tsr1 is a pre-ribosomal factor required for ribosome assembly and is involved in the final maturation step (68).

The second chromatin-bound sub-network in the S2 LTQ data set consists of four underrepresented proteins, called Mat2a, Cept1, Cyc1, Oxa1l. The latter two are not associated with the nucleus, but their role suggest that Mcm7 downregulation leads to reduced activity and assembly of cytochrome C that is involved in the electron transfer in the mitochondrial respiratory chain (193). Methionine adenosyltransferase 2 (Mat2A) is a key enzyme in cellular metabolism. Inhibition of Mat2a has been shown to increase FASL expression and caspase 8-depenent apoptotic cell death (181). It is not clear why these proteins were detected in my analyses of chromatin-bound proteins and whether this is a technical artefact or a genuine association of these proteins with chromatin. Of the three MCODE sub-networks identified in the S1 LTQ dataset, the first network is involved in chromatin remodelling. The proteins affect cell proliferation, including the retinoblastoma binding protein 4 and 7

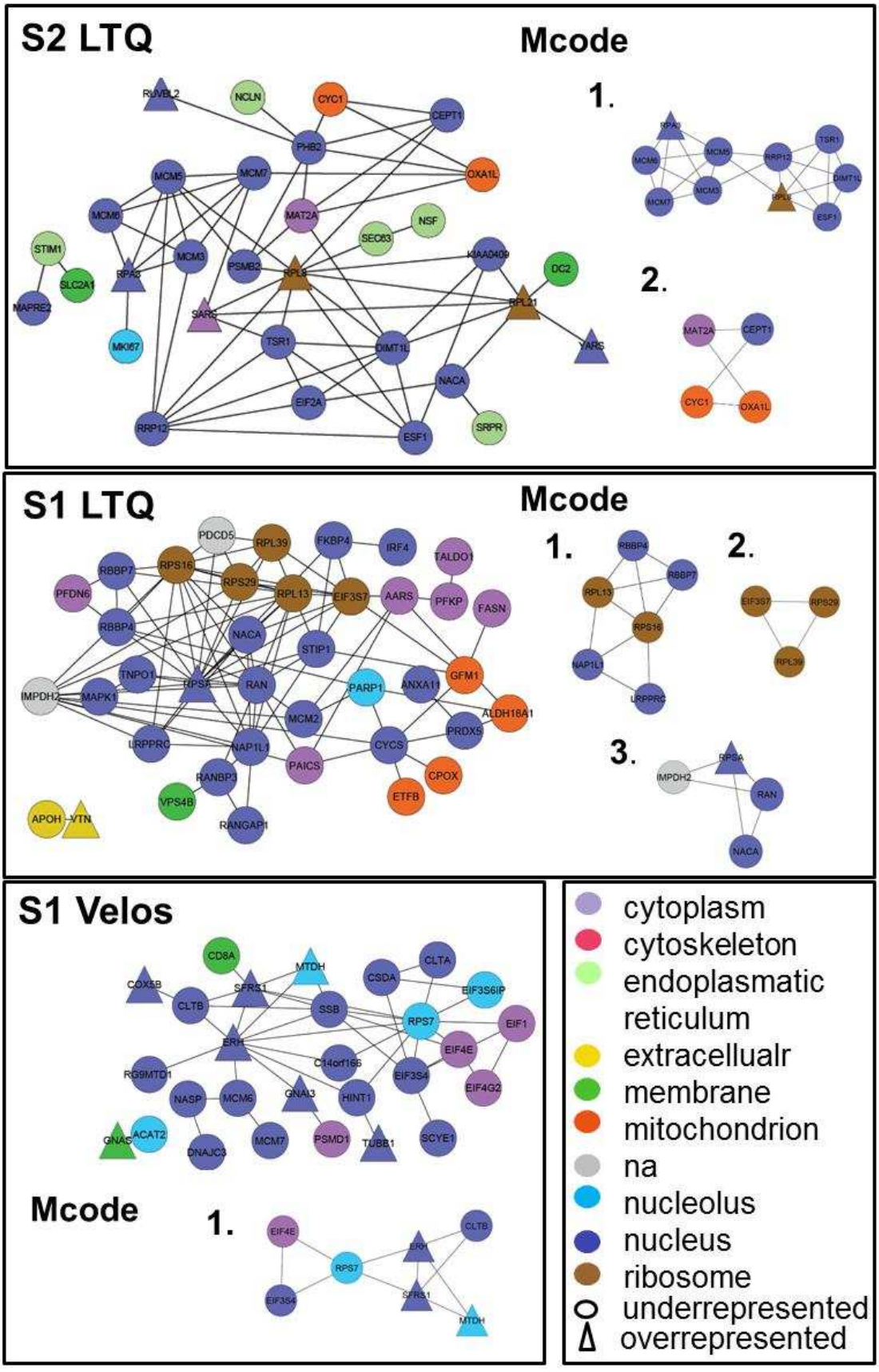
S2 LTQ
Mcode
1.
2.
S1 LTQ
Mcode
1.
2.
3.
S1 Velos
Mcode
1.
cytoplasm
cytoskeleton
endoplasmatic reticulum
extracellualr
membrane
mitochondrion
na
nucleolus
nucleus
ribosome
underrepresented
overrepresented

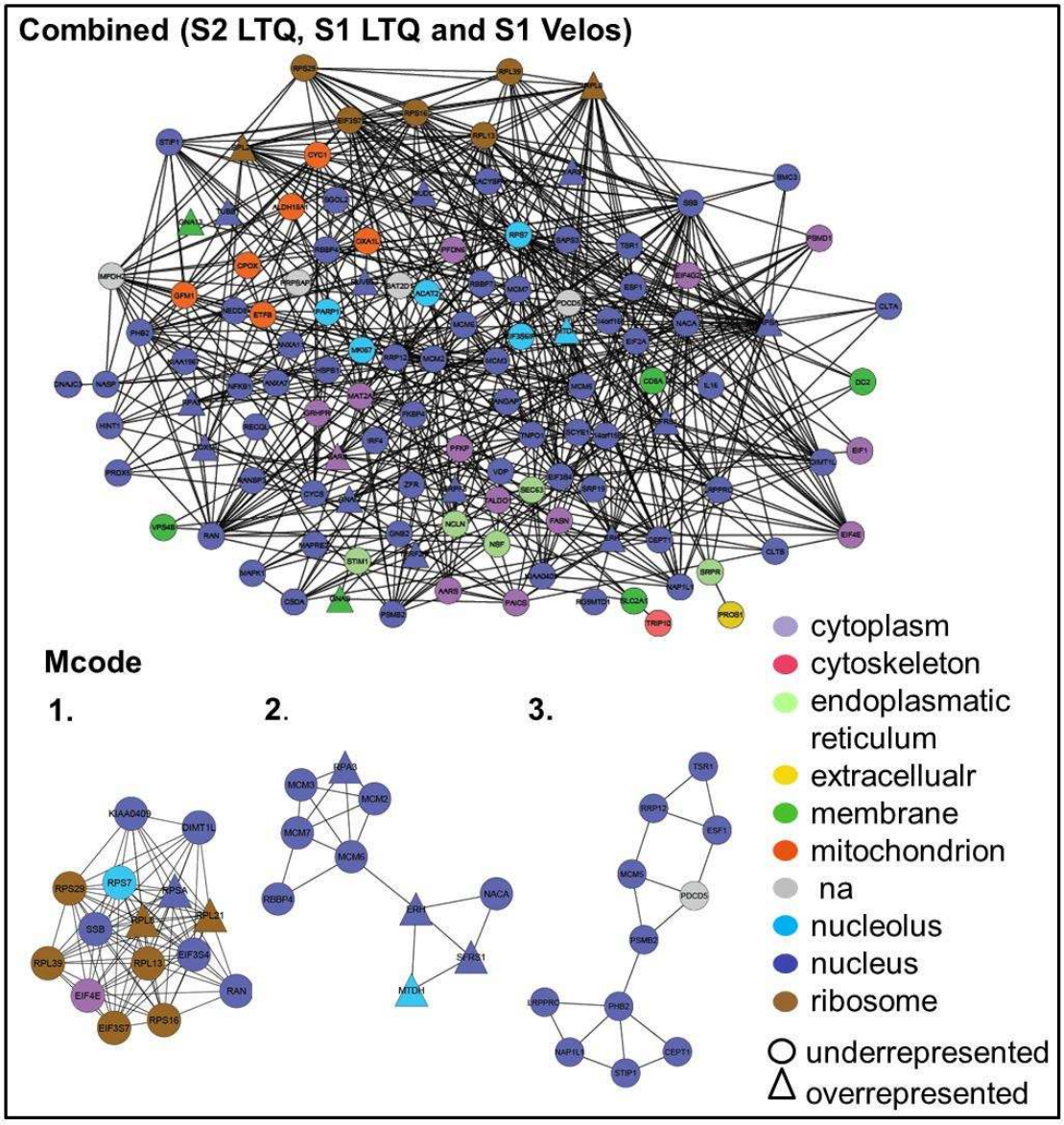

Figure 6.2.5. Protein interaction map of chromatin-bound proteins that change due to Mcm7 depletion.

Chromatin-bound proteins in S1 and S2 fractions that change most significantly in Mcm7-depleted T cells were identified and analysed by HumanNet to obtain the protein:protein interactions. The data sets from the S1 Velos, S1 LTQ, S2 LTQ and a combination of all 3 were visualized using Cytoscape. The node colour represents the sub-cellular location and the node shape indicates whether the protein is over- (triangle) or underrepresented (circle). MCODE analysis was then carried out to identify the most interconnected sub-networks. High-resolution PDFs of these networks are in S 6.2.5 on the CD in the back of this Thesis.

Combined (LTQ S2, LTQS1 and Velos S1)

Protein	Change	Protein	Change
AARS	↓	PARP1	↓
ACAT2	↓	PDCD5	↓
ALDH18A1	↓	PFDN6	↓
ANXA11	↓	PFKP	↓
ANXA7	↓	PHB2	↓
APOH	↓	PRDX5	↓
BAT2D1	↓	PROS1	↓
C14orf156	↓	PRPSAP2	↓
C14orf166	↓	PSMB2	↓
CACYBP	↓	PSMD1	↓
CD8A	↓	RAN	↓
CEPT1	↓	RANBP3	↓
CLTA	↓	RANGAP1	↓
CLTB	↓	RBBP4	↓
CPOX	↓	RBBP7	↓
CSDA	↓	RECQL	↓
CYC1	↓	RG9MTD1	↓
CYCS	↓	RPL13	↓
DC2	↓	RPL39	↓
DIMT1L	↓	RPS16	↓
DNAJC3	↓	RPS29	↓
EIF1	↓	RPS7	↓
EIF2A	↓	RRP12	↓
EIF3S4	↓	SAPS3	↓
EIF3S6IP	↓	SCYE1	↓
EIF3S7	↓	SEC63	↓
EIF4E	↓	SGOL2	↓
EIF4G2	↓	SLC2A1	↓
ESF1	↓	SMC3	↓
ETFB	↓	SRP19	↓
FASN	↓	SRPR	↓
FKBP4	↓	SSB	↓
GFM1	↓	STIM1	↓
GNB2	↓	STIP1	↓
GRHPR	↓	TALDO1	↓
HINT1	↓	TNPO1	↓
HSPB1	↓	TRIP10	↓
IL16	↓	TSR1	↓
IMPDH2	↓	VDP	↓
IRF4	↓	VPS4B	↓
KIAA0409	↓	ZFR	↓
KIAA1967	↓	COX5B	↑
LRPPRC	↓	ERH	↑
MAPK1	↓	GNA13	↑
MAPRE2	↓	GNAI3	↑
MAT2A	↓	GNAS	↑
MCM2	↓	MTDH	↑
MCM3	↓	NUDC	↑
MCM5	↓	PRPF3	↑
MCM6	↓	RPA3	↑
MCM7	↓	RPL21	↑
MKI67	↓	RPL8	↑
NACA	↓	RPSA	↑
NAP1L1	↓	RUVBL2	↑
NASP	↓	SARS	↑
NCLN	↓	SFRS1	↑
NEDD8	↓	TERF2IP	↑
NFKB1	↓	TUBB1	↑
NSF	↓	VTN	↑
OXA1L	↓	YARS	↑
PAICS	↓		

LTQ S2		LTQ S1		Velos S1	
Protein	Change	Protein	Change	Protein	Change
ESF1	↓	AARS	↓	ACAT2	↓
RRP12	↓	ALDH18A1	↓	C14orf166	↓
DC2	↓	ANXA11	↓	CD8A	↓
MCM7	↓	APOH	↓	CLTA	↓
NSF	↓	CPOX	↓	CLTB	↓
EIF2A	↓	CYCS	↓	CSDA	↓
TSR1	↓	EIF3S7	↓	DNAJC3	↓
MCM5	↓	ETFB	↓	EIF1	↓
OXA1L	↓	FASN	↓	EIF3S4	↓
MCM3	↓	FKBP4	↓	EIF3S6IP	↓
MAT2A	↓	GFM1	↓	EIF4E	↓
PHB2	↓	IMPDH2	↓	EIF4G2	↓
DIMT1L	↓	IRF4	↓	HINT1	↓
MKI67	↓	LRPPRC	↓	MCM6	↓
CYC1	↓	MAPK1	↓	MCM7	↓
MAPRE2	↓	MCM2	↓	NASP	↓
NCLN	↓	NACA	↓	PSMD1	↓
SLC2A1	↓	NAP1L1	↓	RG9MTD1	↓
SRPR	↓	PAICS	↓	RPS7	↓
SEC63	↓	PARP1	↓	SCYE1	↓
STIM1	↓	PDCD5	↓	SSB	↓
CEPT1	↓	PFDN6	↓	COX5B	↑
MCM6	↓	PFKP	↓	ERH	↑
PSMB2	↓	PRDX5	↓	GNAI3	↑
KIAA0409	↓	RAN	↓	GNAS	↑
NACA	↓	RANBP3	↓	MTDH	↑
RPL8	↑	RANGAP1	↓	SFRS1	↑
RUVBL2	↑	RBBP4	↓	TUBB1	↑
SARS	↑	RBBP7	↓		
RPL21	↑	RPL13	↓		
YARS	↑	RPL39	↓		
RPA3	↑	RPS16	↓		
		RPS29	↓		
		STIP1	↓		
		TALDO1	↓		
		TNPO1	↓		
		VPS4B	↓		
		RPSA	↑		
		VTN	↑		

Table 6.2.5 A. List of connected proteins that change due to Mcm7-depletion.

The levels of chromatin-bound proteins identified by mass spectrometry in the S2 LTQ, S1 LTQ, S1 Velos or of the 3 combined that change significantly due to Mcm7-depletion were analysed using HumanNet to identify proteins that interact with each other.

LTQ S2				Velos S1	
1st sub-network		2nd sub-network		1st sub-network	
Protein	Change	HGNC syn	Change	Protein	Change
ESF1	↓	CEPT1	↓	CLTB	↓
MCM3	↓	CYC1	↓	EIF3S4	↓
MCM5	↓	MAT2A	↓	EIF4E	↓
MCM6	↓	OXA1L	↓	ERH	↑
MCM7	↓			MTDH	↑
RPA3	↑			RPS7	↓
RPL8	↑			SFRS1	↑
RRP12	↓				
TSR1	↓				

LTQ S1					
1st sub-network		2nd sub-network		3rd sub-network	
Protein	Change	Protein	Change	Protein	Change
LRPPRC	↓	IMPDH2	↓	EIF3S7	↓
NAP1L1	↓	NACA	↓	RPL39	↓
RBBP4	↓	RAN	↓	RPS29	↓
RBBP7	↓	RPSA	↑		
RPL13	↓				
RPS16	↓				

All combined (S1 and S2 LTQ and S1 Velos)					
1st sub-network		2nd sub-network		3rd sub-network	
Protein	Change	Protein	Change	Protein	Change
DIMT1L	↓	ERH	↑	CEPT1	↓
EIF4E	↓	MCM3	↓	ESF1	↓
KIAA0409	↓	MCM6	↓	LRPPRC	↓
RAN	↓	MCM7	↓	MCM5	↓
RPL13	↓	MTDH	↑	NAP1L1	↓
RPL21	↑	NACA	↓	PHB2	↓
RPL39	↓	RBBP4	↓	PSMB2	↓
RPL8	↑	RPA3	↑	RRP12	↓
RPS16	↓	SFRS1	↑	STIP1	↓
RPS29	↓			TSR1	↓
RPSA	↑				
SSB	↓				

Table 6.2.5 B. List of the most inter-connected proteins that change due to Mcm7-depletion.

Chromatin-bound proteins identified by mass spectrometry in the S2 LTQ, S1 LTQ, S1 Velos or of the 3 combined datasets that change significantly due to Mcm7-depletion were analysed using HumanNet to identify proteins that interact with each other. MCODE analysis was performed to identify the most interconnected sub-networks and proteins in each of the top three sub-networks are shown. The under- or over-representation of a protein is indicated by an arrow.

(Rbbp4 and Rbbp7) and the nucleosome assembly protein 1-like (Nap1l). LRPPRC functions in mRNA-binding and export out of the nucleus (254). The second sub-network consists of downregulated ribosomal proteins, such as Rpl29 and Rpl39 and the eIF-3 translation initiation factor protein, EIF3S7/EIF3D. The eIF-3 factor was originally isolated as a five-subunit complex involved in protein synthesis, but subsequent high-content mass spectrometry analysis of yeast eIF-3 identified 230 interacting proteins. These include many proteins associated with nuclear functions, such as the importins Kap123p and Sal3p, which bind to the nuclear pore complex. Sal3p was shown to be required for nuclear import of the Proteasome. Furthermore, eIF3 is associated with 22 proteins involved in ribosome biogenesis (337). Nuclear import of another eIF-3 protein, EIF3S6/EIF3E was also shown to occur in human fibroblasts (410) and this protein interacts directly with Mcm7 and stabilises its association with DNA (410). Reduction of Mcm7 levels therefore inhibits ribosome biogenesis/assembly and potentially a number of other cellular mechanisms mediated by the eIF-3 complex.

In the second sub-network of the S1 LTQ dataset Impdh2 was identified. Impdh2 is involved in *de novo* nucleotide synthesis needed for DNA and RNA synthesis (249). Chromatin-bound Parp1 levels are reduced by depleting Mcm7, as shown by the S1 LTQ dataset. Parp interacts with cytochrome C (Cycs) (292). Parp also interacts with many components of DNA repair pathways, such as Rad21 and Rad18 (294) (156).

6.3 Discussion

The minichromosomal maintenance protein involved in DNA replication was first described in *S. ceravisiae* (381). Later it was also shown that the Mcm2-7 complex binds chromatin in a distributed pattern surrounding the origin recognition complex in *Xenopus* egg extracts (115). The MCM complex has helicase activity and forms complexes with other licensing factors, including Orc4, Cdc6 and Cdt1 that participate in the initiation and elongation of DNA replication (222, 367). The loading and activation of the helicase are regulated by multiple mechanisms to ensure that Mcm2-7 loading can only occur once at each replication origin during the cell cycle (49). Moreover, MCM proteins have been used as bio-markers of cell proliferation and prognostic markers in cancer (412). There is also good evidence that deregulation of DNA replication licensing caused by oncogene activation contributes to cancer by causing genomic instability (46). Work from our laboratory showed that reducing the level of Mcm7 or Mcm4, which are normally induced in primary T cells during entry into the cell cycle from quiescence, caused DNA damage, premature chromatid separation and severe chromosome abnormalities found in genomic instability syndromes (291). In order to understand the molecular changes that occur when Mcm7 levels are reduced, I investigated the changes in the chromatin-bound proteome caused by inhibiting the induction of Mcm7 in primary human T cells. Mcm7 was depleted in three independent isolates of primary human T cells using an siRNA approach, as described in (291). For each, proteins were crosslinked to DNA by incubating the cells with formaldehyde, nuclei were isolated and chromatin was eluted after digestion with micrococcal nuclease (S1 and S2 fractions). Chromatin-bound proteins in each fraction from control or Mcm7-depleted T cells were trypsinised and identified by mass spectrometry (LCMS/MS). Quantitative changes in the chromatin-bound proteome caused by the reduction of Mcm7 were identified by a label-free method, which was used previously by our laboratory (290). Analyses of these data were then carried out using the relaxed and stringent criteria described above to identify the most significant changes. Similar studies have been carried by other groups analysing changes in the proteins on a large scale in response to perturbing DNA replication. Down regulation of the DNA replication protein, Cdc7 in fibroblasts using RNAi, in

combination with SILAC-based MS proteomics of whole cell lysates identified changes in wide-ranging biological processes (266). These changes are associated with active cellular adaptation to cell-cycle arrest and the authors identified proteins involved in several processes such as energetic flux, stress responses and reduced proliferative capacity. This study differs from the analyses described in this Chapter as they addressed changes associated with G_1 arrest rather than genomic instability and they did not analyse the chromatin-bound proteome. Changes in chromatin-associated proteins (of *Xenopus laevis* sperm nuclei), which occurs when DNA replication is inhibited was reported by the Blow laboratory (199), but DNA damage and genomic instability were not investigated. Inhibiting replication licensing with Geminin revealed an unexpectedly broad system-wide effect on the chromatin proteome, including a delay in nuclear pore complex assembly (199).

The results I present in this Chapter show that Mcm7 downregulation affects a number of biological processes. I will highlight some of the processes and give examples of proteins identified in my dataset which have roles in these processes.

DNA replication. First, Mcm7 downregulation decreased levels of several DNA-replication proteins. All of the MCM proteins have to bind to chromatin to form the helicase complex (49) and previous work from the laboratory showed that reducing Mcm7 levels caused a reduction in the levels of all the other MCM proteins bound to chromatin (Figure 2B of (291)). A reduction in the levels of chromatin-bound Mcm2, Mcm3, Mcm5 and Mcm6 were detected by my analyses when Mcm7 was depleted and the largest underrepresentation was observed for Mcm7 (-33-fold combined). These changes validate the methodology I developed and applied here.

The level of expression of MCM proteins has also been used as a marker of proliferation for a number of cancers (for example, see (113, 144)) and reduction in Mcm7 also affects another marker of proliferation MKI67/Ki67 (378). The level of chromatin-bound MKI67/Ki67 is reduced with a combined FC of -10. The function of this protein is unclear, but it is used extensively as a marker of cell proliferation in both scientific and clinical studies (for example, see: (164, 390)). Chromatin binding of Mapre2 was also reduced. This is a microtubule-associated protein that is

necessary for spindle symmetry during mitosis, but it is also important for the proliferative control of normal cells (2).

Transcription. Mcm7 downregulation also reduced the chromatin-binding of Mapk1/ERK2, a crucial player in signal transduction pathways which mediate cell proliferation and survival. When activated, Mapk1 translocates to the nucleus (70), where it phosphorylates many substrates, including several transcription factors, such as Ets, Elk-1, c-Myc and c-Fos (316, 379). Interestingly, MAPK1 and Wnt signalling proteins regulate Cyclin D1. Cdc73 was also reduced when Mcm7 was depleted. Cdc73/parafibromin is involved in different cellular processes, including cell cycle regulation, histone modification and transcriptional pathways (422, 432, 436). This protein interacts with nuclear proteins such as RNA Pol II, Cyclin D1, C-Myc and Wnt targets (263, 363, 423). Parafibromin induces cell cycle arrest in part by repressing the expression of *CCND1* (encodes Cyclin D1) *via* an interaction with the histone methyltransferase Suv31H9 (422). Since Cyclin D1 is not expressed in T cells (373), it is very likely that other cyclins, such as Cyclin D2 and/or Cyclin D3, together with other cell cycle-regulatory proteins could be reduced by depleting Mcm7, but this would need to be investigated. In addition, Mcm7 reduction affects other proteins involved in transcriptional processes, including C14orf166 (positive regulator of RNA Pol II) (297), the interferon-regulated transcription factor Irf4, Nfkb1 (NFκB-p50), Basp1 (co-suppressor of *WT1*) (67), Csda (represses the *GMCSF* promoter) (86), Nedd8 (stabilises HIF1α) (324), Naca (co-activator of c-Jun) (429), Esf1/ABTAB/ABT1 (regulates by binding to TBP) (281) and Phb2 (260). Taken together, these data indicate that inhibiting the induction of Mcm7 in T cells leads to a reduction in chromatin binding of a number of proteins required for the expression of genes involved in cell proliferation and other processes. Data on yeast showed that 88% of gene expression was not affected by conditional inhibition of DNA replication, including genes regulated periodically through the cell cycle. However, 3.5% of genes were affected by inhibition of DNA replication, including reduction in the expression of many genes encoding histones. Also, gene expression was affected by origin licensing near their 3'-ends (283). It would be interesting to determine which genes are regulated in T cells by reducing Mcm7

levels, whether they have binding sites in their promoters for the transcription factors identified here or those regulated by MAPK1/ERK2 and whether any have known DNA replication origins near their 3'- or 5'-ends.

DNA damage. A third class of proteins that is affected by Mcm7 downregulation are DNA damage proteins. The level of chromatin-bound Rpa3 increases when Mcm7 is depleted. The replication protein 3 (Rpa3) is essential for DNA replication and plays an important role in DNA repair of double strand breaks and DNA recombination (268). There is evidence that the DNA repair protein Rad52 interacts directly with Rpa3/Rpa70 to induce DNA repair (179). The previous study from our laboratory showed that reducing Mcm7 caused DNA damage (291) and an increase in chromatin binding of Rpa3 is consistent with the increase in DNA damage caused in these cells. Recruitment of Rpa3 could mediate binding of Rad52 to repair DNA damage caused by replication fork collapse (12, 146). Similarly, the Ruvbl2 protein is up-regulated when Mcm7 is reduced. Ruvbl2 is a DNA helicase essential for homologous recombination and DNA double-strand break repair (185). It has also been shown to be a repressor of *ARF* transcription (420). Mcm7 downregulation also reduces chromatin-binding of the regulatory subunit 1 of protein phosphatase 6 (PP6) (PPP6R1). PP6 binds to the DNA-dependent protein kinase catalytic subunit (DNA-PKcs), which is involved in the repair of DNA double strand breaks by NHEJ. DNA-PKcs recruits PP6 to the sites of DNA damage, where it dephosphorylates p-γH2AX (110). Mcm7-depletion causes nuclear foci of phospho-γH2AX (291) and reduction in PPP6R1 bound to chromatin would enable γ-pH2AX phsosporylation to persist. It is not clear what effect that would have and whether the persistence of a phospho-γH2AX signal would increase mis-repair. In addition, Parp1, which catalyses poly(ADP-ribosyl)ation is downregulated in Mcm7-depleted cells. Parp1 is one of the earliest responses to DNA damage (100) and it is not clear why the level of chromatin binding is decreased in response to depleting Mcm7.

Ribosome biogenesis. The transcription of rRNAs occurs in the nucleolus and the rRNA precursors are processed and assembled into ribosomal subunits, which are

translocated through the nucleus into the cytoplasm to carry out protein synthesis (48, 387). Downregulation of Mcm7 reduced the chromatin binding of a number of rRNA binding proteins, such as Ssb and Dimt1. Dimt1 is an rRNA methyl transferase that di-methylates two adjacent adenosines of the 18S rRNA in the small ribosomal subunit during the normal course of ribosome maturation (301). Ssb/La autoantigen/Sjoegren syndrome type B antigen is an RNA-binding protein that binds the 3' poly(U) termini of RNA polymerase III transcripts (snRNA, tRNA, 5S rRNA) (11, 370). The chromatin binding of other proteins are also reduced, including ribosome proteins Rps7, Rps16, Rps29, Rpl13 and Rpl39, as well as Tsr1 and Larp1. Tsr1 is required for 20S rRNA maturation (68). The ribonucleoprotein Larp1 is found in a complex with poly A-binding protein and EIF4E (described below) and is associated with 60S and 80S ribosomal subunits. A reduction in Larp1 expression by siRNA inhibits global protein synthesis rates and results in mitotic arrest (58). The assembly of ribosomal subunits takes place in the nucleolus and the nuclear import of ribosomal proteins is mediated, for example by importin beta, transportin, RanBP5 and RanBP7 and thus very likely to be affected in the nucleus by Mcm7 reduction (180). Reduction of transportin1 was observed in the in the Mcm7-depleted cells in the relaxed analysis of the S1 LTQ data set. RanBP3 was also reduced in the same sample. Interestingly, in each of the three biological replicates there was a significant reduction in chromatin binding of the GTP-binding protein RAN and RanGAP1 (combined FC each -12). These proteins are required for the nucleo-cytoplasmic transport of proteins and RNA (212) and have a role in DNA synthesis (308). The decreases in a number of ribosomal proteins identified in the datasets reported here are consistent with a decrease in ribosome biogenesis, leading to a reduction of pre-ribosomes exported through the nucleus into the cytoplasm. However, a number of ribosomal proteins also have “extraribosomal” functions in the cell, *i.e.* in processes other than in translation, which include regulating p53 and as a co-factor for NFκB (409). Rps7 binds MDM2 and regulates p53 activity (75). Reducing the binding of Rps7 would be expected to cause an increase in p53 levels. Rps29 also has a role in inducing genes required for apoptosis (197). Rpl13 is part of the GAIT complex, which binds the 3’UTR of specific mRNAs and controls their translation (246). However, a role in the nucleus

has not been described. Abnormalities in ribosomal proteins, including the deletion of one allele, have also been reported to occur in ribosome dysgenesis disorders, including the chromosome 5q- myelodysplastic syndromes and Diamond-Blackfan anaemia (270). It is not yet known whether these disorders occur as a result of ribosomal or extra-ribosomal functions of the proteins affected.

Miscellaneous. The clathrin light chain A and B were also reduced in all three biological datasets when Mcm7 was depleted. Clathrin was originally described as a component of coated vesicles. Clathrins are now know to internalise the epidermal growth factor into the nucleus (99) and additionally clathrins coat the mitotic spindle and are important for chromosome segregation (320). Clathrin light chain A interacts directly with the mitotic protein, MAD2B and depletion of MAD2B with siRNA reduces clathrin light-chain A binding to the mitotic spindle and leads to misaligned chromosomes (250). Downregulating Mcm7 in T cells causes premature chromatid separation and gross chromosomal abnormalities and it would be interesting to determine to what extent the reduction in chromatin binding of Clathrin light chain A and B are responsible for causing these events.

Mcm7 reduction also reduces the chromatin-bound levels of several proteins known to be involved in the initiation of translation, including EIF1, EIF2A, EIF3D, EIF3G, EIF3L, EIF4E. Nuclear translation has been reported (174), but this is contentious. However, these proteins have additional roles in the nucleus. The many functions of EIF3 were described earlier in this Chapter, but include nuclear import/export *via* binding the nuclear pore complex and hnRNA splicing (337). EIF3 also binds to Mcm7 *via* the EIF3S6/EIF3E subunit and stabilises MCM binding to DNA (56). In addition, EIF4G has a role in apoptosis by binding in the nucleus to the apoptosis-inducing factor, AIF (201). A substantial proportion (up to 68%) of the 5' m7G cap-binding protein, EIF4E localises to the nucleus and binds PML as well as RNA (223). This protein has several roles in the nucleus (359), participating in a variety of RNA-processing events including splicing (109) and the nucleo-cytoplasmic transport of specific mRNA, some of which (*e.g.* Cyclin D1 mRNA) are involved in cell proliferation. Its interacting protein, EIF4G, also has a role in RNA decay (298). Both PML and EIF4E bind to the nuclear matrix and PML is a negative regulator of

EIF4E (85). EIF1 is retained in the nucleus when nuclear export is inhibited (256), although its nuclear function is unknown. EIF2A may also have roles in the nucleus (see (290)), but the mechanisms have yet to be investigated in detail.

Conclusion. The study presented here shows that downregulation of Mcm7 affects chromatin binding of proteins involved in biological processes, including DNA replication, DNA damage, transcription, ribosome biogenesis, cell proliferation and others. Studies are now required to investigate the functional consequences of the reduction or induction of chromatin-bound proteins involved in the processes described in my study. In particular, to what extent these account for the DNA damage responses, premature chromatid separation and genomic instability already reported by our laboratory (291).

Chapter 7

7. General Discussion

7.1 Summary

The aim of my PhD work was to apply Systems Biology methods to answer several biological questions, this includes (i) identifying new regulators of a signalling pathway in immune cells using a predictive and advanced imaging approach (ii) investigating whether the orthologues of worm genes predicted by the Phenolog approach are important in maintaining genomic stability in human cells and (iii) systematic identification of changes in the chromatin-bound proteome network in activated T cells caused by depleting a DNA replication protein.

In the first study the work focused on the Rho GTPase, Cdc42 that is involved in regulating changes in the cytoskeleton and motility. The aim was to identify new proteins that are crucial for activation of Cdc42 in NK cells at the immunological synapse. This was addressed by using a novel combination of bioinformatics, imaging and functional cell biology approaches. The bioinformatics analyses predicted a number of proteins that are potentially important for Cdc42 activation. I tested the targets by down regulating each of them using an siRNA approach and then analysing the effects on Cdc42 activity using a FRET biosensor. I measured Cdc42 activity in the NK cells transfected with each siRNA in presence or absence of the target cells by FRET-FLIM. The results showed that two proteins, AKT1 and PI3KR1 are important regulators of Cdc42 activity in NK cells and are important for inducing NK-cell cytotoxicity.

The second study is based on the fact that orthologous genes that are functionally important are frequently conserved between species, but they may be responsible for different phenotypes in different species. The knowledge about the functions of conserved, orthologous genes in other species was used to predict genes that are important in Breast and Ovarian cancer and, based on the functions of the overlapping subsets between humans and worms, may be required to maintain genomic stability in human cells. To determine whether the predicted targets are required for maintaining genomic stability, I used a human primary T cell system

that has been previously used and validated in our laboratory to analyse genomic instability and which has a normal genetic background (291). I isolated human primary T cells and downregulated the proteins of interest using siRNA. The T cells were stimulated with PMA/Ionomycin and DNA damage was analysed by immunofluorescence microscopy of phospho-γH2AX and Rad51. I also carried out karyotype analyses (I-FISH) to analyse chromosomal abnormalities. The results showed that downregulation of the predicted targets result in DNA damage and in an abnormal karyotype.

The final project focused on the effects of depleting Mcm7 on the chromatin-bound proteome of T cells. I optimised the methods to isolate proteins that are strictly associated with chromatin and applied these methods to analyse the changes that occur when Mcm7 is depleted by high content, label-free mass spectrometry and quantitative analysis of the data. In this approach, I depleted Mcm7 using siRNA in primary T cells. The stimulated T cells were crosslinked with formaldehyde and nucleosomes were released from isolated nuclei by digestion with *M.nase*. The nucleosome preparations were digested with Trypsin, separated on a C18 reverse phase column and analysed using tandem MS. I identified chromatin-bound proteins that changed significantly when Mcm7 is depleted and mapped protein:protein interactions using HumanNet. The results showed that the MCM helicase complex proteins were most significant downregulated, which validate the strength of the approach. Downregulation of Mcm7 affects chromatin binding of proteins involved in biological processes, including DNA replication, DNA damage, transcription, ribosome biogenesis and others.

7.2 Future Work

The conclusions from each study are summarized in section 7.1. However, the results raise additional questions which would be interesting to address in future projects.

7.2.1. Cellular location of chromatin-bound proteins identified my mass spectrometry

The proteomics data of the chromatin-bound proteome in Chapter 5 suggest that numerous proteins whose biological function is mainly characterised in the cytoplasm, membrane or in other organelles outside the nucleus have a nuclear form. Therefore, it would be of interest to investigate whether these proteins can exist in the nucleus either at low levels or possibly while passing through the nucleus. This could be achieved experimentally by immunostaining the proteins and defining the localisation of each particular protein in the cell. Co-localisation could be investigated first by multi-colour confocal microscopy and verified by FRET. Some proteins may localise to the nucleus and bind chromatin in a cell cycle-dependent manner. This could be investigated by fixing and isolating cells in different cell cycle phases by staining DNA content with a stain such as Hoechst 33342 and isolating cells in G_0/G_1, early, mid and late S-phase and G_2/M by flow cytometric sorting. Cells in G_2 can be distinguished and isolated from those in M-phase by staining for phospho-Histone H3(S^{10}) (see (291)).

7.2.2. Analysing the effects of reducing Mcm7

The proteomics data obtained from the Mcm7 knockdown experiments in Chapter 6 indicate that many chromatin-bound proteins are downregulated and several biological processes are affected by Mcm7 reduction. It would of interest to validate the proteomics data obtained by mass spectrometry analyses by other means. Preferably, all the chromatin-bound proteins which change in response to reducing Mcm7 should be analysed, but good antibodies may only be available for a subset of proteins (see our recent study for such analyses: (290)). The chromatin-bound

proteins that change significantly in response to depleting Mcm7 could be investigated by western blotting using samples from further siRNA transfection experiments. It is possible that the amount of a given protein in the cell does not change, but the amount bound to chromatin is affected by reducing Mcm7. This could be investigated by carrying out western blot analyses of total cell protein extracts, chromatin-bound protein samples or CSK extracts. Translocation to the nucleus could also be verified by confocal microscopy. Secondly, depending on the protein of interest, functional studies could be carried out to improve the understanding of mechanisms that cause DNA damage, replication fork collapse, premature chromatid separation and genomic instability, which are all caused by reducing Mcm7 (291). Similar studies were carried out in our recent paper (290) in which the functions of eIF6, as well as SF3B2 and SF3B4 proteins were investigated.

The protein complexes containing the chromatin-bound proteins I identified were inferred by using HumanNet. It would be of interest to isolate protein complexes from T cells transfected with control- or Mcm7-siRNA and identify the proteins in each complex by employing methods used by our collaborators in a recent study (156). In this study, the protein complexes in HeLa and HEK293 cytoplasmic and nuclear fractions were separated by extensive biochemical fractionations and proteins in every fraction from each of the fractionation methods were identified by mass spectrometry. One fractionation involves ion exchange chromatography by employing four different optimised analytical column combinations and salt gradients. The same lysates were separated using sucrose gradient centrifugation and also isoelectric focusing. The proteins in each complex were inferred by the fact that proteins which co-purify through several different fractionation methods are likely to be in a complex. The tandem MS analyses led to the identification of more than 13,000 high-confidence physical interactions. This study has provided the biggest database of human protein complexes from cell lines. In a smaller, targeted study, it would be interesting to downregulate Mcm7 and specifically investigate particular proteins that are involved, for example in DNA damage or chromosome segregation, and how the changes affect the protein-complexes identified in (156). This, together with the information obtained in data presented in Chapter 6 might

elucidate more information not only on which nuclear proteins are perturbed, but how they affect part of the cellular ”wiring diagram”.

7.2.3. MCMs in cancer: comparing the effects of increasing and decreasing MCM proteins

It has been shown that DNA replication proteins, including Mcm7 are aberrantly expressed in many cancers. The proteins are either under- or over-expressed as a result of abnormalities in cell cycle control mechanisms (46). It would therefore be interesting to investigate the opposite scenario to that investigated in my Thesis, *i.e.* when Mcm7 is overexpressed in human cells. The changes in the chromatin-bound proteome caused by transfecting T cells with a plasmid expressing Mcm7 would be analysed by the methods established here. Similarly, proteins identified by MS/MS could be classified by sub-cellular location and biological function. The modified nuclear proteome could then be compared with the results in Chapter 6 to identify commonalities and differences caused by increasing or reducing MCM levels.

7.2.4. The chromatin-bound proteome in cancer

The work carried out in (290) elucidated the protein interaction network of primary human T cells during cell cycle entry, whereas my work in Chapter 6 investigated the changes that occur in the chromatin-bound proteome caused by depleting Mcm7, which causes genomic instability. The knowledge obtained from both studies is of use in addressing other biological questions. For example, it would be interesting to apply one of the methodologies to investigate the processes which occur in a blood cancer, such as in cells from patients with chronic lymphocytic leukaemia (CLL). Cells from CLL patients are in an “in cycle G_1” state rather than G_0, indicative of abnormal cell cycle control (280).The chromatin-bound proteome of CLL cells from patients could be isolated using CSK extraction or the chromatin isolation method I used here and analysed by LC-MS/MS. The data obtained could be compared with the reference data in (290) to identify commonalities and differences in cell cycle-dependent changes. This might allow the identification of commonalities and differences in protein interaction networks between normal and

cancerous cells and a more precise definition of the “in cycle G_1” state. Potentially this may allow us to identify new biomarkers for CLL.

7.2.5. Identifying novel genes involved in DNA replication and genome stability by Phenolog analyses.

The Phenolog study enables us to predict novel genes involved in human diseases based on an understanding of the functions of their orthologues in other species. The analyses are based on a given seed set of human genes. The combination of several databases from different species together with bioinformatics analyses used in the Phenolog approach may be used for different biological questions. For instance, the top chromatin-bound proteins which are up- or downregulated by Mcm7 depletion in my proteomic study might be used as a seed set to potentially predict other proteins involved in DNA replication and genomic stability in humans. Based on the seed set, Phenolog analyses may be able to predict additional orthologous genes with different phenotypes in other species, such as worm, yeast or mouse. These analyses may predict novel genes with as yet unrecognised roles in maintaining genomic stability in humans.

7.2.6. Identifying new regulators in solid tumours by a biosensor, FRET-FLIM screen.

The siRNA screen combined with an activity readout for a particular protein:protein interaction using FRET-FLIM is a powerful tool to identify new components of a cellular pathway. This approach is mainly dependant on the protein of interest and the availability of the corresponding biosensor. For instance, a HER2-family biosensor is available (280), which could be used for an analogous study to that reported in Chapter 3. Solid tumours, such as breast, lung or colorectal cancers have an abnormal expression of particular HER2-family proteins. Designing a predictive protein:interaction network and testing each of the predicted targets by downregulating each of the targets with siRNA and quantifying HER family protein activity using the biosensor, may enable us to identify new regulators of this

important pathway. Such regulators could be targets for novel drugs to treat these diseases.

8. References

1. Systems Biology: a vision for engineering and medicine. The Academy of Medical Sciences and The Royal Academy of Engineering.
2. **Abiatari, I., S. Gillen, T. DeOliveira, T. Klose, K. Bo, N. A. Giese, H. Friess, and J. Kleeff.** 2009. The microtubule-associated protein MAPRE2 is involved in perineural invasion of pancreatic cancer cells. Int J Oncol **35:**1111-1116.
3. **Acuto, O., and F. Michel.** 2003. CD28-mediated co-stimulation: a quantitative support for TCR signalling. Nat Rev Immunol **3:**939-951.
4. **Adams, J. M., H. Houston, J. Allen, T. Lints, and R. Harvey.** 1992. The hematopoietically expressed vav proto-oncogene shares homology with the dbl GDP-GTP exchange factor, the bcr gene and a yeast gene (CDC24) involved in cytoskeletal organization. Oncogene **7:**611-618.
5. **Adelaide, J., P. Finetti, I. Bekhouche, L. Repellini, J. Geneix, F. Sircoulomb, E. Charafe-Jauffret, N. Cervera, J. Desplans, D. Parzy, E. Schoenmakers, P. Viens, J. Jacquemier, D. Birnbaum, F. Bertucci, and M. Chaffanet.** 2007. Integrated profiling of basal and luminal breast cancers. Cancer research **67:**11565-11575.
6. **Aebersold, R., and M. Mann.** 2003. Mass spectrometry-based proteomics. Nature **422:**198-207.
7. **Akhtar, A., and S. M. Gasser.** 2007. The nuclear envelope and transcriptional control. Nat Rev Genet **8:**507-517.
8. **Al-Mehdi, A. B., V. M. Pastukh, B. M. Swiger, D. J. Reed, M. R. Patel, G. C. Bardwell, V. V. Pastukh, M. F. Alexeyev, and M. N. Gillespie.** 2012. Perinuclear mitochondrial clustering creates an oxidant-rich nuclear domain required for hypoxia-induced transcription. Sci Signal **5:**ra47.
9. **Alber, F., S. Dokudovskaya, L. M. Veenhoff, W. Zhang, J. Kipper, D. Devos, A. Suprapto, O. Karni-Schmidt, R. Williams, B. T. Chait, M. P. Rout, and A. Sali.** 2007. Determining the architectures of macromolecular assemblies. Nature **450:**683-694.
10. **Aleixo, L. F., M. M. Goodenow, and J. W. Sleasman.** 1995. Molecular analysis of highly enriched populations of T-cell-depleted monocytes. Clin Diagn Lab Immunol **2:**733-739.
11. **Alfano, C., D. Sanfelice, J. Babon, G. Kelly, A. Jacks, S. Curry, and M. R. Conte.** 2004. Structural analysis of cooperative RNA binding by the La motif and central RRM domain of human La protein. Nat Struct Mol Biol **11:**323-329.
12. **Allen, C., A. K. Ashley, R. Hromas, and J. A. Nickoloff.** 2011. More forks on the road to replication stress recovery. J Mol Cell Biol **3:**4-12.
13. **Allen, M. P., M. Xu, D. A. Linseman, J. E. Pawlowski, G. M. Bokoch, K. A. Heidenreich, and M. E. Wierman.** 2002. Adhesion-related kinase repression of gonadotropin-releasing hormone gene expression requires Rac activation of the extracellular signal-regulated kinase pathway. J Biol Chem **277:**38133-38140.
14. **Alter, G., J. M. Malenfant, and M. Altfeld.** 2004. CD107a as a functional marker for the identification of natural killer cell activity. J Immunol Methods **294:**15-22.
15. **Amberger, J., C. A. Bocchini, A. F. Scott, and A. Hamosh.** 2009. McKusick's Online Mendelian Inheritance in Man (OMIM). Nucleic Acids Res **37:**D793-796.
16. **Andersen, J. S., Y. W. Lam, A. K. Leung, S. E. Ong, C. E. Lyon, A. I. Lamond, and M. Mann.** 2005. Nucleolar proteome dynamics. Nature **433:**77-83.

17. **Andjelkovic, M., D. R. Alessi, R. Meier, A. Fernandez, N. J. Lamb, M. Frech, P. Cron, P. Cohen, J. M. Lucocq, and B. A. Hemmings.** 1997. Role of translocation in the activation and function of protein kinase B. J Biol Chem **272:**31515-31524.
18. **Angel, T. E., U. K. Aryal, S. M. Hengel, E. S. Baker, R. T. Kelly, E. W. Robinson, and R. D. Smith.** 2012. Mass spectrometry-based proteomics: existing capabilities and future directions. Chem Soc Rev **41:**3912-3928.
19. **Antharavally, B. S., K. A. Mallia, M. M. Rosenblatt, A. M. Salunkhe, J. C. Rogers, P. Haney, and N. Haghdoost.** 2011. Efficient removal of detergents from proteins and peptides in a spin column format. Anal Biochem **416:**39-44.
20. **Ardouin, L., M. Bracke, A. Mathiot, S. N. Pagakis, T. Norton, N. Hogg, and V. L. Tybulewicz.** 2003. Vav1 transduces TCR signals required for LFA-1 function and cell polarization at the immunological synapse. Eur J Immunol **33:**790-797.
21. **Arnaudo, A. M., R. C. Molden, and B. A. Garcia.** 2011. Revealing histone variant induced changes via quantitative proteomics. Crit Rev Biochem Mol Biol **46:**284-294.
22. **Awasthi, A., A. Samarakoon, X. Dai, R. Wen, D. Wang, and S. Malarkannan.** 2008. Deletion of PI3K-p85alpha gene impairs lineage commitment, terminal maturation, cytokine generation and cytotoxicity of NK cells. Genes Immun **9:**522-535.
23. **Baghdoyan, S., P. Dubreuil, F. Eberle, and S. Gomez.** 2000. Capture of cytokine-responsive genes (NACA and RBM3) using a gene trap approach. Blood **95:**3750-3757.
24. **Bagheri-Yarmand, R., M. Mandal, A. H. Taludker, R. A. Wang, R. K. Vadlamudi, H. J. Kung, and R. Kumar.** 2001. Etk/Bmx tyrosine kinase activates Pak1 and regulates tumorigenicity of breast cancer cells. J Biol Chem **276:**29403-29409.
25. **Baird, D., Q. Feng, and R. A. Cerione.** 2005. The Cool-2/alpha-Pix protein mediates a Cdc42-Rac signaling cascade. Curr Biol **15:**1-10.
26. **Banerjee, P. P., R. Pandey, R. Zheng, M. M. Suhoski, L. Monaco-Shawver, and J. S. Orange.** 2007. Cdc42-interacting protein-4 functionally links actin and microtubule networks at the cytolytic NK cell immunological synapse. The Journal of experimental medicine **204:**2305-2320.
27. **Bantscheff, M., S. Lemeer, M. M. Savitski, and B. Kuster.** 2012. Quantitative mass spectrometry in proteomics: critical review update from 2007 to the present. Anal Bioanal Chem **404:**939-965.
28. **Bantscheff, M., M. Schirle, G. Sweetman, J. Rick, and B. Kuster.** 2007. Quantitative mass spectrometry in proteomics: a critical review. Anal Bioanal Chem **389:**1017-1031.
29. **Barabasi, A. L., and Z. N. Oltvai.** 2004. Network biology: understanding the cell's functional organization. Nat Rev Genet **5:**101-113.
30. **Barbe, L., E. Lundberg, P. Oksvold, A. Stenius, E. Lewin, E. Bjorling, A. Asplund, F. Ponten, H. Brismar, M. Uhlen, and H. Andersson-Svahn.** 2008. Toward a confocal subcellular atlas of the human proteome. Mol Cell Proteomics **7:**499-508.
31. **Barber P. R., Ameer-Beg S. M., Gilbey J., Carlin L. M., Keppler M., Ng T. C., and V. B.** 2008. Multiphoton time-domain fluorescence lifetime imaging microscopy: practical application to protein–protein interactions using global analysis. J R Soc Interface **6:**S93–S105.

32. **Barber, P. R., S. M. Ameer-Beg, J. D. Gilbey, R. J. Edens, I. Ezike, and B. Vojnovic.** 2005. Global and pixel kinetic data analysis for FRET detection by multi-photon time-domain FLIM. Proc. SPIE **5700:**171-181.
33. **Barfod, E. T., Y. Zheng, W. J. Kuang, M. J. Hart, T. Evans, R. A. Cerione, and A. Ashkenazi.** 1993. Cloning and expression of a human CDC42 GTPase-activating protein reveals a functional SH3-binding domain. J Biol Chem **268:**26059-26062.
34. **Barnett, S. F., D. Defeo-Jones, S. Fu, P. J. Hancock, K. M. Haskell, R. E. Jones, J. A. Kahana, A. M. Kral, K. Leander, L. L. Lee, J. Malinowski, E. M. McAvoy, D. D. Nahas, R. G. Robinson, and H. E. Huber.** 2005. Identification and characterization of pleckstrin-homology-domain-dependent and isoenzyme-specific Akt inhibitors. The Biochemical journal **385:**399-408.
35. **Barrios-Rodiles, M., K. R. Brown, B. Ozdamar, R. Bose, Z. Liu, R. S. Donovan, F. Shinjo, Y. Liu, J. Dembowy, I. W. Taylor, V. Luga, N. Przulj, M. Robinson, H. Suzuki, Y. Hayashizaki, I. Jurisica, and J. L. Wrana.** 2005. High-throughput mapping of a dynamic signaling network in mammalian cells. Science **307:**1621-1625.
36. **Beausoleil, S. A., M. Jedrychowski, D. Schwartz, J. E. Elias, J. Villen, J. Li, M. A. Cohn, L. C. Cantley, and S. P. Gygi.** 2004. Large-scale characterization of HeLa cell nuclear phosphoproteins. Proceedings of the National Academy of Sciences of the United States of America **101:**12130-12135.
37. **Benson, V., V. Grobarova, J. Richter, and A. Fiserova.** 2010. Glycosylation regulates NK cell-mediated effector function through PI3K pathway. Int Immunol **22:**167-177.
38. **Bereman, M. S., J. D. Egertson, and M. J. Maccoss.** 2011. Comparison between procedures using SDS for shotgun proteomic analyses of complex samples. Proteomics.
39. **Bermudez, V. P., A. Farina, I. Tappin, and J. Hurwitz.** 2010. Influence of the human cohesion establishment factor Ctf4/AND-1 on DNA replication. J Biol Chem **285:**9493-9505.
40. **Berry, L. D., and K. L. Gould.** 1997. Fission yeast dim1(+) encodes a functionally conserved polypeptide essential for mitosis. The Journal of cell biology **137:**1337-1354.
41. **Biron, C. A.** 1997. Activation and function of natural killer cell responses during viral infections. Curr Opin Immunol **9:**24-34.
42. **Biswas, A. K., and D. G. Johnson.** 2012. Transcriptional and nontranscriptional functions of E2F1 in response to DNA damage. Cancer research **72:**13-17.
43. **Black, W. J., D. Stagos, S. A. Marchitti, D. W. Nebert, K. F. Tipton, A. Bairoch, and V. Vasiliou.** 2009. Human aldehyde dehydrogenase genes: alternatively spliced transcriptional variants and their suggested nomenclature. Pharmacogenet Genomics **19:**893-902.
44. **Blink, E. J., J. A. Trapani, and D. A. Jans.** 1999. Perforin-dependent nuclear targeting of granzymes: A central role in the nuclear events of granule-exocytosis-mediated apoptosis? Immunol Cell Biol **77:**206-215.
45. **Blow, J. J.** 1993. Preventing re-replication of DNA in a single cell cycle: evidence for a replication licensing factor. The Journal of cell biology **122:**993-1002.
46. **Blow, J. J., and P. J. Gillespie.** 2008. Replication licensing and cancer--a fatal entanglement? Nature reviews. Cancer **8:**799-806.

47. **Boehmer, T., J. Enninga, S. Dales, G. Blobel, and H. Zhong.** 2003. Depletion of a single nucleoporin, Nup107, prevents the assembly of a subset of nucleoporins into the nuclear pore complex. Proc Natl Acad Sci U S A **100:**981-985.
48. **Boisvert, F. M., S. van Koningsbruggen, J. Navascues, and A. I. Lamond.** 2007. The multifunctional nucleolus. Nature reviews. Molecular cell biology **8:**574-585.
49. **Boos, D., J. Frigola, and J. F. Diffley.** 2012. Activation of the replicative DNA helicase: breaking up is hard to do. Curr Opin Cell Biol **24:**423-430.
50. **Boulon, S., B. Pradet-Balade, C. Verheggen, D. Molle, S. Boireau, M. Georgieva, K. Azzag, M. C. Robert, Y. Ahmad, H. Neel, A. I. Lamond, and E. Bertrand.** 2010. HSP90 and its R2TP/Prefoldin-like cochaperone are involved in the cytoplasmic assembly of RNA polymerase II. Molecular cell **39:**912-924.
51. **Brady, N., T. J. Gaymes, M. Cheung, G. J. Mufti, and F. V. Rassool.** 2003. Increased error-prone NHEJ activity in myeloid leukemias is associated with DNA damage at sites that recruit key nonhomologous end-joining proteins. Cancer research **63:**1798-1805.
52. **Braisted, J. C., S. Kuntumalla, C. Vogel, E. M. Marcotte, A. R. Rodrigues, R. Wang, S. T. Huang, E. S. Ferlanti, A. I. Saeed, R. D. Fleischmann, S. N. Peterson, and R. Pieper.** 2008. The APEX Quantitative Proteomics Tool: generating protein quantitation estimates from LC-MS/MS proteomics results. BMC Bioinformatics **9:**529.
53. **Brosch, M., L. Yu, T. Hubbard, and J. Choudhary.** 2009. Accurate and sensitive peptide identification with Mascot Percolator. Journal of proteome research **8:**3176-3181.
54. **Bryceson, Y. T., S. C. Chiang, S. Darmanin, C. Fauriat, H. Schlums, J. Theorell, and S. M. Wood.** 2011. Molecular mechanisms of natural killer cell activation. Journal of innate immunity **3:**216-226.
55. **Brynildsen, M. P., and J. J. Collins.** 2009. Systems biology makes it personal. Mol Cell **34:**137-138.
56. **Buchsbaum, S., C. Morris, V. Bochard, and P. Jalinot.** 2007. Human INT6 interacts with MCM7 and regulates its stability during S phase of the cell cycle. Oncogene **26:**5132-5144.
57. **Burkhart, D. L., and J. Sage.** 2008. Cellular mechanisms of tumour suppression by the retinoblastoma gene. Nature reviews. Cancer **8:**671-682.
58. **Burrows, C., N. Abd Latip, S. J. Lam, L. Carpenter, K. Sawicka, G. Tzolovsky, H. Gabra, M. Bushell, D. M. Glover, A. E. Willis, and S. P. Blagden.** 2010. The RNA binding protein Larp1 regulates cell division, apoptosis and cell migration. Nucleic acids research **38:**5542-5553.
59. **Butland, G., J. M. Peregrin-Alvarez, J. Li, W. Yang, X. Yang, V. Canadien, A. Starostine, D. Richards, B. Beattie, N. Krogan, M. Davey, J. Parkinson, J. Greenblatt, and A. Emili.** 2005. Interaction network containing conserved and essential protein complexes in Escherichia coli. Nature **433:**531-537.
60. **Caligiuri, M. A.** 2008. Human natural killer cells. Blood **112:**461-469.
61. **Calleja, V., M. Laguerre, P. J. Parker, and B. Larijani.** 2009. Role of a novel PH-kinase domain interface in PKB/Akt regulation: structural mechanism for allosteric inhibition. PLoS biology **7:**e17.
62. **Canas, B., C. Pineiro, E. Calvo, D. Lopez-Ferrer, and J. M. Gallardo.** 2007. Trends in sample preparation for classical and second generation proteomics. J Chromatogr A **1153:**235-258.

63. **Capelson, M., and M. W. Hetzer.** 2009. The role of nuclear pores in gene regulation, development and disease. EMBO reports **10:**697-705.
64. **Capelson, M., Y. Liang, R. Schulte, W. Mair, U. Wagner, and M. W. Hetzer.** 2010. Chromatin-bound nuclear pore components regulate gene expression in higher eukaryotes. Cell **140:**372-383.
65. **Carmo-Fonseca, M.** 2002. The contribution of nuclear compartmentalization to gene regulation. Cell **108:**513-521.
66. **Carpen, O., I. Virtanen, V. P. Lehto, and E. Saksela.** 1983. Polarization of NK cell cytoskeleton upon conjugation with sensitive target cells. J Immunol **131:**2695-2698.
67. **Carpenter, B., K. J. Hill, M. Charalambous, K. J. Wagner, D. Lahiri, D. I. James, J. S. Andersen, V. Schumacher, B. Royer-Pokora, M. Mann, A. Ward, and S. G. Roberts.** 2004. BASP1 is a transcriptional cosuppressor for the Wilms' tumor suppressor protein WT1. Molecular and cellular biology **24:**537-549.
68. **Carron, C., M. F. O'Donohue, V. Choesmel, M. Faubladier, and P. E. Gleizes.** 2011. Analysis of two human pre-ribosomal factors, bystin and hTsr1, highlights differences in evolution of ribosome biogenesis between yeast and mammals. Nucleic acids research **39:**280-291.
69. **Castilla, L. H., F. J. Couch, M. R. Erdos, K. F. Hoskins, K. Calzone, J. E. Garber, J. Boyd, M. B. Lubin, M. L. Deshano, L. C. Brody, and et al.** 1994. Mutations in the BRCA1 gene in families with early-onset breast and ovarian cancer. Nat Genet **8:**387-391.
70. **Caunt, C. J., and C. A. McArdle.** 2012. ERK phosphorylation and nuclear accumulation: insights from single-cell imaging. Biochem Soc Trans **40:**224-229.
71. **Chakraborty, P., Y. Wang, J. H. Wei, J. van Deursen, H. Yu, L. Malureanu, M. Dasso, D. J. Forbes, D. E. Levy, J. Seemann, and B. M. Fontoura.** 2008. Nucleoporin levels regulate cell cycle progression and phase-specific gene expression. Developmental cell **15:**657-667.
72. **Chan, V., U. S. Khoo, M. S. Wong, K. Lau, D. Suen, G. Li, A. Kwong, and T. K. Chan.** 2008. Localization of hRad9 in breast cancer. BMC cancer **8:**196.
73. **Cheent, K., and S. I. Khakoo.** 2009. Natural killer cells: integrating diversity with function. Immunology **126:**449-457.
74. **Chen, C., A. Wirth, and E. Ponimaskin.** 2011. Cdc42: An important regulator of neuronal morphology. Int J Biochem Cell Biol.
75. **Chen, D., Z. Zhang, M. Li, W. Wang, Y. Li, E. R. Rayburn, D. L. Hill, H. Wang, and R. Zhang.** 2007. Ribosomal protein S7 as a novel modulator of p53-MDM2 interaction: binding to MDM2, stabilization of p53 protein, and activation of p53 function. Oncogene **26:**5029-5037.
76. **Chen, H. Z., S. Y. Tsai, and G. Leone.** 2009. Emerging roles of E2Fs in cancer: an exit from cell cycle control. Nature reviews. Cancer **9:**785-797.
77. **Chen, J. J., D. Silver, S. Cantor, D. M. Livingston, and R. Scully.** 1999. BRCA1, BRCA2, and Rad51 operate in a common DNA damage response pathway. Cancer research **59:**1752s-1756s.
78. **Chin, S. F., A. E. Teschendorff, J. C. Marioni, Y. Wang, N. L. Barbosa-Morais, N. P. Thorne, J. L. Costa, S. E. Pinder, M. A. van de Wiel, A. R. Green, I. O. Ellis, P. L. Porter, S. Tavare, J. D. Brenton, B. Ylstra, and C. Caldas.** 2007. High-resolution aCGH and expression profiling identifies a novel genomic subtype of ER negative breast cancer. Genome Biol **8:**R215.

79. **Chong, J. P., and J. J. Blow.** 1996. DNA replication licensing factor. Prog Cell Cycle Res **2:**83-90.
80. **Chou, Q., M. Russell, D. E. Birch, J. Raymond, and W. Bloch.** 1992. Prevention of pre-PCR mis-priming and primer dimerization improves low-copy-number amplifications. Nucleic Acids Res **20:**1717-1723.
81. **Chow, K. H., R. E. Factor, and K. S. Ullman.** 2012. The nuclear envelope environment and its cancer connections. Nature reviews. Cancer **12:**196-209.
82. **Chow, K. N., and D. C. Dean.** 1996. Domains A and B in the Rb pocket interact to form a transcriptional repressor motif. Mol Cell Biol **16:**4862-4868.
83. **Cloutier, P., and B. Coulombe.** 2010. New insights into the biogenesis of nuclear RNA polymerases? Biochem Cell Biol **88:**211-221.
84. **Cobrinik, D., S. F. Dowdy, P. W. Hinds, S. Mittnacht, and R. A. Weinberg.** 1992. The retinoblastoma protein and the regulation of cell cycling. Trends Biochem Sci **17:**312-315.
85. **Cohen, N., M. Sharma, A. Kentsis, J. M. Perez, S. Strudwick, and K. L. Borden.** 2001. PML RING suppresses oncogenic transformation by reducing the affinity of eIF4E for mRNA. The EMBO journal **20:**4547-4559.
86. **Coles, L. S., P. Diamond, F. Occhiodoro, M. A. Vadas, and M. F. Shannon.** 1996. Cold shock domain proteins repress transcription from the GM-CSF promoter. Nucleic acids research **24:**2311-2317.
87. **Coles, S. J., E. C. Wang, S. Man, R. K. Hills, A. K. Burnett, A. Tonks, and R. L. Darley.** 2011. CD200 expression suppresses natural killer cell function and directly inhibits patient anti-tumor response in acute myeloid leukemia. Leukemia **25:**792-799.
88. **Cook, J. G., D. A. Chasse, and J. R. Nevins.** 2004. The regulated association of Cdt1 with minichromosome maintenance proteins and Cdc6 in mammalian cells. J Biol Chem **279:**9625-9633.
89. **Cooper, M. A., T. A. Fehniger, and M. A. Caligiuri.** 2001. The biology of human natural killer-cell subsets. Trends Immunol **22:**633-640.
90. **Corden, J.** 2011. Going nuclear: transcribers in transit. Molecular cell **42:**143-145.
91. **Crone, J., C. Glas, K. Schultheiss, J. Moehlenbrink, E. Krieghoff-Henning, and T. G. Hofmann.** 2011. Zyxin is a critical regulator of the apoptotic HIPK2-p53 signaling axis. Cancer research **71:**2350-2359.
92. **Cronshaw, J. M., A. N. Krutchinsky, W. Zhang, B. T. Chait, and M. J. Matunis.** 2002. Proteomic analysis of the mammalian nuclear pore complex. The Journal of cell biology **158:**915-927.
93. **Cross, M. K., and M. A. Powers.** 2011. Nup98 regulates bipolar spindle assembly through association with microtubules and opposition of MCAK. Mol Biol Cell **22:**661-672.
94. **Culley, F. J., M. Johnson, J. H. Evans, S. Kumar, R. Crilly, J. Casasbuenas, T. Schnyder, M. Mehrabi, M. P. Deonarain, D. S. Ushakov, V. Braud, G. Roth, R. Brock, K. Kohler, and D. M. Davis.** 2009. Natural killer cell signal integration balances synapse symmetry and migration. PLoS Biol **7:**e1000159.
95. **Das, M., T. Drake, D. J. Wiley, P. Buchwald, D. Vavylonis, and F. Verde.** 2012. Oscillatory Dynamics of Cdc42 GTPase in the Control of Polarized Growth. Science **337** 239-243
96. **Datta, K., T. F. Franke, T. O. Chan, A. Makris, S. I. Yang, D. R. Kaplan, D. K. Morrison, E. A. Golemis, and P. N. Tsichlis.** 1995. AH/PH domain-mediated

interaction between Akt molecules and its potential role in Akt regulation. Mol Cell Biol **15:**2304-2310.
97. **Davis, D. M.** 2002. Assembly of the immunological synapse for T cells and NK cells. Trends Immunol **23:**356-363.
98. **Davis, D. M., I. Chiu, M. Fassett, G. B. Cohen, O. Mandelboim, and J. L. Strominger.** 1999. The human natural killer cell immune synapse. Proc Natl Acad Sci U S A **96:**15062-15067.
99. **De Angelis Campos, A. C., M. A. Rodrigues, C. de Andrade, A. M. de Goes, M. H. Nathanson, and D. A. Gomes.** 2011. Epidermal growth factor receptors destined for the nucleus are internalized via a clathrin-dependent pathway. Biochemical and biophysical research communications **412:**341-346.
100. **De Vos, M., V. Schreiber, and F. Dantzer.** 2012. The diverse roles and clinical relevance of PARPs in DNA damage repair: current state of the art. Biochem Pharmacol **84:**137-146.
101. **Debler, E. W., Y. Ma, H. S. Seo, K. C. Hsia, T. R. Noriega, G. Blobel, and A. Hoelz.** 2008. A fence-like coat for the nuclear pore membrane. Mol Cell **32:**815-826.
102. **Deeds, E. J., O. Ashenberg, and E. I. Shakhnovich.** 2006. A simple physical model for scaling in protein-protein interaction networks. Proc Natl Acad Sci U S A **103:**311-316.
103. **DeFeo-Jones, D., S. F. Barnett, S. Fu, P. J. Hancock, K. M. Haskell, K. R. Leander, E. McAvoy, R. G. Robinson, M. E. Duggan, C. W. Lindsley, Z. Zhao, H. E. Huber, and R. E. Jones.** 2005. Tumor cell sensitization to apoptotic stimuli by selective inhibition of specific Akt/PKB family members. Molecular cancer therapeutics **4:**271-279.
104. **del Pozo, M. A., M. A. Schwartz, J. Hu, W. B. Kiosses, A. Altman, and M. Villalba.** 2003. Guanine exchange-dependent and -independent effects of Vav1 on integrin-induced T cell spreading. J Immunol **170:**41-47.
105. **Denk, W., J. H. Strickler, and W. W. Webb.** 1990. Two-photon laser scanning fluorescence microscopy. Science **248:**73-76.
106. **Denk, W., and K. Svoboda.** 1997. Photon upmanship: why multiphoton imaging is more than a gimmick. Neuron **18:**351-357.
107. **DePamphilis, M. L., J. J. Blow, S. Ghosh, T. Saha, K. Noguchi, and A. Vassilev.** 2006. Regulating the licensing of DNA replication origins in metazoa. Current opinion in cell biology **18:**231-239.
108. **Dickinson, M. E.** 2006. Multiphoton and Multispectral Laser-scanning Microscopy, p. 377. *In* D. L. S. R. D. Goldmann (ed.), Basic Methods in Microscopy. Cold Spring Harbor Laboratory Press, New York.
109. **Dostie, J., F. Lejbkowicz, and N. Sonenberg.** 2000. Nuclear eukaryotic initiation factor 4E (eIF4E) colocalizes with splicing factors in speckles. The Journal of cell biology **148:**239-247.
110. **Douglas, P., J. Zhong, R. Ye, G. B. Moorhead, X. Xu, and S. P. Lees-Miller.** 2010. Protein phosphatase 6 interacts with the DNA-dependent protein kinase catalytic subunit and dephosphorylates gamma-H2AX. Molecular and cellular biology **30:**1368-1381.
111. **Dransfield, I., C. Cabanas, J. Barrett, and N. Hogg.** 1992. Interaction of leukocyte integrins with ligand is necessary but not sufficient for function. J Cell Biol **116:**1527-1535.

112. **Droste, P., S. Miebach, S. Niedenfuhr, W. Wiechert, and K. Noh.** 2011. Visualizing multi-omics data in metabolic networks with the software Omix: a case study. Biosystems **105:**154-161.
113. **Dudderidge, T. J., J. D. Kelly, A. Wollenschlaeger, O. Okoturo, T. Prevost, W. Robson, H. Y. Leung, G. H. Williams, and K. Stoeber.** 2010. Diagnosis of prostate cancer by detection of minichromosome maintenance 5 protein in urine sediments. Br J Cancer **103:**701-707.
114. **Edwards, C. M., B. S. Glisson, C. K. King, S. Smallwood-Kentro, and W. E. Ross.** 1987. Etoposide-induced DNA cleavage in human leukemia cells. Cancer chemotherapy and pharmacology **20:**162-168.
115. **Edwards, M. C., A. V. Tutter, C. Cvetic, C. H. Gilbert, T. A. Prokhorova, and J. C. Walter.** 2002. MCM2-7 complexes bind chromatin in a distributed pattern surrounding the origin recognition complex in Xenopus egg extracts. J Biol Chem **277:**33049-33057.
116. **Elad, N., T. Maimon, D. Frenkiel-Krispin, R. Y. Lim, and O. Medalia.** 2009. Structural analysis of the nuclear pore complex by integrated approaches. Curr Opin Struct Biol **19:**226-232.
117. **Ellenbroek, S. I., and J. G. Collard.** 2007. Rho GTPases: functions and association with cancer. Clin Exp Metastasis **24:**657-672.
118. **Engelmann, D., and B. M. Putzer.** 2012. The dark side of E2F1: in transit beyond apoptosis. Cancer research **72:**571-575.
119. **Enninga, J., A. Levay, and B. M. Fontoura.** 2003. Sec13 shuttles between the nucleus and the cytoplasm and stably interacts with Nup96 at the nuclear pore complex. Mol Cell Biol **23:**7271-7284.
120. **Erickson, J. W., C. Zhang, R. A. Kahn, T. Evans, and R. A. Cerione.** 1996. Mammalian Cdc42 is a brefeldin A-sensitive component of the Golgi apparatus. J Biol Chem **271:**26850-26854.
121. **Errico, A., C. Cosentino, T. Rivera, A. Losada, E. Schwob, T. Hunt, and V. Costanzo.** 2009. Tipin/Tim1/And1 protein complex promotes Pol alpha chromatin binding and sister chromatid cohesion. Embo J **28:**3681-3692.
122. **Etienne-Manneville, S.** 2004. Cdc42--the centre of polarity. J Cell Sci **117:**1291-1300.
123. **Evans, C., J. Noirel, S. Y. Ow, M. Salim, A. G. Pereira-Medrano, N. Couto, J. Pandhal, D. Smith, T. K. Pham, E. Karunakaran, X. Zou, C. A. Biggs, and P. C. Wright.** 2012. An insight into iTRAQ: where do we stand now? Anal Bioanal Chem **404:**1011-1027.
124. **Festy, F., S. M. Ameer-Beg, T. Ng, and K. Suhling.** 2007. Imaging proteins in vivo using fluorescence lifetime microscopy. Mol Biosyst **3:**381-391.
125. **Fey, E. G., G. Krochmalnic, and S. Penman.** 1986. The nonchromatin substructures of the nucleus: the ribonucleoprotein (RNP)-containing and RNP-depleted matrices analyzed by sequential fractionation and resinless section electron microscopy. J Cell Biol **102:**1654-1665.
126. **Fields, S., and O. Song.** 1989. A novel genetic system to detect protein-protein interactions. Nature **340:**245-246.
127. **Finetti, F., S. R. Paccani, M. G. Riparbelli, E. Giacomello, G. Perinetti, G. J. Pazour, J. L. Rosenbaum, and C. T. Baldari.** 2009. Intraflagellar transport is required for polarized recycling of the TCR/CD3 complex to the immune synapse. Nat Cell Biol **11:**1332-1339.

128. **Fitch, W. M.** 1970. Distinguishing homologous from analogous proteins. Systematic zoology **19:**99-113.
129. **Follit, J. A., R. A. Tuft, K. E. Fogarty, and G. J. Pazour.** 2006. The intraflagellar transport protein IFT20 is associated with the Golgi complex and is required for cilia assembly. Mol Biol Cell **17:**3781-3792.
130. **Friedl, P., K. Wolf, and J. Lammerding.** 2011. Nuclear mechanics during cell migration. Current opinion in cell biology **23:**55-64.
131. **Fukuda, T., T. Sumiyoshi, M. Takahashi, T. Kataoka, T. Asahara, H. Inui, M. Watatani, M. Yasutomi, N. Kamada, and K. Miyagawa.** 2001. Alterations of the double-strand break repair gene MRE11 in cancer. Cancer research **61:**23-26.
132. **Funk, J., X. Li, and T. Franz.** 2005. Threshold values for detergents in protein and peptide samples for mass spectrometry. Rapid communications in mass spectrometry : RCM **19:**2986-2988.
133. **Gambus, A., F. van Deursen, D. Polychronopoulos, M. Foltman, R. C. Jones, R. D. Edmondson, A. Calzada, and K. Labib.** 2009. A key role for Ctf4 in coupling the MCM2-7 helicase to DNA polymerase alpha within the eukaryotic replisome. Embo J **28:**2992-3004.
134. **Garcia de Frutos, P., P. Fuentes-Prior, B. Hurtado, and N. Sala.** 2007. Molecular basis of protein S deficiency. Thromb Haemost **98:**543-556.
135. **Gatti, A., Z. Huang, P. T. Tuazon, and J. A. Traugh.** 1999. Multisite autophosphorylation of p21-activated protein kinase gamma-PAK as a function of activation. J Biol Chem **274:**8022-8028.
136. **Gavin, A. C., P. Aloy, P. Grandi, R. Krause, M. Boesche, M. Marzioch, C. Rau, L. J. Jensen, S. Bastuck, B. Dumpelfeld, A. Edelmann, M. A. Heurtier, V. Hoffman, C. Hoefert, K. Klein, M. Hudak, A. M. Michon, M. Schelder, M. Schirle, M. Remor, T. Rudi, S. Hooper, A. Bauer, T. Bouwmeester, G. Casari, G. Drewes, G. Neubauer, J. M. Rick, B. Kuster, P. Bork, R. B. Russell, and G. Superti-Furga.** 2006. Proteome survey reveals modularity of the yeast cell machinery. Nature **440:**631-636.
137. **Gaymes, T. J., G. J. Mufti, and F. V. Rassool.** 2002. Myeloid leukemias have increased activity of the nonhomologous end-joining pathway and concomitant DNA misrepair that is dependent on the Ku70/86 heterodimer. Cancer research **62:**2791-2797.
138. **Gaymes, T. J., P. S. North, N. Brady, I. D. Hickson, G. J. Mufti, and F. V. Rassool.** 2002. Increased error-prone non homologous DNA end-joining--a proposed mechanism of chromosomal instability in Bloom's syndrome. Oncogene **21:**2525-2533.
139. **Gaymes, T. J., S. Shall, L. J. MacPherson, N. A. Twine, N. C. Lea, F. Farzaneh, and G. J. Mufti.** 2009. Inhibitors of poly ADP-ribose polymerase (PARP) induce apoptosis of myeloid leukemic cells: potential for therapy of myeloid leukemia and myelodysplastic syndromes. Haematologica **94:**638-646.
140. **Gehlenborg, N., S. I. O'Donoghue, N. S. Baliga, A. Goesmann, M. A. Hibbs, H. Kitano, O. Kohlbacher, H. Neuweger, R. Schneider, D. Tenenbaum, and A. C. Gavin.** 2010. Visualization of omics data for systems biology. Nat Methods **7:**S56-68.
141. **Giepmans, B. N., S. R. Adams, M. H. Ellisman, and R. Y. Tsien.** 2006. The fluorescent toolbox for assessing protein location and function. Science **312:**217-224.

142. **Giot, L., J. S. Bader, C. Brouwer, A. Chaudhuri, B. Kuang, Y. Li, Y. L. Hao, C. E. Ooi, B. Godwin, E. Vitols, G. Vijayadamodar, P. Pochart, H. Machineni, M. Welsh, Y. Kong, B. Zerhusen, R. Malcolm, Z. Varrone, A. Collis, M. Minto, S. Burgess, L. McDaniel, E. Stimpson, F. Spriggs, J. Williams, K. Neurath, N. Ioime, M. Agee, E. Voss, K. Furtak, R. Renzulli, N. Aanensen, S. Carrolla, E. Bickelhaupt, Y. Lazovatsky, A. DaSilva, J. Zhong, C. A. Stanyon, R. L. Finley, Jr., K. P. White, M. Braverman, T. Jarvie, S. Gold, M. Leach, J. Knight, R. A. Shimkets, M. P. McKenna, J. Chant, and J. M. Rothberg.** 2003. A protein interaction map of Drosophila melanogaster. Science **302:**1727-1736.
143. **Gismondi, A., L. Cifaldi, C. Mazza, S. Giliani, S. Parolini, S. Morrone, J. Jacobelli, E. Bandiera, L. Notarangelo, and A. Santoni.** 2004. Impaired natural and CD16-mediated NK cell cytotoxicity in patients with WAS and XLT: ability of IL-2 to correct NK cell functional defect. Blood **104:**436-443.
144. **Going, J. J., W. N. Keith, L. Neilson, K. Stoeber, R. C. Stuart, and G. H. Williams.** 2002. Aberrant expression of minichromosome maintenance proteins 2 and 5, and Ki-67 in dysplastic squamous oesophageal epithelium and Barrett's mucosa. Gut **50:**373-377.
145. **Grakoui, A., S. K. Bromley, C. Sumen, M. M. Davis, A. S. Shaw, P. M. Allen, and M. L. Dustin.** 1999. The immunological synapse: a molecular machine controlling T cell activation. Science **285:**221-227.
146. **Grimme, J. M., M. Honda, R. Wright, Y. Okuno, E. Rothenberg, A. V. Mazin, T. Ha, and M. Spies.** 2010. Human Rad52 binds and wraps single-stranded DNA and mediates annealing via two hRad52-ssDNA complexes. Nucleic acids research **38:**2917-2930.
147. **Gstaiger, M., and R. Aebersold.** 2009. Applying mass spectrometry-based proteomics to genetics, genomics and network biology. Nat Rev Genet **10:**617-627.
148. **Guerrero, I., and C. Alonso.** 1983. Fractionation by micrococcal nuclease digestion of Drosophila embryo chromatin: isolation of a fraction enriched in two major nonhistone proteins. Cell differentiation **12:**307-316.
149. **Gygi, S. P., Y. Rochon, B. R. Franza, and R. Aebersold.** 1999. Correlation between protein and mRNA abundance in yeast. Mol Cell Biol **19:**1720-1730.
150. **Hanahan, D., and R. A. Weinberg.** 2000. The hallmarks of cancer. Cell **100:**57-70.
151. **Hanahan, D., and R. A. Weinberg.** 2011. Hallmarks of cancer: the next generation. Cell **144:**646-674.
152. **Hardwick, M., D. Fertikh, M. Culty, H. Li, B. Vidic, and V. Papadopoulos.** 1999. Peripheral-type benzodiazepine receptor (PBR) in human breast cancer: correlation of breast cancer cell aggressive phenotype with PBR expression, nuclear localization, and PBR-mediated cell proliferation and nuclear transport of cholesterol. Cancer research **59:**831-842.
153. **Hartl, F. U., and M. Hayer-Hartl.** 2002. Molecular chaperones in the cytosol: from nascent chain to folded protein. Science **295:**1852-1858.
154. **Hashizume, C., H. Nakano, K. Yoshida, and R. W. Wong.** 2010. Characterization of the role of the tumor marker Nup88 in mitosis. Molecular cancer **9:**119.
155. **Hauck, C. R., T. Hunter, and D. D. Schlaepfer.** 2001. The v-Src SH3 domain facilitates a cell adhesion-independent association with focal adhesion kinase. J Biol Chem **276:**17653-17662.
156. **Havugimana, P. C., G. T. Hart, T. Nepusz, H. Yang, A. L. Turinsky, Z. Li, P. I. Wang, D. R. Boutz, V. Fong, S. Phanse, M. Babu, S. A. Craig, P. Hu, C. Wan, J. Vlasblom, V. U. Dar, A. Bezginov, G. W. Clark, G. C. Wu, S. J. Wodak, E. R.**

Tillier, A. Paccanaro, E. M. Marcotte, and A. Emili. 2012. A census of human soluble protein complexes. Cell **150:**1068-1081.
157. **Helmchen, F., and W. Denk.** 2005. Deep tissue two-photon microscopy. Nat Methods **2:**932-940.
158. **Helmchen, F., and W. Denk.** 2002. New developments in multiphoton microscopy. Curr Opin Neurobiol **12:**593-601.
159. **Henley, S. A., and F. A. Dick.** 2012. The retinoblastoma family of proteins and their regulatory functions in the mammalian cell division cycle. Cell Div **7:**10.
160. **Hickman, E. S., M. C. Moroni, and K. Helin.** 2002. The role of p53 and pRB in apoptosis and cancer. Current opinion in genetics & development **12:**60-66.
161. **Hoelz, A., and G. Blobel.** 2004. Cell biology: popping out of the nucleus. Nature **432:**815-816.
162. **Hoffman, G. R., N. Nassar, and R. A. Cerione.** 2000. Structure of the Rho family GTP-binding protein Cdc42 in complex with the multifunctional regulator RhoGDI. Cell **100:**345-356.
163. **Hofmann, T. G., S. P. Hehner, W. Droge, and M. L. Schmitz.** 2000. Caspase-dependent cleavage and inactivation of the Vav1 proto-oncogene product during apoptosis prevents IL-2 transcription. Oncogene **19:**1153-1163.
164. **Hsi, E. D., S. H. Jung, R. Lai, J. L. Johnson, J. R. Cook, D. Jones, S. Devos, B. D. Cheson, L. E. Damon, and J. Said.** 2008. Ki67 and PIM1 expression predict outcome in mantle cell lymphoma treated with high dose therapy, stem cell transplantation and rituximab: a Cancer and Leukemia Group B 59909 correlative science study. Leuk Lymphoma **49:**2081-2090.
165. **Hsieh, C. L., C. L. Lin, H. Liu, Y. J. Chang, C. J. Shih, C. Z. Zhong, S. C. Lee, and B. C. Tan.** 2011. WDHD1 modulates the post-transcriptional step of the centromeric silencing pathway. Nucleic Acids Res **39:**4048-4062.
166. **Hsieh, J. K., F. S. Chan, D. J. O'Connor, S. Mittnacht, S. Zhong, and X. Lu.** 1999. RB regulates the stability and the apoptotic function of p53 via MDM2. Mol Cell **3:**181-193.
167. **Hu, P., and J. Schlessinger.** 1994. Direct association of p110 beta phosphatidylinositol 3-kinase with p85 is mediated by an N-terminal fragment of p110 beta. Mol Cell Biol **14:**2577-2583.
168. **Hu, Q., R. J. Noll, H. Li, A. Makarov, M. Hardman, and R. Graham Cooks.** 2005. The Orbitrap: a new mass spectrometer. Journal of mass spectrometry : JMS **40:**430-443.
169. **Huen, M. S., S. M. Sy, and J. Chen.** 2010. BRCA1 and its toolbox for the maintenance of genome integrity. Nature reviews. Molecular cell biology **11:**138-148.
170. **Hussain, N. K., S. Jenna, M. Glogauer, C. C. Quinn, S. Wasiak, M. Guipponi, S. E. Antonarakis, B. K. Kay, T. P. Stossel, N. Lamarche-Vane, and P. S. McPherson.** 2001. Endocytic protein intersectin-l regulates actin assembly via Cdc42 and N-WASP. Nat Cell Biol **3:**927-932.
171. **Hutchins, J. R., Y. Toyoda, B. Hegemann, I. Poser, J. K. Heriche, M. M. Sykora, M. Augsburg, O. Hudecz, B. A. Buschhorn, J. Bulkescher, C. Conrad, D. Comartin, A. Schleiffer, M. Sarov, A. Pozniakovsky, M. M. Slabicki, S. Schloissnig, I. Steinmacher, M. Leuschner, A. Ssykor, S. Lawo, L. Pelletier, H. Stark, K. Nasmyth, J. Ellenberg, R. Durbin, F. Buchholz, K. Mechtler, A. A. Hyman, and J. M. Peters.** 2010. Systematic analysis of human protein complexes identifies chromosome segregation proteins. Science **328:**593-599.

172. **Hwang, J. U., Y. Gu, Y. J. Lee, and Z. Yang.** 2005. Oscillatory ROP GTPase activation leads the oscillatory polarized growth of pollen tubes. Mol Biol Cell **16:**5385-5399.
173. **Hwang, J. U., G. Wu, A. Yan, Y. J. Lee, C. S. Grierson, and Z. Yang.** 2010. Pollen-tube tip growth requires a balance of lateral propagation and global inhibition of Rho-family GTPase activity. J Cell Sci **123:**340-350.
174. **Iborra, F. J., D. A. Jackson, and P. R. Cook.** 2001. Coupled transcription and translation within nuclei of mammalian cells. Science **293:**1139-1142.
175. **Igarashi, R., M. Suzuki, S. Nogami, and Y. Ohya.** 2005. Molecular dissection of ARP1 regions required for nuclear migration and cell wall integrity checkpoint functions in Saccharomyces cerevisiae. Cell Struct Funct **30:**57-67.
176. **Ingram, W., L. Chan, H. Guven, D. Darling, S. Kordasti, N. Hardwick, L. Barber, G. J. Mufti, and F. Farzaneh.** 2009. Human CD80/IL2 lentivirus-transduced acute myeloid leukaemia (AML) cells promote natural killer (NK) cell activation and cytolytic activity: implications for a phase I clinical study. Br J Haematol **145:**749-760.
177. **Ishiguro, T., J. Saitoh, H. Yawata, H. Yamagishi, S. Iwasaki, and Y. Mitoma.** 1995. Homogeneous quantitative assay of hepatitis C virus RNA by polymerase chain reaction in the presence of a fluorescent intercalater. Anal Biochem **229:**207-213.
178. **Itoh, R. E., K. Kurokawa, Y. Ohba, H. Yoshizaki, N. Mochizuki, and M. Matsuda.** 2002. Activation of rac and cdc42 video imaged by fluorescent resonance energy transfer-based single-molecule probes in the membrane of living cells. Mol Cell Biol **22:**6582-6591.
179. **Jackson, D., K. Dhar, J. K. Wahl, M. S. Wold, and G. E. Borgstahl.** 2002. Analysis of the human replication protein A:Rad52 complex: evidence for crosstalk between RPA32, RPA70, Rad52 and DNA. J Mol Biol **321:**133-148.
180. **Jakel, S., and D. Gorlich.** 1998. Importin beta, transportin, RanBP5 and RanBP7 mediate nuclear import of ribosomal proteins in mammalian cells. The EMBO journal **17:**4491-4502.
181. **Jani, T. S., L. Gobejishvili, P. T. Hote, A. S. Barve, S. Joshi-Barve, G. Kharebava, J. Suttles, T. Chen, C. J. McClain, and S. Barve.** 2009. Inhibition of methionine adenosyltransferase II induces FasL expression, Fas-DISC formation and caspase-8-dependent apoptotic death in T leukemic cells. Cell Res **19:**358-369.
182. **Janssen, A., M. van der Burg, K. Szuhai, G. J. Kops, and R. H. Medema.** 2011. Chromosome segregation errors as a cause of DNA damage and structural chromosome aberrations. Science **333:**1895-1898.
183. **Jasin, M.** 2002. Homologous repair of DNA damage and tumorigenesis: the BRCA connection. Oncogene **21:**8981-8993.
184. **Jenna, S., N. K. Hussain, E. I. Danek, I. Triki, S. Wasiak, P. S. McPherson, and N. Lamarche-Vane.** 2002. The activity of the GTPase-activating protein CdGAP is regulated by the endocytic protein intersectin. J Biol Chem **277:**6366-6373.
185. **Jha, S., and A. Dutta.** 2009. RVB1/RVB2: running rings around molecular biology. Molecular cell **34:**521-533.
186. **Jimenez, C., R. A. Portela, M. Mellado, J. M. Rodriguez-Frade, J. Collard, A. Serrano, A. C. Martinez, J. Avila, and A. C. Carrera.** 2000. Role of the PI3K regulatory subunit in the control of actin organization and cell migration. J Cell Biol **151:**249-262.

187. **Jirawatnotai, S., Y. Hu, W. Michowski, J. E. Elias, L. Becks, F. Bienvenu, A. Zagozdzon, T. Goswami, Y. E. Wang, A. B. Clark, T. A. Kunkel, T. van Harn, B. Xia, M. Correll, J. Quackenbush, D. M. Livingston, S. P. Gygi, and P. Sicinski.** 2011. A function for cyclin D1 in DNA repair uncovered by protein interactome analyses in human cancers. Nature **474:**230-234.
188. **Johnson, K. D., and E. H. Bresnick.** 2002. Dissecting long-range transcriptional mechanisms by chromatin immunoprecipitation. Methods **26:**27-36.
189. **Jongstra-Bilen, J., P. A. Janmey, J. H. Hartwig, S. Galea, and J. Jongstra.** 1992. The lymphocyte-specific protein LSP1 binds to F-actin and to the cytoskeleton through its COOH-terminal basic domain. J Cell Biol **118:**1443-1453.
190. **Jung, J. H., and J. A. Traugh.** 2005. Regulation of the interaction of Pak2 with Cdc42 via autophosphorylation of serine 141. J Biol Chem **280:**40025-40031.
191. **Kakihara, Y., and W. A. Houry.** 2012. The R2TP complex: discovery and functions. Biochim Biophys Acta **1823:**101-107.
192. **Karlebach, G., and R. Shamir.** 2010. Minimally perturbing a gene regulatory network to avoid a disease phenotype: the glioma network as a test case. BMC systems biology **4:**15.
193. **Keil, M., B. Bareth, M. W. Woellhaf, V. Peleh, M. Prestele, P. Rehling, and J. M. Herrmann.** 2012. Oxa1-ribosome complexes coordinate the assembly of cytochrome c oxidase in mitochondria. The Journal of biological chemistry.
194. **Kenworthy, A. K.** 2001. Imaging protein-protein interactions using fluorescence resonance energy transfer microscopy. Methods **24:**289-296.
195. **Keshava Prasad, T. S., R. Goel, K. Kandasamy, S. Keerthikumar, S. Kumar, S. Mathivanan, D. Telikicherla, R. Raju, B. Shafreen, A. Venugopal, L. Balakrishnan, A. Marimuthu, S. Banerjee, D. S. Somanathan, A. Sebastian, S. Rani, S. Ray, C. J. Harrys Kishore, S. Kanth, M. Ahmed, M. K. Kashyap, R. Mohmood, Y. L. Ramachandra, V. Krishna, B. A. Rahiman, S. Mohan, P. Ranganathan, S. Ramabadran, R. Chaerkady, and A. Pandey.** 2009. Human Protein Reference Database--2009 update. Nucleic Acids Res **37:**D767-772.
196. **Ketema, M., K. Wilhelmsen, I. Kuikman, H. Janssen, D. Hodzic, and A. Sonnenberg.** 2007. Requirements for the localization of nesprin-3 at the nuclear envelope and its interaction with plectin. J Cell Sci **120:**3384-3394.
197. **Khanna, N., V. G. Reddy, N. Tuteja, and N. Singh.** 2000. Differential gene expression in apoptosis: identification of ribosomal protein S29 as an apoptotic inducer. Biochemical and biophysical research communications **277:**476-486.
198. **Kharbanda, S., A. Saleem, T. Shafman, Y. Emoto, N. Taneja, E. Rubin, R. Weichselbaum, J. Woodgett, J. Avruch, J. Kyriakis, and et al.** 1995. Ionizing radiation stimulates a Grb2-mediated association of the stress-activated protein kinase with phosphatidylinositol 3-kinase. J Biol Chem **270:**18871-18874.
199. **Khoudoli, G. A., P. J. Gillespie, G. Stewart, J. S. Andersen, J. R. Swedlow, and J. J. Blow.** 2008. Temporal profiling of the chromatin proteome reveals system-wide responses to replication inhibition. Curr Biol **18:**838-843.
200. **Khurana, D., and P. J. Leibson.** 2003. Regulation of lymphocyte-mediated killing by GTP-binding proteins. J Leukoc Biol **73:**333-338.
201. **Kim, J. T., K. D. Kim, E. Y. Song, H. G. Lee, J. W. Kim, S. K. Chae, E. Kim, M. S. Lee, Y. Yang, and J. S. Lim.** 2006. Apoptosis-inducing factor (AIF) inhibits protein synthesis by interacting with the eukaryotic translation initiation factor 3 subunit p44 (eIF3g). FEBS letters **580:**6375-6383.

202. **Kim, N., A. Saudemont, L. Webb, M. Camps, T. Ruckle, E. Hirsch, M. Turner, and F. Colucci.** 2007. The p110delta catalytic isoform of PI3K is a key player in NK-cell development and cytokine secretion. Blood **110:**3202-3208.
203. **Knaus, U. G., and G. M. Bokoch.** 1998. The p21Rac/Cdc42-activated kinases (PAKs). Int J Biochem Cell Biol **30:**857-862.
204. **Knaus, U. G., Y. Wang, A. M. Reilly, D. Warnock, and J. H. Jackson.** 1998. Structural requirements for PAK activation by Rac GTPases. J Biol Chem **273:**21512-21518.
205. **Kohler, A., and E. Hurt.** 2010. Gene regulation by nucleoporins and links to cancer. Mol Cell **38:**6-15.
206. **Koonin, E. V.** 2005. Orthologs, paralogs, and evolutionary genomics. Annual review of genetics **39:**309-338.
207. **Krogan, N. J., G. Cagney, H. Yu, G. Zhong, X. Guo, A. Ignatchenko, J. Li, S. Pu, N. Datta, A. P. Tikuisis, T. Punna, J. M. Peregrin-Alvarez, M. Shales, X. Zhang, M. Davey, M. D. Robinson, A. Paccanaro, J. E. Bray, A. Sheung, B. Beattie, D. P. Richards, V. Canadien, A. Lalev, F. Mena, P. Wong, A. Starostine, M. M. Canete, J. Vlasblom, S. Wu, C. Orsi, S. R. Collins, S. Chandran, R. Haw, J. J. Rilstone, K. Gandi, N. J. Thompson, G. Musso, P. St Onge, S. Ghanny, M. H. Lam, G. Butland, A. M. Altaf-Ul, S. Kanaya, A. Shilatifard, E. O'Shea, J. S. Weissman, C. J. Ingles, T. R. Hughes, J. Parkinson, M. Gerstein, S. J. Wodak, A. Emili, and J. F. Greenblatt.** 2006. Global landscape of protein complexes in the yeast Saccharomyces cerevisiae. Nature **440:**637-643.
208. **Krude, T., C. Musahl, R. A. Laskey, and R. Knippers.** 1996. Human replication proteins hCdc21, hCdc46 and P1Mcm3 bind chromatin uniformly before S-phase and are displaced locally during DNA replication. J Cell Sci **109 (Pt 2):**309-318.
209. **Krutzfeldt, M., M. Ellis, D. B. Weekes, J. J. Bull, M. Eilers, M. D. Vivanco, W. R. Sellers, and S. Mittnacht.** 2005. Selective ablation of retinoblastoma protein function by the RET finger protein. Mol Cell **18:**213-224.
210. **Krzewski, K., and J. L. Strominger.** 2008. The killer's kiss: the many functions of NK cell immunological synapses. Curr Opin Cell Biol **20:**597-605.
211. **Ku, G. M., D. Yablonski, E. Manser, L. Lim, and A. Weiss.** 2001. A PAK1-PIX-PKL complex is activated by the T-cell receptor independent of Nck, Slp-76 and LAT. Embo J **20:**457-465.
212. **Kurisaki, A., K. Kurisaki, M. Kowanetz, H. Sugino, Y. Yoneda, C. H. Heldin, and A. Moustakas.** 2006. The mechanism of nuclear export of Smad3 involves exportin 4 and Ran. Molecular and cellular biology **26:**1318-1332.
213. **Lamarche-Vane, N., and A. Hall.** 1998. CdGAP, a novel proline-rich GTPase-activating protein for Cdc42 and Rac. J Biol Chem **273:**29172-29177.
214. **Lambert, J. P., L. Mitchell, A. Rudner, K. Baetz, and D. Figeys.** 2009. A novel proteomics approach for the discovery of chromatin-associated protein networks. Mol Cell Proteomics **8:**870-882.
215. **Lambie, H., A. Miremadi, S. E. Pinder, J. A. Bell, P. Wencyk, E. C. Paish, R. D. Macmillan, and I. O. Ellis.** 2003. Prognostic significance of BRCA1 expression in sporadic breast carcinomas. The Journal of pathology **200:**207-213.
216. **Lanier, L. L., J. H. Phillips, J. Hackett, Jr., M. Tutt, and V. Kumar.** 1986. Natural killer cells: definition of a cell type rather than a function. J Immunol **137:**2735-2739.
217. **Laurent, J. M., C. Vogel, T. Kwon, S. A. Craig, D. R. Boutz, H. K. Huse, K. Nozue, H. Walia, M. Whiteley, P. C. Ronald, and E. M. Marcotte.** 2010. Protein

abundances are more conserved than mRNA abundances across diverse taxa. Proteomics **10:**4209-4212.
218. **Lea, N. C., Orr, S. J., Stoeber, K., Williams, G. H., Lam, E. W. -F., Ibrahim, M. A. A., Mufti, G. J. and Thomas, N. S. B.** 2003. Commitment point during G0->G1 that controls entry into the cell cycle. Mol Cell Biol **23:**2351-2361.
219. **Lee, I., U. M. Blom, P. I. Wang, J. E. Shim, and E. M. Marcotte.** 2011. Prioritizing candidate disease genes by network-based boosting of genome-wide association data. Genome Res **21:**1109-1121.
220. **Lee, I., B. Lehner, C. Crombie, W. Wong, A. G. Fraser, and E. M. Marcotte.** 2008. A single gene network accurately predicts phenotypic effects of gene perturbation in Caenorhabditis elegans. Nature genetics **40:**181-188.
221. **Lee, M. G., and P. Nurse.** 1987. Complementation used to clone a human homologue of the fission yeast cell cycle control gene cdc2. Nature **327:**31-35.
222. **Lei, M., and B. K. Tye.** 2001. Initiating DNA synthesis: from recruiting to activating the MCM complex. J Cell Sci **114:**1447-1454.
223. **Lejbkowicz, F., C. Goyer, A. Darveau, S. Neron, R. Lemieux, and N. Sonenberg.** 1992. A fraction of the mRNA 5' cap-binding protein, eukaryotic initiation factor 4E, localizes to the nucleus. Proceedings of the National Academy of Sciences of the United States of America **89:**9612-9616.
224. **Levitt, J. A., D. R. Matthews, S. M. Ameer-Beg, and K. Suhling.** 2009. Fluorescence lifetime and polarization-resolved imaging in cell biology. Curr Opin Biotechnol **20:**28-36.
225. **Li, S., C. M. Armstrong, N. Bertin, H. Ge, S. Milstein, M. Boxem, P. O. Vidalain, J. D. Han, A. Chesneau, T. Hao, D. S. Goldberg, N. Li, M. Martinez, J. F. Rual, P. Lamesch, L. Xu, M. Tewari, S. L. Wong, L. V. Zhang, G. F. Berriz, L. Jacotot, P. Vaglio, J. Reboul, T. Hirozane-Kishikawa, Q. Li, H. W. Gabel, A. Elewa, B. Baumgartner, D. J. Rose, H. Yu, S. Bosak, R. Sequerra, A. Fraser, S. E. Mango, W. M. Saxton, S. Strome, S. Van Den Heuvel, F. Piano, J. Vandenhaute, C. Sardet, M. Gerstein, L. Doucette-Stamm, K. C. Gunsalus, J. W. Harper, M. E. Cusick, F. P. Roth, D. E. Hill, and M. Vidal.** 2004. A map of the interactome network of the metazoan C. elegans. Science **303:**540-543.
226. **Liu, D., Y. T. Bryceson, T. Meckel, G. Vasiliver-Shamis, M. L. Dustin, and E. O. Long.** 2009. Integrin-dependent organization and bidirectional vesicular traffic at cytotoxic immune synapses. Immunity **31:**99-109.
227. **Ljunggren, H. G., and K. Karre.** 1990. In search of the 'missing self': MHC molecules and NK cell recognition. Immunol Today **11:**237-244.
228. **Lleres, D., S. Swift, and A. I. Lamond.** 2007. Detecting protein-protein interactions in vivo with FRET using multiphoton fluorescence lifetime imaging microscopy (FLIM). Curr Protoc Cytom **Chapter 12:**Unit12 10.
229. **Loiodice, I., A. Alves, G. Rabut, M. Van Overbeek, J. Ellenberg, J. B. Sibarita, and V. Doye.** 2004. The entire Nup107-160 complex, including three new members, is targeted as one entity to kinetochores in mitosis. Mol Biol Cell **15:**3333-3344.
230. **Lonza.** 2009. Amaxa® Human T Cell Nucleofector® Kit.
231. **Loo, R. R., N. Dales, and P. C. Andrews.** 1996. The effect of detergents on proteins analyzed by electrospray ionization. Methods Mol Biol **61:**141-160.
232. **Low, B. C., K. T. Seow, and G. R. Guy.** 2000. The BNIP-2 and Cdc42GAP homology domain of BNIP-2 mediates its homophilic association and heterophilic interaction with Cdc42GAP. J Biol Chem **275:**37742-37751.

233. **Lu, P., C. Vogel, R. Wang, X. Yao, and E. M. Marcotte.** 2007. Absolute protein expression profiling estimates the relative contributions of transcriptional and translational regulation. Nat Biotechnol **25:**117-124.
234. **Mailand, N., and J. F. Diffley.** 2005. CDKs promote DNA replication origin licensing in human cells by protecting Cdc6 from APC/C-dependent proteolysis. Cell **122:**915-926.
235. **Makarov, A.** 2000. Electrostatic axially harmonic orbital trapping: a high-performance technique of mass analysis. Analytical chemistry **72:**1156-1162.
236. **Makrogianneli, K., L. M. Carlin, M. D. Keppler, D. R. Matthews, E. Ofo, A. Coolen, S. M. Ameer-Beg, P. R. Barber, B. Vojnovic, and T. Ng.** 2009. Integrating receptor signal inputs that influence small Rho GTPase activation dynamics at the immunological synapse. Mol Cell Biol **29:**2997-3006.
237. **Manning, A. L., and N. J. Dyson.** 2012. RB: mitotic implications of a tumour suppressor. Nature reviews. Cancer **12:**220-226.
238. **Manser, E., H. Y. Huang, T. H. Loo, X. Q. Chen, J. M. Dong, T. Leung, and L. Lim.** 1997. Expression of constitutively active alpha-PAK reveals effects of the kinase on actin and focal complexes. Mol Cell Biol **17:**1129-1143.
239. **Manser, E., T. Leung, H. Salihuddin, Z. S. Zhao, and L. Lim.** 1994. A brain serine/threonine protein kinase activated by Cdc42 and Rac1. Nature **367:**40-46.
240. **Manser, E., T. H. Loo, C. G. Koh, Z. S. Zhao, X. Q. Chen, L. Tan, I. Tan, T. Leung, and L. Lim.** 1998. PAK kinases are directly coupled to the PIX family of nucleotide exchange factors. Mol Cell **1:**183-192.
241. **Marmorstein, L. Y., A. V. Kinev, G. K. Chan, D. A. Bochar, H. Beniya, J. A. Epstein, T. J. Yen, and R. Shiekhattar.** 2001. A human BRCA2 complex containing a structural DNA binding component influences cell cycle progression. Cell **104:**247-257.
242. **Marsh, A., S. Healey, A. Lewis, A. B. Spurdle, M. A. Kedda, K. K. Khanna, G. J. Mann, G. M. Pupo, S. R. Lakhani, and G. Chenevix-Trench.** 2007. Mutation analysis of five candidate genes in familial breast cancer. Breast cancer research and treatment **105:**377-389.
243. **Martin, G. A., G. Bollag, F. McCormick, and A. Abo.** 1995. A novel serine kinase activated by rac1/CDC42Hs-dependent autophosphorylation is related to PAK65 and STE20. Embo J **14:**1970-1978.
244. **Mateyak, M. K., and T. G. Kinzy.** 2010. eEF1A: thinking outside the ribosome. The Journal of biological chemistry **285:**21209-21213.
245. **Maurin, J. C., M. L. Couble, M. J. Staquet, F. Carrouel, I. About, J. Avila, H. Magloire, and F. Bleicher.** 2009. Microtubule-associated protein 1b, a neuronal marker involved in odontoblast differentiation. Journal of endodontics **35:**992-996.
246. **Mazumder, B., P. Sampath, V. Seshadri, R. K. Maitra, P. E. DiCorleto, and P. L. Fox.** 2003. Regulated release of L13a from the 60S ribosomal subunit as a mechanism of transcript-specific translational control. Cell **115:**187-198.
247. **Mazzei, T.** 1984. Chemistry and mechanism of action of bleomycin. Chemioterapia : international journal of the Mediterranean Society of Chemotherapy **3:**316-319.
248. **McGary, K. L., T. J. Park, J. O. Woods, H. J. Cha, J. B. Wallingford, and E. M. Marcotte.** 2010. Systematic discovery of nonobvious human disease models through orthologous phenotypes. Proc Natl Acad Sci U S A **107:**6544-6549.
249. **McLean, J. E., N. Hamaguchi, P. Belenky, S. E. Mortimer, M. Stanton, and L. Hedstrom.** 2004. Inosine 5'-monophosphate dehydrogenase binds nucleic acids in vitro and in vivo. The Biochemical journal **379:**243-251.

250. **Medendorp, K., L. Vreede, J. J. van Groningen, L. Hetterschijt, L. Brugmans, P. A. Jansen, W. H. van den Hurk, D. R. de Bruijn, and A. G. van Kessel.** 2010. The mitotic arrest deficient protein MAD2B interacts with the clathrin light chain A during mitosis. PloS one **5:**e15128.
251. **Mellqvist, U. H., M. Hansson, M. Brune, C. Dahlgren, S. Hermodsson, and K. Hellstrand.** 2000. Natural killer cell dysfunction and apoptosis induced by chronic myelogenous leukemia cells: role of reactive oxygen species and regulation by histamine. Blood **96:**1961-1968.
252. **Messiha, F. S.** 1983. Subcellular distribution of oxidoreductases in genital organs of the male rat. Neurobehav Toxicol Teratol **5:**241-245.
253. **Miki, Y., J. Swensen, D. Shattuck-Eidens, P. A. Futreal, K. Harshman, S. Tavtigian, Q. Liu, C. Cochran, L. M. Bennett, W. Ding, and et al.** 1994. A strong candidate for the breast and ovarian cancer susceptibility gene BRCA1. Science **266:**66-71.
254. **Mili, S., and S. Pinol-Roma.** 2003. LRP130, a pentatricopeptide motif protein with a noncanonical RNA-binding domain, is bound in vivo to mitochondrial and nuclear RNAs. Molecular and cellular biology **23:**4972-4982.
255. **Miller, J. S.** 2002. Biology of natural killer cells in cancer and infection. Cancer Invest **20:**405-419.
256. **Mingot, J. M., S. Kostka, R. Kraft, E. Hartmann, and D. Gorlich.** 2001. Importin 13: a novel mediator of nuclear import and export. The EMBO journal **20:**3685-3694.
257. **Mittnacht, S.** 2005. The retinoblastoma protein--from bench to bedside. European journal of cell biology **84:**97-107.
258. **Mittnacht, S., and R. A. Weinberg.** 1991. G1/S phosphorylation of the retinoblastoma protein is associated with an altered affinity for the nuclear compartment. Cell **65:**381-393.
259. **Monks, C. R., B. A. Freiberg, H. Kupfer, N. Sciaky, and A. Kupfer.** 1998. Three-dimensional segregation of supramolecular activation clusters in T cells. Nature **395:**82-86.
260. **Montano, M. M., K. Ekena, R. Delage-Mourroux, W. Chang, P. Martini, and B. S. Katzenellenbogen.** 1999. An estrogen receptor-selective coregulator that potentiates the effectiveness of antiestrogens and represses the activity of estrogens. Proceedings of the National Academy of Sciences of the United States of America **96:**6947-6952.
261. **Moore, H. M., B. Bai, F. M. Boisvert, L. Latonen, V. Rantanen, J. C. Simpson, R. Pepperkok, A. I. Lamond, and M. Laiho.** 2011. Quantitative proteomics and dynamic imaging of the nucleolus reveal distinct responses to UV and ionizing radiation. Mol Cell Proteomics **10:**M111 009241.
262. **Morris, E. J., and N. J. Dyson.** 2001. Retinoblastoma protein partners. Advances in cancer research **82:**1-54.
263. **Mosimann, C., G. Hausmann, and K. Basler.** 2006. Parafibromin/Hyrax activates Wnt/Wg target gene transcription by direct association with beta-catenin/Armadillo. Cell **125:**327-341.
264. **Mott, H. R., D. Nietlispach, K. A. Evetts, and D. Owen.** 2005. Structural analysis of the SH3 domain of beta-PIX and its interaction with alpha-p21 activated kinase (PAK). Biochemistry **44:**10977-10983.
265. **Moynahan, M. E., J. W. Chiu, B. H. Koller, and M. Jasin.** 1999. Brca1 controls homology-directed DNA repair. Mol Cell **4:**511-518.

266. **Mulvey, C., S. Tudzarova, M. Crawford, G. H. Williams, K. Stoeber, and J. Godovac-Zimmermann.** 2010. Quantitative proteomics reveals a "poised quiescence" cellular state after triggering the DNA replication origin activation checkpoint. Journal of proteome research **9:**5445-5460.
267. **Nakatani, Y., H. Konishi, A. Vassilev, H. Kurooka, K. Ishiguro, J. Sawada, T. Ikura, S. J. Korsmeyer, J. Qin, and A. M. Herlitz.** 2005. p600, a unique protein required for membrane morphogenesis and cell survival. Proceedings of the National Academy of Sciences of the United States of America **102:**15093-15098.
268. **Nakaya, R., J. Takaya, T. Onuki, M. Moritani, N. Nozaki, and Y. Ishimi.** 2010. Identification of proteins that may directly interact with human RPA. Journal of biochemistry **148:**539-547.
269. **Nam, E. A., and D. Cortez.** 2011. ATR signalling: more than meeting at the fork. The Biochemical journal **436:**527-536.
270. **Narla, A., and B. L. Ebert.** 2010. Ribosomopathies: human disorders of ribosome dysfunction. Blood **115:**3196-3205.
271. **Nelson, D. E., A. E. Ihekwaba, M. Elliott, J. R. Johnson, C. A. Gibney, B. E. Foreman, G. Nelson, V. See, C. A. Horton, D. G. Spiller, S. W. Edwards, H. P. McDowell, J. F. Unitt, E. Sullivan, R. Grimley, N. Benson, D. Broomhead, D. B. Kell, and M. R. White.** 2004. Oscillations in NF-kappaB signaling control the dynamics of gene expression. Science **306:**704-708.
272. **Neumann, B., M. Held, U. Liebel, H. Erfle, P. Rogers, R. Pepperkok, and J. Ellenberg.** 2006. High-throughput RNAi screening by time-lapse imaging of live human cells. Nature methods **3:**385-390.
273. **Nevanlinna, H., and J. Bartek.** 2006. The CHEK2 gene and inherited breast cancer susceptibility. Oncogene **25:**5912-5919.
274. **Nielsen, A. L.** 2009. The coat protein complex II, COPII, protein Sec13 directly interacts with presenilin-1. Biochem Biophys Res Commun **388:**571-575.
275. **Niforou, K. M., A. K. Anagnostopoulos, K. Vougas, C. Kittas, V. G. Gorgoulis, and G. T. Tsangaris.** 2008. The proteome profile of the human osteosarcoma U2OS cell line. Cancer genomics & proteomics **5:**63-78.
276. **Nishizuka, I., T. Ishikawa, Y. Hamaguchi, M. Kamiyama, Y. Ichikawa, K. Kadota, R. Miki, Y. Tomaru, Y. Mizuno, N. Tominaga, R. Yano, H. Goto, H. Nitanda, S. Togo, Y. Okazaki, Y. Hayashizaki, and H. Shimada.** 2002. Analysis of gene expression involved in brain metastasis from breast cancer using cDNA microarray. Breast Cancer **9:**26-32.
277. **Nobes, C. D., and A. Hall.** 1999. Rho GTPases control polarity, protrusion, and adhesion during cell movement. J Cell Biol **144:**1235-1244.
278. **Nurse, P., and J. Hayles.** 2011. The cell in an era of systems biology. Cell **144:**850-854.
279. **O'Rourke, F. A., J. M. LaPlante, and M. B. Feinstein.** 2003. Antisense-mediated loss of calcium homoeostasis endoplasmic reticulum protein (CHERP; ERPROT213-21) impairs Ca2+ mobilization, nuclear factor of activated T-cells (NFAT) activation and cell proliferation in Jurkat T-lymphocytes. The Biochemical journal **373:**133-143.
280. **Obermann, E. C., K. L. Eward, A. Dogan, E. A. Paul, M. Loddo, P. Munson, G. H. Williams, and K. Stoeber.** 2005. DNA replication licensing in peripheral B-cell lymphoma. J Pathol **205:**318-328.
281. **Oda, T., A. Fukuda, H. Hagiwara, Y. Masuho, M. A. Muramatsu, K. Hisatake, and T. Yamashita.** 2004. ABT1-associated protein (ABTAP), a novel nuclear

protein conserved from yeast to mammals, represses transcriptional activation by ABT1. Journal of cellular biochemistry **93:**788-806.

282. **Olave, I. A., S. L. Reck-Peterson, and G. R. Crabtree.** 2002. Nuclear actin and actin-related proteins in chromatin remodeling. Annual review of biochemistry **71:**755-781.
283. **Omberg, L., J. R. Meyerson, K. Kobayashi, L. S. Drury, J. F. Diffley, and O. Alter.** 2009. Global effects of DNA replication and DNA replication origin activity on eukaryotic gene expression. Molecular systems biology **5:**312.
284. **Ong, S. E., B. Blagoev, I. Kratchmarova, D. B. Kristensen, H. Steen, A. Pandey, and M. Mann.** 2002. Stable isotope labeling by amino acids in cell culture, SILAC, as a simple and accurate approach to expression proteomics. Molecular & cellular proteomics : MCP **1:**376-386.
285. **Onuki-Nagasaki, R., A. Nagasaki, K. Hakamada, T. Q. Uyeda, S. Fujita, M. Miyake, and J. Miyake.** 2010. Transfection microarrays for high-throughput phenotypic screening of genes involved in cell migration. Methods Mol Biol **629:**193-203.
286. **Orange, J. S.** 2008. Formation and function of the lytic NK-cell immunological synapse. Nat Rev Immunol **8:**713-725.
287. **Orange, J. S., K. E. Harris, M. M. Andzelm, M. M. Valter, R. S. Geha, and J. L. Strominger.** 2003. The mature activating natural killer cell immunologic synapse is formed in distinct stages. Proc Natl Acad Sci U S A **100:**14151-14156.
288. **Orange, J. S., N. Ramesh, E. Remold-O'Donnell, Y. Sasahara, L. Koopman, M. Byrne, F. A. Bonilla, F. S. Rosen, R. S. Geha, and J. L. Strominger.** 2002. Wiskott-Aldrich syndrome protein is required for NK cell cytotoxicity and colocalizes with actin to NK cell-activating immunologic synapses. Proc Natl Acad Sci U S A **99:**11351-11356.
289. **Orelli, B. J., and D. K. Bishop.** 2001. BRCA2 and homologous recombination. Breast cancer research : BCR **3:**294-298.
290. **Orr, S. J., D. R. Boutz, R. Wang, C. Chronis, N. C. Lea, T. Thayaparan, E. Hamilton, H. Milewicz, E. Blanc, G. J. Mufti, E. M. Marcotte, and N. S. Thomas.** 2012. Proteomic and protein interaction network analysis of human T lymphocytes during cell-cycle entry. Mol Syst Biol **8:**573.
291. **Orr, S. J., T. Gaymes, D. Ladon, C. Chronis, B. Czepulkowski, R. Wang, G. J. Mufti, E. M. Marcotte, and N. S. Thomas.** 2010. Reducing MCM levels in human primary T cells during the G(0)-->G(1) transition causes genomic instability during the first cell cycle. Oncogene **29:**3803-3814.
292. **Orsucci, D., M. Mancuso, and G. Siciliano.** 2008. Mitochondria, oxidative stress and PARP-1 network: a new target for neuroprotective effects of tetracyclines? J Physiol **586:**2427-2428.
293. **Ostasiewicz, P., D. F. Zielinska, M. Mann, and J. R. Wisniewski.** 2010. Proteome, phosphoproteome, and N-glycoproteome are quantitatively preserved in formalin-fixed paraffin-embedded tissue and analyzable by high-resolution mass spectrometry. Journal of proteome research **9:**3688-3700.
294. **Panigrahi, A. K., N. Zhang, Q. Mao, and D. Pati.** 2011. Calpain-1 cleaves Rad21 to promote sister chromatid separation. Molecular and cellular biology **31:**4335-4347.
295. **Parrini, M. C., M. Lei, S. C. Harrison, and B. J. Mayer.** 2002. Pak1 kinase homodimers are autoinhibited in trans and dissociated upon activation by Cdc42 and Rac1. Mol Cell **9:**73-83.

296. **Paull, T. T., E. P. Rogakou, V. Yamazaki, C. U. Kirchgessner, M. Gellert, and W. M. Bonner.** 2000. A critical role for histone H2AX in recruitment of repair factors to nuclear foci after DNA damage. Curr Biol **10:**886-895.
297. **Perez-Gonzalez, A., A. Rodriguez, M. Huarte, I. J. Salanueva, and A. Nieto.** 2006. hCLE/CGI-99, a human protein that interacts with the influenza virus polymerase, is a mRNA transcription modulator. J Mol Biol **362:**887-900.
298. **Ponting, C. P.** 2000. Novel eIF4G domain homologues linking mRNA translation with nonsense-mediated mRNA decay. Trends in biochemical sciences **25:**423-426.
299. **Provenzano, P. P., K. W. Eliceiri, and P. J. Keely.** 2009. Multiphoton microscopy and fluorescence lifetime imaging microscopy (FLIM) to monitor metastasis and the tumor microenvironment. Clin Exp Metastasis **26:**357-370.
300. **Puig, O., F. Caspary, G. Rigaut, B. Rutz, E. Bouveret, E. Bragado-Nilsson, M. Wilm, and B. Seraphin.** 2001. The tandem affinity purification (TAP) method: a general procedure of protein complex purification. Methods **24:**218-229.
301. **Pulicherla, N., L. A. Pogorzala, Z. Xu, O. F. HC, F. N. Musayev, J. N. Scarsdale, E. A. Sia, G. M. Culver, and J. P. Rife.** 2009. Structural and functional divergence within the Dim1/KsgA family of rRNA methyltransferases. J Mol Biol **391:**884-893.
302. **Punta, M., P. C. Coggill, R. Y. Eberhardt, J. Mistry, J. Tate, C. Boursnell, N. Pang, K. Forslund, G. Ceric, J. Clements, A. Heger, L. Holm, E. L. Sonnhammer, S. R. Eddy, A. Bateman, and R. D. Finn.** 2012. The Pfam protein families database. Nucleic Acids Res **40:**D290-D301.
303. **Qiagen.** 2009. Critical Factors for Successful Real-Time PCR.
304. **Qiang, Y. W., L. Yao, G. Tosato, and S. Rudikoff.** 2004. Insulin-like growth factor I induces migration and invasion of human multiple myeloma cells. Blood **103:**301-308.
305. **Rabut, G., P. Lenart, and J. Ellenberg.** 2004. Dynamics of nuclear pore complex organization through the cell cycle. Curr Opin Cell Biol **16:**314-321.
306. **Rassool, F. V., T. J. Gaymes, N. Omidvar, N. Brady, S. Beurlet, M. Pla, M. Reboul, N. Lea, C. Chomienne, N. S. Thomas, G. J. Mufti, and R. A. Padua.** 2007. Reactive oxygen species, DNA damage, and error-prone repair: a model for genomic instability with progression in myeloid leukemia? Cancer research **67:**8762-8771.
307. **Reddy, S., R. Devlin, C. Menaa, R. Nishimura, S. J. Choi, M. Dallas, T. Yoneda, and G. D. Roodman.** 1998. Isolation and characterization of a cDNA clone encoding a novel peptide (OSF) that enhances osteoclast formation and bone resorption. J Cell Physiol **177:**636-645.
308. **Ren, M., G. Drivas, P. D'Eustachio, and M. G. Rush.** 1993. Ran/TC4: a small nuclear GTP-binding protein that regulates DNA synthesis. The Journal of cell biology **120:**313-323.
309. **Rick, M., S. I. Ramos Garrido, C. Herr, D. R. Thal, A. A. Noegel, and C. S. Clemen.** 2005. Nuclear localization of Annexin A7 during murine brain development. BMC Neurosci **6:**25.
310. **Ridley, A. J.** 1995. Rho-related proteins: actin cytoskeleton and cell cycle. Current opinion in genetics & development **5:**24-30.
311. **Ridley, A. J.** 2001. Rho family proteins: coordinating cell responses. Trends Cell Biol **11:**471-477.
312. **Ridley, A. J.** 2006. Rho GTPases and actin dynamics in membrane protrusions and vesicle trafficking. Trends Cell Biol **16:**522-529.

313. **Rigaut, G., A. Shevchenko, B. Rutz, M. Wilm, M. Mann, and B. Seraphin.** 1999. A generic protein purification method for protein complex characterization and proteome exploration. Nat Biotechnol **17:**1030-1032.
314. **Rogakou, E. P., D. R. Pilch, A. H. Orr, V. S. Ivanova, and W. M. Bonner.** 1998. DNA double-stranded breaks induce histone H2AX phosphorylation on serine 139. J Biol Chem **273:**5858-5868.
315. **Rosenberger, G., I. Jantke, A. Gal, and K. Kutsche.** 2003. Interaction of alphaPIX (ARHGEF6) with beta-parvin (PARVB) suggests an involvement of alphaPIX in integrin-mediated signaling. Human molecular genetics **12:**155-167.
316. **Roskoski, R., Jr.** 2012. ERK1/2 MAP kinases: structure, function, and regulation. Pharmacol Res **66:**105-143.
317. **Rougerie, P., and J. Delon.** 2011. Rho GTPases: Masters of T lymphocyte migration and activation. Immunol Lett.
318. **Rout, M. P., and J. D. Aitchison.** 2001. The nuclear pore complex as a transport machine. J Biol Chem **276:**16593-16596.
319. **Routledge, K. E., V. Gupta, and W. E. Balch.** 2010. Emergent properties of proteostasis-COPII coupled systems in human health and disease. Molecular membrane biology **27:**385-397.
320. **Royle, S. J., N. A. Bright, and L. Lagnado.** 2005. Clathrin is required for the function of the mitotic spindle. Nature **434:**1152-1157.
321. **Rundlett, K. L., and D. W. Armstrong.** 1996. Mechanism of signal suppression by anionic surfactants in capillary electrophoresis-electrospray ionization mass spectrometry. Anal Chem **68:**3493-3497.
322. **Russell, R. B., and P. Aloy.** 2008. Targeting and tinkering with interaction networks. Nat Chem Biol **4:**666-673.
323. **Ryan, K. J., and S. R. Wente.** 2000. The nuclear pore complex: a protein machine bridging the nucleus and cytoplasm. Curr Opin Cell Biol **12:**361-371.
324. **Ryu, J. H., S. H. Li, H. S. Park, J. W. Park, B. Lee, and Y. S. Chun.** 2011. Hypoxia-inducible factor alpha subunit stabilization by NEDD8 conjugation is reactive oxygen species-dependent. The Journal of biological chemistry **286:**6963-6970.
325. **Sabatinos, S. A.** 2010. Replication Fork Stalling and the Fork Protection Complex. Nature Education.
326. **Salazar-Fontana, L. I., V. Barr, L. E. Samelson, and B. E. Bierer.** 2003. CD28 engagement promotes actin polymerization through the activation of the small Rho GTPase Cdc42 in human T cells. J Immunol **171:**2225-2232.
327. **Sato, N., J. Koinuma, M. Fujita, M. Hosokawa, T. Ito, E. Tsuchiya, S. Kondo, Y. Nakamura, and Y. Daigo.** 2010. Activation of WD repeat and high-mobility group box DNA binding protein 1 in pulmonary and esophageal carcinogenesis. Clin Cancer Res **16:**226-239.
328. **Satyanarayana, A., and P. Kaldis.** 2009. Mammalian cell-cycle regulation: several Cdks, numerous cyclins and diverse compensatory mechanisms. Oncogene **28:**2925-2939.
329. **Scanlan, M. J., I. Gout, C. M. Gordon, B. Williamson, E. Stockert, A. O. Gure, D. Jager, Y. T. Chen, A. Mackay, M. J. O'Hare, and L. J. Old.** 2001. Humoral immunity to human breast cancer: antigen definition and quantitative analysis of mRNA expression. Cancer immunity **1:**4.
330. **Schadt, E. E.** 2009. Molecular networks as sensors and drivers of common human diseases. Nature **461:**218-223.

331. **Schmittgen, T. D., and K. J. Livak.** 2008. Analyzing real-time PCR data by the comparative C(T) method. Nat Protoc **3:**1101-1108.
332. **Segovis, C. M., R. A. Schoon, C. J. Dick, L. P. Nacusi, P. J. Leibson, and D. D. Billadeau.** 2009. PI3K links NKG2D signaling to a CrkL pathway involved in natural killer cell adhesion, polarity, and granule secretion. J Immunol **182:**6933-6942.
333. **Sehl, M. E., L. R. Langer, J. C. Papp, L. Kwan, J. L. Seldon, G. Arellano, J. Reiss, E. F. Reed, S. Dandekar, Y. Korin, J. S. Sinsheimer, Z. F. Zhang, and P. A. Ganz.** 2009. Associations between single nucleotide polymorphisms in double-stranded DNA repair pathway genes and familial breast cancer. Clin Cancer Res **15:**2192-2203.
334. **Sekar, R. B., and A. Periasamy.** 2003. Fluorescence resonance energy transfer (FRET) microscopy imaging of live cell protein localizations. J Cell Biol **160:**629-633.
335. **Sentman, C. L., M. A. Barber, A. Barber, and T. Zhang.** 2006. NK cell receptors as tools in cancer immunotherapy. Advances in cancer research **95:**249-292.
336. **Serrano-Pertierra, E., E. Cernuda-Morollon, and C. Lopez-Larrea.** 2012. The Wiskott-Aldrich syndrome proteins are involved in the regulation of natural killer cell migration upon NKG2D activation. Eur J Immunol.
337. **Sha, Z., L. M. Brill, R. Cabrera, O. Kleifeld, J. S. Scheliga, M. H. Glickman, E. C. Chang, and D. A. Wolf.** 2009. The eIF3 interactome reveals the translasome, a supercomplex linking protein synthesis and degradation machineries. Molecular cell **36:**141-152.
338. **Shannon, P., A. Markiel, O. Ozier, N. S. Baliga, J. T. Wang, D. Ramage, N. Amin, B. Schwikowski, and T. Ideker.** 2003. Cytoscape: a software environment for integrated models of biomolecular interaction networks. Genome Res **13:**2498-2504.
339. **Sharkey, D. J., E. R. Scalice, K. G. Christy, Jr., S. M. Atwood, and J. L. Daiss.** 1994. Antibodies as thermolabile switches: high temperature triggering for the polymerase chain reaction. Biotechnology (N Y) **12:**506-509.
340. **Shibuya, K., L. L. Lanier, J. H. Phillips, H. D. Ochs, K. Shimizu, E. Nakayama, H. Nakauchi, and A. Shibuya.** 1999. Physical and functional association of LFA-1 with DNAM-1 adhesion molecule. Immunity **11:**615-623.
341. **Shiio, Y., R. N. Eisenman, E. C. Yi, S. Donohoe, D. R. Goodlett, and R. Aebersold.** 2003. Quantitative proteomic analysis of chromatin-associated factors. J Am Soc Mass Spectrom **14:**696-703.
342. **Shimizu, Y., D. E. Geraghty, B. H. Koller, H. T. Orr, and R. DeMars.** 1988. Transfer and expression of three cloned human non-HLA-A,B,C class I major histocompatibility complex genes in mutant lymphoblastoid cells. Proc Natl Acad Sci U S A **85:**227-231.
343. **Shin, E. Y., K. S. Shin, C. S. Lee, K. N. Woo, S. H. Quan, N. K. Soung, Y. G. Kim, C. I. Cha, S. R. Kim, D. Park, G. M. Bokoch, and E. G. Kim.** 2002. Phosphorylation of p85 beta PIX, a Rac/Cdc42-specific guanine nucleotide exchange factor, via the Ras/ERK/PAK2 pathway is required for basic fibroblast growth factor-induced neurite outgrowth. J Biol Chem **277:**44417-44430.
344. **Shoemaker, B. A., and A. R. Panchenko.** 2007. Deciphering protein-protein interactions. Part I. Experimental techniques and databases. PLoS Computational Biology **3:**337-344.

345. **Shoemaker, B. A., and A. R. Panchenko.** 2007. Deciphering protein-protein interactions. Part II. Computational methods to predict protein and domain interaction partners. PLoS Comput Biol **3:**e43.
346. **Sihn, C. R., E. J. Suh, K. H. Lee, and S. H. Kim.** 2005. Sec13 induces genomic instability in U2OS cells. Experimental & molecular medicine **37:**255-260.
347. **Simpson, J. L., R. H. Gray, A. Perez, P. Mena, M. Barbato, E. E. Castilla, R. T. Kambic, F. Pardo, G. Tagliabue, W. S. Stephenson, A. Bitto, C. Li, V. H. Jennings, J. M. Spieler, and J. T. Queenan.** 1997. Pregnancy outcome in natural family planning users: cohort and case-control studies evaluating safety. Advances in contraception : the official journal of the Society for the Advancement of Contraception **13:**201-214.
348. **Sinai, P., C. Nguyen, J. D. Schatzle, and C. Wulfing.** 2010. Transience in polarization of cytolytic effectors is required for efficient killing and controlled by Cdc42. Proc Natl Acad Sci U S A **107:**11912-11917.
349. **Slomiany, P., T. Baker, E. R. Elliott, and M. J. Grossel.** 2006. Changes in motility, gene expression and actin dynamics: Cdk6-induced cytoskeletal changes associated with differentiation in mouse astrocytes. Journal of cellular biochemistry **99:**635-646.
350. **Smith, A. E., C. Chronis, M. Christodoulakis, S. J. Orr, N. C. Lea, N. A. Twine, A. Bhinge, G. J. Mufti, and N. S. Thomas.** 2009. Epigenetics of human T cells during the G0-->G1 transition. Genome Res **19:**1325-1337.
351. **Smith, J. C., J. P. Lambert, F. Elisma, and D. Figeys.** 2007. Proteomics in 2005/2006: developments, applications and challenges. Anal Chem **79:**4325-4343.
352. **Snyder, J. T., D. K. Worthylake, K. L. Rossman, L. Betts, W. M. Pruitt, D. P. Siderovski, C. J. Der, and J. Sondek.** 2002. Structural basis for the selective activation of Rho GTPases by Dbl exchange factors. Nature structural biology **9:**468-475.
353. **Squirrell, J. M., D. L. Wokosin, J. G. White, and B. D. Bavister.** 1999. Long-term two-photon fluorescence imaging of mammalian embryos without compromising viability. Nat Biotechnol **17:**763-767.
354. **Stabile, H., C. Carlino, C. Mazza, S. Giliani, S. Morrone, L. D. Notarangelo, A. Santoni, and A. Gismondi.** 2010. Impaired NK-cell migration in WAS/XLT patients: role of Cdc42/WASp pathway in the control of chemokine-induced beta2 integrin high-affinity state. Blood **115:**2818-2826.
355. **Stagg, S. M., P. LaPointe, A. Razvi, C. Gurkan, C. S. Potter, B. Carragher, and W. E. Balch.** 2008. Structural basis for cargo regulation of COPII coat assembly. Cell **134:**474-484.
356. **Stevens, W. K., W. Vranken, N. Goudreau, H. Xiang, P. Xu, and F. Ni.** 1999. Conformation of a Cdc42/Rac interactive binding peptide in complex with Cdc42 and analysis of the binding interface. Biochemistry **38:**5968-5975.
357. **Stewart, M.** 2010. Nuclear export of mRNA. Trends Biochem Sci **35:**609-617.
358. **Stinchcombe, J. C., and G. M. Griffiths.** 2007. Secretory mechanisms in cell-mediated cytotoxicity. Annu Rev Cell Dev Biol **23:**495-517.
359. **Strudwick, S., and K. L. Borden.** 2002. The emerging roles of translation factor eIF4E in the nucleus. Differentiation **70:**10-22.
360. **Sutherland, B. W., J. Toews, and J. Kast.** 2008. Utility of formaldehyde cross-linking and mass spectrometry in the study of protein-protein interactions. Journal of mass spectrometry : JMS **43:**699-715.

361. **Sutherland, C. L., N. J. Chalupny, K. Schooley, T. VandenBos, M. Kubin, and D. Cosman.** 2002. UL16-binding proteins, novel MHC class I-related proteins, bind to NKG2D and activate multiple signaling pathways in primary NK cells. J Immunol **168:**671-679.
362. **Tadeu, A. M., S. Ribeiro, J. Johnston, I. Goldberg, D. Gerloff, and W. C. Earnshaw.** 2008. CENP-V is required for centromere organization, chromosome alignment and cytokinesis. The EMBO journal **27:**2510-2522.
363. **Takahashi, A., R. Tsutsumi, I. Kikuchi, C. Obuse, Y. Saito, A. Seidi, R. Karisch, M. Fernandez, T. Cho, N. Ohnishi, O. Rozenblatt-Rosen, M. Meyerson, B. G. Neel, and M. Hatakeyama.** 2011. SHP2 tyrosine phosphatase converts parafibromin/Cdc73 from a tumor suppressor to an oncogenic driver. Molecular cell **43:**45-56.
364. **Takeda, D. Y., and A. Dutta.** 2005. DNA replication and progression through S phase. Oncogene **24:**2827-2843.
365. **Talluri, S., and F. A. Dick.** 2012. Regulation of transcription and chromatin structure by pRB: Here, there and everywhere. Cell cycle **11**.
366. **Tanaka, S., and J. F. Diffley.** 2002. Deregulated G1-cyclin expression induces genomic instability by preventing efficient pre-RC formation. Genes Dev **16:**2639-2649.
367. **Tanaka, S., and J. F. Diffley.** 2002. Interdependent nuclear accumulation of budding yeast Cdt1 and Mcm2-7 during G1 phase. Nat Cell Biol **4:**198-207.
368. **Tang, K., D. Nie, Y. Cai, and K. V. Honn.** 1999. The beta4 integrin subunit rescues A431 cells from apoptosis through a PI3K/Akt kinase signaling pathway. Biochem Biophys Res Commun **264:**127-132.
369. **Tchapyjnikov, D., Y. Li, T. Pisitkun, J. D. Hoffert, M. J. Yu, and M. A. Knepper.** 2010. Proteomic profiling of nuclei from native renal inner medullary collecting duct cells using LC-MS/MS. Physiological genomics **40:**167-183.
370. **Teplova, M., Y. R. Yuan, A. T. Phan, L. Malinina, S. Ilin, A. Teplov, and D. J. Patel.** 2006. Structural basis for recognition and sequestration of UUU(OH) 3' temini of nascent RNA polymerase III transcripts by La, a rheumatic disease autoantigen. Molecular cell **21:**75-85.
371. **Terasaki, M. E. D. E. M. D. R. S. M.** 2006. Confocal Microscopy of Living Cells. *In* J. B. Pawley (ed.), Handbook of Biological Confocal Microscopy, Third Edition ed. Springer Science+Business Media., LLC, Madison.
372. **Thomas, N. S., A. R. Pizzey, S. Tiwari, C. D. Williams, and J. Yang.** 1998. p130, p107, and pRb are differentially regulated in proliferating cells and during cell cycle arrest by alpha-interferon. J Biol Chem **273:**23659-23667.
373. **Thomas, N. S. B.** 2004. Cell cycle regulation, p. 33-63. *In* L. Degos, Griffin, J. D., Linch, D. C. and Lowenberg, B. (ed.), Textbook of Malignant Haematology, 2nd ed. Martin Dunitz, London.
374. **Tiedje, C., I. Sakwa, U. Just, and T. Hofken.** 2008. The Rho GDI Rdi1 regulates Rho GTPases by distinct mechanisms. Mol Biol Cell **19:**2885-2896.
375. **Trinchieri, G.** 1989. Biology of natural killer cells. Adv Immunol **47:**187-376.
376. **Tsutsui, Y., T. Morishita, T. Natsume, K. Yamashita, H. Iwasaki, F. Yamao, and H. Shinagawa.** 2005. Genetic and physical interactions between Schizosaccharomyces pombe Mcl1 and Rad2, Dna2 and DNA polymerase alpha: evidence for a multifunctional role of Mcl1 in DNA replication and repair. Current genetics **48:**34-43.

377. **Tu, S., and R. A. Cerione.** 2001. Cdc42 is a substrate for caspases and influences Fas-induced apoptosis. J Biol Chem **276:**19656-19663.
378. **Turbitt, M. L., and R. M. Mackie.** 1986. An assessment of the diagnostic value of the monoclonal antibodies Leu 8, OKT9, OKT10 and Ki67 in cutaneous lymphocytic infiltrates. Br J Dermatol **115:**151-158.
379. **Turjanski, A. G., J. P. Vaque, and J. S. Gutkind.** 2007. MAP kinases and the control of nuclear events. Oncogene **26:**3240-3253.
380. **Turner, C. E., M. C. Brown, J. A. Perrotta, M. C. Riedy, S. N. Nikolopoulos, A. R. McDonald, S. Bagrodia, S. Thomas, and P. S. Leventhal.** 1999. Paxillin LD4 motif binds PAK and PIX through a novel 95-kD ankyrin repeat, ARF-GAP protein: A role in cytoskeletal remodeling. J Cell Biol **145:**851-863.
381. **Tye, B. K.** 1999. MCM proteins in DNA replication. Annual review of biochemistry **68:**649-686.
382. **Uhrberg, M.** 2005. The CD107 mobilization assay: viable isolation and immunotherapeutic potential of tumor-cytolytic NK cells. Leukemia **19:**707-709.
383. **Van Aelst, L., and C. D'Souza-Schorey.** 1997. Rho GTPases and signaling networks. Genes Dev **11:**2295-2322.
384. **Vanhaesebroeck, B., K. Ali, A. Bilancio, B. Geering, and L. C. Foukas.** 2005. Signalling by PI3K isoforms: insights from gene-targeted mice. Trends Biochem Sci **30:**194-204.
385. **Vanhaesebroeck, B., S. J. Leevers, G. Panayotou, and M. D. Waterfield.** 1997. Phosphoinositide 3-kinases: a conserved family of signal transducers. Trends Biochem Sci **22:**267-272.
386. **Vanherberghen, B., K. Andersson, L. M. Carlin, E. N. Nolte-'t Hoen, G. S. Williams, P. Hoglund, and D. M. Davis.** 2004. Human and murine inhibitory natural killer cell receptors transfer from natural killer cells to target cells. Proc Natl Acad Sci U S A **101:**16873-16878.
387. **Venema, J., and D. Tollervey.** 1999. Ribosome synthesis in Saccharomyces cerevisiae. Annual review of genetics **33:**261-311.
388. **Venkitaraman, A. R.** 2001. Functions of BRCA1 and BRCA2 in the biological response to DNA damage. J Cell Sci **114:**3591-3598.
389. **Venkitaraman, A. R., and R. J. Cowling.** 1994. Interleukin-7 induces the association of phosphatidylinositol 3-kinase with the alpha chain of the interleukin-7 receptor. Eur J Immunol **24:**2168-2174.
390. **Viale, G.** 2011. Pathological work up of the primary tumor: getting the proper information out of it. Breast **20 Suppl 3:**S82-86.
391. **Villalonga, P., and A. J. Ridley.** 2006. Rho GTPases and cell cycle control. Growth Factors **24:**159-164.
392. **Vlahos, C. J., W. F. Matter, K. Y. Hui, and R. F. Brown.** 1994. A specific inhibitor of phosphatidylinositol 3-kinase, 2-(4- morpholinyl)-8-phenyl-4H-1-benzopyran-4-one (LY294002). J Biol Chem **269:**5241-5248.
393. **Vogel, C., S. Abreu Rde, D. Ko, S. Y. Le, B. A. Shapiro, S. C. Burns, D. Sandhu, D. R. Boutz, E. M. Marcotte, and L. O. Penalva.** 2010. Sequence signatures and mRNA concentration can explain two-thirds of protein abundance variation in a human cell line. Mol Syst Biol **6:**400.
394. **Vogel, C., and E. M. Marcotte.** 2012. Label-free protein quantitation using weighted spectral counting. Methods in molecular biology **893:**321-341.

395. **Vogel, L. B., and D. J. Fujita.** 1995. p70 phosphorylation and binding to p56lck is an early event in interleukin-2-induced onset of cell cycle progression in T-lymphocytes. J Biol Chem **270:**2506-2511.
396. **Vogel, S. S., C. Thaler, and S. V. Koushik.** 2006. Fanciful FRET. Sci STKE **2006:**re2.
397. **Voskoboinik, I., M. J. Smyth, and J. A. Trapani.** 2006. Perforin-mediated target-cell death and immune homeostasis. Nat Rev Immunol **6:**940-952.
398. **Vyas, Y. M., K. M. Mehta, M. Morgan, H. Maniar, L. Butros, S. Jung, J. K. Burkhardt, and B. Dupont.** 2001. Spatial organization of signal transduction molecules in the NK cell immune synapses during MHC class I-regulated noncytolytic and cytolytic interactions. J Immunol **167:**4358-4367.
399. **Walhout, A. J., R. Sordella, X. Lu, J. L. Hartley, G. F. Temple, M. A. Brasch, N. Thierry-Mieg, and M. Vidal.** 2000. Protein interaction mapping in C. elegans using proteins involved in vulval development. Science **287:**116-122.
400. **Wallrabe, H., and A. Periasamy.** 2005. Imaging protein molecules using FRET and FLIM microscopy. Curr Opin Biotechnol **16:**19-27.
401. **Walter, B. N., Z. Huang, R. Jakobi, P. T. Tuazon, E. S. Alnemri, G. Litwack, and J. A. Traugh.** 1998. Cleavage and activation of p21-activated protein kinase gamma-PAK by CPP32 (caspase 3). Effects of autophosphorylation on activity. J Biol Chem **273:**28733-28739.
402. **Wang, G. G., L. Cai, M. P. Pasillas, and M. P. Kamps.** 2007. NUP98-NSD1 links H3K36 methylation to Hox-A gene activation and leukaemogenesis. Nat Cell Biol **9:**804-812.
403. **Wang, J., S. Rao, J. Chu, X. Shen, D. N. Levasseur, T. W. Theunissen, and S. H. Orkin.** 2006. A protein interaction network for pluripotency of embryonic stem cells. Nature **444:**364-368.
404. **Wang, J. B., W. J. Wu, and R. A. Cerione.** 2005. Cdc42 and Ras cooperate to mediate cellular transformation by intersectin-L. J Biol Chem **280:**22883-22891.
405. **Wang, K., Y. Ye, Z. Xu, X. Zhang, Z. Hou, Y. Cui, and Y. Song.** 2010. Interaction between BRCA1/BRCA2 and ATM/ATR associate with breast cancer susceptibility in a Chinese Han population. Cancer genetics and cytogenetics **200:**40-46.
406. **Wang, L., K. Zhu, and Y. Zheng.** 2004. Oncogenic Dbl, Cdc42, and p21-activated kinase form a ternary signaling intermediate through the minimum interactive domains. Biochemistry **43:**14584-14593.
407. **Wang, X., X. Wei, B. Thijssen, J. Das, S. M. Lipkin, and H. Yu.** 2012. Three-dimensional reconstruction of protein networks provides insight into human genetic disease. Nature biotechnology **30:**159-164.
408. **Wang, Y., J. Y. Shyy, and S. Chien.** 2008. Fluorescence proteins, live-cell imaging, and mechanobiology: seeing is believing. Annu Rev Biomed Eng **10:**1-38.
409. **Warner, J. R., and K. B. McIntosh.** 2009. How common are extraribosomal functions of ribosomal proteins? Molecular cell **34:**3-11.
410. **Watkins, S. J., and C. J. Norbury.** 2004. Cell cycle-related variation in subcellular localization of eIF3e/INT6 in human fibroblasts. Cell Prolif **37:**149-160.
411. **Weber, K. S., L. B. Klickstein, P. C. Weber, and C. Weber.** 1998. Chemokine-induced monocyte transmigration requires cdc42-mediated cytoskeletal changes. Eur J Immunol **28:**2245-2251.
412. **Williams, G. H., and K. Stoeber.** 2012. The cell cycle and cancer. The Journal of pathology **226:**352-364.

413. **Wisniewski, J. R., A. Zougman, N. Nagaraj, and M. Mann.** 2009. Universal sample preparation method for proteome analysis. Nat Methods **6:**359-362.
414. **Wittwer, C. T., M. G. Herrmann, A. A. Moss, and R. P. Rasmussen.** 1997. Continuous fluorescence monitoring of rapid cycle DNA amplification. Biotechniques **22:**130-131, 134-138.
415. **Wong, J. V., P. Dong, J. R. Nevins, B. Mathey-Prevot, and L. You.** 2011. Network calisthenics: control of E2F dynamics in cell cycle entry. Cell cycle **10:**3086-3094.
416. **Wooster, R., and B. L. Weber.** 2003. Breast and ovarian cancer. N Engl J Med **348:**2339-2347.
417. **Wu, L. C., Z. W. Wang, J. T. Tsan, M. A. Spillman, A. Phung, X. L. Xu, M. C. Yang, L. Y. Hwang, A. M. Bowcock, and R. Baer.** 1996. Identification of a RING protein that can interact in vivo with the BRCA1 gene product. Nat Genet **14:**430-440.
418. **Wu, Z., S. Zheng, and Q. Yu.** 2009. The E2F family and the role of E2F1 in apoptosis. The international journal of biochemistry & cell biology **41:**2389-2397.
419. **Wulfing, C., B. Purtic, J. Klem, and J. D. Schatzle.** 2003. Stepwise cytoskeletal polarization as a series of checkpoints in innate but not adaptive cytolytic killing. Proc Natl Acad Sci U S A **100:**7767-7772.
420. **Xie, C., W. Wang, F. Yang, M. Wu, and Y. Mei.** 2012. RUVBL2 is a novel repressor of ARF transcription. FEBS letters **586:**435-441.
421. **Xu, S., and M. A. Powers.** 2009. Nuclear pore proteins and cancer. Seminars in cell & developmental biology **20:**620-630.
422. **Yang, Y. J., J. W. Han, H. D. Youn, and E. J. Cho.** 2010. The tumor suppressor, parafibromin, mediates histone H3 K9 methylation for cyclin D1 repression. Nucleic acids research **38:**382-390.
423. **Yart, A., M. Gstaiger, C. Wirbelauer, M. Pecnik, D. Anastasiou, D. Hess, and W. Krek.** 2005. The HRPT2 tumor suppressor gene product parafibromin associates with human PAF1 and RNA polymerase II. Molecular and cellular biology **25:**5052-5060.
424. **Yodoi, J., K. Teshigawara, T. Nikaido, K. Fukui, T. Noma, T. Honjo, M. Takigawa, M. Sasaki, N. Minato, M. Tsudo, and et al.** 1985. TCGF (IL 2)-receptor inducing factor(s). I. Regulation of IL 2 receptor on a natural killer-like cell line (YT cells). J Immunol **134:**1623-1630.
425. **Yoo, Y., X. Wu, and J. L. Guan.** 2007. A novel role of the actin-nucleating Arp2/3 complex in the regulation of RNA polymerase II-dependent transcription. J Biol Chem **282:**7616-7623.
426. **Yoshida, T., H. Kitaura, Y. Hagio, T. Sato, S. M. Iguchi-Ariga, and H. Ariga.** 2008. Negative regulation of the Wnt signal by MM-1 through inhibiting expression of the wnt4 gene. Exp Cell Res **314:**1217-1228.
427. **Yoshizaki, H., Y. Ohba, K. Kurokawa, R. E. Itoh, T. Nakamura, N. Mochizuki, K. Nagashima, and M. Matsuda.** 2003. Activity of Rho-family GTPases during cell division as visualized with FRET-based probes. J Cell Biol **162:**223-232.
428. **Yoshizawa-Sugata, N., and H. Masai.** 2009. Roles of human AND-1 in chromosome transactions in S phase. J Biol Chem **284:**20718-20728.
429. **Yotov, W. V., A. Moreau, and R. St-Arnaud.** 1998. The alpha chain of the nascent polypeptide-associated complex functions as a transcriptional coactivator. Molecular and cellular biology **18:**1303-1311.

430. **Yung, E., S. Sekulovic, B. Argiropoulos, C. K. Lai, M. Leung, T. Berg, S. Vollett, V. C. Chang, A. Wan, S. Wong, and R. K. Humphries.** 2011. Delineating domains and functions of NUP98 contributing to the leukemogenic activity of NUP98-HOX fusions. Leukemia research **35:**545-550.
431. **Zanello, S. B., R. Nayak, L. P. Zanello, and P. Farthing-Nayak.** 2006. Identification and distribution of 14.3.3sigma (stratifin) in the human cornea. Current eye research **31:**825-833.
432. **Zhang, C., D. Kong, M. H. Tan, D. L. Pappas, Jr., P. F. Wang, J. Chen, L. Farber, N. Zhang, H. M. Koo, M. Weinreich, B. O. Williams, and B. T. Teh.** 2006. Parafibromin inhibits cancer cell growth and causes G1 phase arrest. Biochemical and biophysical research communications **350:**17-24.
433. **Zhang, Y., T. Lindblom, A. Chang, M. Sudol, A. E. Sluder, and E. A. Golemis.** 2000. Evidence that dim1 associates with proteins involved in pre-mRNA splicing, and delineation of residues essential for dim1 interactions with hnRNP F and Npw38/PQBP-1. Gene **257:**33-43.
434. **Zhao, Z. S., E. Manser, and L. Lim.** 2000. Interaction between PAK and nck: a template for Nck targets and role of PAK autophosphorylation. Mol Cell Biol **20:**3906-3917.
435. **Zhou, X., Q. Hao, J. Liao, Q. Zhang, and H. Lu.** 2012. Ribosomal protein S14 unties the MDM2-p53 loop upon ribosomal stress. Oncogene.
436. **Zhu, B., Y. Zheng, A. D. Pham, S. S. Mandal, H. Erdjument-Bromage, P. Tempst, and D. Reinberg.** 2005. Monoubiquitination of human histone H2B: the factors involved and their roles in HOX gene regulation. Molecular cell **20:**601-611.
437. **Zhu, W., C. Ukomadu, S. Jha, T. Senga, S. K. Dhar, J. A. Wohlschlegel, L. K. Nutt, S. Kornbluth, and A. Dutta.** 2007. Mcm10 and And-1/CTF4 recruit DNA polymerase alpha to chromatin for initiation of DNA replication. Genes Dev **21:**2288-2299.